Thesis for the degree of Philosophiae Doctor

Modelling tropospheric ozone production on different scales

Øivind Hodnebrog

Meteorology and Oceanography Section

Department of Geosciences

Faculty of Mathematics and Natural Sciences

University of Oslo

Series of dissertations submitted to the
Faculty of Mathematics and Natural Sciences, University of Oslo
No. 1162

ISSN 1501-7710

Cover: Inger Sandved Anfinsen.
Printed in Norway: AIT Oslo AS.

Produced in co-operation with Unipub.
The thesis is produced by Unipub merely in connection with the
thesis defence. Kindly direct all inquiries regarding the thesis to the copyright
holder or the unit which grants the doctorate.

Acknowledgements

The work presented here has been carried out at the Section for Meteorology and Oceanography (MetOs), Department of Geosciences, University of Oslo. Financial support has been received from the European Union's Seventh Framework Programme (FP7/2007-2013) through the CITYZEN project (no. 212095), and Sixth Framework Programme (FP6/2002-2006) through the QUANTIFY Integrated Project (no. 003893) and ECATS Network of Excellence (no. 012284).

First and foremost I would like to thank Professor Frode Stordal, who has been an excellent supervisor ever since I started working on my master thesis and throughout the work with my PhD thesis. His extensive knowledge and great willingness to help have been essential for the completion of this thesis. I would also like to thank my co-supervisors, Professor emeritus Ivar S. A. Isaksen, Dr. Michael Gauss, Professor Terje K. Berntsen and Professor II Øystein Hov, for valuable discussions and feedback. My supervisors have given me the opportunity to establish valuable contacts through participation in international project meetings and conferences. In particular, I would like to mention my enriching stay at the Atmospheric Chemistry Division, National Center for Atmospheric Research in Boulder, Colorado in October 2010.

Special thanks go to my friends and colleagues at MetOs, Met.no and my new workplace CICERO for all the help and support I have received. MetOs has really been a great place to work during these years. My friends and family also deserve big thanks for their support and encouragement, and for being there for me when I needed a break from work. Lastly, I am thankful that my fiancée Siri has been incredibly patient and supportive.

Oslo, November 2011

Øivind Hodnebrog

List of papers presented in this thesis

1. Hodnebrog, Ø., Stordal, F., and Berntsen, T. K.: Does the resolution of megacity emissions impact large scale ozone?, Atmospheric Environment, 45 (38), 6852-6862, 10.1016/j.atmosenv.2011.01.012, 2011.

2. Hodnebrog, Ø., Berntsen, T. K., Dessens, O., Gauss, M., Grewe, V., Isaksen, I. S. A., Koffi, B., Myhre, G., Olivié, D., Prather, M. J., Pyle, J. A., Stordal, F., Szopa, S., Tang, Q., van Velthoven, P., Williams, J. E., and Ødemark, K.: Future impact of non-land based traffic emissions on atmospheric ozone and OH – an optimistic scenario and a possible mitigation strategy, Atmos. Chem. Phys., 11 (21), 11293-11317, 10.5194/acp-11-11293-2011, 2011.

3. Colette, A., Granier, C., Hodnebrog, Ø., Jakobs, H., Maurizi, A., Nyiri, A., Bessagnet, B., D'Angiola, A., D'Isidoro, M., Gauss, M., Meleux, F., Memmesheimer, M., Mieville, A., Rouïl, L., Russo, F., Solberg, S., Stordal, F., and Tampieri, F.: Air quality trends in Europe over the past decade: a first multi-model assessment, Atmos. Chem. Phys., 11 (22), 11657-11678, 10.5194/acp-11-11657-2011, 2011.

4. Hodnebrog, Ø., Solberg, S., Stordal, F., Svendby, T. M., Simpson, D., Hilboll, A., Pfister, G. G., Turquety, S., Richter, A., Burrows, J. P., Denier van der Gon, H. A. C.: A model study of the Eastern Mediterranean ozone levels during the hot summer of 2007. *Submitted to Atmos. Chem. Phys., 2011.*

Contents

1 Introduction

The UN Secretary-General recently addressed some of the main challenges for the future as the world's population reached 7 billion (UN, 2011). Climate change and degradation of the environment were two of the main obstacles he emphasized. Extensive research over the last decades has shown that ozone (O_3) is a key species concerning both these issues. The levels of tropospheric ozone has increased significantly since pre-industrial times, and widespread environmental impacts are projected also for the future (Fowler et al., 2008). Anthropogenic activity, leading to higher emissions of O_3 precursors, is the main driver for changes in tropospheric ozone. However, its abundance is also strongly influenced by dry deposition, biomass burning emissions, biogenic emissions and stratosphere-troposphere exchange, all of which are affected by changes in climate, and some also by land use changes. Atmospheric computer models are useful tools which help to understand the interactions between these processes as well as the complex photochemistry leading to ozone formation. Although substantial model improvements have been made over the past few decades, tropospheric ozone modelling remains a challenging task.

Ozone in the atmosphere has several different impacts, therefore it is an essential species for studies dealing with climate and environment. In the stratosphere, ozone is favourable because of the ozone layer which protects humans from dangerous solar UV radiation. Since the 1970s, when scientists discovered that chlorine and bromine containing compounds (CFCs and halons) could destroy the ozone layer (Molina and Rowland, 1974), the topic of stratospheric ozone depletion has been subject to extensive research and debate. The Montreal Protocol was signed in 1987 in order to reduce the emissions of ozone-depleting substances. Although this international agreement has been considered a major success, future projections show that the ozone layer will not reach pre-1980 levels before the middle of this century (WMO, 2010), due to the long atmospheric lifetimes of CFCs and halons.

The focus of this study is tropospheric ozone, which is currently the third most important anthropogenic greenhouse gas, contributing approximately 0.35 W m^{-2} to the radiative forcing (RF) (IPCC, 2007). In contrast to the long-lived greenhouse gases, e.g. CO_2

and CH_4, ozone has the ability to cause regional forcing, and hence regional climate change. The uncertainty of the estimated global RF from tropospheric O_3 is fairly large, ranging from 0.25 to 0.65 W m^{-2}, and this suggests that work remains in order to fully understand the chemical and physical processes involved in ozone formation and destruction.

High concentrations of ozone occurring near the surface are harmful for humans, animals and vegetation. Ozone pollution is an increasing problem as the background ozone concentrations have more than doubled to about 35-40 ppb in the Northern Hemisphere mid-latitudes since the late 19th century (Fowler et al., 2008, and references therein). Locally, and particularly near urban environments, ozone concentrations can reach up to 200 ppb, which may have fatal consequences knowing that impacts on human health occur above 50 ppb (WHO, 2006) and impacts on vegetation generally occur above 40 ppb. The WHO guideline value of 50 ppb is exceeded in many countries, and in the EU 21,400 premature deaths are associated with ozone each year (EEA, 2007). Additionally, loss of arable crop production due to O_3 were estimated to cost approximately €6.7 billion in the EU in 2000 (Holland et al., 2006). Ozone is also known to cause reductions in tree growth and carbon sequestration, and to modify species composition (Ashmore, 2005). Emission controls are needed in order to avoid increasing concentrations in the future, but climate change is also likely to influence future O_3 levels due to the many links between meteorology and chemistry (e.g. Isaksen et al., 2009). As an example of climate-chemistry interactions, a severe heat wave in Europe during August 2003 was estimated to have led to an excess of between 423 and 769 deaths in England and Wales due to elevated ozone and particle concentrations (Stedman, 2004). Additional record-breaking heat waves took place in southeast Europe during summer 2007, causing severe forest fires and air pollution episodes. Such episodes are expected to occur more frequently in a future warmer climate (Founda and Giannakopoulos, 2009), thus increasing the potential for negative impacts of ozone pollution. Studies of ozone pollution during heat waves (given in Paper IV and partly in Paper I) are important because they may include signs of what to expect in the future.

When the various ozone impacts are studied with numerical models, the issue of scales needs to be considered. As the temporal and spatial scales of various physical and chemical processes differ substantially, the choice of numerical model depends on the problem at hand. The role of ozone in the radiative forcing budget of the atmosphere is normally studied using

global Chemistry-Transport Models (CTMs), while regional or urban scale models often are used to study the effect of ozone on air quality. However, the limited-area domains in the regional and urban scale models make it difficult to properly account for processes occurring on a global scale, such as long-range transport of air pollution. Similarly for global CTMs, important information may be lost as small-scale processes are often not well represented due to poor resolution combined with non-linearities in the ozone chemistry. The inaccuracies that arise due to neglection of urban-scale processes in coarse-resolution models may become increasingly important for studies of the future because of rapid urbanization leading to intense hotspots of ozone precursor emissions. Only 13% of the world's population lived in cities in 1900, while in 2007 this number reached 50%, and is projected to increase to 60% by 2030 (UNFPA, 2007).

The scale issue is a common theme for the work presented in this thesis. More specifically, this study deals with the impacts of tropospheric ozone on scales varying from approximately 10 km, typical of urban scale models, to approximately 100 km and more, typical of global CTMs, as well as interactions between these scales. Main objectives are summarized here:

- Increase knowledge on interactions between different spatial scales, from urban to global scales, focusing on megacity ozone formation.
- Estimate how regional air pollution may respond to climate change by investigating extreme summer episodes.
- Quantify and understand how current ozone levels have responded to past emission changes, and estimate how the global ozone distribution may change in the future, mainly focusing on the rapidly growing transport sector.

Most of these topics are not only interesting to other researchers in the scientific community, but also highly relevant for policy makers. E.g. in order to mitigate climate change, it is useful to know how ozone and the resulting radiative forcing are affected under various emission scenarios. Similarly, in the context of air pollution, a detailed insight into the interactions between ozone precursor emissions, and chemical and meteorological processes is needed in order to derive effective strategies to avoid potential health impacts and vegetation damages. Such collaboration between researchers and policy makers has previously shown to give

positive results. Recently, a review of the Gothenburg Protocol (UNECE, 2007) showed that emission controls have led to substantial decreases in European emissions of NO_X and NMVOCs, which are important precursors in ozone formation.

Large parts of this work have been carried out in the framework of the EU FP7 project CITYZEN (http://www.cityzen-project.eu), where provision of policy-relevant results was an important task. CITYZEN aimed at determining the air pollution distribution and change in and around selected megacities and hotspot regions by using a range of numerical models as well as ground-based and satellite observations. Parts of the research presented in this thesis have also been performed within the EU FP6 project QUANTIFY (http://www.ip-quantify.eu) and the ongoing FP6 network ECATS (http://www.ecats-network.eu). The first project dealt with quantifying the global climate impacts of air, sea and land traffic, while the latter focuses on the climate and environmental impacts of aviation. Two additional studies are still ongoing and not included in this thesis, but they are subjects of follow-up studies and are briefly mentioned here. The first ongoing work is within CITYZEN and concerns climate-chemistry interactions. More specifically, the effects of future climate changes and emission changes are studied by running a global CTM (Oslo CTM2) using meteorological data from a climate model (ECHAM5-HAM) and various emission scenarios. Secondly, in QUANTIFY, simulations with six different global atmospheric chemistry models (ACMs) have been performed using a high emission scenario, and these results will complement the results from the optimistic scenario described in Paper II.

The following section presents scientific background information with the purpose of setting the thesis work in a broader perspective. Section 3 is devoted to atmospheric chemistry modelling, including descriptions of the two models used in this thesis. The individual papers are summarized in Section 4, while main conclusions and prospects of future research are given in Section 5.

2 Scientific background

The research described in this thesis focuses on two important roles of tropospheric ozone; as an important greenhouse gas and as an air pollutant – harmful to humans and vegetation when exposed to large quantities. Processes governing the abundance of tropospheric ozone are investigated in more detail with a special focus on anthropogenic impacts and scale issues, and these topics are emphasized in the background information given in this section.

2.1 Processes governing tropospheric ozone abundance

Ozone is not emitted directly, but is a secondary pollutant produced chemically in the atmosphere. Its abundance strongly depends on the concentrations of the ozone precursors carbon monoxide (CO), nitrogen oxides (NO_X), methane (CH_4), and non-methane volatile organic compounds (NMVOCs), but it is also dependent on deposition and meteorological processes, such as advection, cloud cover formation and precipitation release (Section 2.5). Emissions of ozone precursors come from three sources: anthropogenic sources, particularly fossil fuel combustion; biogenic sources, including emissions from vegetation, soil and ocean; and the third source is biomass burning, which is particularly important near the tropics. Transport of ozone from the stratosphere is another source of tropospheric ozone, but is less important than chemical production on a global scale, although comparable to the net chemistry. Ozone abundance in the upper troposphere is important for radiative forcing (relevant for Paper II), and O_3 also has a longer lifetime in this region compared to the lower troposphere. It is suggested that the stratosphere-troposphere exchange could increase significantly in the future due to climate change (e.g. Pyle et al., 2007). Dry deposition is a major loss for ozone, while wet deposition of e.g. HNO_3 leads to a reduction of ozone precursor concentrations. The main sources and sinks of tropospheric O_3 are illustrated in Figure 1 along with estimated global budgets. The processes that are most important for this work (chemical production and loss, and dry deposition) have been explained in more detail in the following sections.

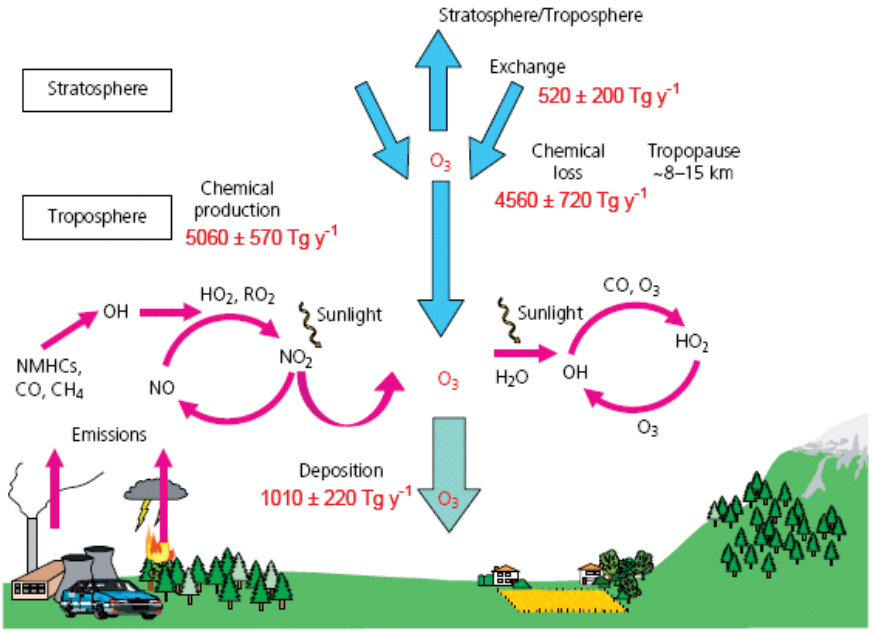

Figure 1. Illustration of the main processes governing the tropospheric O_3 abundance (modified from Fowler et al., 2008). The annual global fluxes and uncertainties are from Stevenson et al. (2006) and have been estimated using 25 models.

2.1.1 Ozone chemistry in the troposphere

Tropospheric O_3 is produced from peroxy radicals RO_2 (e.g. HO_2, CH_3O_2) in the presence of NO_X and sunlight:

$$NO + RO_2 \rightarrow NO_2 + RO \quad (1)$$

$$NO_2 + h\nu \rightarrow NO + O \qquad \lambda < 420 \text{ nm} \quad (2)$$

$$O + O_2 + M \rightarrow O_3 + M \quad (3)$$

The RO_2 radicals result mainly from oxidation by the highly reactive hydroxyl radical OH, which breaks down many trace gases and is thus known as the scavenger of the atmosphere. In the free troposphere, the main reactions producing RO_2 radicals are through the oxidations of CO and CH_4:

$$CO + OH \rightarrow CO_2 + H \quad (4)$$

$$H + O_2 + M \rightarrow HO_2 + M \quad (5)$$

$$CH_4 + OH \rightarrow CH_3 + H_2O \quad (6)$$

$$CH_3 + O_2 + M \rightarrow CH_3O_2 + M \quad (7)$$

In urban air and close to biogenic sources, however, emissions of NMVOCs become much more important in ozone formation. The most reactive NMVOCs with respect to ozone formation, such as aromatics, alkenes and ethenes, have lifetimes of a few hours to a few days, hence they are broken down before they reach the free troposphere. The break down of NMVOCs occurs mainly through photolysis and reaction with OH, HO_2, O, NO_3 and O_3, and leads to ozone formation through the production of free radicals, similar as for CO and CH_4 in Eqs. (4)-(7). However, an important difference from the longer-lived gases CO and CH_4 is that the location of NMVOC emissions largely determines where ozone is produced. For this reason, the issue of scales is essential when it comes to modelling ozone formation near urban areas.

One of the major loss mechanisms of ozone is also the major source of OH in the free troposphere, and requires the presence of sunlight and water vapour:

$$O_3 + h\nu \rightarrow O(^1D) + O_2 \qquad \lambda < 310 \text{ nm} \quad (8)$$

$$O(^1D) + H_2O \rightarrow 2OH \quad (9)$$

Other chemical sinks of ozone include reactions with HO_X (HO_2 and OH), NO_X (NO and NO_2), and NMVOCs, but there are major differences between the loss mechanisms in the free troposphere and in urban air. For instance, in many regions of the troposphere the ozone mixing ratio is controlled by the so-called photostationary-state relationship which includes the reaction

$$NO + O_3 \rightarrow NO_2 + O_2 \quad (10)$$

followed by Eqs. (2)-(3). In contrast to the free troposphere, mixing ratios of NO often exceed O_3 mixing ratios in urban air and Eq. (10) may deplete ozone.

2.1.2 Surface dry deposition

Dry deposition to land and water surfaces is the main loss of boundary layer O_3, constituting a global average flux of approximately 1000 Tg yr^{-1} (Figure 1). Ozone is a very reactive trace gas but not very soluble, hence the dry deposition to land surfaces is much more efficient compared to water surfaces. The amount of ozone removed by dry deposition also depends largely on the type of land surface (e.g. forest, cropland, residential). As a consequence, the representation of dry removal in atmospheric computer models is subject to large uncertainties. The type of land use in each model grid box is critically dependent on the horizontal resolution used and on the applied land use dataset, which often has limitations in quality and resolution. Further, the dry deposition parameterization needs to take into account several meteorological factors, and this adds to the complexity and uncertainties involved.

The time rate of change in concentration due to dry deposition is often determined by a deposition velocity (v_d), which depends on various resistances. For example, in the commonly used Wesely (1989) scheme the deposition velocity is expressed as the inverse of three resistances:

$$v_d = \frac{1}{r} = \frac{1}{r_a + r_b + r_c}$$

where r_a is the aerodynamic resistance between the surface and a specified height above the canopy, r_b is the resistance of a sub layer adjacent to the surface, and r_c is the bulk surface resistance, which is computed as the sum of seven minor resistances. The aerodynamic and sub layer resistances are dependent on meteorological conditions such as stability, and therefore they often have a strong diurnal cycle. The bulk surface resistance represents the plant canopy and the soil, and includes the stomatal resistance, which describes the resistance encountered when trace gases pass through the plant's stomatal openings. In reality the opening and closing of stomata depend on the meteorological factors water vapour, temperature and solar radiation, while in the Wesely scheme only the latter two variables are taken into account. As mentioned in Paper I and Paper IV, this could have led to overestimation of modelled dry removal of O_3 during the summer heat waves of 2003 and 2007, respectively, because the stomata close to protect the plants during drought conditions. An experiment by Vautard et al. (2005) showed that a doubling of the bulk deposition

resistances in the Wesely scheme for two land use types increased the performance when modelling the summer 2003 heat wave.

2.2 Ozone precursor emissions

2.2.1 Anthropogenic

Emissions of the ozone precursors NO_X, CO, CH_4 and NMVOC have increased substantially over the last couple of centuries due to anthropogenic activity. Fossil fuel combustion is the most important anthropogenic source, and takes place in a variety of emission sectors including e.g. power generation, industry and transport. However, the importance of each sector depends strongly on the precursor gas and on the location. Different countries have different levels of economic development and emission legislations. Access to natural resources also plays a role in the relative contributions of anthropogenic emission sources, for instance in Norway, hydroelectric power constitutes most of the power generation, leading to a very low share of O_3 precursor emissions from this sector. Besides fossil fuel combustion, sources such as deforestation, savannah burning and the burning of agricultural waste are important, especially for CO where the sum of these three sources accounts for half of the global anthropogenic emissions of CO (Fowler et al., 2008). In the future, significant changes in anthropogenic emissions are expected, mainly due to population growth, economic development and technological progress.

Detailed information on the spatial and temporal distributions of emissions is critical input to atmospheric chemistry models (ACMs). Such information often has limitations in spatial and temporal resolution, and it is subject to large uncertainties as different countries have different methods of reporting their emissions. In Europe the quality is relatively good as the European Monitoring and Evaluation Programme (EMEP; http://www.emep.int) puts large efforts into developing up-to-date emission inventories suitable for atmospheric modelling. In some countries so-called bottom-up inventories (based on local statistics) may be of low quality or even non-existent, and emission estimates have to be complemented by top-down methods (involving measurements and modelling). As an example, Richter et al.

(2005) used satellite observations and an ACM to find that bottom-up inventories underestimated NO_2 emissions over industrial areas in China.

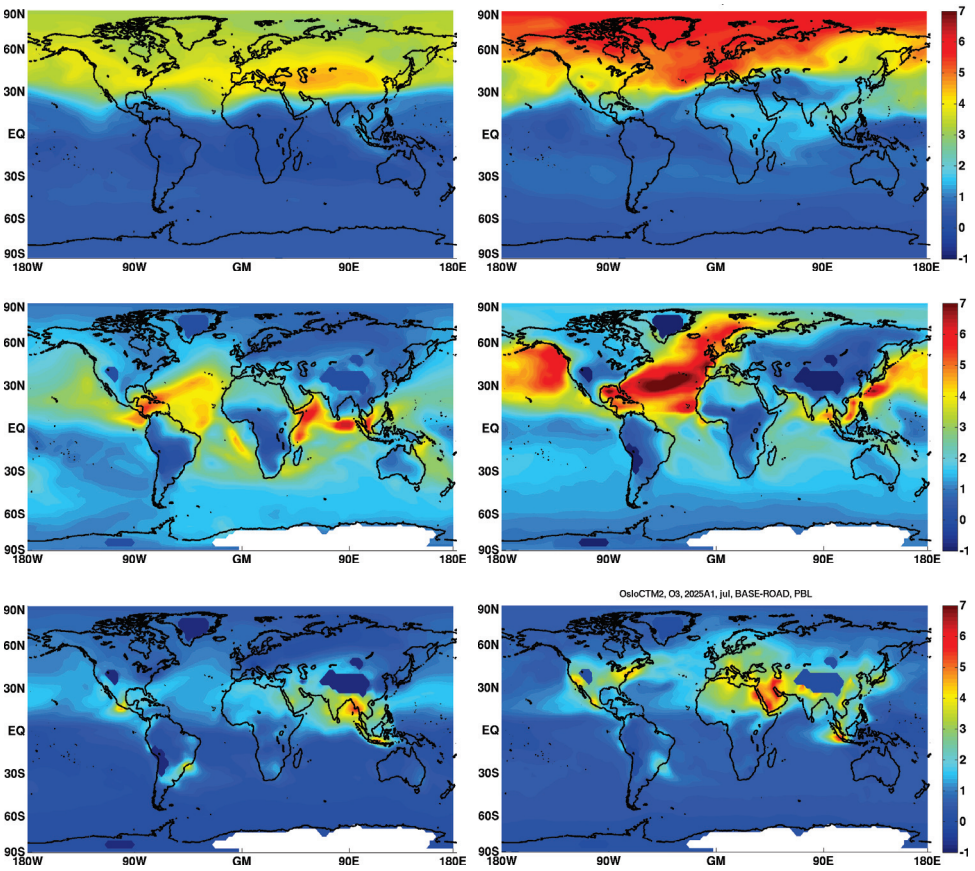

Figure 2. Mean perturbations of O_3 (Δppb) in January (left) and July (right) in the upper troposphere (300 – 200 hPa) due to a 5% perturbation of aircraft emissions (top), and in the lower troposphere (> 800 hPa) due to a 5% perturbation of ship emissions (middle) and road emissions (bottom). The results are from Hodnebrog et al. (manuscript in preparation) and show the estimated impact in 2025 under the A1B scenario, as calculated by the Oslo CTM2 model. The O_3 response caused by the 5% emission perturbation has been scaled to 100% by multiplying with a factor 20.

This work focuses specifically on how transport sector emissions may impact tropospheric ozone in the future. Emissions from this sector have large impacts on both air pollution and climate. On a 100 year time scale, CO_2 constitutes the largest positive radiative forcing term due to present-day (year 2000) traffic emissions, while tropospheric ozone is the second largest term (Fuglestvedt et al., 2008). The total climate impact from transportation is expected to increase in the future as a consequence of increasing population and economic turnover. In terms of ozone, one study predicts that in 2030 ozone RF from the traffic sector will constitute 26% of the total anthropogenic O_3 forcing (Unger et al., 2008). In addition, projected regional changes in emissions and expected technological developments make transportation impacts on atmospheric chemical composition a highly interesting topic for the future.

While road traffic accounted for 33% of the anthropogenic NO_X emissions in 2000 (Cofala et al., 2007), substantial decreases are expected in the future due to stricter vehicle emission standards and already available technological improvements (Uherek et al., 2010). Figure 2 shows that consequently the near-future (2025) road traffic impact on lower tropospheric O_3 is expected to decrease, when comparing with the year 2000 results of Hoor et al. (2009). On the other hand, the ozone impact of the non-land based traffic sectors, aircraft and shipping, is expected to increase. It is also evident from Figure 2 that the global distribution of impacts on ozone varies significantly between the three sectors and between the winter and summer seasons. The ozone impact from aircraft emissions is more well-mixed and occur in the upper troposphere / lower stratosphere (UTLS) region where the climate impact is large due to the low temperatures near the tropopause (e.g. Hansen et al., 1997). The shipping emissions, however, are emitted into the relatively clean maritime boundary layer and the large share of NO_X emissions from this sector leads to increased OH levels and thereby a reduction of methane lifetimes (Hoor et al., 2009). Previous studies have shown that for shipping the CH_4 cooling effect will dominate over the O_3 warming (e.g. Myhre et al., 2011), and this is described further in Paper II.

2.2.2 Natural

A number of natural sources exist for ozone precursor emissions, and in the case of NMVOCs the global sum of emissions from terrestrial plant species (known as biogenic emissions) is even larger than from the anthropogenic sources (Fowler et al., 2008). The most important natural sources of NO_X emissions are bacterial and volcanic activity, lightning and open burning of biomass from forest fires. For CO, the primary sources are vegetation, oceans and biomass burning, while natural CH_4 emissions mainly stem from wetlands. Common for all of these sources is that large uncertainties are involved in the magnitude and global distribution of these emissions. The uncertainties are at least a factor of 2 for natural emissions (Simpson et al., 1999), and this could have major implications for atmospheric modelling studies focusing on ozone.

Of particular interest is isoprene, which is the most important biogenic emission species due to the large emission rate and reactivity with OH. It has been estimated that isoprene is about a factor of three more photochemically reactive than a weighted average of VOCs emitted by e.g. motor vehicle exhaust (Benjamin et al., 1997), hence its potential impact on O_3 production is strong. Additionally, the emission rate of biogenic isoprene is closely dependent on meteorological conditions, especially temperature and solar radiation, but also humidity, wind speed and soil moisture. As biogenic emissions normally increase with temperature, their contribution to ozone formation could increase significantly in a future climate (Pyle et al., 2007). In paper IV, the impact of biogenic emissions on O_3 during an extremely hot summer period has been investigated for the Eastern Mediterranean region, where biogenic emissions are important and typically represent 70-80% of the annual total NMVOC emissions (Symeonidis et al., 2008).

2.3 Scale interactions in the ozone chemistry

Ever since the first two- and three-dimensional numerical air-quality models designed to simulate the atmospherical chemical composition were developed in the 1960s and 1970s, computational requirements have put restrictions on the temporal and spatial model resolutions. Even today, more than one model is needed in order to represent all scales concerning air quality and climate change issues. It is well-known that coarse resolution leads to inaccuracies in the calculations, both regarding meteorological and chemical processes.

One grid box in global CTM models often represents an area exceeding 100 km × 100 km, well beyond the size of a typical large city. In reality, however, inhomogeneous distribution and composition of emissions will lead to large spatial variations in concentrations of ozone precursors within an urban area. Significant production and loss of ozone may take place before a pollution plume, e.g. from a megacity, is diluted to the scale of the model grid box. Consequently, inaccuracies will arise when emissions and concentrations are averaged in a large grid box.

Similarly, small-scale meteorological processes are likely to cause additional inaccuracies in coarse-resolution models since the atmospheric chemical composition is strongly dependent on meteorological conditions (e.g. Jacob and Winner, 2009). Many of the meteorological processes occur on small temporal and spatial scales and therefore needs to be parameterized. For instance convection, which is important to determine the vertical transport and washout of chemical species, can occur on spatial scales less than a kilometer, much lower than the resolution of the global-scale models that exist today. Other meteorological variables which are important for chemistry and may be inaccurately represented in coarse resolution models include, but are not limited to, temperature (affecting e.g., chemical reaction rates, biogenic emissions, dry deposition), cloud cover (photodissociation rates), precipitation (wet deposition) and turbulence (dispersion), whereas the latter is also a good example of a process where there is a lack of physical understanding.

The ozone chemistry is known to be non-linear (e.g. Jacob, 1999), implying that increases in precursor emissions do not necessarily cause a corresponding increase in ozone levels. In urban air, the ozone abundance is largely dependent on the ratio between NO_X and NMVOCs concentrations. When the initial mixing ratio of NO_X is low, an increase in the abundance of NMVOCs does not affect the amount of ozone. At high NO_X levels, an increase

in NMVOC mixing ratios causes increasing ozone values. The latter case is called the NMVOC-limited regime as ozone production is limited by the abundance of NMVOCs. When NMVOC levels are low, an increase in NO_X could even decrease the amount of ozone. The reason is that Eq. (10) is the main reaction converting NO to NO_2 and when Eq. (2) ceases at night, the net reaction is ozone loss. At high NMVOC levels, an increase in NO_X causes increasing ozone values, and this case is called the NO_X-limited regime.

The non-linearities in ozone chemistry, described above, implies that coarse-resolution models may overestimate the ozone enhancement efficiency (number of ozone molecules produced per NO_X molecule emitted) in a NO_X rich emission plume because the size of a model grid box may be too large to ensure that the mixing time between grid boxes is shorter than the NO_X lifetime. However, there are competing effects and the O_3 overestimation could be partly compensated by the fact that the lifetime of NO_X during daytime is underestimated in coarse-resolution models. The reason for this is that high NO_X levels lead to a major reduction of OH (Poppe et al., 1993) through the reaction

$$NO_2 + OH + M \rightarrow HNO_3 + M \quad (11)$$

Consequently, OH is depleted and the lifetime of NO_X increases in the plume (e.g. Franke et al., 2008), while in coarse-resolution models the high NO_X levels are suppressed, thus the NO_X lifetime is too short. On the other hand, during nighttime the overestimation of O_3 production could be intensified. In the absence of sunlight, NO_X is lost by the reactions

$$NO_2 + O_3 \rightarrow NO_3 + O_2 \quad (12)$$

$$NO_2 + NO_3 + M \rightarrow N_2O_5 + M \quad (13)$$

$$N_2O_5 + H_2O(aq) \rightarrow 2HNO_3 \quad (14)$$

which lead to an overestimation of the NO_X lifetime in coarse-resolution models because the reaction rate in (13) is quadratic in NO_X.

In order to account for non-linearities in the ozone chemistry, parameterizations have been developed and implemented into CTMs for aviation plumes (e.g. Meijer et al., 1997; Kraabøl et al., 2002; Cariolle et al., 2009). The impact of non-linear chemistry on ozone levels has also been studied for ship plumes (e.g. Kasibhatla et al., 2000; Franke et al., 2008; Huszar et al., 2010), but the effect is more complex than for aircraft partly due to interaction with other emission sources near the surface. The effect of aircraft and ship plumes is also

different from that of a megacity plume because of the large impact of NMVOCs in the latter, whereas ozone precursor emissions from the aircraft and ship sectors are mostly dominated by NO_X. In the frameworks of the QUANTIFY and ECATS projects, the Cariolle et al. (2009) parameterization for aircraft plumes has been implemented in the Oslo CTM2 model and compared against results obtained with the previously developed Kraabøl et al. (2002) method which used so-called effective emissions. Figure 3 shows the effect on O_3 when applying the two parameterizations, and it can be seen that the inclusion of sub-grid scale chemistry leads to a reduction of ozone, mainly in the region of the North Atlantic Flight Corridor. However, the magnitude is different between the Kraabøl and Cariolle methods, reflecting some of the uncertainties. Considering that the maximum zonal mean ozone contribution from aircraft (without plume parameterization) is up to 4 ppb (not shown), the plume effects, which could reach -0.4 ppb (Figure 3), have a significant impact on ozone chemistry in large-scale models. The effect of neglecting small-scale chemistry in megacity plumes has been investigated in Paper I.

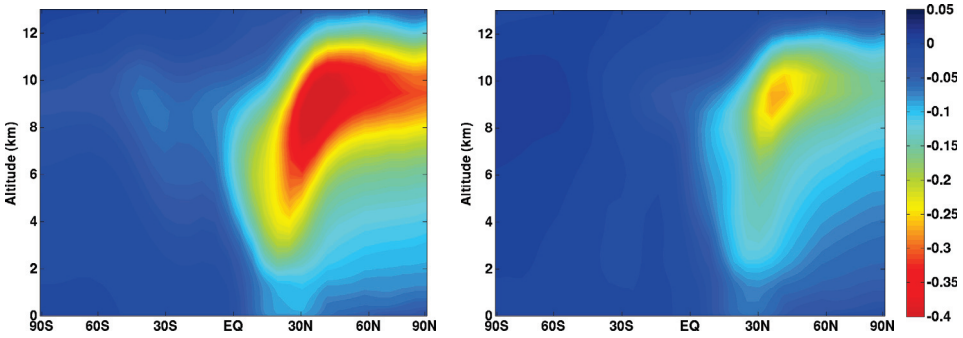

Figure 3. Zonally averaged O_3 changes (Δppb) due to aviation plume effects for January 2003 using the Kraabøl et al. (2002) parameterization (left), and the Cariolle et al. (2009) parameterization (right) calculated with the Oslo CTM2 model. The model results are produced by Ø. Hodnebrog (not published).

2.4 Trends in near-surface ozone

Measurements show that there has been a doubling in hemispheric background O_3 levels in the northern mid-latitudes from 10-15 to 20-30 ppb between 1900 and 1980, and the levels have further increased to a present-day level of 25-35 ppb (Fowler et al., 2008). Despite the hemispheric O_3 increase, many countries, mainly in Europe and North America, have reduced their precursor emissions over the last couple of decades, and consequently reduced peak O_3 concentrations (Solberg et al., 2005). The 1979 Convention on Long-range Transboundary Air Pollution (CLRTAP) with its 1999 Gothenburg Protocol is an international effort to reduce O_3 precursor emissions. The Protocol set national limits based on scientific assessments of thresholds of health effects and vegetation damages, as well as cost effectiveness of the control measures, and is now ratified by 24 parties including the US and many European countries.

The use of atmospheric chemistry models enables the possibility to derive trends with a regional or global coverage, given that sufficient information of the spatial distribution and temporal evolution of emissions and meteorology is available. Trends can be derived for places where measurement data are sparse or not available, and another advantage is that model sensitivity tests can be performed to help explain the causes of observed trends, for instance by keeping the emissions constant while including year-to-year variability in the meteorology. The issue of scales is important also for trend studies, as the choice of model and horizontal resolution depend for instance on whether urban or rural trends are being calculated.

Figure 4 shows the global distribution of the 10-year near-surface O_3 trend from 1998 to 2007 calculated with the Oslo CTM2 model for the study presented in Paper III (note that global trends were not included in Paper III which focused on European trends). Southeast Asia, with eastern China in particular, sticks out as the region with the strongest positive trend, exceeding 0.5 ppb O_3 per year over large areas. Substantial O_3 reductions can be seen in North America, specifically along the east coast of the US, presumably as a consequence of the emission controls that have been applied to reduce O_3 precursor emissions. Over Europe, however, the abatement strategies did not seem to have the same effect since the trend is mostly non-significant (p-value > 0.05) and only slightly negative. This is a good example of how the ozone response not necessarily reflects local emission controls. Ozone needs to be

treated as a regional or global pollutant, and a 10-year period may be too short to assess its trend due to the strong year-to-year variability. There is a strong link between meteorology and ozone formation and it is likely that recent pollution events, such as during the summers of 2003 and 2007, could have counter-acted the effects of reducing precursor emissions. Other possible explanations are: non-linearities in ozone production, forest fires (e.g., Paper IV shows a strong impact of Eastern Mediterranean fires on ozone during summer 2007), increases in background O_3 (including increased import from the stratosphere), meteorological impact on biogenic NMVOC emissions, and changes in the NO to NO_2 emission ratio (important in urban areas). A further discussion of the 10-year European O_3 trends is given in Paper III.

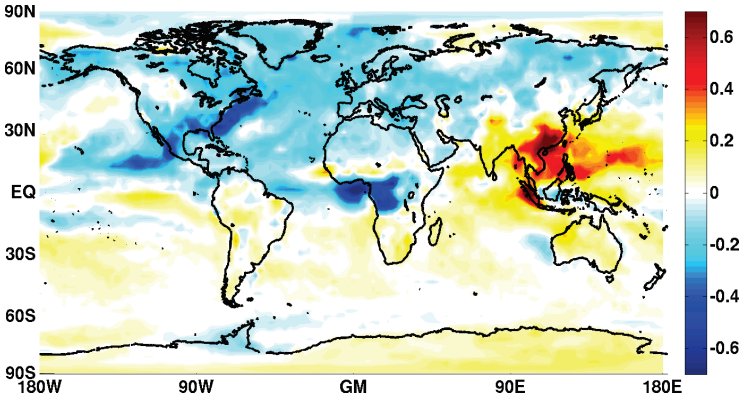

Figure 4. Distribution of near-surface O_3 trends (ppb yr^{-1}) for the period 1998-2007 calculated with the Oslo CTM2 model. The results are from the simulations described in Paper III.

2.5 Climate-ozone interactions

Weather and climate have major impacts on the ozone abundance (e.g. Isaksen et al., 2009; Jacob and Winner, 2009). On the other hand, changes in ozone levels contribute to climate change, both regionally and globally. Increasing attention has been drawn to such kinds of climate-chemistry interactions since their importance was recognized more than 20 years ago (Ramanathan et al., 1987), and currently fully-coupled climate-chemistry models are being developed and used to estimate how climate and air pollution may change in the future.

Ozone is affected by climate in many different ways. Temperature impacts ozone directly as most of the gas-phase reactions in the ozone chemistry are thermal chemical reactions. Additionally, temperature affects ozone levels indirectly through surface dry deposition and biogenic VOC emissions. The amount of solar radiation also affects biogenic emissions, as well as rate constants in photochemical reactions. Furthermore, precipitation affects loss of trace gases and particles by wet deposition, which is mainly relevant for ozone through washout of nitric acid (HNO_3). HNO_3 is a reservoir species of NO_X and its high solubility leads to effective loss when precipitation is present. Another important link between meteorology and chemistry is the formation of the OH radical which is strongly dependent on cloud cover, sunlight and water vapour, as shown in Eqs. (8)-(9). Advection (large-scale) and diffusion (small-scale) determine how ozone and its precursors are transported in the atmosphere. Typical time scales for global transport vary significantly with horizontal and vertical location (e.g. Jacob, 1999), and of major importance for tropospheric O_3 is ventilation from the boundary layer to the free troposphere, and intrusion from the stratosphere.

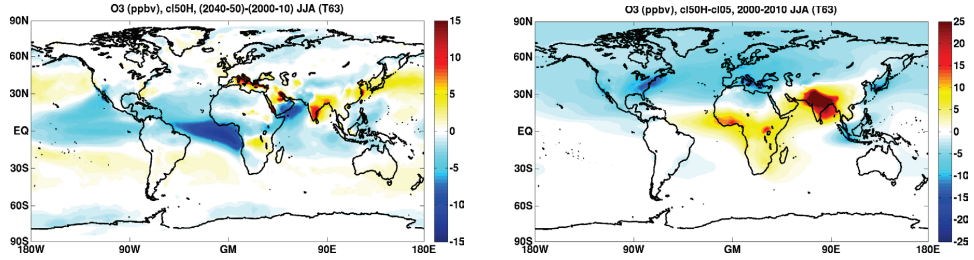

Figure 5. Predicted change in daily maximum near-surface O_3 (Δppb) during summer (June, July, August) due to changes in climate from 2000-2010 to 2040-2050 (left), and due to changes in anthropogenic emissions from 2005 to 2050 (right) calculated with the Oslo CTM2 model. Please note that different scales have been used. The model results are produced by Ø. Hodnebrog (not yet published).

Figure 5 shows a potential scenario of how climate changes and emission changes may impact the global near-surface O_3 distribution during northern hemisphere summers in the middle of this century. The estimates are calculated with the one-way coupled ECHAM5→Oslo CTM2 model system developed within the CITYZEN project. Climate data for present time and for the future have been calculated with the ECHAM5-HAM model, and these data have then been used as the meteorological driver for the Oslo CTM2 model. The figure illustrates the complexity of the problem showing ozone enhancements in some regions and ozone reductions in other regions. Although most regions show a stronger ozone response due to expected changes in emissions, the impact of climate change on O_3 is clearly evident with increases for instance in India and the Mediterranean region. The indication that future climate-induced O_3 changes may be more important on regional and local scales than on global scales is also highlighted in other studies (e.g. Fowler et al., 2008), but it should be noted that current global chemistry models (GCMs) are not able to simulate all processes governing ground-level O_3 with sufficiently high resolution. Recommendations for future research on this topic focus specifically on the ability of GCMs to simulate the climate change impacts on regional air pollution meteorology and natural emissions, whereas the latter is also strongly affected by changes in land cover (Jacob and Winner, 2009). Nevertheless, several climate change impacts on ozone have already been identified with a good level of scientific understanding; including consequences of changes in temperature, humidity, sunlight, drought and CO_2 (Fowler et al., 2008). It is also suggested that heat waves in Europe, such as the summer 2003 and 2007 episodes, will occur more frequently in a future climate (Schär et al., 2004; Founda and Giannakopoulos, 2009), potentially leading to increased number of occurrences of severe air pollution episodes.

As mentioned before, tropospheric ozone is not only affected by changes in climate, but it is also an important greenhouse gas and thereby a driver of climate change. Additionally, a recent study has highlighted the indirect warming effect of O_3, which occurs through suppression of plant growth and hence reductions in the land carbon sink for CO_2 (Sitch et al., 2007). The ozone precursor gases also have important effects on climate, not only through the formation of O_3. Increases in NO_X emissions lead to cooling due to associated increases in OH which will reduce concentrations of CH_4 – the second most important anthropogenic greenhouse gas (IPCC, 2007). On the other hand, emissions of CO,

NMVOC and CH_4 lead to reductions in OH concentrations and thereby induce warming of the climate. In this work, the effect of ozone and its precursors on forcing of climate is studied in Paper II, while Paper IV focuses on the effect of meteorological conditions on ozone.

3 Modelling – from global to local scales

Computer modelling of atmospheric chemical reactions started already in the 1950s when so-called box models were used. The first two and three dimensional air-quality models were developed 10-20 years later, including treatment of emissions, transport, gas chemistry and gas deposition to the ground. Since then, models simulating the chemical composition of the atmosphere have undergone substantial improvements, especially as a consequence of increased computer capacity, but also in the way we understand various atmospheric processes. Additionally, the areas of application have expanded from pure urban air pollution modelling to also include simulations of regional acid deposition, stratospheric ozone depletion and global climate change. Fully coupled climate-chemistry models are being developed, but are not yet widely used in atmospheric chemistry studies due to their complexity and computational demands. More commonly, different issues regarding air pollution and climate change are addressed using different models, and the model choice depends particularly on the spatial scales in question.

In this work, two different atmospheric chemistry models have been applied; namely Oslo CTM2 and WRF-Chem. The combination of these two models covers a wide range of temporal and spatial scales necessary to address topics relevant for this thesis, such as ozone impacts on climate and ozone formation from megacity emissions. Both models divide the atmosphere into a three-dimensional grid and solve a number of differential equations for each grid box. However, since the area of application differ between the models, the treatment of processes and the possible range of scales also differ, as described below.

3.1 Oslo CTM2

The Oslo Chemistry-Transport Model has been developed in the atmospheric chemistry group at the Department of Geosciences over many years and is now in its second version with Oslo CTM3 soon to come. Oslo CTM2 is a global offline CTM capable of simulating both tropospheric and stratospheric chemistry. The model is normally driven by meteorological data from the European Centre for Medium-Range Weather Forecasts (ECMWF) Integrated

Forecast System (IFS)[1], although meteorological data from a general circulation model (ECHAM5) have recently been used to estimate the impact of climate change on air pollution (Figure 5).

Advective transport is critically important in a CTM, and in the Oslo CTM2 the highly accurate Second Order Moments scheme is used (Prather, 1986). In addition, tracers undergo convective transport (Tiedtke, 1989), boundary layer mixing (Holtslag et al., 1990), wet and dry deposition (Wesely, 1989), chemical reactions and emissions. The chemistry scheme for the troposphere (Berntsen and Isaksen, 1997), the focus of this thesis, consists of 51 species and takes into account 86 thermal reactions, 17 photolytic reactions and 2 heterogeneous reactions. The numerical solution is based on the Quasi-Steady-State Approximation (QSSA) (Hesstvedt et al., 1978), using three different integration methods depending on the chemical lifetime of the species. Calculation of photolysis rates is done online using the FAST-J2 method (Wild et al., 2000; Bian and Prather, 2002).

The model resolution is flexible, and in this thesis the horizontal resolution is Gaussian T42 (approx. 2.8° × 2.8°), while in the vertical, 60 layers extend from the surface to 0.1 hPa. This resolution serves as a good compromise between computational demands and accuracy, although higher resolution is always desirable, especially for the 10-year trend study focusing on emission hotspots (Paper III). Natural emissions are taken from the POET inventory (Granier et al., 2005) and from the QUANTIFY project (Jöckel et al., 2006), biomass burning emissions are from the Global Fire Emissions Database (GFED) (van der Werf et al., 2006), while anthropogenic emissions are provided through the CITYZEN and QUANTIFY projects. A comprehensive model description and evaluation is given in Søvde et al. (2008). In this thesis, the model has been applied in Paper II and paper III, where brief model descriptions are given, but Oslo CTM2 model results from Paper III have also been used as input to WRF-Chem in Paper I and Paper IV.

[1] Documentation available online at http://www.ecmwf.int/research/ifsdocs/.

3.2 WRF-Chem v. 3.2

The Weather Research and Forecasting model with chemistry (WRF-Chem) is developed as a collaborative effort between several research institutes (Grell et al., 2005). The principal contributors are the National Oceanic and Atmospheric Administration (NOAA) and the National Center for Atmospheric Research (NCAR). Contrary to the Oslo CTM2 model, WRF-Chem consists of a numerical weather prediction model (WRF) (Skamarock and Klemp, 2008), which is fully coupled with the chemistry module. The model is non-hydrostatic and therefore able to simulate small-scale processes, such as those leading to urban air pollution, but is also commonly used for regional scale studies.

There are a number of choices for schemes related both to the dynamics and the chemistry, but the focus here is on the setup used in this thesis. The advection scheme is a third-order Runge-Kutta based time-splitting scheme which offers the best combination of efficiency and simplicity for non-hydrostatic atmospheric models (Wicker and Skamarock, 2002). Further, the model has been set up with treatment of convection using the Grell-3 cumulus scheme, boundary layer mixing (Janjic, 2002), dry deposition (Wesely, 1989) (same as in Oslo CTM2), chemical reactions and emissions. The chemistry scheme is the Regional Acid Deposition Model version 2 (RADM2) (Stockwell et al., 1990), which also is based on QSSA, and consists of 63 chemical species, 135 thermal reactions and 21 photochemical reactions. Photolysis rates for the photochemical reactions are calculated using the FTUV scheme (Madronich, 1987). By default, a fixed overhead O_3 column is used in the FTUV calculations, but as a part of the work with this thesis, the model now uses a domain-averaged total O_3 column for each day taken from the 10-year Oslo CTM2 simulation described in Paper III.

As WRF-Chem is in principal a regional model (a global version is under development), meteorological and chemical data are needed at the domain boundaries in addition to initial fields. These data are taken from ECMWF-IFS re-analysis for the meteorological variables, while the chemical species are updated every 6 hours from results obtained with the Oslo CTM2 model. As the Oslo CTM2 and RADM2 chemistry schemes differ, the NMVOC species in the first had to be mapped to the appropriate RADM2 components. Figure 6 shows that WRF-Chem is able to reproduce the observed tropospheric

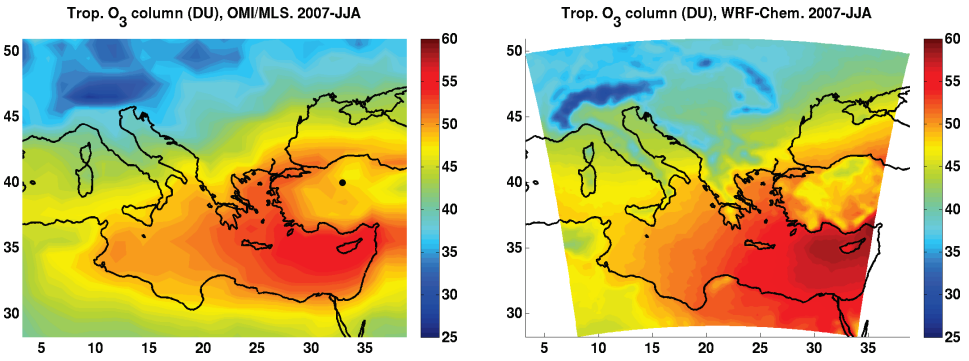

Figure 6. Tropospheric O_3 column (DU) for the summer (June-July-August) 2007 from OMI/MLS observations (left) and from a WRF-Chem simulation using initial and boundary conditions from Oslo CTM2 (right). The black dot in the left plot marks the location of the Ankara sonde measurements depicted in Figure 7. Monthly mean OMI/MLS level 3 data have been downloaded from NASA (Ziemke et al., 2006) and the model results are from Paper IV.

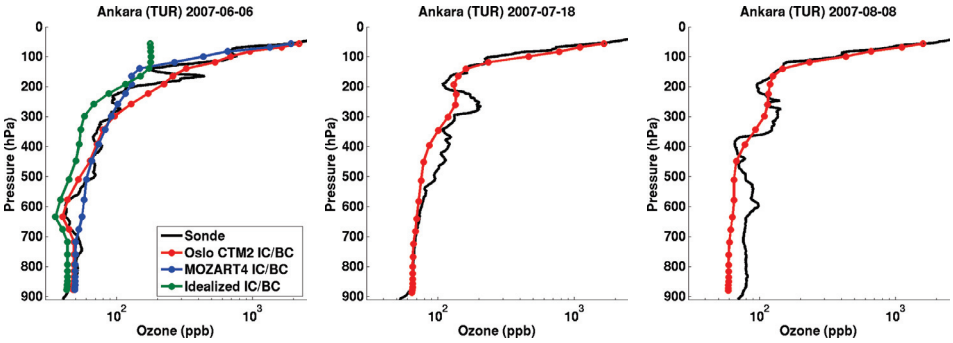

Figure 7. Vertical ozone profiles (ppbv) modelled by WRF-Chem using three different setups for initial and boundary conditions, and measured by balloon sondes released at Ankara, Turkey in the afternoon on 6 June (left), 18 July (middle), and 8 August (right) in 2007. Note that the scale on the bottom axis is logarithmic and ranges from 30 to 2500 ppb. Ozone sonde measurements were retrieved from the World Ozone and Ultraviolet Radiation Data Centre (http://www.woudc.org) and the model results are from Paper IV.

ozone column relatively well when using initial and boundary conditions (IC/BC) from Oslo CTM2. The modelled maximum tropospheric ozone column near Cyprus is about 5 DU higher than the observed, but this could partly be due to the differences in horizontal resolution (25 km × 25 km in the model versus 1.25° longitude × 1.0° latitude in the observations). The tropospheric ozone column in regional models is very sensitive to boundary conditions as a large column contribution comes from the upper troposphere, where the lifetime of ozone is longer and advection is more rapid. Hence, the Oslo CTM2 initial and boundary conditions play an essential role for the WRF-Chem results presented in Figure 6. The importance of using realistic IC/BC for the chemical species is shown in Figure 7. During the period of the simulations of the Eastern Mediterranean region (presented in Paper IV), three ozone sonde measurements were available for the summer 2007; one for each month at Ankara, Turkey. The WRF-Chem simulation with Oslo CTM2 IC/BC compares well with the sonde measurements in the upper troposphere, except that some of the fluctuations are missing, but this is not surprising given the relatively coarse vertical model resolution. Below ~600 hPa, WRF-Chem shows excellent agreement with the observations in June and July, while there is an underestimation up to 20 ppb for the sonde observation in August. For the comparison in June, results from two additional simulations are available. The WRF-Chem simulation with IC/BC from the MOZART-4 model[2] (Emmons et al., 2010) shows a vertical O_3 profile similar to the observations, but with a slight overestimation near 600 hPa. The ozone mixing ratios from the simulation using idealized vertical profiles as IC/BC for the chemical species, however, are underestimated at all height levels. The mixing ratios are particularly low in the UTLS region when comparing with the observations and the simulations using Oslo CTM2 and MOZART-4 as initial and boundary conditions.

The horizontal resolutions applied here range from 9 km × 9 km (local/regional scale) to 81 km × 81 km (regional/global scale) while the number of vertical layers is 27, covering the region between the surface and 50 hPa. Biogenic emissions are calculated online in the model using the Model of Emissions of Gases and Aerosols from Nature (MEGAN) version 2.04 (Guenther et al., 2006), while anthropogenic emissions are taken from several different sources. An emission pre-processor program, WRF-EMIS, has been developed, making it

[2] MOZART-4 data have been downloaded from http://www.acd.ucar.edu/wrf-chem/mozart.shtml.

possible to include anthropogenic emissions from five different inventories. Each emission inventory has different resolution and coverage, e.g. 1 km × 1 km resolution for the UK (NAEI, 2007) and 0.5° × 0.5° resolution with global coverage (RETRO, 2006). The WRF-EMIS program interpolates the original data to the WRF-Chem domain, maps NMVOCs to RADM2 components, and adds monthly, weekly and diurnal cycles as well as approximate vertical profiles, all dependent on the emission sectors. Further descriptions of the WRF-Chem model and the treatments of emissions are given in Paper I and Paper IV.

4 Summary of papers

4.1 Paper I

Hodnebrog, Ø., Stordal, F., and Berntsen, T. K.: Does the resolution of megacity emissions impact large scale ozone?, Atmospheric Environment, 45 (38), 6852-6862, 10.1016/j.atmosenv.2011.01.012, 2011.

This paper investigated the importance of using high resolution when modelling the impact of megacity emissions on large scale tropospheric ozone. The regional WRF-Chem model was run for two 3-day summer periods in July and August 2003, focusing on three megacities; London, Ruhr, and Cairo. We have used various resolutions in megacity emission fields (ranging from 9×9 km^2 to 81×81 km^2), while the model resolution was kept constant at 9×9 km^2 in all simulations. Results from the six case studies show that the inaccuracies that arise on a large scale when using megacity emission resolution at a typical scale of a global Chemistry-Transport Model (81×81 km^2) were relatively small (12% or less), but they depend strongly on meteorological conditions. A change in megacity emission resolution induced small-scale spatial changes in ozone fields, but relatively small changes when integrating over a large volume. Thus, our study suggests that high resolution is more important for local air pollution studies than for large scale ozone changes relevant for climate studies, and indicates that parameterization of megacity emissions in large-scale models may be unnecessary. However, the impact of a finer resolution of the meteorology was not studied here and could possibly give larger effects seen from a climate perspective.

4.2 Paper II

Hodnebrog, Ø., Berntsen, T. K., Dessens, O., Gauss, M., Grewe, V., Isaksen, I. S. A., Koffi, B., Myhre, G., Olivié, D., Prather, M. J., Pyle, J. A., Stordal, F., Szopa, S., Tang, Q., van Velthoven, P., Williams, J. E., and Ødemark, K.: Future impact of non-land based traffic emissions on atmospheric ozone and OH – an optimistic scenario and a possible mitigation strategy, Atmos. Chem. Phys., 11 (21), 11293-11317, 10.5194/acp-11-11293-2011, 2011.

The impact of future emissions from aviation and shipping on the atmospheric chemical composition was studied in this paper. Six different atmospheric chemistry models were run with emissions from an optimistic scenario (B1) and a mitigation option for the aircraft sector (B1 ACARE). The model results show that emissions from both aircraft and shipping will have a larger impact on atmospheric ozone and OH in near future (2025; B1) and for longer time horizons (2050; B1) compared to recent time (2000). However, there is a large potential for reducing the impact of aviation in 2050 if the technological improvements considered in the B1 ACARE will be introduced. Aircraft emissions have about 4 times higher ozone enhancement efficiency (ozone molecules enhanced relative to NO_X molecules emitted) than shipping emissions and the maximum impact is found in the UTLS region. Zonal mean aircraft-induced ozone could reach up to 5 ppbv at northern mid- and high latitudes during future summer (July 2050; B1). Shipping emissions have the largest impact in the marine boundary layer and their ozone contribution may exceed 4 ppbv over the North Atlantic Ocean in the future (2050; B1) during northern summer (July). Net radiative forcings from the six models have been calculated, taking into account ozone, methane (including stratospheric water vapour), and methane-induced ozone changes. For the B1 scenario, shipping leads to a net cooling with radiative forcings of -28.0 (±5.1) and -30.8 (±4.8) mW m^{-2} in 2025 and 2050, respectively, due to the large impact on OH and, thereby, methane lifetime reductions. Corresponding values for the aviation sector shows a net warming effect with 3.8 (±6.1) and 1.9 (±6.3) mW m^{-2}, respectively, but with a small net cooling of -0.6 (±4.6) mW m^{-2} for B1 ACARE in 2050.

4.3 Paper III

Colette, A., Granier, C., Hodnebrog, Ø., Jakobs, H., Maurizi, A., Nyiri, A., Bessagnet, B., D'Angiola, A., D'Isidoro, M., Gauss, M., Meleux, F., Memmesheimer, M., Mieville, A., Rouïl, L., Russo, F., Solberg, S., Stordal, F., and Tampieri, F.: Air quality trends in Europe over the past decade: a first multi-model assessment, Atmos. Chem. Phys., 11 (22), 11657-11678, 10.5194/acp-11-11657-2011, 2011.

In this paper the capability of current state-of-the-art chemistry-transport models (CTMs) to reproduce air quality trends and interannual variability is discussed. It is important to document strengths and weaknesses based on historical simulations before the models are used to investigate future air quality projections. Two global and four regional CTMs were applied to simulate air quality over the past decade (1998-2007) in the Western European anthropogenic emissions hotspots. Comparisons between models and observations show that trends of the primary atmospheric constituent NO_2 are well reproduced, while capturing the more moderate trends of secondary species such as O_3 is more challenging. Apart from the long term trend, the modelled monthly variability is consistent with the observations, but the year-to-year variability is generally underestimated. Comparisons with simulations where anthropogenic emissions are kept constant throughout the 10-year period show that the magnitude of the emission-driven trend exceeds the natural variability for primary compounds. Thus, we can conclude that emission management strategies have had a significant impact over the past 10 years, hence supporting further emission reductions.

4.4 Paper IV

Hodnebrog, Ø., Solberg, S., Stordal, F., Svendby, T. M., Simpson, D., Hilboll, A., Pfister, G. G., Turquety, S., Richter, A., Burrows, J. P., Denier van der Gon, H. A. C.: A model study of the Eastern Mediterranean ozone levels during the hot summer of 2007. *Submitted to Atmos. Chem. Phys., 2011.*

Processes leading to O_3 formation during the hot summer of 2007 in southeast Europe have been studied using two regional atmospheric chemistry models; WRF-Chem and EMEP MSC-W. Three heat waves and a number of forest fire episodes struck the region during this period, greatly affecting air pollution levels. Comparisons with satellite observations of CO and NO_2 columns show that the model simulations reflect the location and influence of the forest fires relatively well, but the modelled magnitude of CO in the plume core is too low. Most likely, this is caused by underestimation of CO in the emission inventories, suggesting that the CO/NO_X ratios of fire emissions should be re-assessed. Comparisons with surface O_3 measurements show fairly good agreement for both models. Biogenic VOC emissions reacting with anthropogenic NO_X emissions are calculated to contribute significantly to the levels of ozone in the region, but the magnitude and geographical distribution depend strongly on the model and biogenic emission module used. Ozone levels increased substantially during the July and August heat waves due to a combination of forest fire emissions and the effect of high temperatures. The largest temperature impact on ozone was through the temperature dependence of the biogenic emissions, closely followed by the effect of decreased dry deposition, while the impact of high temperatures on the ozone chemistry was much lower. Considering the projected increase in the number of heat wave episodes in a warmer climate, our results suggest that forest fire emissions, and the temperature effect on biogenic emissions and dry deposition, will potentially lead to substantial ozone increases in the future.

5 Main conclusions and future outlook

The four papers presented have dealt with modelling of tropospheric ozone on scales ranging from urban to global and addressed issues related to local air pollution and global climate change. The main conclusions are given below and have been sorted by the objectives stated in the introduction, in order to better show the interrelationship between the individual studies.

Increase knowledge on interactions between different spatial scales, from urban to global scales, focusing on megacity ozone formation.

One of the original goals of the thesis was to derive an effective emission parameterization, which would take into account subgrid-scale processes in megacity emission plumes, similar to what has been done for aircraft and ship emissions. However, we found out in Paper I that this task was much more complex than anticipated, and concluded that the development of a general parameterization of ozone chemistry following emissions from megacities may even be unnecessary. The large-scale changes in ozone fields due to increased megacity emission resolution were found to be relatively small. There are several reasons why megacity plume chemistry is more difficult and less important to parameterize than aircraft and ship plumes. First, the emissions from a megacity generally have lower ratios of NO_X to NMVOC and a much more heterogeneous spatial and temporal distribution compared to the emissions from the aircraft and ship sectors. Additionally, interaction with surrounding chemistry and meteorology is more complex for a megacity, especially due to its location in the continental boundary layer. In sum, the subgrid-scale effects of a megacity emission plume consist of several competing effects where some cancel each other out, and consequently the total contribution does not seem to have a major impact on a large scale. It should be noted, however, that these results are based on relatively short simulations of 3 megacity regions for the scales from 9 km to 81 km. The effects could be larger in other megacities, at other times and at other resolutions. Also, the effects of changing the resolution of the meteorology has not been tested and could give larger impacts.

The most striking result in Paper III, focusing on European rural and urban air pollution, is the consistency of model performance between regional and global CTMs.

Although the difference in resolution between the regional CTMs and the global Oslo CTM2 was approximately a factor of 5 in each horizontal direction, the performance in terms of daily mean NO_2 and O_3 comparisons (correlation, bias and root-mean-square error) was not significantly better for the higher resolution models. However, all models showed better scores when compared to rural background sites than for urban and suburban background sites. This is expected as even the regional CTMs used a quite coarse resolution (50 km × 50 km), and is also in line with the conclusion of Paper I, stating that high resolution is more important for local air quality studies than for climate studies.

The issue of scales was also briefly discussed in Paper IV, where the need for high temporal and spatial resolution of emission data in studies of regional air pollution was highlighted. A comparison between two forest fire emission inventories, differing largely in resolution, showed better agreement with satellite observations of tropospheric NO_2 columns for the simulation using the high temporal and spatial resolution emission inventory.

This thesis has not only dealt with the impact of small-scale processes on ozone from a climate perspective, but also the importance of taking into account large-scale processes when determining local air pollution. In this context, a one-way offline coupling has been made between the global Oslo CTM2 model and the regional WRF-Chem model. With this method, processes taking place outside the boundaries of the model domain, such as long-range transport of air pollutants, are taken into account in the WRF-Chem simulations. This one-way coupled system has been used successfully in Paper I and Paper IV.

Estimate how regional air pollution may respond to climate change by investigating extreme summer episodes.

Previous literature has strongly indicated that heat waves over Europe will occur more frequently in a future climate. These episodes often lead to high ozone levels and may have detrimental impacts on human health and vegetation. Thus, studies of recent heat wave episodes may include signs of what to expect in a future climate. WRF-Chem simulations of the heat wave episode in August 2003 were presented in Paper I, with a main focus on the UK. Observed surface O_3 values exceeded 100 ppb, mainly due to stable air, high temperatures and large amounts of incoming solar radiation triggering photochemistry. The

model underestimated the peak values, presumably because the dry deposition scheme does not include moisture-dependence, leading to overestimation of O_3 loss due to dry removal.

The importance of dry deposition for O_3 during high temperature episodes was studied in more detail in Paper IV. This study focused on the three heat waves and numerous forest fires that took place in the Eastern Mediterranean region during the summer of 2007. The model results showed a substantial increase in ozone due to emissions from forest fires, which are also likely to occur more frequently in a future climate. Ozone formation was further intensified by the high temperatures causing a reduction of dry deposition and an increase in biogenic VOC emissions. The latter effect was even more important near the large cities and ship tracks in the area, as the biogenic VOC emissions reacted with anthropogenic NO_X emissions leading to efficient O_3 production. The direct impact of high temperatures on the chemical reactions was on average surprisingly low, although there were large spatial differences. In sum, the temperature impacts on biogenic emissions and dry deposition, along with increased risk of forest fire emissions, need to be taken into account when assessing mitigation options for the future.

Quantify and understand how current ozone levels have responded to past emission changes, and estimate how the global ozone distribution may change in the future, mainly focusing on the rapidly growing transport sector.

Abatement strategies over the last decades have caused a reduction of O_3 precursor emissions in Europe. The results presented in Paper III show that the observed European trend of surface NO_2 concentrations for the past decade reflects the emission reductions, and that the regional and global CTMs are able to reproduce the observed decreasing trend relatively well. However, neither the observations nor the models show a clear decreasing trend in surface O_3 concentrations. Partly, this can be explained by the non-linear nature of ozone chemistry. If NO_X emissions are reduced more effectively than NMVOC emissions, this may result in ozone increases, particularly over urban areas. Additionally, simulations with constant emissions and varying meteorology show that the inter-annual meteorological variability influenced the ozone trend. This is also expected for a study comprising only 10 years, which is probably a lower limit for deriving trends of surface ozone.

Estimates of how emissions from aircraft and shipping may influence ozone distributions in the future have been presented in Paper II. The meteorological data were kept constant in order to only quantify the impacts of emission changes and not climate changes. Results from global CTMs show that the impacts on ozone will be larger in the future (2025 and 2050) compared to recent time (2000), even in the case of an optimistic scenario. Ship traffic emissions lead to strong ozone increases in the marine boundary layer, and may have significant impacts on European air pollution levels during northern hemisphere summer. From a climate perspective, O_3 precursor emissions from shipping are expected to continue to cool the atmosphere in the future, because the effect of reduced methane lifetime dominates the warming effect of O_3 increases. As the majority of aircraft emissions take place in the UTLS region, they have less influence on air pollution, but stronger impacts on climate through O_3 formation. Model results show that the warming effect from aviation-induced O_3 can be reduced substantially in the far future (2050) if technological NO_X improvements were to be applied. Another main conclusion is that expected changes in the spatial distribution of emissions from both aircraft and shipping will lead to more efficient O_3 enhancement in the far future. This is a result of non-linearity in ozone chemistry as future emissions of O_3 precursor emissions from these transport sectors are expected to shift further south, where the background pollution levels are lower.

Future outlook

Over the last few decades, substantial improvements have been made in the way we understand the processes governing tropospheric ozone, and in the development of atmospheric computer models. However, as has been shown in this thesis, the impacts of ozone on climate and environment are manifold, and similarly there is a large number of complex processes affecting ozone production and destruction. In order to properly take into account climate-chemistry interactions, further development of fully-coupled Earth system models is needed to make them more robust. Although these types of models can be used to study many of the issues related to climate change and air pollution, they can not replace all models dealing with atmospheric ozone, at least in the near future. For example, the scientific community will still need box models with a comprehensive set of chemical reactions to increase knowledge on small-scale chemistry, and backward trajectory or particle dispersion

models will still be useful to identify locations of emission sources. Nevertheless, the need for multiple models when studying a range of scales may decrease, keeping in mind that the computer capacity has undergone vast improvements and is expected to continue to improve in the future.

As a consequence of the expected increase in spatial and temporal model resolutions, the subject of scale inaccuracies will become less important, but not insignificant as non-linearities in meteorology and ozone chemistry occur also at very small scales. Until global models are able to represent these scales explicitly, there is still a need to parameterize subgrid scale processes, and such parameterizations induce new uncertainties. One way to reduce the uncertainties, or at least get a figure of how large the uncertainties are, is to increase the use of ensemble model simulations. Both the use of ensemble simulations for one model and the use of multi-model ensembles, will lead to less uncertainties and more robust results. This will be made more feasible in the future as the computer capacity increases. However, an important question will remain; how to find the best balance between complexity (e.g. number of processes to be considered) and resolution of a model, and the number of ensemble simulations to be performed.

When modelling tropospheric ozone, the input data are of critical importance, in particular the emission data which are subject to large uncertainties. As the model performance often is limited by the quality of the emission data, more emphasis should be put on the development of detailed emission parameterizations and inventories for present-day and future scenarios. With the advances in model resolution, higher resolution is also needed for the emission data in order to model air pollution more accurately. In particular, efforts should be made to improve our knowledge of the magnitude of biogenic emissions, which is a major source of uncertainty in tropospheric ozone modelling.

References

Ashmore, M. R.: Assessing the future global impacts of ozone on vegetation, Plant, Cell & Environment, 28 (8), 949-964, 10.1111/j.1365-3040.2005.01341.x, 2005.

Benjamin, M. T., Sudol, M., Vorsatz, D., and Winer, A. M.: A spatially and temporally resolved biogenic hydrocarbon emissions inventory for the California South Coast Air Basin, Atmospheric Environment, 31 (18), 3087-3100, 10.1016/s1352-2310(97)00014-9, 1997.

Berntsen, T. K., and Isaksen, I. S. A.: A global three-dimensional chemical transport model for the troposphere .1. Model description and CO and ozone results, J. Geophys. Res.-Atmos., 102 (D17), 21239-21280, 10.1029/97jd01140, 1997.

Bian, H. S., and Prather, M. J.: Fast-J2: Accurate simulation of stratospheric photolysis in global chemical models, J. Atmos. Chem., 41 (3), 281-296, 10.1023/a:1014980619462, 2002.

Cariolle, D., Caro, D., Paoli, R., Hauglustaine, D. A., Cuenot, B., Cozic, A., and Paugam, R.: Parameterization of plume chemistry into large-scale atmospheric models: Application to aircraft NOx emissions, J. Geophys. Res.-Atmos., 114, 21, D1930210.1029/2009jd011873, 2009.

Cofala, J., Amann, M., Klimont, Z., Kupiainen, K., and Hoglund-Isaksson, L.: Scenarios of global anthropogenic emissions of air pollutants and methane until 2030, Atmospheric Environment, 41 (38), 8486-8499, 10.1016/j.atmosenv.2007.07.010, 2007.

EEA: Air Pollution in Europe 1990–2004. EEA Report No2/2007, European Environment Agency: Copenhagen, 2007.

Emmons, L. K., Walters, S., Hess, P. G., Lamarque, J. F., Pfister, G. G., Fillmore, D., Granier, C., Guenther, A., Kinnison, D., Laepple, T., Orlando, J., Tie, X., Tyndall, G., Wiedinmyer, C., Baughcum, S. L., and Kloster, S.: Description and evaluation of the Model for Ozone and Related chemical Tracers, version 4 (MOZART-4), Geosci. Model Dev., 3 (1), 43-67, 10.5194/gmd-3-43-2010, 2010.

Founda, D., and Giannakopoulos, C.: The exceptionally hot summer of 2007 in Athens, Greece - A typical summer in the future climate?, Glob. Planet. Change, 67 (3-4), 227-236, 10.1016/j.gloplacha.2009.03.013, 2009.

Fowler, D., Amann, M., Anderson, R., Ashmore, M. R., Cox, P., Depledge, M., Derwent, D., Grennfelt, P., Hewitt, N., Hov, Ø., Jenkin, M. E., Kelly, F., Liss, P., Pilling, M. J., Pyle, J., Slingo, J., and Stevenson, D.: Ground-level ozone in the 21st century: future trends, impacts and policy implications. 15/08, The Royal Society, London, 2008.

Franke, K., Eyring, V., Sander, R., Hendricks, J., Lauer, A., and Sausen, R.: Toward effective emissions of ships in global models, Meteorol. Z., 17 (2), 117-129, 10.1127/0941-2948/2008/0277, 2008.

Fuglestvedt, J., Berntsen, T., Myhre, G., Rypdal, K., and Skeie, R. B.: Climate forcing from the transport sectors, Proc. Natl. Acad. Sci. U. S. A., 105 (2), 454-458, 10.1073/pnas.0702958104, 2008.

Granier, C., Lamarque, J. F., Mieville, A., Muller, J. F., Olivier, J., Orlando, J., Peters, J., Petron, G., Tyndall, G., and Wallens, S.: POET, a database of surface emissions of ozone precursors, available on internet at http://www.aero.jussieu.fr/projet/ACCENT/POET.php, 2005.

Grell, G. A., Peckham, S. E., Schmitz, R., McKeen, S. A., Frost, G., Skamarock, W. C., and Eder, B.: Fully coupled "online" chemistry within the WRF model, Atmospheric Environment, 39 (37), 6957-6975, 2005.

Guenther, A., Karl, T., Harley, P., Wiedinmyer, C., Palmer, P. I., and Geron, C.: Estimates of global terrestrial isoprene emissions using MEGAN (Model of Emissions of Gases and Aerosols from Nature), Atmospheric Chemistry and Physics, 6, 3181-3210, 2006.

Hansen, J., Sato, M., and Ruedy, R.: Radiative forcing and climate response, J. Geophys. Res.-Atmos., 102 (D6), 6831-6864, 1997.

Hesstvedt, E., Hov, O., and Isaksen, I. S. A.: Quasi-steady-state approximations in air pollution modeling - Comparison of two numerical schemes for oxidant prediction, Int. J. Chem. Kinet., 10 (9), 971-994, 1978.

Holland, M., Kinghorn, S., Emberson, L., Cinderby, S., Ashmore, M., Mills, G., and Harmens, H.: Development of a framework for probabilistic assessment of the economic losses caused by ozone damage to crops in Europe, NERC/Centre for Ecology and Hydrology, 50 pp., 2006.

Holtslag, A. A. M., Debruijn, E. I. F., and Pan, H. L.: A High Resolution Air Mass Transformation Model for Short-Range Weather Forecasting, Mon. Weather Rev., 118 (8), 1561-1575, 10.1175/1520-0493(1990)118<1561:ahramt>2.0.co;2, 1990.

Hoor, P., Borken-Kleefeld, J., Caro, D., Dessens, O., Endresen, O., Gauss, M., Grewe, V., Hauglustaine, D., Isaksen, I. S. A., Jöckel, P., Lelieveld, J., Myhre, G., Meijer, E., Olivie, D., Prather, M., Schnadt Poberaj, C., Shine, K. P., Staehelin, J., Tang, Q., van Aardenne, J., van Velthoven, P., and Sausen, R.: The impact of traffic emissions on atmospheric ozone and OH: results from QUANTIFY, Atmos. Chem. Phys., 9 (9), 3113-3136, 2009.

Huszar, P., Cariolle, D., Paoli, R., Halenka, T., Belda, M., Schlager, H., Miksovsky, J., and Pisoft, P.: Modeling the regional impact of ship emissions on NOx and ozone levels over the Eastern Atlantic and Western Europe using ship plume parameterization, Atmos. Chem. Phys., 10 (14), 6645-6660, 10.5194/acp-10-6645-2010, 2010.

IPCC: Climate Change 2007: The Physical Science Basis. Contribution of Working Group I to the Fourth Assessment Report of the Intergovernmental Panel on Climate Change, Cambridge University Press, Cambridge, United Kingdom and New York, NY, USA., 2007.

Isaksen, I. S. A., Granier, C., Myhre, G., Berntsen, T. K., Dalsoren, S. B., Gauss, M., Klimont, Z., Benestad, R., Bousquet, P., Collins, W., Cox, T., Eyring, V., Fowler, D., Fuzzi, S., Jockel, P., Laj, P., Lohmann, U., Maione, M., Monks, P., Prevot, A. S. H., Raes, F., Richter, A., Rognerud, B., Schulz, M., Shindell, D., Stevenson, D. S., Storelvmo, T., Wang, W. C., van Weele, M., Wild, M., and Wuebbles, D.: Atmospheric composition change: Climate-Chemistry interactions, Atmospheric Environment, 43 (33), 5138-5192, 10.1016/j.atmosenv.2009.08.003, 2009.

Jacob, D.: Introduction to Atmospheric Chemistry, Princeton University Press, 1999.

Jacob, D. J., and Winner, D. A.: Effect of climate change on air quality, Atmospheric Environment, 43 (1), 51-63, 10.1016/j.atmosenv.2008.09.051, 2009.

Janjic, Z. I.: Nonsingular Implementation of the Mellor-Yamada Level 2.5 Scheme in the NCEP Meso model, NCEP Office Note(No. 437), 61, 2002.

Jöckel, P., Tost, H., Pozzer, A., Bruhl, C., Buchholz, J., Ganzeveld, L., Hoor, P., Kerkweg, A., Lawrence, M. G., Sander, R., Steil, B., Stiller, G., Tanarhte, M., Taraborrelli, D., Van Aardenne, J., and Lelieveld, J.: The atmospheric chemistry general circulation model ECHAM5/MESSy1: consistent simulation of ozone from the surface to the mesosphere, Atmos. Chem. Phys., 6, 5067-5104, 2006.

Kasibhatla, P., Levy, H., Moxim, W. J., Pandis, S. N., Corbett, J. J., Peterson, M. C., Honrath, R. E., Frost, G. J., Knapp, K., Parrish, D. D., and Ryerson, T. B.: Do emissions from ships have a significant impact on concentrations of nitrogen oxides in the marine boundary layer?, Geophys. Res. Lett., 27 (15), 2229-2232, 2000.

Kraabøl, A. G., Berntsen, T. K., Sundet, J. K., and Stordal, F.: Impacts of NOx emissions from subsonic aircraft in a global three-dimensional chemistry transport model including plume processes, J. Geophys. Res.-Atmos., 107 (D22), 4655, 10.1029/2001jd001019, 2002.

Madronich, S.: Photodissociation in the atmosphere .1. Actinic flux and the effects of ground reflections and clouds, J. Geophys. Res.-Atmos., 92 (D8), 9740-9752, 1987.

Meijer, E. W., vanVelthoven, P. F. J., Wauben, W. M. F., Beck, J. P., and Velders, G. J. M.: The effects of the conversion of nitrogen oxides in aircraft exhaust plumes in global models, Geophys. Res. Lett., 24 (23), 3013-3016, 1997.

Molina, M. J., and Rowland, F. S.: Stratospheric Sink for Chlorofluoromethanes - Chlorine Atomic-Catalysed Destruction of Ozone, Nature, 249 (5460), 810-812, 10.1038/249810a0, 1974.

Myhre, G., Shine, K. P., Rädel, G., Gauss, M., Isaksen, I. S. A., Tang, Q., Prather, M. J., Williams, J. E., van Velthoven, P., Dessens, O., Koffi, B., Szopa, S., Hoor, P., Grewe, V., Borken-Kleefeld, J., Berntsen, T. K., and Fuglestvedt, J. S.: Radiative forcing due to changes in ozone and methane caused by the transport sector, Atmospheric Environment, 45 (2), 387-394, 10.1016/j.atmosenv.2010.10.001, 2011.

NAEI: National Atmospheric Emissions Inventory. http://www.naei.co.uk, 2007.

Poppe, D., Wallasch, M., and Zimmermann, J.: The Dependence of the Concentration of OH on its Precursors under Moderately Polluted Conditions - A Model Study, J. Atmos. Chem., 16 (1), 61-78, 1993.

Prather, M. J.: Numerical advection by conservation of 2nd-order moments, J. Geophys. Res.-Atmos., 91 (D6), 6671-6681, 1986.

Pyle, J. A., Warwick, N., Yang, X., Young, P. J., and Zeng, G.: Climate/chemistry feedbacks and biogenic emissions, Philos. Trans. R. Soc. A-Math. Phys. Eng. Sci., 365 (1856), 1727-1740, 10.1098/rsta.2007.2041, 2007.

Ramanathan, V., Callis, L., Cess, R., Hansen, J., Isaksen, I., Kuhn, W., Lacis, A., Luther, F., Mahlman, J., Reck, R., and Schlesinger, M.: Climate-Chemical Interactions and Effects of

Changing Atmospheric Trace Gases, Rev. Geophys., 25 (7), 1441-1482, 10.1029/RG025i007p01441, 1987.

RETRO: REanalysis of the TROpospheric chemical composition over the past 40 years. http://retro.enes.org, 2006.

Richter, A., Burrows, J. P., Nuss, H., Granier, C., and Niemeier, U.: Increase in tropospheric nitrogen dioxide over China observed from space, Nature, 437 (7055), 129-132, 10.1038/nature04092, 2005.

Schär, C., Vidale, P. L., Luthi, D., Frei, C., Haberli, C., Liniger, M. A., and Appenzeller, C.: The role of increasing temperature variability in European summer heatwaves, Nature, 427 (6972), 332-336, 10.1038/nature02300, 2004.

Simpson, D., Winiwarter, W., Borjesson, G., Cinderby, S., Ferreiro, A., Guenther, A., Hewitt, C. N., Janson, R., Khalil, M. A. K., Owen, S., Pierce, T. E., Puxbaum, H., Shearer, M., Skiba, U., Steinbrecher, R., Tarrason, L., and Oquist, M. G.: Inventorying emissions from nature in Europe, J. Geophys. Res.-Atmos., 104 (D7), 8113-8152, 1999.

Sitch, S., Cox, P. M., Collins, W. J., and Huntingford, C.: Indirect radiative forcing of climate change through ozone effects on the land-carbon sink, Nature, 448 (7155), 791-U794, 10.1038/nature06059, 2007.

Skamarock, W. C., and Klemp, J. B.: A time-split nonhydrostatic atmospheric model for weather research and forecasting applications, J. Comput. Phys., 227 (7), 3465-3485, 10.1016/j.jcp.2007.01.037, 2008.

Solberg, S., Derwent, R. G., Hov, O., Langner, J., and Lindskog, A.: European abatement of surface ozone in a global perspective, Ambio, 34 (1), 47-53, 2005.

Søvde, O. A., Gauss, M., Smyshlyaev, S. P., and Isaksen, I. S. A.: Evaluation of the chemical transport model Oslo CTM2 with focus on arctic winter ozone depletion, J. Geophys. Res.-Atmos., 113 (D09304), 10.1029/2007jd009240, 2008.

Stedman, J. R.: The predicted number of air pollution related deaths in the UK during the August 2003 heatwave, Atmospheric Environment, 38 (8), 1087-1090, 10.1016/j.atmosenv.2003.11.011, 2004.

Stevenson, D. S., Dentener, F. J., Schultz, M. G., Ellingsen, K., van Noije, T. P. C., Wild, O., Zeng, G., Amann, M., Atherton, C. S., Bell, N., Bergmann, D. J., Bey, I., Butler, T., Cofala, J., Collins, W. J., Derwent, R. G., Doherty, R. M., Drevet, J., Eskes, H. J., Fiore, A. M., Gauss, M., Hauglustaine, D. A., Horowitz, L. W., Isaksen, I. S. A., Krol, M. C., Lamarque, J. F., Lawrence, M. G., Montanaro, V., Muller, J. F., Pitari, G., Prather, M. J., Pyle, J. A., Rast, S., Rodriguez, J. M., Sanderson, M. G., Savage, N. H., Shindell, D. T., Strahan, S. E., Sudo, K., and Szopa, S.: Multimodel ensemble simulations of present-day and near-future tropospheric ozone, J. Geophys. Res.-Atmos., 111 (D08301), 10.1029/2005jd006338, 2006.

Stockwell, W. R., Middleton, P., Chang, J. S., and Tang, X. Y.: The 2nd generation regional acid deposition model chemical mechanism for regional air-quality modeling, J. Geophys. Res.-Atmos., 95 (D10), 16343-16367, 1990.

Symeonidis, P., Poupkou, A., Gkantou, A., Melas, D., Yay, O. D., Pouspourika, E., and Balis, D.: Development of a computational system for estimating biogenic NMVOCs emissions

based on GIS technology, Atmospheric Environment, 42 (8), 1777-1789, 10.1016/j.atmosenv.2007.11.019, 2008.

Tiedtke, M.: A comprehensive mass flux scheme for cumulus parameterization in large-scale models, Mon. Weather Rev., 117 (8), 1779-1800, 1989.

Uherek, E., Halenka, T., Borken-Kleefeld, J., Balkanski, Y., Berntsen, T., Borrego, C., Gauss, M., Hoor, P., Juda-Rezler, K., Lelieveld, J., Melas, D., Rypdal, K., and Schmid, S.: Transport impacts on atmosphere and climate: Land transport, Atmospheric Environment, 44 (37), 4772-4816, 10.1016/j.atmosenv.2010.01.002, 2010.

UN: As global population nears 7 billion, UN capitalizes on new opportunities, United Nations News Centre, www.un.org/news/, Accessed on October 18, 2011.

UNECE: Review of the 1999 Gothenburg Protocol, Report by the Secretariat. UNECE Executive Body for the Convention on Long-Range Transboundary Air Pollution. ECE/EB.AIR/2007/10, 2007.

UNFPA: State of world population 2007, United Nations Population Fund, New York, 2007.

Unger, N., Shindell, D. T., Koch, D. M., and Streets, D. G.: Air pollution radiative forcing from specific emissions sectors at 2030, J. Geophys. Res., 113 (D2), D02306, 10.1029/2007jd008683, 2008.

van der Werf, G. R., Randerson, J. T., Giglio, L., Collatz, G. J., Kasibhatla, P. S., and Arellano, A. F.: Interannual variability in global biomass burning emissions from 1997 to 2004, Atmos. Chem. Phys., 6, 3423-3441, 2006.

Vautard, R., Honore, C., Beekmann, M., and Rouil, L.: Simulation of ozone during the August 2003 heat wave and emission control scenarios, Atmospheric Environment, 39 (16), 2957-2967, 10.1016/j.atmosenv.2005.01.039, 2005.

Wesely, M. L.: Parameterization of surface resistances to gaseous dry deposition in regional-scale numerical-models, Atmospheric Environment, 23 (6), 1293-1304, 1989.

WHO: Air quality guidelines: global update 2005, particulate matter, ozone, nitrogen dioxide and sulphur dioxide, WHO Regional Office for Europe: Copenhagen, 2006.

Wicker, L. J., and Skamarock, W. C.: Time-splitting methods for elastic models using forward time schemes, Mon. Weather Rev., 130 (8), 2088-2097, 10.1175/1520-0493(2002)130<2088:tsmfem>2.0.co;2, 2002.

Wild, O., Zhu, X., and Prather, M. J.: Fast-j: Accurate simulation of in- and below-cloud photolysis in tropospheric chemical models, J. Atmos. Chem., 37 (3), 245-282, 2000.

WMO: Scientific Assessment of Ozone Depletion: 2010, Global Ozone Research and Monitoring Project - Report No. 50, 572 pp., Geneva, Switzerland, 2010.

Ziemke, J. R., Chandra, S., Duncan, B. N., Froidevaux, L., Bhartia, P. K., Levelt, P. F., and Waters, J. W.: Tropospheric ozone determined from aura OMI and MLS: Evaluation of measurements and comparison with the Global Modeling Initiative's Chemical Transport Model, J. Geophys. Res.-Atmos., 111 (D19), D19303 10.1029/2006jd007089, 2006.

I

II

Atmos. Chem. Phys., 11, 11293–11317, 2011
www.atmos-chem-phys.net/11/11293/2011/
doi:10.5194/acp-11-11293-2011

Atmospheric Chemistry and Physics

Future impact of non-land based traffic emissions on atmospheric ozone and OH – an optimistic scenario and a possible mitigation strategy

Ø. Hodnebrog[1,*], T. K. Berntsen[1], O. Dessens[2,], M. Gauss[1,3], V. Grewe[4], I. S. A. Isaksen[1], B. Koffi[5], G. Myhre[6], D. Olivié[7,***], M. J. Prather[8], J. A. Pyle[2], F. Stordal[1], S. Szopa[5], Q. Tang[8], P. van Velthoven[9], J. E. Williams[9], and K. Ødemark[1]**

[1]Department of Geosciences, University of Oslo, Norway
[2]Centre for Atmospheric Science, Department of Chemistry, Cambridge, UK
[3]Norwegian Meteorological Institute, Oslo, Norway
[4]Deutsches Zentrum für Luft- und Raumfahrt, Institut für Physik der Atmosphäre, Oberpfaffenhofen, Germany
[5]Laboratoire des Sciences du Climat et de l'Environment (LSCE-IPSL), Gif-sur-Yvette, France
[6]Center for International Climate and Environmental Research-Oslo (CICERO), Oslo, Norway
[7]Centre National de Recherches Météorologiques GAME/CNRM (Météo-France, CNRS), Toulouse, France
[8]Department of Earth System Science, University of California, Irvine, USA
[9]Royal Netherlands Meteorological Institute, KNMI, De Bilt, The Netherlands
[*]now at: CICERO, Oslo, Norway
[**]now at: UCL Energy Institute, University College London, London, UK
[***]now at: Department of Geosciences, University of Oslo, Norway and CICERO, Oslo, Norway

Received: 20 April 2011 – Published in Atmos. Chem. Phys. Discuss.: 16 June 2011
Revised: 24 September 2011 – Accepted: 31 October 2011 – Published: 14 November 2011

Abstract. The impact of future emissions from aviation and shipping on the atmospheric chemical composition has been estimated using an ensemble of six different atmospheric chemistry models. This study considers an optimistic emission scenario (B1) taking into account e.g. rapid introduction of clean and resource-efficient technologies, and a mitigation option for the aircraft sector (B1 ACARE), assuming further technological improvements. Results from sensitivity simulations, where emissions from each of the transport sectors were reduced by 5 %, show that emissions from both aircraft and shipping will have a larger impact on atmospheric ozone and OH in near future (2025; B1) and for longer time horizons (2050; B1) compared to recent time (2000). However, the ozone and OH impact from aircraft can be reduced substantially in 2050 if the technological improvements considered in the B1 ACARE will be achieved.

Shipping emissions have the largest impact in the marine boundary layer and their ozone contribution may exceed 4 ppbv (when scaling the response of the 5 % emission perturbation to 100 % by applying a factor 20) over the North Atlantic Ocean in the future (2050; B1) during northern summer (July). In the zonal mean, ship-induced ozone relative to the background levels may exceed 12 % near the surface. Corresponding numbers for OH are 6.0×10^5 molecules cm^{-3} and 30 %, respectively. This large impact on OH from shipping leads to a relative methane lifetime reduction of 3.92 (±0.48) % on the global average in 2050 B1 (ensemble mean CH_4 lifetime is 8.0 (±1.0) yr), compared to 3.68 (±0.47) % in 2000.

Aircraft emissions have about 4 times higher ozone enhancement efficiency (ozone molecules enhanced relative to NO_x molecules emitted) than shipping emissions, and the maximum impact is found in the UTLS region. Zonal mean aircraft-induced ozone could reach up to 5 ppbv at northern mid- and high latitudes during future summer (July 2050; B1), while the relative impact peaks during northern winter (January) with a contribution of 4.2 %. Although the aviation-induced impact on OH is lower than for shipping, it still causes a reduction in the relative methane lifetime of 1.68 (±0.38) % in 2050 B1. However, for B1 ACARE the perturbation is reduced to 1.17 (±0.28) %, which is lower than the year 2000 estimate of 1.30 (±0.30) %.

Based on the fully scaled perturbations we calculate net radiative forcings from the six models taking into account

Correspondence to: Ø. Hodnebrog
(oivind.hodnebrog@geo.uio.no)

ozone, methane (including stratospheric water vapour), and methane-induced ozone changes. For the B1 scenario, shipping leads to a net cooling with radiative forcings of −28.0 (±5.1) and −30.8 (±4.8) mW m^{-2} in 2025 and 2050, respectively, due to the large impact on OH and, thereby, methane lifetime reductions. Corresponding values for the aviation sector shows a net warming effect with 3.8 (±6.1) and 1.9 (±6.3) mW m^{-2}, respectively, but with a small net cooling of -0.6 (±4.6) mW m^{-2} for B1 ACARE in 2050.

1 Introduction

Increasing population and economic turnover will lead to increasing transport demand notably for aviation (AIR) and maritime shipping (SHIP). This will outpace technological improvements and lead to increasing emissions of various air pollutants, affecting air quality and climate through a complex system of chemical reactions and aerosol interactions. From a climate perspective, the present (2000) impact on radiative forcing (RF) is positive for AIR and negative for SHIP (Fuglestvedt et al., 2008; Balkanski et al., 2010), mostly due to formation of contrail cirrus in the first and sulphate in the latter. A first estimate of aircraft-induced cloudiness based on a climate model study was just recently given (Burkhardt and Karcher, 2011), however, the magnitude of positive RF from contrail cirrus is under debate (Lee et al., 2010). Substantial contributions also stem from the emissions of nitrogen oxides (NO_x), carbon monoxide (CO) and non-methane hydrocarbons (NMHCs). These relatively short-lived gases change the oxidative state of the atmosphere and tend to give a positive radiative forcing through the increase in ozone (e.g. Ramanathan and Dickinson, 1979; Berntsen et al., 1997), while enhanced OH levels are known to reduce the lifetime of methane (CH_4) and thereby cause negative RF (e.g. Crutzen, 1987; Shindell et al., 2005). Among the various transport sectors, previous studies have shown that the warming effect is most efficient (relative to the number of NO_x molecules emitted) for AIR (e.g. Fuglestvedt et al., 2008) because changes in ozone have their largest impact on climate when they occur in the UTLS (upper troposphere/lower stratosphere) region, due to the low temperatures found near the tropopause (Wang and Sze, 1980; Lacis et al., 1990; Hansen et al., 1997). On the other hand, the cooling effect caused by changes in methane lifetimes dominates the SHIP impact (e.g. Myhre et al., 2011) because of the large amounts of NO_x emitted into the clean maritime boundary layer. Due to the different effects on the atmospheric composition, it is important to study the AIR and SHIP sectors individually, especially when it comes to initiating mitigation measures. Another important aspect regarding non-land based traffic emissions, as opposed to land based traffic emissions, is the fact that the background conditions are usually relatively clean and this is known to increase the enhancement efficiencies of ozone and OH (e.g. Hoor et al., 2009).

IPCC (1999) published an assessment of the impact of aviation on climate, which was later updated by Sausen et al. (2005), and recently by Lee et al. (2009). Several other studies have also investigated how aircraft NO_x emissions alter the chemical composition of the atmosphere (e.g. Hidalgo and Crutzen, 1977; Johnson et al., 1992; Brasseur et al., 1996; Schumann, 1997; Grewe et al., 1999, 2007; Schumann et al., 2000; Kraabøl et al., 2002; Stevenson et al., 2004; Gauss et al., 2006; Søvde et al., 2007). The studies dealing with impact from future subsonic aircraft NO_x emissions project an increase in aircraft-induced ozone in 2050 compared to the present day atmosphere, but the effect depends on the emission scenario used. Søvde et al. (2007) estimated a maximum zonal mean aircraft-induced ozone increase of about 10 ppbv in the UTLS region for 2050 (annual mean) (aircraft NO_x emissions of 2.18 TgN yr^{-1}). In another study, Grewe et al. (1999) calculated 7 to 10 % increased ozone mixing ratios due to aviation for the same year and region, but for two different emission scenarios (aircraft NO_x emissions of 2.15 and 3.42 TgN yr^{-1}, respectively).

Among the studies on impacts from ship emissions (e.g. Lawrence and Crutzen, 1999; Corbett and Koehler, 2003; Endresen et al., 2003, 2007; Eyring et al., 2005, 2007; Dalsøren and Isaksen, 2006; Dalsøren et al., 2009, 2010), only one has made future projections with atmospheric chemistry models (Eyring et al., 2007). They estimate maximum near-surface ozone contributions from shipping of 5–6 ppbv (annual mean) in the North Atlantic for the year 2000, increasing to 8 ppbv in one of the 2030 scenarios (ship NO_x emissions of 3.10 and 5.95 TgN yr^{-1}, respectively). In a second 2030 scenario the ship emissions were assumed to stabilize at 2000 levels, but the higher background NO_x levels caused a slight decrease in the ozone impact from shipping.

The present study is performed within the EU project QUANTIFY (Quantifying the Climate Impact of Global and European Transport Systems), which was the first attempt of investigating the global scale impact on the atmospheric composition due to emissions from each of the transport sectors. Fuglestvedt et al. (2008) investigated the climate forcing from the transport sectors for year 2000, and later Skeie et al. (2009) estimated transport-induced RF for future scenarios. A multi-model study of the year 2000 impact of transport emissions on the atmospheric chemical composition was performed by Hoor et al. (2009) using the preliminary QUANTIFY emissions. They found a maximum ozone increase from aircraft of 3.69 ppbv in the upper troposphere between 30 and 60° N, and they also found that shipping emissions contributed the most to ozone perturbations in the lower troposphere with around 50 % of the total traffic induced perturbation. The RF results from Hoor et al. (2009) were recently updated by Myhre et al. (2011) who used the final version of the QUANTIFY emissions data to estimate the year 2000 impact. The future impacts of both the

Table 1. Global annual emissions of NO_x, CO and NMHC provided by QUANTIFY (http://www.ip-quantify.eu) for the years 2000, 2025 and 2050 in the B1 scenario. The 2000 emissions are from the final QUANTIFY dataset and thereby differ from the preliminary emissions used in Hoor et al. (2009).

	NO_x emissions in Tg(N)			CO emissions in Tg(C)			NMHC emissions in Tg(C)		
Source	2000	2025B1	2050B1	2000	2025B1	2050B1	2000	2025B1	2050B1
Aircraft	0.85	1.18/1.13*	1.04/0.79*	–	–	–	–	–	–
Ship	4.56	4.93	5.05	0.6	1.0	1.5	0.36	0.51	0.63
Road	8.89	3.29	0.52	47.2	14.8	1.7	11.37	2.74	0.53
Non-traffic	28.9	30.8	31.4	365.3	220.5	196.5	108.1	108.4	109.0
Biogenic, soil	6.89	6.89	6.89	48.2	48.2	48.2	340.5	340.5	340.5

* B1 ACARE aircraft emissions.

emissions and climate changes on transport-induced ozone have so far only been studied by Koffi et al. (2010), using the climate-chemistry model LMDz-INCA (also used in this study). Cariolle et al. (2009) investigated the effect of including an aircraft plume parameterization in large-scale atmospheric models, and similarly the inclusion of a ship plume parameterization was studied by Huszar et al. (2010). Both studies suggested significant reductions in non-land based traffic-induced ozone when plume processes were taken into account. Main results obtained in QUANTIFY are summarized in Lee et al. (2010) (aviation), Eyring et al. (2010) (shipping), and Uherek et al. (2010) (land transport).

The objective of this study is to investigate how emissions from the non-land based traffic sectors (AIR and SHIP) impact atmospheric ozone, OH, and the resulting RF, if precursor emissions from all sectors show reductions due to environmental concerns leading to improved technology. The effects of possible future high emission scenarios will be dealt with in a follow-up study, using the same set of atmospheric chemistry models. The scenarios selected for this purpose are the SRES (Special Report on Emission Scenarios) optimistic B1 and pessimistic A1B (Nakicenovic et al., 2000), respectively, whereas results from the first are presented in this study. As the B1 scenario is considered to be far more optimistic than the A1B scenario (both for transport and non-transport emissions), due to assumptions of e.g. rapid introduction of clean and resource-efficient technologies in the first, the combined results represent possible low or high developments, respectively, of the transport-induced impact on the atmospheric chemical composition, taking into account uncertainties related to the evolution of e.g. economy and technology. More specifically, the B1 scenario is characterized by environmental concerns leading to improved NO_x technology and a relatively smooth transition to alternative energy systems, but without assumptions of climate policies (in accordance with the SRES terms of reference) (Nakicenovic et al., 2000). We have also studied the effect of utilizing additional technological improvements to the aircraft through the B1 ACARE mitigation option (Owen et al., 2010). The fuel efficiency improvements in B1 ACARE probably require the technology to be driven by concerns over climate change and is thus considered a mitigation scenario. In the following we describe the simulation setup and the emission scenarios (Sect. 2), before giving a short presentation of each of the models in the ensemble (Sect. 3). The impacts on ozone and OH are dealt with in Sects. 4 and 5, respectively, while global radiative forcing calculations are presented in Sect. 6. Finally, our conclusions are given in Sect. 7.

2 Emissions and simulation setup

Traffic emissions of the ozone precursors NO_x, CO and NMHC have been developed for year 2000 and for future scenarios through QUANTIFY (data can be downloaded from www.ip-quantify.eu). Anthropogenic emissions from non-traffic sources were taken from the EDGAR3.2-FT2000 inventory (Olivier et al., 2005; van Aardenne et al., 2005) for year 2000, while the future non-traffic emissions evolve according to the IPCC (Intergovernmental Panel on Climate Change) SRES (Nakicenovic et al., 2000) B1 scenario. Table 1 lists the global annual emissions used in this study, and Fig. 1 shows the time development of NO_x emissions from different transport sectors and for several scenarios. Although the future increase in the global NO_x emissions from AIR and SHIP is relatively small for the B1 scenario, important changes in the regional distribution of emissions can be seen for these transport sectors (Figs. 2–4).

New aircraft emissions scenarios have been developed using the FAST model and are described in Owen et al. (2010). B1 ACARE is a mitigation scenario for aviation and contains additional emission reductions on top of the reductions that are assumed in the B1 scenario. B1 ACARE can be seen as a very optimistic, but feasible, scenario due to concern over climate change. The traffic demand is the same in both scenarios, but excellent fuel efficiency and NO_x improvements are assumed in the mitigation scenario, in accordance with the targets set by the Advisory Council for

Aeronautical Research in Europe (ACARE, 2002). Consequently, the B1 ACARE scenario has 4 and 24 % lower aircraft NO_x emissions than B1 in 2025 and 2050, respectively, and the emissions for 2050 are even lower than the year 2000 estimate. Figure 2 shows that the increase in Europe and Asia in 2025 is smaller for B1 ACARE compared to the B1 scenario, and the emission reductions over the US are stronger in the first scenario. When comparing 2050 with 2025, only a few flight routes have increased emissions in B1 ACARE, and major emission reductions can be seen in Europe, the US, and Japan. The dependency of aircraft NO_x emissions on different latitude intervals can be seen in Fig. 4.

Shipping emissions are based on Endresen et al. (2007) (year 2000) and Eide et al. (2007) (years 2025 and 2050), and are characterized by increased NO_x emissions in the future, even for the optimistic B1 scenario. Already in 2025 the shipping sector could have become the largest emitter of NO_x among the three transport sectors (Fig. 1). Most of the increase for the B1 scenario is distributed among 12 new shipping routes (Fig. 3) that are predicted by Eide et al. (2007). It is worth noting the Northern Sea Route which has increasing emissions from 2000 to 2025, and then shows a slight decline from 2025 to 2050.

Emissions from road transport are based on Borken et al. (2007). Future emissions are documented in Uherek et al. (2010). While road traffic was the dominating source of NO_x emissions among the transport sectors in 2000, assumptions of stricter vehicle emission standards and improvements in technology will lead to a substantial decrease of NO_x emissions in the future scenarios (Fig. 1), particularly for B1. Technology with low NO_x emissions is already available for the road sector, and is faster to implement than for aircraft and shipping as the lifetime of vehicles is shorter. Koffi et al. (2010) showed that the rapid decline in NO_x emissions from road transport will lead to a drastic decrease in the ozone impact of road emissions in 2050. For this reason the impact of road traffic on ozone and OH has not been dealt with in this study, but model results from a policy failure scenario (A1B HIGH) for the road transport sector are subject of a follow-up study.

Additional emissions used in this study include biogenic emissions of isoprene and NO from soils (Jöckel et al., 2006), lightning NO_x emissions specified at 5 TgN yr^{-1} (Schumann and Huntrieser, 2007), and biomass burning emissions based on monthly mean Global Fire Emissions Database (GFED) estimates for 2000 (van der Werf et al., 2006) with multi-year (1997–2002) averaged activity data using emission factors from Andreae and Merlet (2001). The biogenic and soil emissions are fixed using the climatology described in Hoor et al. (2009).

Regarding methane, all models used prescribed surface boundary conditions with global CH_4 abundances taken from IPCC (2001), but with a hemispheric scaling such that the mixing ratios were approximately 5 % higher in the Northern than the Southern Hemisphere. Two of the models (p-TOMCAT and MOCAGE) used the IPCC (2001) value for 2000 (1760 ppbv) in all simulations, while the other four models (TM4, OsloCTM2, LMDz-INCA and UCI CTM) updated to the 2025B1 and 2050B1 values (1909 and 1881 ppbv, respectively) in the future simulations. The effect of using 2000 rather than 2025B1 surface methane in the future 2025B1 simulations has been investigated with the OsloCTM2 model and found to have a small impact (up to 1–2 %) on aircraft- and ship-induced relative methane lifetime changes, and on global distributions of ozone and OH perturbations.

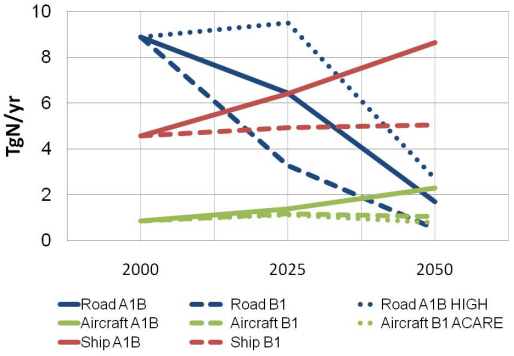

Fig. 1. Time development of NO_x emissions from different transport sectors in the SRES A1B and B1 scenarios, together with the alternative scenarios B1 ACARE and A1B HIGH (unit: TgN yr^{-1}).

The global models included in the ensemble have been run with year 2000 emissions and with the future emission scenarios B1 and B1 ACARE for the years 2025 and 2050. For the year 2000 and for the future B1 simulations, a reference run (BASE) and perturbation runs, one for aircraft (AIR) and one for ship (SHIP), have been performed by each model for each year. For the future B1 ACARE simulations, new reference runs and new aircraft perturbation runs were required in order to study the atmospheric chemistry impact of aircraft emissions under this scenario. In the perturbation simulations, a 5 % reduction has been applied to all emitted species of the respective traffic sector. The reasons not to switch off the emissions in the various transport sectors completely are both to reduce non-linearities in chemistry, and because the unscaled response (i.e. impacts due to 5 % emission perturbation) of the chemical system is expected to be closer to the effect of realistic emission changes than a total removal of the emissions (Hoor et al., 2009). The 5 % reduction approach was used to derive the sensitivity of the atmospheric chemical composition, e.g. ozone concentration, to an emission category with an appropriate accuracy (Hoor et al., 2009). The effect of, e.g. road traffic emissions is obtained by multiplying this sensitivity, e.g. change in ozone concentration per kg emission from road traffic, with the total road traffic

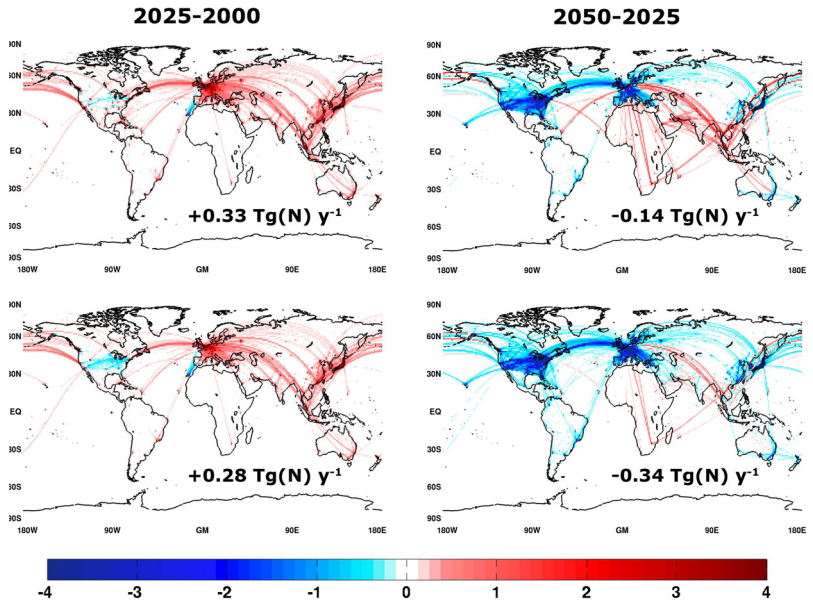

Fig. 2. Spatial distribution of the absolute difference in NO_x emission flux from aircraft for the B1 (top) and B1 ACARE (bottom) scenarios (unit: 10^{13} Δmolecules NO_2 m^{-2} s^{-1}) used in QUANTIFY.

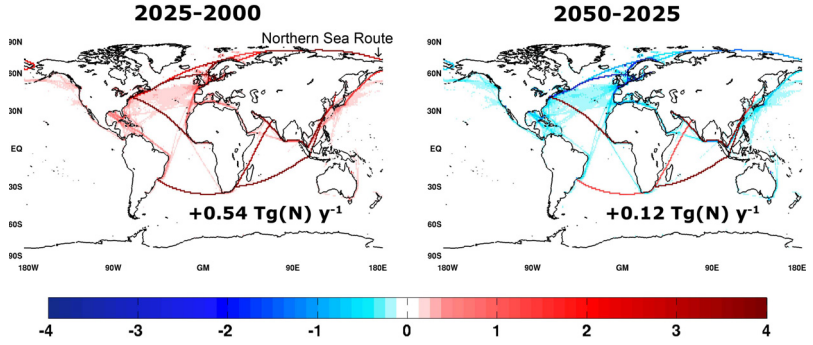

Fig. 3. Spatial distribution of the absolute difference in NO_x emission flux from shipping for the B1 scenario (unit: 10^{13} Δmolecules NO_2 m^{-2} s^{-1}) used in QUANTIFY.

emissions. When comparing results from this study with other studies, it is important to note that the 5 % perturbation approach is very different from removing an emission source by 100 %. Non-linearities in chemistry can lead to large differences between the two approaches as described in Hoor et al. (2009) and Koffi et al. (2010). For further discussions on the small perturbation approach, the reader is referred to Grewe et al. (2010) who state that the method of perturbing an emission source by a small amount (e.g. 5 %), in order to derive its sensitivity, is well suited to address impacts of e.g. future emission policies. In order to simplify the comparison with Hoor et al. (2009) and Myhre et al. (2011), the ozone and OH results (Sects. 4 and 5.1) are shown unscaled (i.e. the direct difference between BASE-AIR and BASE-SHIP), while calculations of methane lifetime changes and radiative forcings (Sects. 5.2 and 6) have been scaled to 100 % by multiplying the impacts caused by the 5 % emission perturbation with 20 (i.e. 20 × (BASE-AIR) and 20 × (BASE-SHIP)).

Table 2. Specifications of the participating models in this study (modified from Hoor et al., 2009).

Model	TM4	p-TOMCAT	OsloCTM2	LMDz-INCA	UCI CTM	MOCAGE
Operated	KNMI	UCAM-DCHEM	UiO	LSCE	UCI	Météo-France
Model type	CTM	CTM	CTM	CCM (nudged)	CTM	CTM
Meteorology	ECMWF OD	ECMWF OD	ECMWF OD	ECMWF OD	ECMWF OD	ECMWF OD
Hor. resolution	$2° \times 3°$	T21	T42	$3.75° \times 2.5°$	T42	T21
Levels	34	31	60	19	40	60
Model top (hPa)	0.1	10	0.1	3	2	0.1
Transport scheme	Russell and Lerner (1981)	Prather (1986)	Prather (1986)	van Leer (1977)	Prather (1986)	Williamson and Rasch (1989)
Convection	Tiedtke (1989)	Tiedtke (1989)	Tiedtke (1989)	Emanuel (1991, 1993)	Tiedtke (1989)	Bechtold et al. (2001)
Lightning	Meijer et al. (2001)	Price and Rind (1992)	Price and Rind (1992)	Price and Rind (1992), modified	Price and Rind (1992)	Climatology
Transp. species	26	35	76	66	28	65
Total species	42	51	98	96	38	82
Gas phase reactions	68+16	112+27	163+47	291+51	90+22	186+47
Het. Reactions	2	1	7	4	0	9
Strat. chemistry	no	no	yes	no	LINOZ	yes
NMHC chemistry	yes, CBM4	yes	yes	yes	yes	yes
Lightning NO_X ($TgN\,yr^{-1}$)	5	5	5	2	5	5
References	Williams et al. (2010)	O'Connor et al. (2005)	Gauss et al. (2003), Søvde et al. (2008)	Hauglustaine et al. (2004), Folberth et al. (2006)	Wild et al. (2003), Hsu et al. (2005)	Teyssèdre et al. (2007)

3 Model descriptions

An ensemble of six models has been applied in order to estimate the future impact of non-land based traffic emissions on atmospheric ozone and OH, when considering optimistic scenarios. For the results presented in Sects. 4–6, equally weighted average values of the six models are shown along with the standard deviations, representing the spread in the model results (selected individual model results are shown in Appendix B). Five global Chemistry Transport Models (CTMs) were driven by operational meteorological data from the European Centre for Medium-Range Weather Forecasts (ECMWF) and updated every 6 h (TM4, p-TOMCAT, OsloCTM2, UCI CTM and MOCAGE), while one Climate Chemistry Model (CCM) was nudged towards the ECMWF data (LMDz-INCA). In all simulations the meteorological data are from year 2003 while 2002 data were used to spin-up the models. General model properties are synthesized in Table 2, and short descriptions are given below.

The models have been evaluated by Schnadt et al. (2010) who compared simulated CO to aircraft measurements from 2003, and found underestimation of tropospheric CO at northern hemispheric middle and subtropical latitudes. The discrepancies were possibly related to the biomass burning emissions which were abnormally high in 2003 (e.g. Yurganov et al., 2005), while biomass burning emissions from 2000 were used in the simulations. Comparisons of the annual cycle of ozone from multi-year sonde observations and from the six models are shown in Appendix A (Fig. A1). Overall, the ensemble mean of the model results agrees relatively well with the observations.

3.1 TM4

TM4 is a global chemistry transport model with a horizontal resolution of $3° \times 2°$ and 34 vertical layers up to 0.1 hPa. The version used here has been comprehensively described in Williams et al. (2010). The chemical scheme is the modified CBM4 mechanism decribed by Houweling et al. (1998), supplemented with sulphur chemistry and with the chemical reaction data being updated by Williams and van Noije (2008). The advection scheme is the slopes method developed by Russell and Lerner (1981), while convection is based on the Tiedtke mass flux scheme (Tiedtke, 1989).

3.2 p-TOMCAT

The global offline chemistry transport model p-TOMCAT is an updated version (see O'Connor et al., 2005) of a model previously used for a range of tropospheric chemistry studies (Law et al., 1998, 2000; Savage et al., 2004). The model is used here with a horizontal resolution of $5.6° \times 5.6°$ (T21) and extends from the surface to 10 hPa in 31 vertical levels. The chemical mechanism includes the reactions of methane, ethane and propane plus their oxidation products and of sulphur species. The model chemistry uses the atmospheric chemistry integration package ASAD (Carver et al., 1997) and is integrated with the IMPACT scheme of Carver and Stott (2000). The chemical rate coefficients used by p-TOMCAT are taken from the IUPAC summary of March 2005. The Prather (1986) scheme is used for advection while convective transport is based on the mass flux parameterization of Tiedtke (1989).

3.3 OsloCTM2

The OsloCTM2 chemistry transport model is used here with both tropospheric and stratospheric chemistry (Gauss et al., 2003; Søvde et al., 2008). It extends from the surface to 0.1 hPa in 60 vertical layers and a horizontal resolution of Gaussian T42 ($2.8° \times 2.8°$) is used. Advection in OsloCTM2 is done using the second order moment scheme (Prather, 1986), while convection is based on the Tiedtke mass flux scheme (Tiedtke, 1989). The Quasi Steady-State Approximation (Hesstvedt et al., 1978) is used for the numerical

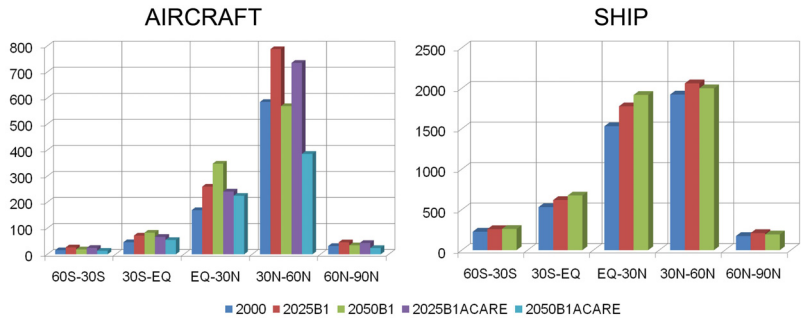

Fig. 4. NO_X emissions (Gg(N) yr^{-1}) from aircraft (left) and shipping (right) for different latitude intervals and for different years/scenarios. Note that 90° S–60° S is not shown in the figures because the emissions in this region are close to zero.

solution in the chemistry scheme, and photodissociation is done on-line using the FAST-J2 method (Wild et al., 2000; Bian and Prather, 2002).

3.4 LMDz-INCA

The LMDz-INCA model consists of the LMDz General Circulation Model (Le Treut et al., 1998), coupled on-line with the chemistry and aerosol model INCA (Folberth et al., 2006). The version 4.0 of the LMDz model has 19 hybrid levels on the vertical from the ground to 3 hPa and a horizontal resolution of 2.5° in latitude and 3.75° in longitude. The large-scale advection of tracers is performed using the finite volume transport scheme of Van Leer (1977), as described in Hourdin and Armengaud (1999). The turbulent mixing in the planetary boundary layer is based on a second-order closure model. The INCA model considers the surface and 3-D emissions, calculates dry deposition and wet scavenging rates, and integrates in time the concentration of atmospheric species with a time step of 30 min. The CH_4-NO_x-CO-O_3 photochemistry, as well as the oxidation pathways of non-methane hydrocarbons and non-methane volatile organic compounds are taken into account. The winds and temperature predicted by LMDz have been nudged to 6-hourly ECMWF data over the whole model domain with a relaxation time of 2.5 h (Hauglustaine et al., 2004).

3.5 UCI CTM

In this study, the University of California, Irvine (UCI) chemistry transport model extends from the surface to 2 hPa with 40 vertical layers and is run at T42 horizontal resolution. The UCI CTM contains separate tropospheric and stratospheric chemistry. The tropospheric chemistry is simulated by the ASAD (A Self-contained Atmospheric chemistry coDe) software package (Carver et al., 1997) with UCI updates (Tang and Prather, 2010), which include the chemical kinetics and photochemical coefficients from the JPL publication 06–2 (Sander et al., 2006), and quasi steady-state initial guesses for radicals, and $O(^1D)$ included with O_3. The stratospheric chemistry uses the linearized ozone scheme (Linoz), which can include up to four independent species (e.g. O_3, N_2O, NO_y, CH_4), but in this case consists only ozone (Prather and Hsu, 2010). The tropopause, the boundary between the troposphere and the stratosphere, is determined by an artificial tracer (e90) (Prather et al., 2011; Tang et al., 2011). The advection and convection use the same schemes as OsloCTM2.

3.6 MOCAGE

The MOCAGE chemistry transport model is used here with a horizontal resolution of 5.6° × 5.6° (T21) and 60 levels up to 0.1 hPa (Teyssèdre et al., 2007). The chemical scheme is a combination of the tropospheric RELACS scheme (Crassier et al., 2000) (a reduced version of the RACM scheme, Stockwell et al., 1997) and of the stratospheric REPROBUS scheme (Lefèvre et al., 1994) including the heterogeneous chemistry described in Luo et al. (1995). The large-scale transport of the tracers is done using a semi-Lagrangian transport scheme (Williamson and Rasch, 1989), while the convective transport is as described in Bechtold et al. (2001).

4 Ozone

The 2050 B1 annual mean ozone column response to a 5 % perturbation in emissions is shown in Fig. 5 for the aircraft and shipping sectors. The ozone impact from AIR is zonally well mixed, and mostly confined to the Northern Hemisphere (NH) in accordance with the latitudinal distribution of emissions shown in Fig. 4. A method to estimate the contribution of a source is to estimate the sensitivity (ozone change per emission) with a 5 %-perturbation and then to multiply it with the total emission of the source category (e.g. AIR), which effectively equals a scaling of impacts to 100 % by multiplying the response of the 5 % emission perturbation by

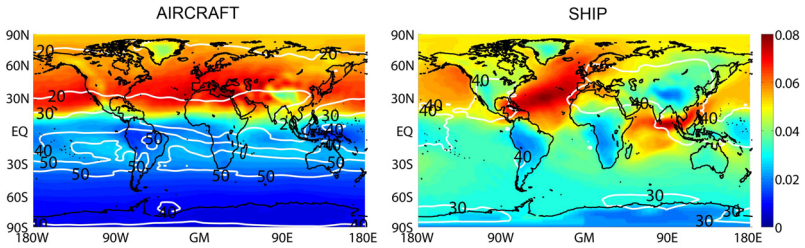

Fig. 5. Yearly mean perturbations of the ozone column (ΔDU, up to 40 hPa) due to a 5 % perturbation of aircraft emissions (left) and ship emissions (right) for the 2050 B1 scenario. The white contour lines show the standard deviation relative to the ensemble mean column perturbation (%), and have been smoothed to improve readability.

20 (Grewe et al., 2010). The results show a maximum ozone column response of 1.6 DU. The corresponding perturbation for SHIP is also 1.6 DU, but much less homogeneously distributed with maximum values occurring over the North Atlantic Ocean and at the coastal areas of South East Asia. These two areas were also identified as peaks in the 2030 model simulations performed by Eyring et al. (2007), who attributed the increased ship-induced tropospheric ozone column over the Indian Ocean to the higher tropopause and more effective vertical transport found there.

Figure 5 also shows the relative standard deviation which represents the spread in results between the different models (see Appendix B for individual model results). Only results for 2050 B1 are shown in Fig. 5, but the relative standard deviations for the other years and scenarios also have similar distributions. The robustness of the models is quite good for the aircraft perturbation case, with a relative standard deviation less than 20 % in most of the areas where the perturbation effect is strong. However, model differences in interhemispheric transport result in a larger relative standard deviation in the Southern Hemisphere (SH). The relative standard deviation for shipping demonstrates larger deviations between the models compared to the aircraft case, and is mainly in the range 30–40 %. One of the models (OsloCTM2) gives large impacts from shipping with a scaled maximum value of 2.5 DU, while another model (MOCAGE) has a corresponding value of only 0.9 DU. However, as model intercomparison is beyond the scope of this study, the reader is referred to e.g. Danilin et al. (1998) and Rogers et al. (2002) for thorough discussions of differences between CTMs.

4.1 Effects of aircraft emissions

Figure 6 shows the impact of aircraft emissions on ozone in the UTLS region for January and July along with the difference between the B1 and B1 ACARE scenarios (represented by the red lines). When focusing on the B1 scenario, the results indicate an increase in ozone impact from aircraft between 2000 (black dotted line) and 2025 (black dashed line), while the difference between 2025 and 2050 (black solid line) depends on the season and on the latitude. Because of the strong net decrease in NO_x emissions from aircraft at northern mid- and high latitudes from 2025 to 2050 (Fig. 4), the resulting ozone effect is a decrease in zonal mean values north of 30° N during summer (Fig. 6, bottom right) when the photochemistry is more intense. This signal is to a large extent consistent between the models, but it depends strongly on the model whether or not there is an ozone decrease in the NH during winter. In the SH, the ozone impact from aircraft emissions is likely to increase in 2025 and further to 2050, if emissions evolve according to the B1 scenario. The zonal mean local maximum of 0.066 ppbv (or 1.3 ppbv scaled to 100 %) at about 25° S in 2050 B1 (July) is caused by a combination of increased emissions in the tropics (Fig. 4) and transport across the hemispheres.

The local maximum can also be seen in Fig. 7, which shows the zonal mean ozone impact for 2050 B1 (see Fig. B1 for individual model results), together with the average vertical profile of the NH impact on ozone for each year and scenario. The results show that the maximum absolute impact in the UTLS region is larger in July compared to January, because of the difference in the length of the day between both months. However, the maximum ozone impact relative to the reference simulation (BASE) in 2050 B1 is larger in January with a peak value of 0.21 % (or 4.2 % scaled) located in the middle to upper troposphere at 20–30° N. This peak in the tropics during winter arises because aircraft-induced NO_x and O_3 are transported from the northern mid-latitude UTLS to the low-latitude middle troposphere where the background levels of NO_x and O_3 are lower. For comparison, Grewe et al. (1999) calculated annual maximum relative ozone changes due to aircraft emissions of 7 % in a 2050 scenario, but the aircraft NO_x emissions used in their study were about twice as large as the 2050 B1 emissions that are used here (2.15 TgN yr^{-1} compared to 1.05 TgN yr^{-1}), and the surface NO_x emissions were 60 % larger (69.7 TgN yr^{-1} compared to 43.8 TgN yr^{-1}). The comparison is also influenced by several other factors such as the difference in year of meteorology used and potential model developments (e.g.

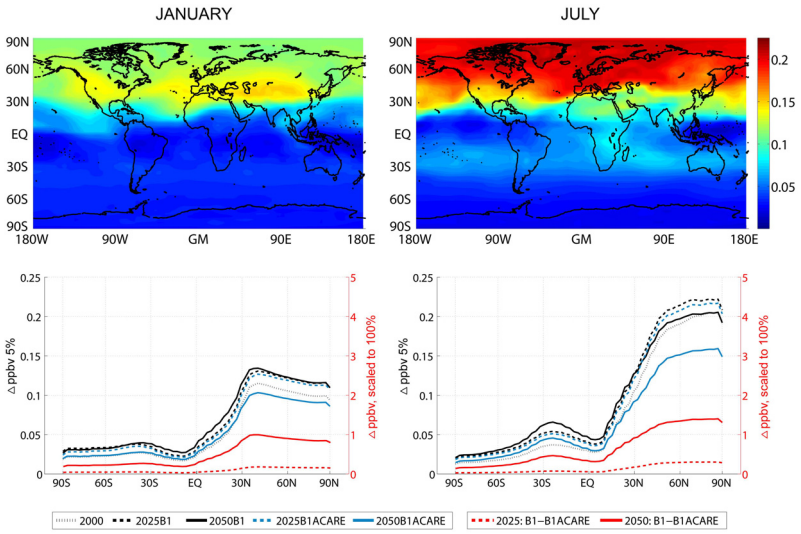

Fig. 6. Mean perturbations of ozone (Δppbv) in the upper troposphere (300–200 hPa) during January (left) and July (right) for the 2050 B1 scenario (top) and as zonal means for all scenarios (bottom). The color bar and the left y-axis show the unscaled impact of the 5 % perturbation of aircraft emissions (simulations BASE – AIR), while the red scales in the bottom figures are scaled up by a factor 20 from 5 % to 100 % and refer to all lines. The red lines show the difference between the B1 and B1ACARE scenarios and refer to the red axis only.

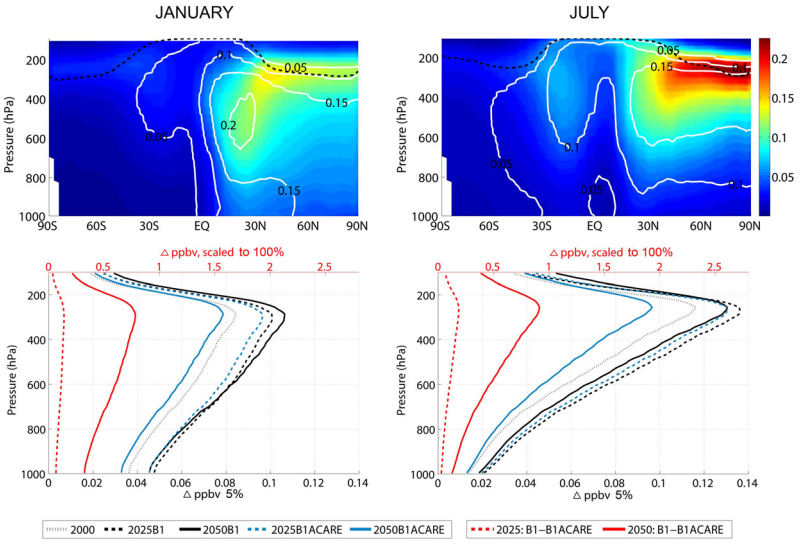

Fig. 7. Zonal mean perturbations of ozone (Δppbv) during January (left) and July (right) for the 2050 B1 scenario (top) and as Northern Hemisphere average for all years (bottom). In the top figures, solid contour lines show the change relative to the BASE simulation while the dashed line indicates the tropopause. The color bar and the bottom x-axis show the unscaled impact of the 5 % perturbation of aircraft emissions (simulations BASE – AIR), while the red scales in the bottom figures are scaled up by a factor 20 from 5 % to 100 % and refer to all lines. The red lines show the difference between the B1 and B1ACARE scenarios and refer to the red axis only.

Table 3. Global annual average of the change in O_3 molecules per NO_x molecule emitted from aviation and shipping, given as ensemble means and standard deviations.

	2000	2025B1	2050B1	2025B1ACARE	2050B1ACARE
AIR	2.05 (±0.51)	1.90 (±0.42)	2.16 (±0.52)	1.95 (±0.42)	2.31 (±0.59)
SHIP	0.509 (±0.185)	0.508 (±0.185)	0.535 (±0.194)	–	–

chemical reaction rates, deposition parameterizations, improved resolution) since the Grewe et al. (1999) study. Also worth noting is the fact that ozone perturbations in the lower troposphere are weaker during summer than in winter, presumably because the surface deposition to plants is faster and the photochemical lifetime of ozone is shorter (because increased water vapour gives more HO_x and thereby ozone loss) at lower altitudes during summer.

If emissions evolve according to the B1 ACARE mitigation option rather than the B1 scenario, Figs. 6 and 7 show that ozone will only be reduced by a small amount in 2025 (red dashed line), while in 2050 (red solid line) the mitigation option will have a substantial effect on reducing ozone levels. A direct comparison between B1 and B1 ACARE yields mean ozone differences poleward of 30° N in the UTLS of 0.18–0.30 ppbv and 0.94–1.40 ppbv during summers of 2025 and 2050, respectively (Fig. 6, red lines). Notably in the NH, the average ozone perturbation from aircraft in 2050 for B1 ACARE (blue solid line) is reduced to considerably lower values than the estimated impact in year 2000 (black dotted line) for altitudes below 200 hPa (Fig. 7). The fact that the mitigation option only has a minor effect in 2025 could be associated with the long lifetime of aircraft.

Hoor et al. (2009) found that the change in ozone burden per NO_x-emission was highest for aircraft when comparing with the road and ship transport sectors. In Table 3 we have presented the ozone enhancement efficiency in order to investigate how the sensitivity changes with different years and scenarios. Previous studies (e.g. Grooß et al., 1998; Grewe et al., 1999) have found that the non-linearity in the ozone production normally leads to a smaller positive ozone perturbation per aircraft emitted NO_x-molecule when the emissions are higher. This is also the case when we compare the ozone change per aircraft NO_x-emission in 2000 with 2025 (Table 3), when the emissions are expected to increase. However, when looking at the 2050 B1 scenario, all models show a higher ozone enhancement efficiency compared to year 2000, although the aircraft NO_x emissions also are higher. This unexpected effect can be explained by the change in the location of the emissions. In 2050, the aircraft NO_x emissions are shifted further south compared to year 2025 (Fig. 4), and will then take place in more pristine regions where the background NO_x levels are lower. Additionally, Hoor et al. (2009) emphasized the role of road traffic for the chemical state of the UTLS, and as NO_x emissions from this transport sector are assumed to decrease rapidly in the future, the NO_x background levels at cruise altitude are affected. Not surprisingly, the highest ozone enhancement efficiency is found in 2050 B1 ACARE, which is the scenario with the lowest aircraft emissions. For this case, the models estimate that the ozone abundance increases by 2.31 molecules for every NO_x molecule emitted from aircraft.

4.2 Effects of ship emissions

Figures 8 and 9 show the effects of shipping emissions on atmospheric ozone in January and July for different years and scenarios (see Fig. B2 for individual model results). Even if emissions evolve according to the optimistic B1 scenario, model results show that the shipping sector will increase its effect on ozone in the future. Focusing on the estimated ozone impact in the lower troposphere in 2050 B1 (Fig. 8), the largest effect from shipping can be found in the North Atlantic Ocean with ozone values of about 0.2 ppbv (or 4 ppbv scaled) during summer when the photochemical activity reaches a maximum. Notably, the impact in the Arctic region is expected to increase in the future due to the expected introduction of new ship tracks associated with melting of the polar ice cap. This area is especially sensitive to emission perturbations because of the low background NO_x levels which lead to higher ozone enhancement efficiencies. Consequently, the maximum relative effects in July are found in this region, showing zonal mean impacts exceeding 0.6 % (or 12 % scaled) near the surface (Fig. 9).

Interestingly, Fig. 8 shows that the ozone impact from shipping at northern mid- and high latitudes will increase from 2025 (dashed line) to 2050 (solid line), especially during winter, although the emissions in these regions are expected to decrease (Fig. 4). Except for transport from lower latitudes, where the emissions increase, this feature can be explained by lower ambient levels of NO_x which act to increase the change in ozone burden per NO_x emitted from ships. The increase in ozone enhancement efficiency can also be seen in Table 3, where global annual average values are given. In the future B1 scenario, large reductions in anthropogenic non-traffic and road emissions of NO_x are assumed over the Eastern US and Europe. This significantly increases the ozone enhancement efficiency from shipping, as transport from these polluted continental areas normally leads to higher levels of NO_x over the Atlantic Ocean and the North Sea.

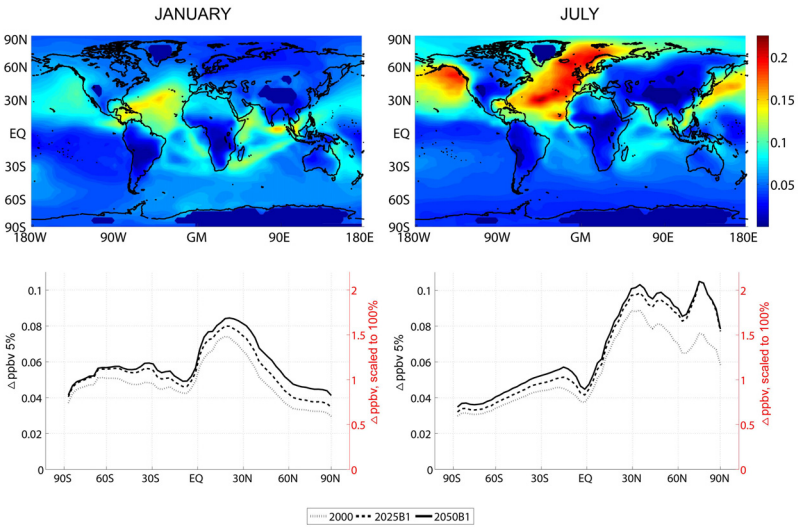

Fig. 8. Mean perturbations of ozone (Δppbv) in the lower troposphere (>800 hPa) during January (left) and July (right) for the 2050 B1 scenario (top) and as zonal means for all years (bottom). The color bar and the left y-axis show the impact caused by a 5 % perturbation of ship emissions (simulations BASE – SHIP), while the red scales in the bottom figures are scaled up by a factor 20 from 5 % to 100 %.

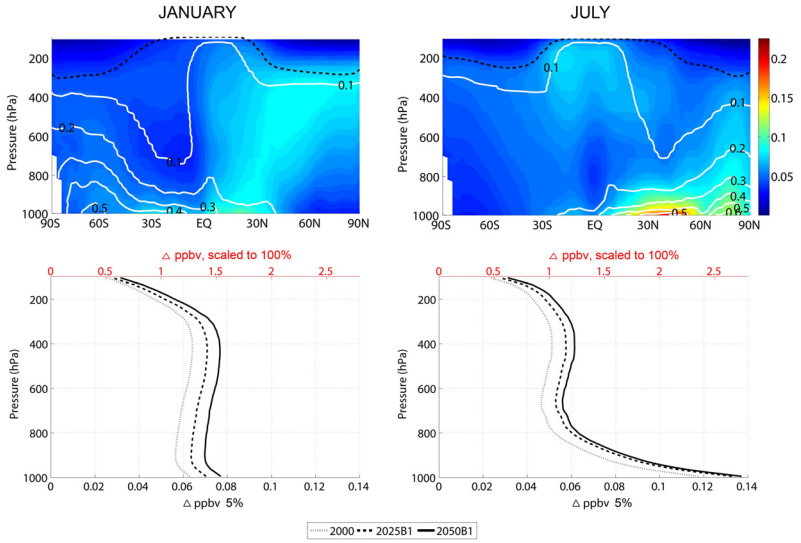

Fig. 9. Zonal mean perturbations of ozone (Δppbv) during January (left) and July (right) for the 2050 B1 scenario (top) and as Northern Hemisphere average for all years (bottom). In the top figures, solid contour lines show the change relative to the BASE simulation while the dashed line indicates the tropopause. The color bar and the bottom x-axis show the impact caused by a 5 % perturbation of ship emissions (simulations BASE – SHIP), while the red scales in the bottom figures are scaled up by a factor 20 from 5 % to 100 %.

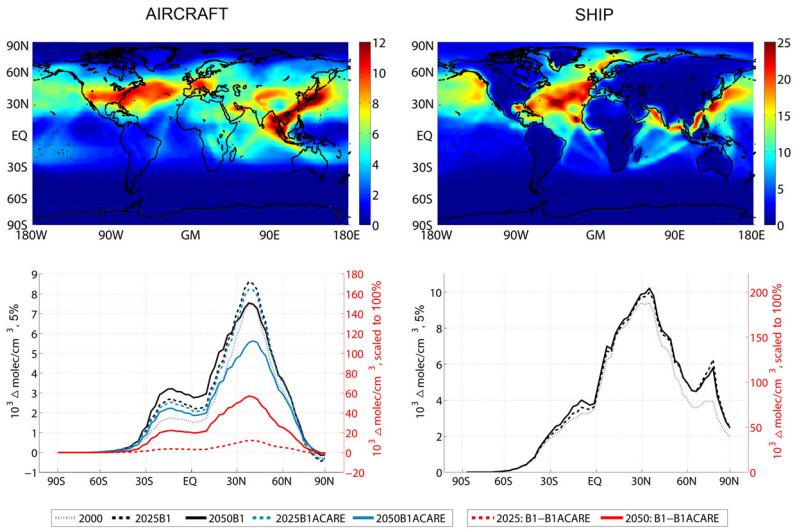

Fig. 10. Mean perturbations of OH (10^3 Δmolec cm^{-3}) in July in the upper troposphere (300–200 hPa) due to a 5 % perturbation of aircraft emissions (left), and in the lower troposphere (>800 hPa) due to a 5 % perturbation of ship emissions (right). The top row figures show results from the 2050 B1 scenario, and the bottom row figures show zonal means for all years and scenarios. The colorbars and the left y-axis show the unscaled impact of the 5 % perturbation of the emissions, while the red scales in the bottom figures are scaled up by a factor 20 from 5 % to 100 % and refer to all lines. The red lines show the difference between the B1 and B1ACARE scenarios and refer to the red axis only. Note that different scales are used for AIR and SHIP.

5 OH

5.1 Global OH

Changes in the concentration and distribution of the hydroxyl radical (OH) are important for air pollution and the self-cleaning capacity of the atmosphere (Lelieveld et al., 2002) as OH is the main oxidant in the troposphere. Validation of modelled OH is difficult, however, particularly because of its short lifetime (less than one second) which makes it almost impossible to measure directly. In a recent study by Montzka et al. (2011), indirect measurements of the interannual variability of global OH are consistent with past model studies (Dentener et al., 2003; Dalsøren and Isaksen, 2006; Lelieveld et al., 2006; Duncan and Logan, 2008), and this suggest that larger confidence should be given to models than previously assumed (Isaksen and Dalsøren, 2011).

The impact of aircraft and shipping emissions on tropospheric OH is shown in Figs. 10 and 11 for July, when the effect is largest due to enhanced photochemistry in the NH. For aircraft emissions, there is an indication of a future increase in the impact on tropospheric OH. Figure 10 shows that enhanced OH levels in the UTLS are expected at all latitudes in 2025 (black and blue dashed lines), with an exception near the Arctic region where increased aircraft emissions seem to cause a slight decrease in OH levels. However, when comparing the impacts between 2025 and 2050, the OH response depends strongly on both scenario and latitude. In 2050 (black and blue solid lines), a decrease is seen between approximately 30 and 60° N, associated with a strong decrease in aircraft NO_x emissions (Fig. 4), while a zonal mean increase is expected elsewhere, in particular near the equator where aircraft NO_x emissions are assumed to increase. In 2025 B1, the zonal mean average in the UTLS region for July peaks at 40° N with a value of 8.6×10^3 molecules cm^{-3} (unscaled). When averaging the aircraft-induced OH vertical profile over the entire NH, 2025 B1 and 2050 B1 both show a maximum of 5.4×10^3 molecules cm^{-3} (unscaled) near 250 hPa (Fig. 11).

The largest effects from aircraft emissions during northern summer in the future (July 2050; B1) can be found east and southeast of Asia, but also with significant impacts close to the North Atlantic flight corridor (Fig. 10, top left). The zonal mean OH impact peaks above 300 hPa, and this is also the region of maximum relative impact with a value of 0.6 % (or 12 % scaled) (Fig. 11, top left). In the SH, the absolute values are lower, but due to low background levels the relative impact is fairly high with a value of almost 0.5 % (or 10 % scaled).

As was the case with ozone, the technological improvements that are assumed in the B1 ACARE mitigation scenario have significant effects on OH. If the ACARE targets

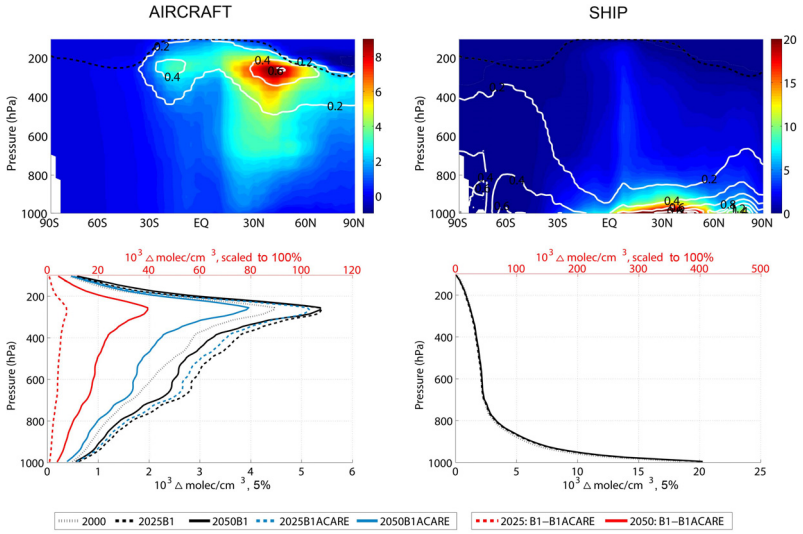

Fig. 11. Zonal mean perturbations of OH (10^3 Δmolec cm^{-3}) in July due to a 5 % perturbation of aircraft emissions (left) and ship emissions (right), for the 2050 B1 scenario (top) and the average Northern Hemisphere vertical profile for all years and scenarios (bottom). In the top figures, solid contour lines show the change relative to the BASE simulation while the dashed line indicates the tropopause. The colorbar and the bottom x-axis show the unscaled impact of the 5 % perturbation of the emissions, while the red scales in the bottom figures are scaled up by a factor 20 from 5 % to 100 % and refer to all lines. The red lines show the difference between the B1 and B1ACARE scenarios and refer to the red axis only. Note that different scales are used for AIR and SHIP.

will be met in 2050, the northern summer OH levels in the UTLS region (red solid line) could be reduced by up to 5.7×10^4 molecules cm^{-3} (Fig. 10, bottom left). The reductions are substantial also in the NH as a whole, showing average differences between B1 and B1 ACARE of 3.9×10^4 molecules cm^{-3} near 250 hPa (Fig. 11, bottom left), and with significant effects also in the middle troposphere. In the near future (2025), the gain of fulfilling the ACARE targets is much lower, but still the maximum difference between B1 and B1 ACARE is 7.6×10^3 molecules cm^{-3} (red dashed line).

Hoor et al. (2009) emphasized the large impact of ship emissions on the boundary layer OH levels, and concluded that the effect of ship emissions is more important for the global OH budget than road and aircraft emissions. Figure 10 shows that the impact from ship emissions on OH in the boundary layer is expected to increase in the future if emissions evolve according to the B1 scenario. Between 2025 and 2050, OH will continue to increase at all latitudes except north of 60° N where a small reduction in ship NO_x emissions is expected.

Focusing on northern summer in the future (July 2050; B1), the largest impact from ship emissions can be found in the North Atlantic Ocean with maximum values reaching 3.0×10^4 molecules cm^{-3} (unscaled) (Fig. 10, top right). As discussed in Sect. 4.2, ozone production in this area is largely sensitive to an increase in NO_x emissions, and because of high humidity and strong incoming solar radiation, additional OH is produced when O(^{1}D) reacts with H_2O. Additionally, the background levels of CO and NMHCs, which act to deplete OH, are relatively low in these pristine regions. In the zonal mean, maximum absolute values are found near the surface at 45° N (Fig. 11, top right), while the relative impact reaches a maximum of about 1.5 % (or 30 % scaled) near 75° N. The reason is the low background values of OH, as shipping is a dominant source of air pollutants at these high latitudes, and because the production of additional OH caused by ship emissions is more effective in the summer month of July.

5.2 Methane lifetime

Emissions from the aircraft and shipping sectors greatly affect the OH concentration, and this leads to changes in the methane lifetime. Methane lifetimes due to reaction with OH have been calculated for each model and for each year and scenario. As in Hoor et al. (2009), monthly mean 3-D-fields of methane and OH were used, and the resulting lifetime changes were then scaled from a 5 % perturbation in emissions to a 100 % perturbation (to get a stronger signal in the RF calculations) by multiplying with a factor of 20

Table 4. Relative changes (%) in methane lifetimes (integrated up to 50 hPa) due to a 5 % decrease in traffic emissions. Values are given relative to the BASE case, and are scaled to 100 % by multiplying with 20. Both the mean of the six models and the standard deviations (indicating the spread of the models) are given. Note that this table does not include the feedback effect of methane changes on its own lifetime.

	AIR	SHIP
2000	1.30 (±0.30)	3.68 (±0.47)
2025B1	1.69 (±0.35)	3.73 (±0.40)
2050B1	1.68 (±0.38)	3.92 (±0.48)
2025B1ACARE	1.59 (±0.34)	–
2050B1ACARE	1.17 (±0.28)	–

(Grewe et al., 2010). The resulting model mean and standard deviation of the methane lifetime changes are given in Table 4 (see Tables B1–B2 for individual model results), while the model mean of the methane lifetime is 8.0 (±1.0) yr in the 2050 B1 BASE simulation and 8.3 (±1.0) yr in the 2000 BASE simulation. The rather low relative standard deviation of 12 % is similar for the BASE simulations of the other scenarios, and indicates that the ensemble mean of the models is relatively robust when calculating methane lifetimes.

As discussed in Sect. 5.1, SHIP exhibits the largest impact on OH levels and consequently the largest impact on methane lifetime. The model ensemble predicts that the shipping sector contributed to a methane lifetime reduction of 3.68 % in year 2000, and that this number will increase to 3.92 % in 2050, if emissions evolve according to the B1 scenario (Table 4). Eyring et al. (2007) calculated methane lifetime changes from shipping in 2030, and their estimates range from 1.14 % to 1.81 % for a low and high emission scenario, respectively. Their result is much lower than both 2025 B1 and 2050 B1 from this study, and that was also the case for the year 2000 results discussed in Hoor et al. (2009). According to Hoor et al. (2009), part of the differences could be attributed to the very different distribution of ship emissions. The same reasoning applies here as the future ship emissions in Eyring et al. (2007) are more concentrated along the major shipping routes in contrast to the QUANTIFY future ship emissions, which are spread out over larger areas.

The methane lifetime changes for SHIP do not follow the trend in ship NO_x emissions, which increased a lot more between 2000 and 2025 B1 than between 2025 B1 and 2050 B1 (Fig. 1). The reason is the assumption of large reductions in land based NO_x emissions, particularly from road traffic, in Europe and the US between 2025 B1 and 2050 B1 (not shown). This effect exceeds the impact of increased ship emissions, as a decrease in background NO_x levels leads to a more efficient OH production from shipping.

The future methane lifetime changes for AIR are to a certain degree in accordance with the evolution of the aircraft B1 emissions; an increased impact in 2025 followed by stabilization in 2050 (Table 4). The model ensemble predicts a much lower impact of aircraft on methane lifetimes for the B1 ACARE scenario, especially in 2050 when the relative methane lifetime change is lower than the year 2000 value.

6 Radiative forcings

Radiative forcings have been calculated using the same method as in Myhre et al. (2011). The Oslo radiative transfer model (Myhre et al., 2000) was used to calculate ozone radiative forcings based on monthly mean ozone fields from each model simulation. In order to obtain a robust signal the fully scaled perturbations have been used in the RF calculations, i.e. the ozone change resulting from the 5 % perturbation has been multiplied by 20 (Hoor et al., 2009; Grewe et al., 2010). According to Myhre et al. (2011), the non-linearities arising from the perturbation magnitude are of little importance compared to the inter-model differences in the RF.

Figure 12 shows the yearly averaged ozone RF for the 2050 B1 scenario as means of all models and with absolute standard deviations. The aircraft sector has a larger impact than ship emissions in the NH and the changes in RF are relatively homogeneous throughout different latitude zones. The impacts are large throughout the NH and have maximum values reaching 76 mW m^{-2} near 30° N. In the SH the ozone RF from aircraft is low, except in the region 0–30° S. This latitude band also shows a large spread of the models with standard deviations up to 21 mW m^{-2}, indicating possible model uncertainties related to convection and transport between the hemispheres. For SHIP, the ozone RF is stronger in the SH compared to AIR, but the RF in the NH is much weaker. Maximum impact from SHIP takes place between 30° N and 30° S, and peaks at 50 mW m^{-2}.

Global average ozone RF for all scenarios is given in Table 5 (see Tables B3–B4 for individual model results). For the B1 scenario there is a small increase in the ozone RF from AIR between 2025 and 2050, although the NO_x emissions from aircraft are assumed to decrease slightly during this time span. As explained in Sect. 4.1, this is probably caused by the latitudinal shift in the location of the aircraft emissions leading to higher ozone enhancement efficiencies in 2050. For comparison, Myhre et al. (2011) calculated a five model average of 17 mW m^{-2} for AIR in year 2000. The increase to 25.7 mW m^{-2} for 2025 B1 (Table 5) is consistent with the aircraft NO_x emissions, which also are assumed to increase (Fig. 1). For the 2050 B1 scenario, Skeie et al. (2009) estimated ozone RF from AIR to be 38 mW m^{-2} using a simple climate model. The relatively large difference to our study can be partly explained by a lower normalized radiative forcing in this study (36.3 compared to 42.9 mW $m^{-2}DU^{-1}$), and partly by lower ozone enhancement efficiencies (2.16 compared to 2.69 ozone molecules enhanced per NO_x molecule emitted from AIR). In Lee et al. (2009), a scaling approach

Table 5. Radiative forcings (mW m^{-2}) from changes in ozone, methane (including stratospheric water vapour), and methane-induced ozone for different transport sectors and years/scenarios given as ensemble means and standard deviations. Note that the history of emissions has been taken into account, and that the fully scaled perturbations were used.

	AIRCRAFT				SHIPPING			
	O_3	CH_4	$O_{3(CH4)}$	total	O_3	CH_4	$O_{3(CH4)}$	total
2025B1	25.7 (±8.3)	−16.0 (±3.4)	−5.9 (±1.2)	3.8 (±6.1)	23.6 (±8.4)	−37.8 (±4.1)	−13.8 (±1.5)	−28.0 (±5.1)
2050B1	26.2 (±9.0)	−17.8 (±4.0)	−6.5 (±1.5)	1.9 (±6.4)	25.2 (±9.6)	−41.0 (±5.0)	−15.0 (±1.8)	−30.8 (±4.8)
2025B1ACARE	24.1 (±7.7)	−15.5 (±3.3)	−5.7 (±1.2)	2.9 (±5.8)	–	–	–	–
2050B1ACARE	18.9 (±6.8)	−14.3 (±3.4)	−5.2 (±1.2)	−0.6 (±4.6)	–	–	–	–

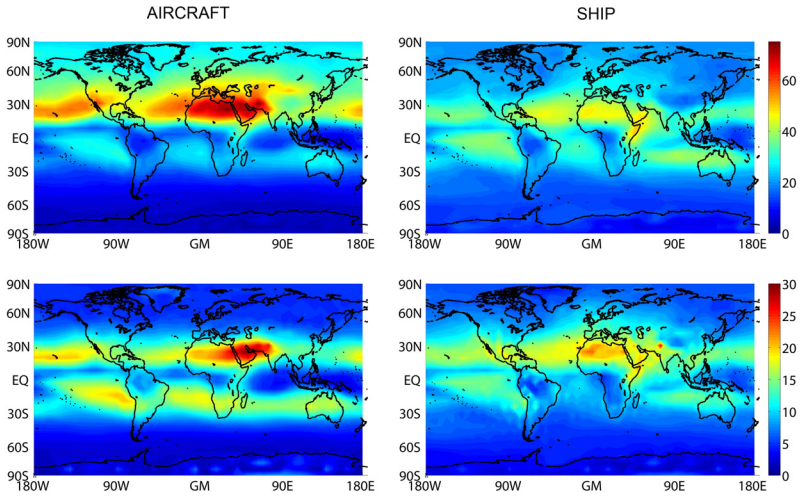

Fig. 12. Radiative forcing (mW m^{-2}) from short-term O_3 due to emissions from aircraft (left) and shipping (right), shown as ensemble mean for the 2050 B1 scenario (top) along with the absolute standard deviation (bottom). Note that the fully scaled perturbations were used to calculate the forcings.

was used to estimate the aviation RF of ozone in 2050 to be in the range 59.4–109.8 mW m^{-2}, depending on the scenario. Their estimates are much higher than in this study, but this is expected because even their lowest emission scenario (SRES B2 with technology 2, see IPCC, 1999) had larger aircraft NO_x emissions than the 2050 B1 scenario used here. The effect of the B1 ACARE mitigation strategy is evident already in 2025, with a 1.6 mW m^{-2} lower ozone RF than in the B1 scenario (Table 5). However, in 2050 the corresponding number has increased to 7.3 mW m^{-2}, showing the large potential impact of technological improvements in the aircraft sector.

The ozone RF from SHIP is calculated to increase between 2025 and 2050, this time due to a combination of the slight increase in ozone precursor emissions for this transport sector, and the stronger ozone enhancement efficiency in 2050 (see Sect. 4.2). Despite the assumed increase in ship emissions between 2000 and 2025 B1, Myhre et al. (2011) have a larger estimate for 2000 (24 mW m^{-2}) than our results for 2025 B1. The reason is that the MOCAGE model is included in our study, and this model is at the lower end of the spectrum when calculating ozone RF from SHIP (Table B4). Again, Eyring et al. (2007) calculated lower impacts than in this study, with ozone RF from shipping ranging from 7.9 to 13.6 mW m^{-2} in 2030. On the other hand, Skeie et al. (2009) estimated a larger impact from shipping with short-lived ozone RF at 36 mW m^{-2} for the 2050 B1 scenario, also this time due to lower ozone enhancement efficiencies in this study (0.535 compared to 0.859 ozone molecules enhanced per NO_x molecule emitted from SHIP).

Emissions of NO_x from aircraft and shipping sectors normally lead to an increase in OH concentrations, resulting in a reduction of methane lifetime. The forcing due to the changes in methane is given in the second column in Table 5, and has been calculated mainly using the method described by Berntsen et al. (2005). For each year and scenario, the

changes in methane lifetime were multiplied by the estimated methane concentrations reported in IPCC (2001). Further, to account for the impact of methane changes on its own lifetime, a feedback factor of 1.4 was used (IPCC, 2001). The linearized methane specific forcing of $0.35\,\mathrm{mW\,m^{-2}\,ppbv^{-1}}$ was then applied, assuming a background methane mixing ratio of 1909 ppbv and 1881 ppbv for 2025 B1 and 2050 B1, respectively. In Table 5, the CH_4 RF term includes the impact of methane changes on stratospheric water vapour (SWV), and the RF of SWV is assumed to be 0.15 times that of the methane RF (Myhre et al., 2007).

RF from changes in methane-induced ozone is calculated assuming that a 10 % increase in methane leads to a 0.64 DU increase in ozone (IPCC, 2001), and that this ozone has a specific forcing of $42\,\mathrm{mW\,m^{-2}\,DU^{-1}}$ (IPCC, 2001). As explained in Myhre et al. (2011), the chemical model calculations are one year simulations only, hence the methane concentration may not be in steady state with the change in OH during that year, but depends on the time-history of the emissions. In order to correct for this transient response, factors have been applied based on the method described in Grewe and Stenke (2008). The factors for 2025 are 0.88, 0.91 and 0.94 for AIR B1, AIR B1ACARE and SHIP B1, respectively. Corresponding factors for 2050 are 1.00, 1.15 and 0.99. Note that the factor for 2050 B1 ACARE is larger than 1 because the aircraft emissions are assumed to decrease in the preceding years for this scenario.

The sum of the three RF components in Table 5 shows a negative RF from SHIP, and this is consistent with what has been found in previous studies (Fuglestvedt et al., 2008; Skeie et al., 2009; Myhre et al., 2011). For AIR, however, the total RF is slightly positive in three out of four cases. Interestingly, a slightly negative RF is predicted for the 2050 B1 ACARE scenario. It is important to note that the net effect for AIR is the sum of a fairly large positive number (O_3 RF) and two smaller negative numbers (CH_4 plus CH_4-induced O_3 RF), each associated with uncertainties. The subtle difference between these effects results in a small net value, and considering the uncertainties it is difficult to say for sure whether or not the net effect is positive or negative. However, the general tendency of an increasing importance of methane RF relative to the ozone RF for future air traffic emissions is consistent for both B1 scenarios. It reflects the decreasing rate of ozone RF increase, whereas the CH_4 RF decreases are effective with a time-lag associated with the methane lifetime. For the B1 scenario, a reduction of $1.9\,\mathrm{mW\,m^{-2}}$ is predicted between 2025 and 2050, and for B1 ACARE the reduction is $3.5\,\mathrm{mW\,m^{-2}}$. Compared to Myhre et al. (2011), our estimates of total RF may seem low considering that the aircraft NO_x emissions are higher for the B1 scenario in 2025 and 2050 than they were in 2000. The reason is related to the factors used to correct for the time-history of the emissions, which has to be kept in mind when interpreting RF from methane plus induced ozone changes. The aircraft NO_x emissions increased rapidly prior to year 2000, while the increase levelled off towards 2025, and further turned to a reduction towards 2050 in the B1 and B1 ACARE scenarios. As a consequence, the cooling effect caused by changes in methane and methane-induced ozone RF may compensate the warming from short-term ozone RF (which is unaffected by the time-history of emissions), if emissions evolve according to the optimistic B1 or B1 ACARE scenarios.

7 Conclusions

Six atmospheric chemistry models have been applied in order to investigate how emissions from the non-land based traffic sectors (AIR and SHIP) impact the distributions of ozone and OH according to the B1 and B1 ACARE emission scenarios. Although the B1 scenario is considered optimistic, model results show that the impacts of both AIR and SHIP emissions on ozone and OH will increase in the future (2025 and 2050) compared to recent time (2000). We used the perturbation approach to calculate both, the contributions of the individual sectors to ozone and OH, and their changes over time, knowing that this methodology has principle limitations in the calculation of contributions (Grewe et al., 2010). The choice of -5 % emission perturbations guarantees a consistent calculation of the atmospheric sensitivity with respect to aircraft and ship emissions (Hoor et al., 2009). Our contribution calculation highlights the large impact of ship emissions on the chemistry in the lower troposphere, and indicates that ship-induced ozone could exceed 4 ppbv over the North Atlantic Ocean during future summer (July 2050; B1). At the same time, aircraft emissions dominate in the UTLS region with a maximum zonal mean ozone impact that could reach 5 ppbv polewards of 30° N.

Model simulations with the B1 ACARE mitigation scenario for aviation show modest reductions in ozone levels in 2025, while substantial reductions can be expected in 2050. Zonal means of the UTLS region at northern mid- and high latitudes show that B1 ACARE yields 0.9–1.4 ppbv lower ozone values than the already optimistic B1 scenario during future summer (July 2050), and this is even lower than for recent time (2000). However, all of our future simulations predict an increase in aircraft-induced ozone in the SH compared to year 2000, and this is mainly a response to the assumed increase in aircraft NO_x emissions in this region. Additionally, the shift in emission location between 2025 and 2050, from the already polluted mid- and high northern latitudes to the more pristine regions in the south, leads to an increase in the ozone enhancement efficiency with an increase in the ozone concentration of 2.31 molecules per emitted aircraft NO_x molecule for the 2050 B1 ACARE scenario.

Emissions from SHIP have important effects on the OH concentrations, particularly in the marine boundary layer, and this impact will become increasingly important in the future. As a consequence, the models estimate a relative methane lifetime reduction of 3.9 % (scaled) due to SHIP in

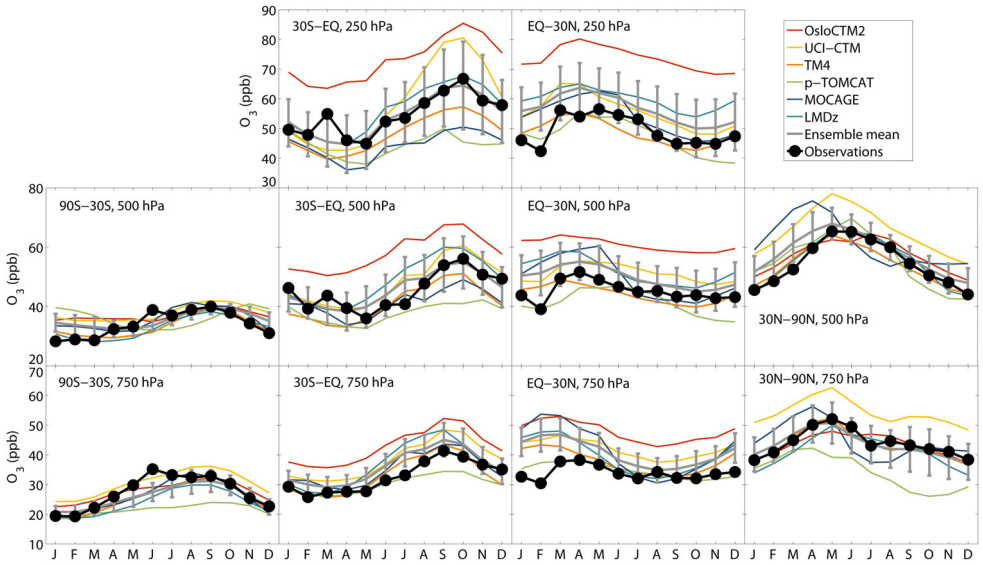

Fig. A1. Comparison of the monthly mean ozone observations (black line with dots) from Logan (1999) with the model ensemble mean and standard deviation (grey line with error bars), and the individual model results (see legend for color codes) at different latitude bands (from left to right: 90° S–30° S, 30° S–EQ, EQ–30° N, 30° N–90° N) and different pressure levels (from top to bottom: 250 hPa, 500 hPa, 750 hPa) for the 2003 model simulations. For comparison, the figure has been made similar to Fig. 2 in the multi-model study by Stevenson et al. (2006).

2050 B1. The corresponding value for AIR is 1.7 %, but if the ACARE targets will be achieved, this number is reduced to 1.2 %.

The large impact of SHIP on OH is reflected in the radiative forcing calculations. When considering RF from changes in short-term ozone, methane (including stratospheric water vapour), and methane-induced ozone, our results suggest that SHIP will have a net cooling effect in 2025 and 2050 of −28.0 (±5.1) and −30.8 (±4.8) mW m^{-2}, respectively, for the B1 scenario. The uncertainties relative to net RF are larger for AIR, but positive RF from short-term ozone normally dominates. The resulting RF for AIR in the B1 scenario is 3.8 (±6.1) and 1.9 (±6.3) mW m^{-2} in 2025 and 2050, respectively. Interestingly, a small cooling effect of -0.6 (±4.6) mW m^{-2} is estimated for 2050 B1 ACARE, but it is important to note that the time-history of emissions has been taken into account, and this leads to a dominance of RF caused by changes in methane and methane-induced ozone, as the larger aviation emissions prior to 2050 have no impact on the 2050 short-term ozone RF (due to shorter lifetime of ozone compared to methane). In order to obtain knowledge of the total impact from AIR and SHIP on future climate, the RF from CO_2, contrails (including contrail-cirrus) and aerosols must be considered in addition to the RF from ozone and methane presented here.

To summarize, emissions from the two transport sectors aviation and shipping will have an increased impact on atmospheric ozone and OH in the future, even if emissions evolve according to the optimistic B1 scenario. However, the aviation impact through ozone formation can be reduced significantly by initiating the ACARE mitigation option, which is purely based on technological improvements. The long operating time of aircraft suggests that mitigation measures for this traffic sector should be considered at an early stage.

Appendix A

Comparison with ozone observations

Results from the BASE simulation of each model have been compared to ozonesonde observations from Logan (1999) and are shown in Fig. A1. In general, the model results agree relatively well with the observations both regarding magnitude and annual cycle. However, a few exceptions can be found, particularly in the tropics where the OsloCTM2 model is biased high. This bias is well-known from previous studies and recent model development has shown that the inclusion of an HNO_3 forming branch of the $HO_2 + NO$ reaction reduced tropical tropospheric O_3 modelled by OsloCTM2 significantly and improved the agreement with ozonesonde

Table B1. Relative changes (%) in methane lifetimes (integrated up to 50 hPa) due to a 5 % decrease in aircraft emissions. Values are given relative to the BASE case, and are scaled to 100 % by multiplying with 20. Note that this table does not include the feedback effect of methane changes on its own lifetime.

	TM4	p-TOMCAT	OsloCTM2	LMDz-INCA	UCI CTM	MOCAGE
2000	1.27	1.61	0.85	1.07	1.60	1.41
2025B1	1.82	2.03	1.11	1.40	1.93	1.84
2050B1	1.77	2.04	1.09	1.37	2.04	1.78
2025B1ACARE	1.71	1.93	1.05	1.32	1.82	1.73
2050B1ACARE	1.22	1.47	0.75	0.94	1.43	1.23

Table B2. Same as Table B1, but due to a 5 % decrease in ship emissions.

	TM4	p-TOMCAT	OsloCTM2	LMDz-INCA	UCI CTM	MOCAGE
2000	4.17	3.44	3.77	3.20	4.28	3.24
2025B1	4.20	3.49	3.96	3.36	4.08	3.27
2050B1	4.38	3.56	4.14	3.51	4.52	3.43

Table B3. Radiative forcings ($mW\,m^{-2}$) from changes in ozone, methane (including stratospheric water vapour), and methane-induced ozone for different years/scenarios, due to emissions from aircraft. Note that the history of emissions has been taken into account, and that the fully scaled perturbations were used.

	TM4				p-TOMCAT				OsloCTM2			
	O_3	CH_4	$O_{3(CH_4)}$	total	O_3	CH_4	$O_{3(CH_4)}$	total	O_3	CH_4	$O_{3(CH_4)}$	total
2025B1	19.8	−17.3	−6.3	−3.8	40.1	−19.3	−7.0	13.8	20.6	−10.6	−3.9	6.2
2050B1	21.1	−18.8	−6.9	−4.5	42.7	−21.6	−7.9	13.2	20.4	−11.5	−4.2	4.7
2025B1ACARE	18.7	−16.6	−6.1	−4.0	38.2	−18.8	−6.9	12.6	20.3	−10.2	−3.7	6.4
2050B1ACARE	15.1	−14.8	−5.4	−5.2	31.4	−17.8	−6.5	7.1	14.6	−9.1	−3.3	2.1
	LMDz-INCA				UCI CTM				MOCAGE			
	O_3	CH_4	$O_{3(CH_4)}$	total	O_3	CH_4	$O_{3(CH_4)}$	total	O_3	CH_4	$O_{3(CH_4)}$	total
2025B1	18.0	−13.3	−4.9	−0.2	26.6	−18.3	−6.7	1.6	29.2	−17.5	−6.4	5.4
2050B1	18.0	−14.5	−5.3	−1.8	28.1	−21.6	−7.9	−1.4	27.2	−18.9	−6.9	1.4
2025B1ACARE	16.9	−12.8	−4.7	−0.6	25.1	−17.7	−6.5	0.9	25.5	−16.8	−6.1	2.5
2050B1ACARE	12.5	−11.4	−4.2	−3.1	19.9	−17.4	−6.4	−3.8	20.1	−14.9	−5.5	−0.3

measurements in the tropics (Søvde et al., 2011). Furthermore, modelling of tropospheric ozone and its precursors is particularly difficult in the tropics due to uncertainties related to convective mixing and lightning parameterizations (e.g. Doherty et al., 2005). At mid- and high latitudes, the UCI CTM model overestimates ozone while there is an underestimation of ozone by p-TOMCAT in the lower troposphere in these regions. As model validation is beyond the scope of this study, interested readers are refered to e.g. van Noije et al. (2006), Shindell et al. (2006) and Dentener et al. (2006) for evaluations of NO_2 columns, CO distributions and deposition budgets, respectively. When interpreting the comparison in Fig. A1, one should be aware that the Logan data are mainly from sondes launched at northern midlatitudes, hence the observations may not be as representative in the tropics and in the Southern Hemisphere. Additionally, the observations are collected from the period 1980–1993, while the models have used emissions from year 2000 and meteorological data from 2003. Nevertheless, Stevenson et al. (2006) found that there have only been minor ozone trends between the Logan data period and year 2000, suggesting that comparisons with Logan data are still meaningful. All in all, we can conclude that the six models are capable of representing atmospheric ozone, and the ensemble mean provides a robust result as individual model errors tend to counterbalance.

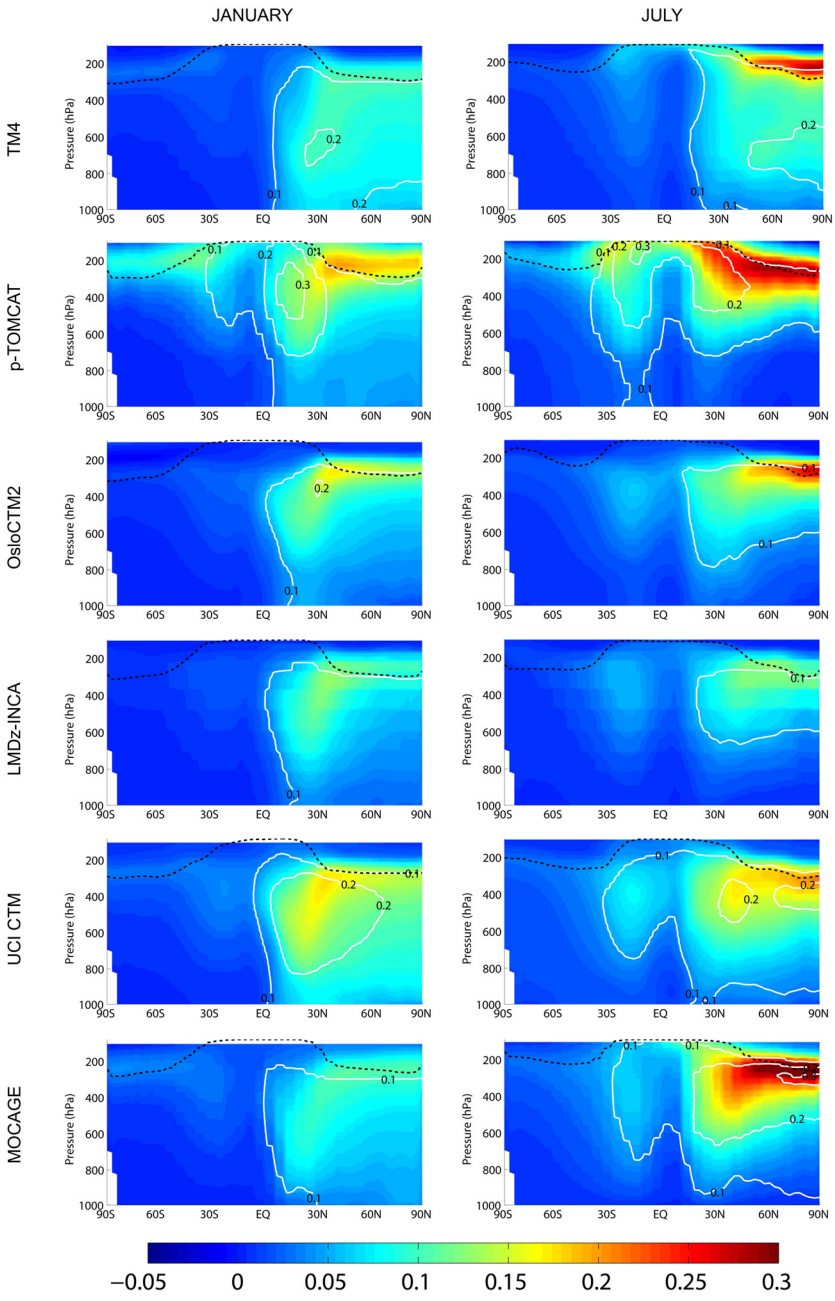

Fig. B1. Zonal mean perturbations of ozone (Δppbv) during January (left) and July (right) for the 2050 B1 scenario, due to a 5 % perturbation of aircraft emissions (simulations BASE – AIR). Solid contour lines show the change relative to the BASE simulation while the dashed line indicates the tropopause.

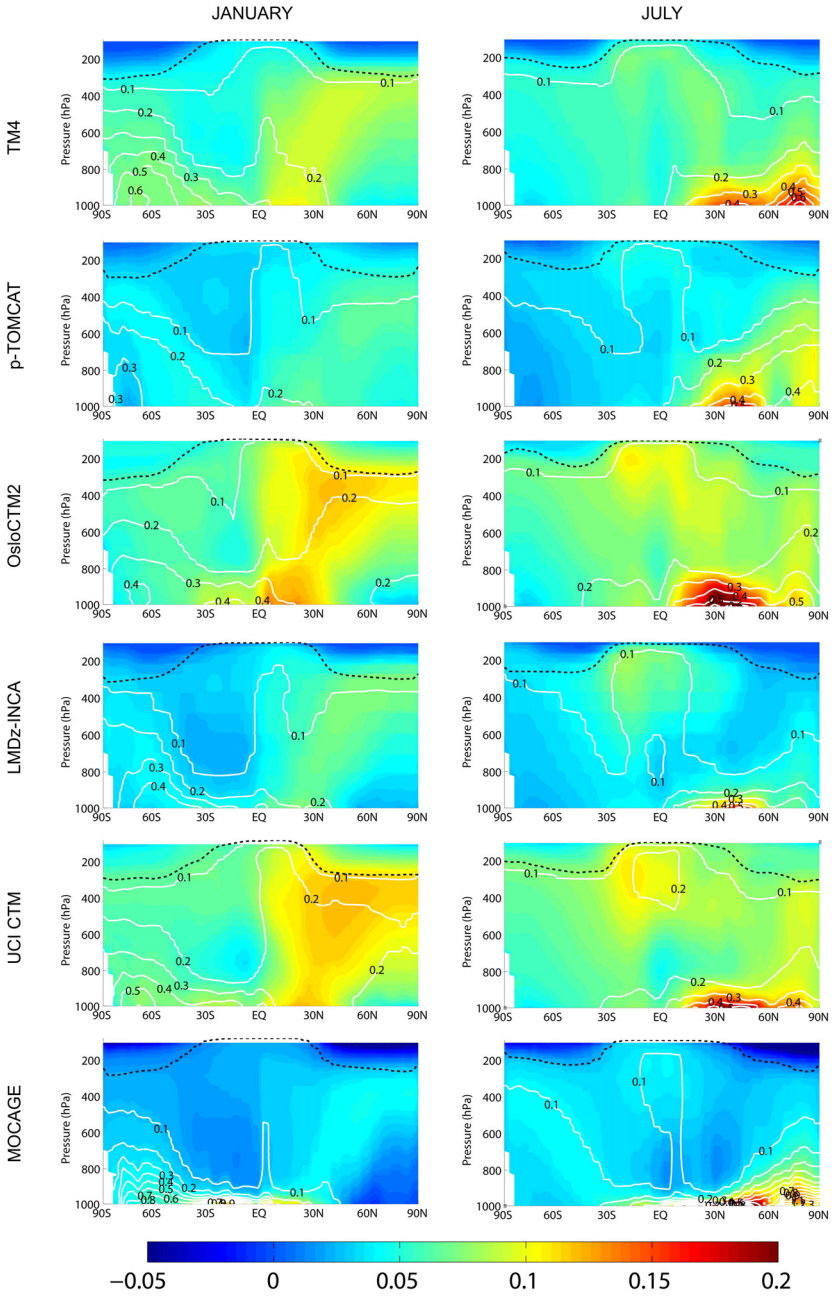

Fig. B2. Same as Fig. B1, but due to a 5 % perturbation of ship emissions (BASE – SHIP).

Table B4. Same as Table B3, but due to emissions from shipping.

	TM4				p-TOMCAT				OsloCTM2			
	O_3	CH_4	$O_{3(CH_4)}$	total	O_3	CH_4	$O_{3(CH_4)}$	total	O_3	CH_4	$O_{3(CH_4)}$	total
2025B1	23.6	−42.6	−15.6	−34.6	19.2	−35.5	−13.0	−29.2	33.9	−40.2	−14.7	−21.0
2050B1	26.9	−45.7	−16.7	−35.5	20.0	−37.2	−13.6	−30.8	35.5	−43.2	−15.8	−23.5
	LMDz-INCA				UCI CTM				MOCAGE			
	O_3	CH_4	$O_{3(CH_4)}$	total	O_3	CH_4	$O_{3(CH_4)}$	total	O_3	CH_4	$O_{3(CH_4)}$	total
2025B1	18.6	−34.1	−12.4	−28.0	33.3	−41.5	−15.2	−23.4	13.3	−33.2	−12.1	−32.0
2050B1	19.6	−36.7	−13.4	−30.4	36.6	−47.2	−17.3	−27.9	12.5	−35.9	−13.1	−36.5

Appendix B

Results from individual models

Individual model results are shown for the 2050 B1 scenario as zonal mean ozone perturbations for AIR and SHIP in Fig. B1 and Fig. B2, respectively. Relative changes in methane lifetimes are listed in Tables B1–B2, and RF calculations are given in Tables B3–B4.

Acknowledgements. This work was funded by the European Union's Sixth Framework Programme (FP6/2002-2006) through the QUANTIFY Integrated Project under contract no. 003893 (GOCE), and through the Network of Excellence ECATS (Project no. ANE4-CT-2005-012284). GM has received funding from the Research Council of Norway through the TEMPO project. Emission data sets were provided by the QUANTIFY partners MMU (aircraft), DNV (shipping), DLR (road traffic) and JRC (other anthropogenic emissions). The authors would like to thank Jens Borken-Kleefeld (IIASA) and Magnus S. Eide (DNV) for their helpful comments on the manuscript.

Edited by: L. Ganzeveld

References

ACARE: Strategic Research Agenda; Advisory Council for Aeronautics Research in Europe, Brussels, 2002.

Andreae, M. O. and Merlet, P.: Emission of trace gases and aerosols from biomass burning, Global Biogeochem. Cy., 15, 955–966, 2001.

Balkanski, Y., Myhre, G., Gauss, M., Rädel, G., Highwood, E. J., and Shine, K. P.: Direct radiative effect of aerosols emitted by transport: from road, shipping and aviation, Atmos. Chem. Phys., 10, 4477–4489, doi:10.5194/acp-10-4477-2010, 2010.

Bechtold, P., Bazile, E., Guichard, F., Mascart, P., and Richard, E.: A mass-flux convection scheme for regional and global models, Q. J. Roy. Meteorol. Soc., 127, 869–886, 2001.

Berntsen, T. K., Isaksen, I. S. A., Myhre, G., Fuglestvedt, J. S., Stordal, F., Larsen, T. A., Freckleton, R. S., and Shine, K. P.: Effects of anthropogenic emissions on tropospheric ozone and its radiative forcing, J. Geophys. Res.-Atmos., 102, 28101–28126, 1997.

Berntsen, T. K., Fuglestvedt, J. S., Joshi, M. M., Shine, K. P., Stuber, N., Ponater, M., Sausen, R., Hauglustaine, D. A., and Li, L.: Response of climate to regional emissions of ozone precursors: sensitivities and warming potentials, Tellus B, 57, 283–304, 2005.

Bian, H. S. and Prather, M. J.: Fast-J2: Accurate simulation of stratospheric photolysis in global chemical models, J. Atmos. Chem., 41, 281–296, doi:10.1023/a:1014980619462, 2002.

Borken, J., Steller, H., Meretei, T., and Vanhove, F.: Global and country inventory of road passenger and freight transportation - Fuel consumption and emissions of air pollutants in year 2000, Transp. Res. Record, 2011, 127–136, doi:10.3141/2011-14, 2007.

Brasseur, G. P., Muller, J. F., and Granier, C.: Atmospheric impact of NOx emissions by subsonic aircraft: A three-dimensional model study, J. Geophys. Res.-Atmos., 101, 1423–1428, 1996.

Burkhardt, U. and Karcher, B.: Global radiative forcing from contrail cirrus, Nat. Clim. Chang., 1, 54–58, doi:10.1038/nclimate1068, 2011.

Cariolle, D., Caro, D., Paoli, R., Hauglustaine, D. A., Cuenot, B., Cozic, A., and Paugam, R.: Parameterization of plume chemistry into large-scale atmospheric models: Application to aircraft NOx emissions, J. Geophys. Res.-Atmos., 114, D19302, doi:10.1029/2009jd011873, 2009.

Carver, G. D. and Stott, P. A.: IMPACT: an implicit time integration scheme for chemical species and families, Ann. Geophys.-Atmos. Hydrospheres Space Sci., 18, 337–346, 2000.

Carver, G. D., Brown, P. D., and Wild, O.: The ASAD atmospheric chemistry integration package and chemical reaction database, Comput. Phys. Commun., 105, 197–215, 1997.

Corbett, J. J. and Koehler, H. W.: Updated emissions from ocean shipping, J. Geophys. Res.-Atmos., 108, 4650–4665, doi:10.1029/2003jd003751, 2003.

Crassier, V., Suhre, K., Tulet, P., and Rosset, R.: Development of a reduced chemical scheme for use in mesoscale meteorological models, Atmos. Environ., 34, 2633–2644, doi:10.1016/s1352-2310(99)00480-x, 2000.

Crutzen, P. J.: Role of the tropics in atmospheric chemistry, in: The Geophysiology of Amazonia, edited by: Dickinson, R. E., John Wiley, New York, 107–130, 1987.

Dalsøren, S. B. and Isaksen, I. S. A.: CTM study of changes in tropospheric hydroxyl distribution 1990-2001 and its impact on methane, Geophys. Res. Lett., 33, L23811, doi:10.1029/2006gl027295, 2006.

Dalsøren, S. B., Eide, M. S., Endresen, Ø., Mjelde, A., Gravir, G., and Isaksen, I. S. A.: Update on emissions and environmental impacts from the international fleet of ships: the contribution from major ship types and ports, Atmos. Chem. Phys., 9, 2171–2194, doi:10.5194/acp-9-2171-2009, 2009.

Dalsøren, S. B., Eide, M. S., Myhre, G., Endresen, O., Isaksen, I. S. A., and Fuglestvedt, J. S.: Impacts of the Large Increase in International Ship Traffic 2000–2007 on Tropospheric Ozone and Methane, Environ. Sci. Technol., 44, 2482–2489, doi:10.1021/es902628e, 2010.

Danilin, M. Y., Fahey, D. W., Schumann, U., Prather, M. J., Penner, J. E., Ko, M. K. W., Weisenstein, D. K., Jackman, C. H., Pitari, G., Kohler, I., Sausen, R., Weaver, C. J., Douglass, A. R., Connell, P. S., Kinnison, D. E., Dentener, F. J., Fleming, E. L., Berntsen, T. K., Isaksen, I. S. A., Haywood, J. M., and Karcher, B.: Aviation fuel tracer simulation: Model intercomparison and implications, Geophys. Res. Lett., 25, 3947–3950, 1998.

Dentener, F., Peters, W., Krol, M., van Weele, M., Bergamaschi, P., and Lelieveld, J.: Interannual variability and trend of CH_4 lifetime as a measure for OH changes in the 1979–1993 time period, J. Geophys. Res.-Atmos., 108, 4442, doi:10.1029/2002jd002916, 2003.

Dentener, F., Drevet, J., Lamarque, J. F., Bey, I., Eickhout, B., Fiore, A. M., Hauglustaine, D., Horowitz, L. W., Krol, M., Kulshrestha, U. C., Lawrence, M., Galy-Lacaux, C., Rast, S., Shindell, D., Stevenson, D., Van Noije, T., Atherton, C., Bell, N., Bergman, D., Butler, T., Cofala, J., Collins, B., Doherty, R., Ellingsen, K., Galloway, J., Gauss, M., Montanaro, V., Muller, J. F., Pitari, G., Rodriguez, J., Sanderson, M., Solmon, F., Strahan, S., Schultz, M., Sudo, K., Szopa, S., and Wild, O.: Nitrogen and sulfur deposition on regional and global scales: A multimodel evaluation, Global Biogeochem. Cy., 20, GB4003, doi:10.1029/2005gb002672, 2006.

Doherty, R. M., Stevenson, D. S., Collins, W. J., and Sanderson, M. G.: Influence of convective transport on tropospheric ozone and its precursors in a chemistry-climate model, Atmos. Chem. Phys., 5, 3205–3218, doi:10.5194/acp-5-3205-2005, 2005.

Duncan, B. N. and Logan, J. A.: Model analysis of the factors regulating the trends and variability of carbon monoxide between 1988 and 1997, Atmos. Chem. Phys., 8, 7389–7403, doi:10.5194/acp-8-7389-2008, 2008.

Eide, M. S., Endresen, O., Mjelde, A., Mangset, L. E., and Gravir, G.: Ship emissions of the future. Technical Report No 2007-1325, Det Norske Veritas, Høvik, Norway, 2007.

Emanuel, K. A.: A scheme for representing cumulus convection in large-scale models, J. Atmos. Sci., 48, 2313–2335, 1991.

Emanuel, K. A.: A cumulus representation based on the episodic mixing model: the importance of mixing and microphysics in predicting humidity, AMS Meteorol. Monogr., 24, 185–192, 1993.

Endresen, O., Sorgard, E., Sundet, J. K., Dalsøren, S. B., Isaksen, I. S. A., Berglen, T. F., and Gravir, G.: Emission from international sea transportation and environmental impact, J. Geophys. Res.-Atmos., 108, 4560, doi:10.1029/2002jd002898, 2003.

Endresen, O., Sorgard, E., Behrens, H. L., Brett, P. O., and Isaksen, I. S. A.: A historical reconstruction of ships' fuel consumption and emissions, J. Geophys. Res.-Atmos., 112, D12301, doi:10.1029/2006jd007630, 2007.

Eyring, V., Kohler, H. W., Lauer, A., and Lemper, B.: Emissions from international shipping: 2. Impact of future technologies on scenarios until 2050, J. Geophys. Res.-Atmos., 110, D17306, doi:10.1029/2004jd005620, 2005.

Eyring, V., Stevenson, D. S., Lauer, A., Dentener, F. J., Butler, T., Collins, W. J., Ellingsen, K., Gauss, M., Hauglustaine, D. A., Isaksen, I. S. A., Lawrence, M. G., Richter, A., Rodriguez, J. M., Sanderson, M., Strahan, S. E., Sudo, K., Szopa, S., van Noije, T. P. C., and Wild, O.: Multi-model simulations of the impact of international shipping on Atmospheric Chemistry and Climate in 2000 and 2030, Atmos. Chem. Phys., 7, 757–780, doi:10.5194/acp-7-757-2007, 2007.

Eyring, V., Isaksen, I. S. A., Berntsen, T., Collins, W. J., Corbett, J. J., Endresen, O., Grainger, R. G., Moldanova, J., Schlager, H., and Stevenson, D. S.: Transport impacts on atmosphere and climate: Shipping, Atmos. Environ., 44, 4735–4771, doi:10.1016/j.atmosenv.2009.04.059, 2010.

Folberth, G. A., Hauglustaine, D. A., Lathière, J., and Brocheton, F.: Interactive chemistry in the Laboratoire de Mtorologie Dynamique general circulation model: model description and impact analysis of biogenic hydrocarbons on tropospheric chemistry, Atmos. Chem. Phys., 6, 2273–2319, doi:10.5194/acp-6-2273-2006, 2006.

Fuglestvedt, J., Berntsen, T., Myhre, G., Rypdal, K., and Skeie, R. B.: Climate forcing from the transport sectors, P. Natl. Acad. Sci. USA, 105, 454–458, doi:10.1073/pnas.0702958104, 2008.

Gauss, M., Isaksen, I. S. A., Wong, S., and Wang, W. C.: Impact of H_2O emissions from cryoplanes and kerosene aircraft on the atmosphere, J. Geophys. Res.-Atmos., 108, 4304, doi:10.1029/2002jd002623, 2003.

Gauss, M., Isaksen, I. S. A., Lee, D. S., and Søvde, O. A.: Impact of aircraft NO_x emissions on the atmosphere – tradeoffs to reduce the impact, Atmos. Chem. Phys., 6, 1529–1548, doi:10.5194/acp-6-1529-2006, 2006.

Grewe, V. and Stenke, A.: AirClim: an efficient tool for climate evaluation of aircraft technology, Atmos. Chem. Phys., 8, 4621–4639, doi:10.5194/acp-8-4621-2008, 2008.

Grewe, V., Dameris, M., Hein, R., Kohler, I., and Sausen, R.: Impact of future subsonic aircraft NOx emissions on the atmospheric composition, Geophys. Res. Lett., 26, 47–50, 1999.

Grewe, V., Stenke, A., Ponater, M., Sausen, R., Pitari, G., Iachetti, D., Rogers, H., Dessens, O., Pyle, J., Isaksen, I. S. A., Gulstad, L., Søvde, O. A., Marizy, C., and Pascuillo, E.: Climate impact of supersonic air traffic: an approach to optimize a potential future supersonic fleet results from the EU-project SCENIC, Atmos. Chem. Phys., 7, 5129–5145, doi:10.5194/acp-7-5129-2007, 2007.

Grewe, V., Tsati, E., and Hoor, P.: On the attribution of contributions of atmospheric trace gases to emissions in atmospheric model applications, Geosci. Model Dev., 3, 487–499, doi:10.5194/gmd-3-487-2010, 2010.

Grooß, J. U., Bruhl, C., and Peter, T.: Impact of aircraft emissions on tropospheric and stratospheric ozone. Part I: Chemistry and 2-D model results, Atmos. Environ., 32, 3173–3184, 1998.

Hansen, J., Sato, M., and Ruedy, R.: Radiative forcing and climate response, J. Geophys. Res.-Atmos., 102, 6831–6864, 1997.

Hauglustaine, D. A., Hourdin, F., Jourdain, L., Filiberti, M. A., Walters, S., Lamarque, J. F., and Holland, E. A.: Interactive chemistry in the Laboratoire de Meteorologie Dynamique general circulation model: Description and background tropospheric

chemistry evaluation, J. Geophys. Res.-Atmos., 109, D04314, doi:10.1029/2003jd003957, 2004.

Hesstvedt, E., Hov, O., and Isaksen, I. S. A.: Quasi-steady-state approximations in air pollution modeling - Comparison of two numerical schemes for oxidant prediction, Int. J. Chem. Kinet., 10, 971–994, 1978.

Hidalgo, H. and Crutzen, P. J.: Tropospheric and stratospheric composition perturbed by NO_x emissions of high-altitude aircraft, J. Geophys. Res.-Oceans, 82, 5833–5866, 1977.

Hoor, P., Borken-Kleefeld, J., Caro, D., Dessens, O., Endresen, O., Gauss, M., Grewe, V., Hauglustaine, D., Isaksen, I. S. A., Jöckel, P., Lelieveld, J., Myhre, G., Meijer, E., Olivie, D., Prather, M., Schnadt Poberaj, C., Shine, K. P., Staehelin, J., Tang, Q., van Aardenne, J., van Velthoven, P., and Sausen, R.: The impact of traffic emissions on atmospheric ozone and OH: results from QUANTIFY, Atmos. Chem. Phys., 9, 3113–3136, doi:10.5194/acp-9-3113-2009, 2009.

Hourdin, F. and Armengaud, A.: The use of finite-volume methods for atmospheric advection of trace species. Part I: Test of various formulations in a general circulation model, Mon. Weather Rev., 127, 822–837, 1999.

Houweling, S., Dentener, F., and Lelieveld, J.: The impact of nonmethane hydrocarbon compounds on tropospheric photochemistry, J. Geophys. Res.-Atmos., 103, 10673–10696, 1998.

Hsu, J., Prather, M. J., and Wild, O.: Diagnosing the stratosphere-to-troposphere flux of ozone in a chemistry transport model, J. Geophys. Res.-Atmos., 110, D19305, doi:10.1029/2005jd006045, 2005.

Huszar, P., Cariolle, D., Paoli, R., Halenka, T., Belda, M., Schlager, H., Miksovsky, J., and Pisoft, P.: Modeling the regional impact of ship emissions on NO_x and ozone levels over the Eastern Atlantic and Western Europe using ship plume parameterization, Atmos. Chem. Phys., 10, 6645–6660, doi:10.5194/acp-10-6645-2010, 2010.

IPCC: Aviation and the Global Atmosphere, edited by: Penner, J. E., Lister, D. H., Griggs, D. J., Dokken, D. J., and McFarland, M., Cambridge University Press, Cambridge, United Kingdom and New York, NY, USA, 1999.

IPCC: Climate Change 2001: The Scientific Basis. Contribution of Working Group I to the Third Assessment Report of the Intergovernmental Panel on Climate Change, edited by: Houghton, J. T., Ding, Y., Griggs, D. J., Noguer, M., van der Linden, P. J., Dai, X., Maskell, K., and Johnson, C. A., Cambridge University Press, Cambridge, United Kingdom and New York, NY, USA., 881 pp., 2001.

Isaksen, I. S. A. and Dalsøren, S. B.: Getting a Better Estimate of an Atmospheric Radical, Science, 331, 38–39, doi:10.1126/science.1199773, 2011.

Jöckel, P., Tost, H., Pozzer, A., Brühl, C., Buchholz, J., Ganzeveld, L., Hoor, P., Kerkweg, A., Lawrence, M. G., Sander, R., Steil, B., Stiller, G., Tanarhte, M., Taraborrelli, D., van Aardenne, J., and Lelieveld, J.: The atmospheric chemistry general circulation model ECHAM5/MESSy1: consistent simulation of ozone from the surface to the mesosphere, Atmos. Chem. Phys., 6, 5067–5104, doi:10.5194/acp-6-5067-2006, 2006.

Johnson, C., Henshaw, J., and McInnes, G.: Impact of aircraft and surface emissions of nitrogen-oxides on tropospheric ozone and global warming, Nature, 355, 69–71, 1992.

Koffi, B., Szopa, S., Cozic, A., Hauglustaine, D., and van Velthoven, P.: Present and future impact of aircraft, road traffic and shipping emissions on global tropospheric ozone, Atmos. Chem. Phys., 10, 11681–11705, doi:10.5194/acp-10-11681-2010, 2010.

Kraabøl, A. G., Berntsen, T. K., Sundet, J. K., and Stordal, F.: Impacts of NOx emissions from subsonic aircraft in a global three-dimensional chemistry transport model including plume processes, J. Geophys. Res.-Atmos., 107, 4655, doi:10.1029/2001jd001019, 2002.

Lacis, A. A., Wuebbles, D. J., and Logan, J. A.: Radiative forcing of climate by changes in the vertical-distribution of ozone, J. Geophys. Res.-Atmos., 95, 9971–9981, 1990.

Law, K. S., Plantevin, P. H., Shallcross, D. E., Rogers, H. L., Pyle, J. A., Grouhel, C., Thouret, V., and Marenco, A.: Evaluation of modeled O-3 using Measurement of Ozone by Airbus In-Service Aircraft (MOZAIC) data, J. Geophys. Res.-Atmos., 103, 25721–25737, 1998.

Law, K. S., Plantevin, P. H., Thouret, V., Marenco, A., Asman, W. A. H., Lawrence, M., Crutzen, P. J., Muller, J. F., Hauglustaine, D. A., and Kanakidou, M.: Comparison between global chemistry transport model results and Measurement of Ozone and Water Vapor by Airbus In-Service Aircraft (MOZAIC) data, J. Geophys. Res.-Atmos., 105, 1503–1525, 2000.

Lawrence, M. G. and Crutzen, P. J.: Influence of NOx emissions from ships on tropospheric photochemistry and climate, Nature, 402, 167–170, 1999.

Le Treut, H., Forichon, M., Boucher, O., and Li, Z. X.: Sulfate aerosol indirect effect and CO2 greenhouse forcing: Equilibrium response of the LMD GCM and associated cloud feedbacks, J. Clim., 11, 1673–1684, 1998.

Lee, D. S., Fahey, D. W., Forster, P. M., Newton, P. J., Wit, R. C. N., Lim, L. L., Owen, B., and Sausen, R.: Aviation and global climate change in the 21st century, Atmos. Environ., 43, 3520–3537, doi:10.1016/j.atmosenv.2009.04.024, 2009.

Lee, D. S., Pitari, G., Grewe, V., Gierens, K., Penner, J. E., Petzold, A., Prather, M. J., Schumann, U., Bais, A., Berntsen, T., Iachetti, D., Lim, L. L., and Sausen, R.: Transport impacts on atmosphere and climate: Aviation, Atmos. Environ., 44, 4678–4734, doi:10.1016/j.atmosenv.2009.06.005, 2010.

Lefèvre, F., Brasseur, G. P., Folkins, I., Smith, A. K., and Simon, P.: Chemistry of the 1991-1992 stratospheric winter: Three-dimensional model simulations, J. Geophys. Res., 99, 8183–8195, doi:10.1029/93jd03476, 1994.

Lelieveld, J., Peters, W., Dentener, F. J., and Krol, M. C.: Stability of tropospheric hydroxyl chemistry, J. Geophys. Res.-Atmos., 107, 4715, doi:10.1029/2002jd002272, 2002.

Lelieveld, J., Brenninkmeijer, C. A. M., Joeckel, P., Isaksen, I. S. A., Krol, M. C., Mak, J. E., Dlugokencky, E., Montzka, S. A., Novelli, P. C., Peters, W., and Tans, P. P.: New Directions: Watching over tropospheric hydroxyl (OH), Atmos. Environ., 40, 5741–5743, doi:10.1016/j.atmosenv.2006.04.008, 2006.

Logan, J. A.: An analysis of ozonesonde data for the troposphere: Recommendations for testing 3-D models and development of a gridded climatology for tropospheric ozone, J. Geophys. Res., 104, 16115–16149, doi:10.1029/1998jd100096, 1999.

Luo, B., Carslaw, K. S., Peter, T., and Clegg, S. L.: Vapour pressures of $H_2SO_4/HNO_3/HCl/HBr/H_2O$ solutions to low stratospheric temperatures, Geophys. Res. Lett., 22, 247–250, doi:10.1029/94gl02988, 1995.

Meijer, E. W., van Velthoven, P. F. J., Brunner, D. W., Huntrieser, H., and Kelder, H.: Improvement and evaluation of the parameterisation of nitrogen oxide production by lightning, Phys. Chem. Earth Pt. C-Solar-Terr. Planet. Sci., 26, 577–583, 2001.

Montzka, S. A., Krol, M., Dlugokencky, E., Hall, B., Jöckel, P., and Lelieveld, J.: Small Interannual Variability of Global Atmospheric Hydroxyl, Science, 331, 67–69, doi:10.1126/science.1197640, 2011.

Myhre, G., Karlsdottir, S., Isaksen, I. S. A., and Stordal, F.: Radiative forcing due to changes in tropospheric ozone in the period 1980 to 1996, J. Geophys. Res.-Atmos., 105, 28935–28942, 2000.

Myhre, G., Nilsen, J. S., Gulstad, L., Shine, K. P., Rognerud, B., and Isaksen, I. S. A.: Radiative forcing due to stratospheric water vapour from CH_4 oxidation, Geophys. Res. Lett., 34, L01807, doi:10.1029/2006gl027472, 2007.

Myhre, G., Shine, K. P., Rädel, G., Gauss, M., Isaksen, I. S. A., Tang, Q., Prather, M. J., Williams, J. E., van Velthoven, P., Dessens, O., Koffi, B., Szopa, S., Hoor, P., Grewe, V., Borken-Kleefeld, J., Berntsen, T. K., and Fuglestvedt, J. S.: Radiative forcing due to changes in ozone and methane caused by the transport sector, Atmos. Environ., 45, 387–394, doi:10.1016/j.atmosenv.2010.10.001, 2011.

Nakicenovic, N., Davidson, O., Davis, G., Grübler, A., Kram, T., La Rovere, E. L., Metz, B., Morita, T., Pepper, W., Pitcher, H., Sankovski, A., Shukla, P., Swart, R., Watson, R., and Dadi, Z.: Special Report on Emissions Scenarios, Cambridge University Press, Cambridge, 599 pp., 2000.

O'Connor, F. M., Carver, G. D., Savage, N. H., Pyle, J. A., Methven, J., Arnold, S. R., Dewey, K., and Kent, J.: Comparison and visualisation of high-resolution transport modelling with aircraft measurements, Atmos. Sci. Lett., 6, 164–170, doi:10.1002/asl.111, 2005.

Olivier, J. G. J., Van Aardenne, J. A., Dentener, F., Ganzeveld, L., and Peters, J. A. H. W.: Recent trends in global greenhouse gas emissions: regional trends and spatial distribution of key sources, in: Non-CO2 Greenhouse Gases (NCGG-4), Millpress, Rotterdam, 325–330, 2005.

Owen, B., Lee, D. S., and Lim, L.: Flying into the Future: Aviation Emissions Scenarios to 2050, Environ. Sci. Technol., 44, 2255-2260, doi:10.1021/es902530z, 2010.

Prather, M. J.: Numerical advection by conservation of 2nd-order moments, J. Geophys. Res.-Atmos., 91, 6671–6681, 1986.

Prather, M. J. and Hsu, J.: Coupling of Nitrous Oxide and Methane by Global Atmospheric Chemistry, Science, 330, 952–954, doi:10.1126/science.1196285, 2010.

Prather, M. J., Zhu, X., Tang, Q., Hsu, J., and Neu, J. L.: An atmospheric chemist in search of the tropopause, J. Geophys. Res., 116, D04306, doi:10.1029/2010JD014939, 2011.

Price, C. and Rind, D.: A simple lightning parameterization for calculating global lightning distributions, J. Geophys. Res.-Atmos., 97, 9919–9933, 1992.

Ramanathan, V. and Dickinson, R. E.: Role of stratospheric ozone in the zonal and seasonal radiative energy-balance of the Earth-troposphere system, J. Atmos. Sci., 36, 1084–1104, 1979.

Rogers, H., Teyssèdre, H., Pitari, G., Grewe, V., van Velthoven, P., and Sundet, J.: Model intercomparison of the transport of aircraft-like emissions from sub- and supersonic aircraft, Meteorol. Z., 11, 151–159, doi:10.1127/0941-2948/2002/0011-0151, 2002.

Russell, G. L. and Lerner, J. A.: A new finite-differencing scheme for the tracer transport-equation, J. Appl. Meteorol., 20, 1483–1498, 1981.

Sander, S. P., Orkin, V. L., Kurylo, M. J., Golden, D. M., Barker, J. R., Huie, R. E., Kolb, C. E., Abbatt, J. P. D., Friedl, R. R., Burkholder, J. B., Moortgat, G. K., and Wine, P. H.: Chemical kinetics and photochemical data for use in atmospheric studies, JPL Publication 06–2, NASA/JPL, Jet Propulsion Laboratory, California Institute of Technology, Pasadena, California, Evaluation Number 15, 2006.

Sausen, R., Isaksen, I., Grewe, V., Hauglustaine, D., Lee, D. S., Myhre, G., Kohler, M. O., Pitari, G., Schumann, U., Stordal, F., and Zerefos, C.: Aviation radiative forcing in 2000: An update on IPCC (1999), Meteorol. Z., 14, 555–561, doi:10.1127/0941-2948/2005/0049, 2005.

Savage, N. H., Law, K. S., Pyle, J. A., Richter, A., Nüß, H., and Burrows, J. P.: Using GOME NO_2 satellite data to examine regional differences in TOMCAT model performance, Atmos. Chem. Phys., 4, 1895–1912, doi:10.5194/acp-4-1895-2004, 2004.

Schnadt Poberaj, C., Staehelin, J., Bintania, R., van Velthoven, P., Dessens, O., Gauss, M., Isaksen, I. S. A., Grewe, V., Jöckel, P., Hoor, P., Koffi, B., Hauglustaine, D., and Olivié, D.: QUANTIFY model evaluation of global chemistry models: carbon monoxide, Proceedings of the 2nd International Conference on Transport, Atmosphere and Climate, DLR Forschungsbericht 2010-10, ISSN 1434-8454,163-168, 2010,

Schumann, U.: The impact of nitrogen oxides emissions from aircraft upon the atmosphere at flight altitudes - Results from the AERONOX project, Atmos. Environ., 31, 1723–1733, 1997.

Schumann, U. and Huntrieser, H.: The global lightning-induced nitrogen oxides source, Atmos. Chem. Phys., 7, 3823–3907, doi:10.5194/acp-7-3823-2007, 2007.

Schumann, U., Schlager, H., Arnold, F., Ovarlez, J., Kelder, H., Hov, O., Hayman, G., Isaksen, I. S. A., Staehelin, J., and Whitefield, P. D.: Pollution from aircraft emissions in the North Atlantic flight corridor: Overview on the POLINAT projects, J. Geophys. Res.-Atmos., 105, 3605–3631, 2000.

Shindell, D. T., Faluvegi, G., Bell, N., and Schmidt, G. A.: An emissions-based view of climate forcing by methane and tropospheric ozone, Geophys. Res. Lett., 32, L04803, doi:10.1029/2004gl021900, 2005.

Shindell, D. T., Faluvegi, G., Stevenson, D. S., Krol, M. C., Emmons, L. K., Lamarque, J. F., Petron, G., Dentener, F. J., Ellingsen, K., Schultz, M. G., Wild, O., Amann, M., Atherton, C. S., Bergmann, D. J., Bey, I., Butler, T., Cofala, J., Collins, W. J., Derwent, R. G., Doherty, R. M., Drevet, J., Eskes, H. J., Fiore, A. M., Gauss, M., Hauglustaine, D. A., Horowitz, L. W., Isaksen, I. S. A., Lawrence, M. G., Montanaro, V., Muller, J. F., Pitari, G., Prather, M. J., Pyle, J. A., Rast, S., Rodriguez, J. M., Sanderson, M. G., Savage, N. H., Strahan, S. E., Sudo, K., Szopa, S., Unger, N., van Noije, T. P. C., and Zeng, G.: Multimodel simulations of carbon monoxide: Comparison with observations and projected near-future changes, J. Geophys. Res.-Atmos., 111, D19306, doi:10.1029/2006jd007100, 2006.

Skeie, R. B., Fuglestvedt, J., Berntsen, T., Lund, M. T., Myhre, G., and Rypdal, K.: Global temperature change from the transport sectors: Historical development and future scenarios, Atmos.

Environ., 43, 6260–6270, doi:10.1016/j.atmosenv.2009.05.025, 2009.

Søvde, O. A., Gauss, M., Isaksen, I. S. A., Pitari, G., and Marizy, C.: Aircraft pollution – a futuristic view, Atmos. Chem. Phys., 7, 3621–3632, doi:10.5194/acp-7-3621-2007, 2007.

Søvde, O. A., Gauss, M., Smyshlyaev, S. P., and Isaksen, I. S. A.: Evaluation of the chemical transport model Oslo CTM2 with focus on arctic winter ozone depletion, J. Geophys. Res.-Atmos., 113, D09304, doi:10.1029/2007jd009240, 2008.

Søvde, O. A., Hoyle, C. R., Myhre, G., and Isaksen, I. S. A.: The HNO_3 forming branch of the HO_2 + NO reaction: pre-industrial-to-present trends in atmospheric species and radiative forcings, Atmos. Chem. Phys., 11, 8929–8943, doi:10.5194/acp-11-8929-2011, 2011.

Stevenson, D. S., Doherty, R. M., Sanderson, M. G., Collins, W. J., Johnson, C. E., and Derwent, R. G.: Radiative forcing from aircraft NOx emissions: Mechanisms and seasonal dependence, J. Geophys. Res.-Atmos., 109, D17307, doi:10.1029/2004jd004759, 2004.

Stevenson, D. S., Dentener, F. J., Schultz, M. G., Ellingsen, K., van Noije, T. P. C., Wild, O., Zeng, G., Amann, M., Atherton, C. S., Bell, N., Bergmann, D. J., Bey, I., Butler, T., Cofala, J., Collins, W. J., Derwent, R. G., Doherty, R. M., Drevet, J., Eskes, H. J., Fiore, A. M., Gauss, M., Hauglustaine, D. A., Horowitz, L. W., Isaksen, I. S. A., Krol, M. C., Lamarque, J. F., Lawrence, M. G., Montanaro, V., Muller, J. F., Pitari, G., Prather, M. J., Pyle, J. A., Rast, S., Rodriguez, J. M., Sanderson, M. G., Savage, N. H., Shindell, D. T., Strahan, S. E., Sudo, K., and Szopa, S.: Multimodel ensemble simulations of present-day and near-future tropospheric ozone, J. Geophys. Res.-Atmos., 111, D08301, doi:10.1029/2005jd006338, 2006.

Stockwell, W. R., Kirchner, F., Kuhn, M., and Seefeld, S.: A new mechanism for regional atmospheric chemistry modeling, J. Geophys. Res., 102, 25847–25879, doi:10.1029/97jd00849, 1997.

Tang, Q. and Prather, M. J.: Correlating tropospheric column ozone with tropopause folds: the Aura-OMI satellite data, Atmos. Chem. Phys., 10, 9681–9688, doi:10.5194/acp-10-9681-2010, 2010.

Tang, Q., Prather, M. J., and Hsu, J.: Stratosphere-troposphere exchange ozone flux related to deep convection, Geophys. Res. Lett., 38, L03806, doi:10.1029/2010gl046039, 2011.

Teyssèdre, H., Michou, M., Clark, H. L., Josse, B., Karcher, F., Olivié, D., Peuch, V.-H., Saint-Martin, D., Cariolle, D., Attié, J.-L., Nédélec, P., Ricaud, P., Thouret, V., van der A, R. J., Volz-Thomas, A., and Chéroux, F.: A new tropospheric and stratospheric Chemistry and Transport Model MOCAGE-Climat for multi-year studies: evaluation of the present-day climatology and sensitivity to surface processes, Atmos. Chem. Phys., 7, 5815–5860, doi:10.5194/acp-7-5815-2007, 2007.

Tiedtke, M.: A comprehensive mass flux scheme for cumulus parameterization in large-scale models, Mon. Weather Rev., 117, 1779–1800, 1989.

Uherek, E., Halenka, T., Borken-Kleefeld, J., Balkanski, Y., Berntsen, T., Borrego, C., Gauss, M., Hoor, P., Juda-Rezler, K., Lelieveld, J., Melas, D., Rypdal, K., and Schmid, S.: Transport impacts on atmosphere and climate: Land transport, Atmos. Environ., 44, 4772–4816, doi:10.1016/j.atmosenv.2010.01.002, 2010.

van Aardenne, J. A., Dentener, F. D., Olivier, J. G. J., Peters, J. A. H. W., and Ganzeveld, L. N.: The EDGAR 3.2 Fast Track 2000 dataset (32FT2000), available at: http://themasites.pbl.nl/images/Description_of_EDGAR_32FT2000(v8)_tcm61-46462.pdf, Joint Research Center, Institute for Environment and Sustainability (JRC-IES), Climate Change Unit, Ispra, Italy, 2005.

van der Werf, G. R., Randerson, J. T., Giglio, L., Collatz, G. J., Kasibhatla, P. S., and Arellano Jr., A. F.: Interannual variability in global biomass burning emissions from 1997 to 2004, Atmos. Chem. Phys., 6, 3423–3441, doi:10.5194/acp-6-3423-2006, 2006.

Van Leer, B.: Towards the ultimate conservative difference scheme. IV. A new approach to numerical convection, J. Comput. Phys., 23, 276–299, doi:10.1016/0021-9991(77)90095-x, 1977.

van Noije, T. P. C., Eskes, H. J., Dentener, F. J., Stevenson, D. S., Ellingsen, K., Schultz, M. G., Wild, O., Amann, M., Atherton, C. S., Bergmann, D. J., Bey, I., Boersma, K. F., Butler, T., Cofala, J., Drevet, J., Fiore, A. M., Gauss, M., Hauglustaine, D. A., Horowitz, L. W., Isaksen, I. S. A., Krol, M. C., Lamarque, J.-F., Lawrence, M. G., Martin, R. V., Montanaro, V., Müller, J.-F., Pitari, G., Prather, M. J., Pyle, J. A., Richter, A., Rodriguez, J. M., Savage, N. H., Strahan, S. E., Sudo, K., Szopa, S., and van Roozendael, M.: Multi-model ensemble simulations of tropospheric NO2 compared with GOME retrievals for the year 2000, Atmos. Chem. Phys., 6, 2943–2979, doi:10.5194/acp-6-2943-2006, 2006.

Wang, W. C. and Sze, N. D.: Coupled effects of atmospheric N_2O and O_3 on the Earth's climate, Nature, 286, 589–590, 1980.

Wild, O., Zhu, X., and Prather, M. J.: Fast-j: Accurate simulation of in- and below-cloud photolysis in tropospheric chemical models, J. Atmos. Chem., 37, 245–282, 2000.

Wild, O., Sundet, J. K., Prather, M. J., Isaksen, I. S. A., Akimoto, H., Browell, E. V., and Oltmans, S. J.: Chemical transport model ozone simulations for spring 2001 over the western Pacific: Comparisons with TRACE-P lidar, ozonesondes, and Total Ozone Mapping Spectrometer columns, J. Geophys. Res.-Atmos., 108, 8826, doi:10.1029/2002jd003283, 2003.

Williams, J. E. and van Noije, T. P. C.: On the updating of the modified Carbon Bond Mechanism IV for use in global Chemistry Transport Models, KNMI Scientific Report WR 2008-02, De Bilt, The Netherlands, 64 pp., 2008.

Williams, J. E., Scheele, M. P., van Velthoven, P. F. J., Thouret, V., Saunois, M., Reeves, C. E., and Cammas, J.-P.: The influence of biomass burning and transport on tropospheric composition over the tropical Atlantic Ocean and Equatorial Africa during the West African monsoon in 2006, Atmos. Chem. Phys., 10, 9797–9817, doi:10.5194/acp-10-9797-2010, 2010.

Williamson, D. L. and Rasch, P. J.: Two-dimensional semi-lagrangian transport with shape-preserving interpolation, Mon. Weather Rev., 117, 102–129, 1989.

Yurganov, L. N., Duchatelet, P., Dzhola, A. V., Edwards, D. P., Hase, F., Kramer, I., Mahieu, E., Mellqvist, J., Notholt, J., Novelli, P. C., Rockmann, A., Scheel, H. E., Schneider, M., Schulz, A., Strandberg, A., Sussmann, R., Tanimoto, H., Velazco, V., Drummond, J. R., and Gille, J. C.: Increased Northern Hemispheric carbon monoxide burden in the troposphere in 2002 and 2003 detected from the ground and from space, Atmos. Chem. Phys., 5, 563–573, doi:10.5194/acp-5-563-2005, 2005.

III

Atmos. Chem. Phys., 11, 11657–11678, 2011
www.atmos-chem-phys.net/11/11657/2011/
doi:10.5194/acp-11-11657-2011

Atmospheric Chemistry and Physics

Air quality trends in Europe over the past decade: a first multi-model assessment

A. Colette[1], C. Granier[2,3,4,5], Ø. Hodnebrog[6], H. Jakobs[7], A. Maurizi[8], A. Nyiri[9], B. Bessagnet[1], A. D'Angiola[2], M. D'Isidoro[8,*], M. Gauss[9], F. Meleux[1], M. Memmesheimer[7], A. Mieville[10], L. Rouïl[1], F. Russo[8], S. Solberg[11], F. Stordal[6], and F. Tampieri[8]

[1]Institut National de l'Environnement Industriel et des Risques (INERIS), Verneuil-en-Halatte, France
[2]Université Paris 6 Pierre et Marie Curie, CNRS-INSU, LATMOS-IPSL, Paris, France
[3]NOAA Earth System Research Laboratory, Boulder, CO, USA
[4]Cooperative Institute for Research in Environmental Sciences, University of Colorado, Boulder, CO, USA
[5]Max Planck Institute for Meteorology, Hamburg, Germany
[6]Universitetet i Oslo (UiO), Oslo, Norway
[7]Rhenish Institute for Environmental Research at the University of Cologne (FRIUUK), Köln, Germany
[8]Institute of Atmospheric Sciences and Climate, Consiglio Nazionale Delle Ricerche, Bologna, Italy
[9]Meteorologisk institutt (met.no), Oslo, Norway
[10]Laboratoire d'Aerologie, Toulouse, France
[11]Norsk Institutt for Luftforskning (NILU), Oslo, Norway
[*]now at: ENEA, Bologna, Italy

Received: 16 June 2011 – Published in Atmos. Chem. Phys. Discuss.: 4 July 2011
Revised: 19 October 2011 – Accepted: 30 October 2011 – Published: 22 November 2011

Abstract. We discuss the capability of current state-of-the-art chemistry and transport models to reproduce air quality trends and interannual variability. Documenting these strengths and weaknesses on the basis of historical simulations is essential before the models are used to investigate future air quality projections. To achieve this, a coordinated modelling exercise was performed in the framework of the CityZEN European Project. It involved six regional and global chemistry-transport models (BOLCHEM, CHIMERE, EMEP, EURAD, OSLOCTM2 and MOZART) simulating air quality over the past decade in the Western European anthropogenic emissions hotspots.

Comparisons between models and observations allow assessing the skills of the models to capture the trends in basic atmospheric constituents (NO_2, O_3, and PM_{10}). We find that the trends of primary constituents are well reproduced (except in some countries – owing to their sensitivity to the emission inventory) although capturing the more moderate trends of secondary species such as O_3 is more challenging. Apart from the long term trend, the modelled monthly variability is consistent with the observations but the year-to-year variability is generally underestimated.

A comparison of simulations where anthropogenic emissions are kept constant is also investigated. We find that the magnitude of the emission-driven trend exceeds the natural variability for primary compounds. We can thus conclude that emission management strategies have had a significant impact over the past 10 yr, hence supporting further emission reductions.

Correspondence to: A. Colette
(augustin.colette@ineris.fr)

1 Introduction

Air quality (AQ) management is an essential aspect of environmental policy. Since the major pollution smog events that occurred in the United Kingdom in the 1950s, the awareness of policy makers, economical stakeholders and the general public kept increasing at a steady pace over the last decades. The issue soon became the focus of international negotiations as it appeared that polluting activities in a given country could have a significant impact on the air quality of its neighbours – making internationally coordinated management strategies more relevant at the regional scale. In addition, the need for coordinated political actions was further

justified as it became obvious that the economic cost of innovative technologies and stringent management policies to control pollutant emissions in the competitive and interrelated economic context should be shared and optimised at the European level. Scientific collaboration and multilateral policy negotiation led thus to the 1979 Convention on Long-range Transboundary Air Pollution (LRTAP) and its Gothenburg Protocol accepted in 1999 (UNECE, 1999) as well as the EU National Emissions Ceiling (NEC) Directive (EC, 2001). In 2005, the European Commission published its Thematic Strategy on Air Pollution under the 6th Environmental Action Programme: The Clean Air For Europe (CAFE, 2005) programme has established a long-term policy strategy targeting the adverse effects of air pollution on human health and environment. It determined a set of objectives to be reached within the ongoing revision of the Gothenburg protocol and the NEC directive. Therefore, it is now timely to assess the actual efficiency of the adopted control measures on air quality trends.

European Air Quality management caused the development of operational air pollution monitoring networks throughout the whole of Europe. Such regulatory AQ monitoring networks started in the 1990s, and the observed records are now long enough to assess trends. These initiatives have been accompanied by a number of scientific programmes aimed at improving our understanding of processes playing a role in air quality. Complex numerical models designed to capture air quality variability have been built, and these models reflect our understanding and ability to simulate atmospheric physical and chemical processes. Hence, we now have the suitable tools and observational data for a detailed assessment of our capability to reproduce current atmospheric pollution trends and assess the efficiency of existing control strategies.

Furthermore, the changing economic and industrial context requires periodical revisions of regulations. Currently, the compatibility of climate and air quality policies is questioned and it is unclear whether current mitigation strategies will be as efficient as expected a few decades ahead. Similar impact assessment studies were performed in the context of previous negotiations (Gothenburg Protocol and EC Directive). But uncertainties in emission projections and modelling were high and the actual impact of adopted policies was not correctly foreseen. In the present phase of revision of the emission control legislation, it is thus essential to ensure that current chemistry transport models used to assess the impact of future projections can capture air quality trends and variability over the past decade.

The goal of the present paper is thus to investigate air quality trends and verify if the processes involved are suitably reproduced in existing chemistry and transport models in order to assess their strengths and weaknesses in dealing with policy-related issues such as the impact of future emission projections. To address this question, a coordinated modelling exercise was conducted in the context of the CityZen Project (megaCITY – Zoom for the Environment, http://www.cityzen-project.eu/) funded by the Seventh European Framework Programme for research. The scope was to attempt to reproduce air quality trends in air pollution hotspots with an ensemble of models in order to investigate the performance of existing tools. Six chemistry-transport models were involved: BOLCHEM, CHIMERE, OSLOCTM2, EMEP, EURAD and MOZART, reflecting a variety of approaches: regional or global coverage, online or offline chemistry and transport coupling. Only anthropogenic emissions (based on national totals officially reported within the CLRTAP) were prescribed uniformly for all models while the choice of remaining forcing data (meteorology, biogenic emissions, boundary conditions, etc...) was left open. That way, we ensured the ensemble of simulations would constitute an envelope of trajectories that adequately represents our understanding of the processes involved. The geographical focus is centred on the Western Europe air pollution hotspots constituted by the densely populated cluster of large cities in Benelux, Southern United Kingdom, Western Germany and Northern France. This area was chosen because it is both an area of high emissions and high population exposure. In addition, it offers some degree of homogeneity in terms of economical activities and air pollution regulation trends. The 1998–2007 decade was chosen because of (1) the availability of monitoring data and (2) the robustness of emissions inventories during that period.

This paper is organized as follows: observed air quality trends in the Western European pollution hotspots are investigated in Sect. 2, the modelling setup is presented in Sect. 3 and a short model evaluation is discussed in Sect. 4. The discussion of the capability of the models involved to capture observed trends is detailed in Sect. 5 and the interannual variability is addressed in Sect. 6. Section 7 is devoted to the investigation of the respective roles of anthropogenic emission reduction and meteorological variability on the observed evolution of air pollution.

2 Observed air quality trends

2.1 Scope and available databases

Before proceeding to the assessment of model performance in terms of air quality trend modelling, we present the observational data that will be used as a reference for the model validation. We limited our scope to the comparison to in-situ surface monitoring stations and we left aside total vertical columns derived by satellite (Konovalov et al., 2010) or tropospheric profiles (Thouret et al., 1998; Logan et al., 1999).

Also, we focus only on ozone (O_3), nitrogen dioxide (NO_2) and particulate matter with a diameter smaller than 10 µm (PM_{10}). Since these basic compounds have been regulated for several years, they are widely monitored, so that we can compile a significant dataset of stations offering a good

coverage (including in urban areas) over the past 10 yr. Unfortunately the same does not hold true for $PM_{2.5}$, whereas this metric would have been better suited to investigate trends in human health exposure.

Building a reliable dataset to assess long term trends is a notoriously difficult task. Two main approaches are found in the literature. The first one consists of using a subset of well documented records (Vautard et al., 2006; Løvblad et al., 2004) follow this strategy by focusing on stations of the EMEP network – i.e. records that are specifically designed for trend assessments. But such stations are all located in rural background areas (because they are designed to monitor transboundary fluxes of air pollution) making it impossible to study urban agglomerations (Derwent et al., 2003; Harrison et al., 2008; Ordonez et al., 2005) include urban sites but limit their geographical scope to a given area – making it possible to check the consistency of individual records. Our aim to document trends over a large hotspot of emissions could thus only be fulfilled by using an alternative approach that consists of relying on a much larger set of stations (at the cost of including sites not designed specifically for trend assessment studies). Here we follow an approach similar to (EEA, 2009) or (Konovalov et al., 2010), considering that the hypothetical degradation of the dataset is compensated by its statistical significance (dubious records having less weights on the statistical indicators inferred).

The focus of the present work being a study of anthropogenic emissions hotspots, regulatory air quality monitoring stations constitute the main source of data. These data were obtained through the public database of the European Environmental Agency AIRBASE (http://air-climate.eionet.europa.eu/databases/AIRBASE/, version 3 downloaded in spring 2010).

We also included a few measurements of Sulphate (SO_{4p}), total Nitrate ($NO_{3t} = NO_{3p} + HNO_{3g}$) and total Ammonia ($NH_{4t} = NH_{4p} + NH_{3g}$) (subscripts are defined as follow: "p" for particulate, "g" for gaseous, "t" for total) collected at remote background sites of the EMEP network (Co-operative programme for monitoring and evaluation of the long range transmission of air pollutants in Europe) reported by the parties of the CLRTAP and available through the EBAS repository (http://ebas.nilu.no/). However, we could not gather enough records for a robust assessment of 10-yr trends for these compounds in the emission hotspots. Hence these data will be used exclusively in the model evaluation to discuss the uncertainty of total particulate matter modelling.

2.2 Data filtering

The temporal consistency of the record is a major concern in trend assessment studies. This issue is especially relevant when using surface AQ monitoring stations considering that the networks are often designed for population exposure and regulatory purposes rather than trend assessment. As such, the experimental setup can be modified following a change in the legislation. Monitoring networks have improved significantly since 1998, but unfortunately the present trend assessment has to be based on a fraction of the network that offers a satisfactory coverage of the past decade.

The consistency of the subset used here was ensured using the following three criteria derived from the guidelines of the European Environmental Agency (EEA, 2009):

- the annual coverage should be larger than 75 %;
- at least 8 of the 10 yr between 1998 and 2007 should be recorded;
- a visual screening of each individual record was performed to discard time series with obvious peculiar behaviour. Developing an automated screening algorithm was beyond the scope of the present study. However the subjective character of visual inspection is balanced by a superior capability of detecting a wide spectrum of awkward features. The visual inspection should thus not be considered as a limitation of the present approach as long as the number of discarded records is as small as possible.

The number of selected stations for each constituent and for both the European region (geographic box extending from 12° W to 30° E and 35° N to 65° N) and the Benelux region (1° W–8° E, 48° N–54° N) is given on Table 1. It is noted that the quantitative thresholds on the annual coverage (first two bullet points above) constitute a much more stringent criterion than the subsequent visual inspection.

2.3 Observed trends

The trends observed at each of the selected stations are displayed in Fig. 1 for NO_2, O_3 and PM_{10}. These trends are computed using time series of monthly averages of daily mean values at each individual location. Each record is deseasonalised by removing the average seasonal cycle from the raw monthly record and the slope is then computed using a standard linear least square method. Given the fact that the record is only 10 yr long (in the best case), it was considered un-necessary to implement a more elaborate deseasonalisation procedure. The limited length of the record also led us to focus on linear trends although there are ongoing initiatives to identify change points, piecewise linear or non-linear trends in air quality monitoring (Konovalov et al., 2010; Carslaw et al., 2011). To account for auto-correlation and seasonality, the significance of the trend is assessed with a Mann-Kendall test at the 95 % confidence level (Kendall, 1976; Hipel and McLeod, 2005).

The decrease of NO_2 concentration is quite robust throughout Europe, except in South-Eastern France and Northern Italy plus a couple of isolated stations. It appears on these maps that the average trend is more pronounced at

Table 1. Number of available in-situ surface records obtained from the AIRBASE repository (O_3, NO_2, and PM_{10}) or the EMEP network (SO_2, SO_{4p}, NO_{3t}, and NH_{4t}) before and after applying the quality check criteria, and for both the whole European domain and the Benelux hotspot.

	Europe			Benelux		
	Total available	8 yr with 75 % annual coverage	Passed visual screening	Total available	8 yr with 75 % annual coverage	Passed visual screening
O_3	1855	717	705	339	166	162
NO_2	1997	669	649	354	160	158
PM_{10}	1533	166	164	252	30	30
SO_2	56	38	37	5	0	0
SO_{4p}	54	41	37	3	3	3
NO_{3t}	41	24	22	0	0	0
NH_{4t}	37	25	21	0	0	0

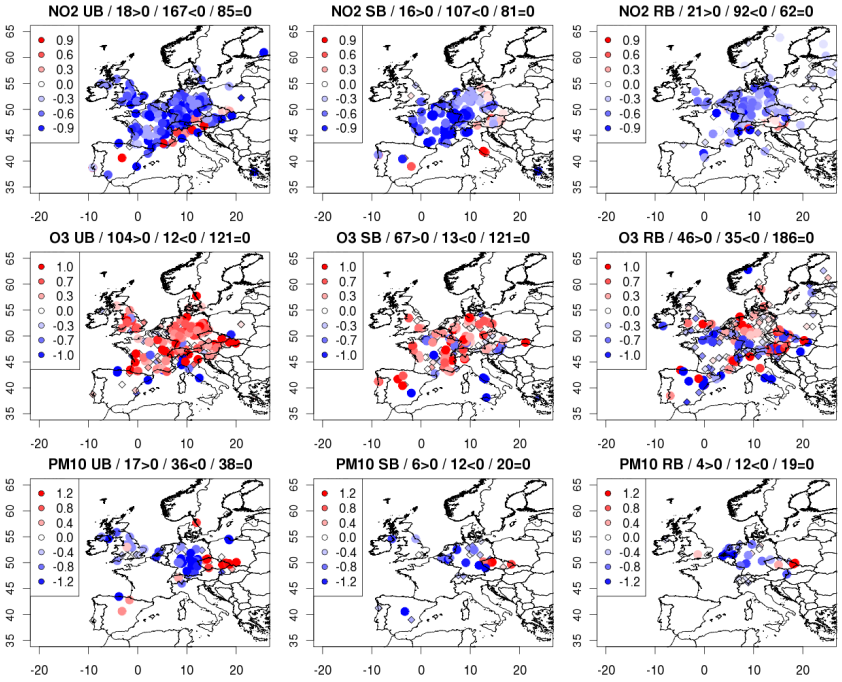

Fig. 1. Trends of daily means of NO_2, O_3, and PM_{10} ($\mu g\,m^{-3}\,yr^{-1}$) observed at urban background (UB), suburban background (SB) and rural background (RB) AIRBASE stations. Stations where a statistically significant trend is observed are shown with a large dot a small diamond is used otherwise. The title of each panel also provides the number of stations with a positive, negative or null (not significant) slope.

urban stations: the median trend for all UB (urban background), SB (suburban background) and RB (rural background) stations are -0.37, -0.27 and $-0.14\,\mu g\,m^{-3}\,yr^{-1}$, respectively. We find an absolute majority of European stations with a significant negative trend: 62 %, 52 % and 53 % (UB, SB and RB), in line with existing studies with similar temporal and geographical focus (Konovalov et al., 2010; Løvblad et al., 2004; Monks et al., 2009).

These decreasing trends for nitrogen dioxide are reflected in the evolution of O_3 where a slight increase is observed especially at urban sites in and around the Benelux region because anthropogenic emissions are high enough so that a decrease of NO_x has primarily an impact on the reduction of night-time titration. Hence we find that the average daily mean O_3 trend at UB, SB and RB sites is 0.37, 0.27 and 0.05 $\mu g\, m^{-3}\, yr^{-1}$, respectively.

The proportion of sites where the O_3 trend is positive is 30.8 % when considering daily means but this number drops to 18.5 % when considering O_3 daily peaks, reflecting qualitatively the findings of (Vautard et al., 2006) as they found an opposite trend for background and peak ozone. We find however a smaller difference than in their study because they focused on a different time period (1990–2002) and on remote EMEP stations.

To summarize, the relatively strong decrease of nitrogen oxides over the past decade was unfortunately not accompanied by a sufficient decrease of the other precursors of ozone, notably VOCs, thus leading to moderate observed increases in background ozone in urban areas. Also, in places such as the Benelux region, this decrease was not strong enough to change the photochemical regimes leading to a predominant role of reduced titration of O_3 as a result of NO_x decrease.

The number of PM_{10} monitoring stations that pass the filtering described in Sect. 2.2 is by far lower than for O_3 or NO_2. For instance in France PM_{10} reporting in AIRBASE started in 2001 and the trend is affected by a change in the metrological correction applied to the measurements in 2007 (Favez et al., 2007) so that no station could be included in the present study. In Germany, UK, and Benelux, PM_{10} concentrations are systematically decreasing, thanks to the air quality regulation enforced during the past decade. However, the trend of total PM_{10} levels-off in Northern Germany and the UK as noted by Harrison et al. (2008). In parts of Spain and the Czech Republic, a positive trend is found. This behaviour was discussed by Braniš (2008) who reported a decrease of PM_{10} during the 1990s due to the economic downturn followed by an increase as a consequence of the increased car traffic in Eastern European countries (of which the Czech Republic is almost the unique representative to pass the filtering of Sect. 2.2).

2.4 Sensitivity of the estimated trend to the filtering

In Sect. 2.2, we required somewhat arbitrarily that selected records should cover at least 8 yr in the 1998–2007 decade. One could however question to what extent the findings reported in this paper are sensitive to that threshold.

The number of stations that would have been selected if we had used a threshold of 5, 6, 7, 8, 9, or 10 yr are provided on Table 2 as well as the corresponding median trend. Here we focus only on stations in the larger Benelux region to enhance the homogeneity of the subset. The most stringent criteria of a minimum coverage of 10 yr would have led to a much smaller subset, hence changing the significance of the set. This is illustrated by looking at the median trend obtained for a 10 yr threshold: it differs from the median obtained with the other thresholds. However it does not mean that it is more representative since the number of stations is lower.

The choice of a 8-yr threshold is further justified by the comparison of the distribution of trends for various thresholds. Figure 2 displays quantile-quantile plots of the distribution of PM_{10} (O_3 and NO_2 not represented for concision purposes) trends in the Benelux area, taking as reference the distribution of de-seasonalised trends covering at least 8 yr over the 1998–2007 decade. It appears that central quantiles are quite insensitive to that threshold, but the tails of the distribution can be dramatically different when using only stations that cover 5, 6, or 10 yr.

A closer look at the median of the distribution of trends (Table 2) shows that strong differences can be found when using different criteria, even if the sign of the trend is quite robust. The table also features the result of the Wilcoxon test (Hollander and Wolfe, 1999) that measures the similarity of two distributions by comparing the rank of individuals (offering a similar yet more quantitative information than the quantile-quantile plot). The p-value of that test is given, it provides the probability that the distribution is similar to the distribution obtained when using all stations covering at least 8 yr. It can be seen that for all three pollutants, using 7, 8 or 9 yr as a threshold yields similar distributions. But using 5, 6, or 10 yr as a threshold would give quite different estimates.

3 Modelling setup

In order to produce an ensemble of models that best represents our ability to capture air quality trends, it was decided to keep the modelling setup as flexible as possible, the only restriction being to use the same emission inventory for anthropogenic emissions. As such, the present experiment is not a model inter-comparison initiative, but rather an attempt to assess the uncertainties in air pollution trend modelling.

3.1 Inventory of anthropogenic emissions

We use the EMEP emission inventory (Vestreng et al., 2005) which is based on official emission data reported by individual countries under the LRTAP convention. This inventory is the most widely used and the only available for the whole decade 1998–2007. When launching the experiment (August 2009) only the 1998–2007 period was available from the website http://www.emep.int. Beyond the European domain (for global CTMs), these emissions are merged into the so-called MACCity inventory (Granier et al., 2011). Several published studies documented the shortcomings of anthropogenic emission inventories in general (Granier et al., 2011; Monks et al., 2009) or for the EMEP inventory in particular (Vestreng et al., 2009; Jonson et al., 2006; Konovalov

Table 2. Sensitivity of the trend computed in the Benelux region to the threshold used in the quality checking procedure. For each minimum number of years covered and each pollutant, we provide the number of available stations, the p-value of the Wilcoxon test of similarity of the distributions compared to the reference (with a 8-yr threshold), and the median of the distribution of the trends at all stations.

	NO_2 # sta.	p-val.	Median trend ($\mu g\,m^{-3}\,yr^{-1}$)	O_3 # sta.	p-val.	Median trend ($\mu g\,m^{-3}\,yr^{-1}$)	PM_{10} # sta.	p-val.	Median trend ($\mu g\,m^{-3}\,yr^{-1}$)
5	194	0.69	−0.343	203	0.91	0.188	91	0.08	−0.228
6	180	0.60	−0.322	186	0.92	0.204	65	0.06	−0.222
7	167	0.87	−0.344	174	0.99	0.204	39	0.91	−0.303
8	158	1	−0.347	162	1	0.204	30	1	−0.290
9	110	0.54	−0.366	132	0.72	0.178	25	0.93	−0.277
10	49	0.33	−0.315	51	0.49	0.203	13	0.46	−0.338

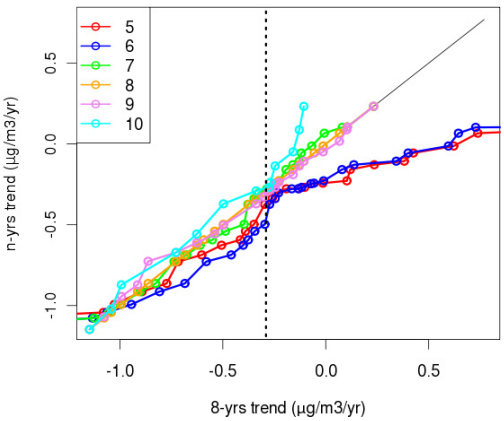

Fig. 2. Comparison of the distributions of PM_{10} trends ($\mu g\,m^{-3}\,yr^{-1}$) in Benelux, depending on the threshold of minimum number of years used in the data quality check procedure (8 yr being used as a reference on the x-axis). The vertical dashed line shows the median of the reference distribution.

et al., 2006). The main advantage of this inventory is that it is built from officially reported national emissions. Nevertheless because of national regulatory issues, some countries might choose not to report emission for given activity sectors, which leads to the problem of data completeness and gap-filling process. In a context of changing regulatory context, this issue is especially relevant for trend assessment. In addition to this issue which is specifically relevant for the EMEP inventories, other shortcomings are well known for any anthropogenic emissions inventory. The injection height or temporal (seasonal or daily) profiles are also an issue. Last but not least, only a few species are reported and hypothesis have to be made regarding the chemical speciation (the ratio between NO and NO_2 amongst the total NO_x, the speciation of primary particulate matter or volatile organic compounds).

In addition to the above shortcomings, a couple of hypothesis had to be made to these emissions to improve their inter-annual consistency. Particulate matter (PM) emitted in North African countries were not reported before 2007, hence they were reset to zero for that year. There are no reported PM emissions over the sea areas in 1999, hence for that year, and over the sea exclusively, we used PM emissions reported for 2000. There are no PM emissions reported in 1998, hence we used PM emissions of 1999. These assumptions will certainly have an impact on the results discussed below, especially over sea surfaces where PM emission are constant during the first three years of the decade.

For each grid point of the inventory we fitted a linear least square regression for the total emissions of PM, NO_x, and non-methane volatile organic compounds, as well as the NMVOC/NO_x ratio and we plotted the map of the slope on Fig. 3. NO_x emissions decreased throughout Europe, except on the ship tracks because of a significant increase of the traffic (Eyring et al., 2010; Endresen et al., 2007). NMVOC decreased also, except in Poland. And the trend in the ratio NMVOC/NO_x shows some interesting patterns with regards to the modelled trends of O_3 that will be discussed later. Note that the trend of primary PM emission is much more variable geographically.

3.2 Chemistry transport models

The main technical characteristics of the four regional and two global chemistry-transport models used in the present study are summarized in Table 3.

3.2.1 BOLCHEM

The BOLCHEM model is developed by the Institute of Atmospheric Sciences and Climate of the Italian National Council of Research. It is an online coupled atmospheric dynamics and composition model. The meteorological part is BOLAM (http://www.isac.cnr.it/~dinamica/bolam) while the composition part deals with gas and aerosol chemistry and

Table 3. Technical characteristics of the chemistry-transport models used in the present study.

		BOLCHEM	CHIMERE	EMEP	EURAD	OSLOCTM2	MOZART 4
Chemical Mechanism	Gas-phase	SAPRC90 (Carter, 1990)	Melchior 2 reduced: 44 species, 120 reactions (Lattuati, 1997).	EMEP (Simpson et al., 1993), with subsequent updates (Simpson et al., 2011)	RADM2, RACM-MIM (Stockwell et al., 1997; Geiger et al., 2003; Karl et al., 2006)	QSSA solver (Hesstvedt et al., 1978) (Berntsen and Isaksen, 1997) for ozone/NO_x/hydrocarbon (51 species, 104 reactions)	MOZART chemical scheme (Emmons et al., 2010)
	Aerosols	Aero3 (Binkowski and Roselle, 2003)	ISORROPIA (equilibrium), 14 aerosols species, 8 size bins (Nenes et al., 1998)	EQSAM (Metzger et al., 2002)	MADE/SORGAM (Ackermann et al., 1998; Schell et al., 2001)	M7 aerosol model (Vignati et al., 2004) for BC/OC, sea salt, dust and sulfate. Nitrate according to Myhre et al. (2006)	MOZART aerosol scheme (Emmons et al., 2010), includes BC/OC, Sulphate, Nitrate, Secondary Organic aerosols
Geometry	Modelling domain (resolution)	Europe (0.5 deg)	Europe (0.5 deg)	Europe (50 km)	Europe (50 km)	Global (T42, ∼2.81 deg)	Global (T63, ∼1.8 deg)
	Number of vertical levels (min, max)	16 (40 m a.g.l.–500 hPa)	8 (30 m a.g.l.–500 hPa)	20 (90 m a.g.l.–100 hPa)	23 (20 m a.g.l.–100 hPa)	60 (8 m a.g.l.–0.1 hPa)	28
Meteorology	Mesoscale model	Hydrostatic limited area model BOLAM coupled online with atmospheric composition modules (Buzzi et al., 1994)	WRF v3.2.1. (Skamarock et al., 2008). Simulations compliant with the CORDEX requirements (Giorgi et al., 2009)	PARLAM-PS (for 1998–2006), HIRLAM (2007) (Undén et al., 2003)	MM5 (Grell et al., 1994)	N/A	N/A
	Large scale Forcing	ERA-interim.	ERA-Interim	IFS (ECMWF) run in-house with data assimilation	NCEP/GFS	IFS (ECMWF) run in-house with data assimilation	NCEP/NCAR analyses
Boundary Conditions		LMDz-INCA monthly climatology (1997–2001) (Hauglustaine et al., 2004)	LMDz-INCA monthly climatology (1997–2001) (Hauglustaine et al., 2004)	O_3: observation-based climatology modulated by potential vorticity, latitude and inter-annually (Logan, 1999)	O_3: observation-based climatology modulated inter-annually (Logan, 1999)	N/A	N/A
Biogenic emissions		Isoprene, monoterpenes and other VOCs computed according to Symeonidis et al. (2008)	MEGAN v. 2.04 (Guenther et al., 2006)	Isoprene computed according to Simpson (1995)	Isoprene and Monoterpene emissions according to Lamb et al. (1993)	POET (Granier et al., 2005; Olivier et al., 2003)	MEGAN v2.04 (Guenther et al., 2006)
Natural emissions		none	none	Volcano emissions for Italy according to EMEP emission data base	none	Volcanic emissions of SO_2 taken from Spiro et al. (1992) with vertical distribution from Graf et al. (1997).	POET (Granier et al., 2005)
Biomass burning		none	GFED monthly (A. Heil, personal communication, 2010)	N/A	none	RETRO (monthly, 1998–2000) (Schultz et al., 2008) and GFEDv2 (8-days, 2001–2007) (Van Der Werf et al., 2006)	GFED monthly (A. Heil, personal communication, 2010)

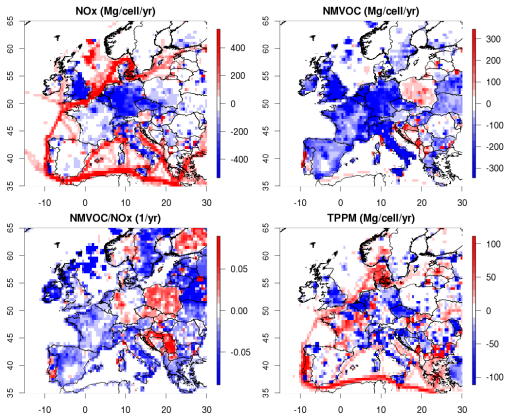

Fig. 3. Map of EMEP expert emissions trends (linear least square fit of annual totals) over 1998–2007 for NO_x, NMVOC, NMVOC/NO_x and total primary PM (TPPM). Units are Mg/yr except for NMVOC/NO_x (yr^{-1}).

physics. More details can be found in Mircea et al. (2008) and at http://bolchem.isac.cnr.it.

3.2.2 CHIMERE

The CHIMERE model is developed, maintained and distributed by Institut Pierre Simon Laplace (CNRS) and INERIS (Bessagnet et al., 2008). It is used for daily operational forecasting in France (Honoré et al., 2007) and beyond (e.g. through the MACC project of the European Global Monitoring for Environment and Security Programme) as well as long-term studies (Vautard et al., 2006; Beekmann and Vautard, 2010). More details can be found on the website: http://www.lmd.polytechnique.fr/chimere.

3.2.3 EMEP

The EMEP model is a Eulerian Chemical Transport Model developed at the EMEP Centre MSC-W, hosted by the Norwegian Meteorological Institute. It has been publicly available as Open Source code since 2008. The latest version can be obtained from https://wiki.met.no/emep/page1/unimodopensource2011. The model has been documented by Simpson et al. (2003) and Simpson et al. (2011). It is used to provide the scientific basis to the LRTAP convention, in particular for establishing source-receptor relationships of air pollution, but also for daily chemical weather forecasting within the MACC project.

3.2.4 EURAD

The EURAD model (Jakobs et al., 2002; Memmesheimer et al., 2004, 2007) is used to carry out chemical transport simulations for the area considered. The model calculates the transport, chemical transformations and deposition of air pollutants in the troposphere from the surface up to about 16 km. It is being implemented operationally for daily forecast in Germany and beyond in the framework of the European project MACC. Meteorological fields are provided by the meteorological model MM5. Gas phase kinetics is computed using the RACM-MIM chemistry mechanism (Geiger et al., 2003). The MADE-SORGAM (Schell et al., 2001) model is used to account for the formation of secondary organic and inorganic particles in the atmosphere. More details can be found on the website: http://www.eurad.uni-koeln.de.

3.2.5 OSLOCTM2

OSLOCTM2 is a global offline chemistry transport model driven by ECMWF meteorological data (Isaksen et al., 2005; Søvde et al., 2008). In this study the model was run with tropospheric and stratospheric chemistry including both gas-phase chemistry using the Quasi Steady-State Approximation (Hesstvedt et al., 1978; Berntsen and Isaksen, 1997), and aerosols using the M7 (Vignati et al., 2004) and nitrate (Myhre et al., 2006) modules. The period 1997–2007 was simulated, the first year of which was considered as spin-up. In OSLOCTM2 advection is done using the second order moment scheme (Prather, 1986), convection is based on the Tiedtke mass flux parameterization (Tiedtke, 1989), and transport in the boundary layer is treated according to the Holtslag K-profile method (Holtslag et al., 1990). The calculation of dry deposition is based on Wesely (1989).

3.2.6 MOZART

MOZART (Model for OZone And Related chemical Tracers) is a chemistry transport model (CTM) developed jointly by the (US) National Center for Atmospheric Research (NCAR), the Geophysical Fluid Dynamics Laboratory (GFDL), and the Max Planck Institute for Meteorology (MPI-Met) to simulate the distribution of gaseous and particulate compounds in the Earth's atmosphere. The MOZART-4 version of the model (Emmons et al., 2010) was used in this study. The MOZART-4 source code and standard input files are available for download from the NCAR Community Data Portal (http://cdp.ucar.edu).

4 Model evaluation

The present model ensemble was designed to assess the capability of state-of-the-art chemistry transport models to capture the trends of main pollutants. This chapter presents a short model evaluation to understand where the models stand.

The O_3, NO_2 and PM_{10} scores of each model compared to AIRBASE suburban stations are given on Table 4. Only one type of station is discussed for concision purposes. Bias,

Table 4. Model performances at AIRBASE suburban stations computed over 10 yr on the basis of daily means.

	NO_2			O_3			PM_{10}		
	R	Bias ($\mu g\,m^{-3}$)	RMSE ($\mu g\,m^{-3}$)	R	Bias ($\mu g\,m^{-3}$)	RMSE ($\mu g\,m^{-3}$)	R	Bias ($\mu g\,m^{-3}$)	RMSE ($\mu g\,m^{-3}$)
BOLCHEM	0.658	−1.46	12.6	0.782	−4.31	17.6	0.37	−4.48	13.9
CHIMERE	0.633	−13.4	16.6	0.797	18.5	23.5	0.576	−11.3	15.5
EMEP	0.574	−14.1	17.4	0.74	13.3	21	0.542	−14.4	17.9
EURAD	0.644	−6.46	16.0	0.659	15	25.2	0.524	−3.75	15.1
OSLOCTM2	0.544	−14.7	18.0	0.75	17.1	23.5			
MOZART	0.35	−18.1	21.3	0.627	4.76	22			

Root Mean Square Error (RMSE) and correlation are all computed from daily mean values. Note that aggregated metrics or daily maxima are often used for model performances assessment but daily values were considered more appropriate for the investigation of trends. Figure 4 displays the mean seasonal cycles (monthly values based on 10 yr of daily means) observed and modelled at AIRBASE stations. Model and data are displayed for all types of stations (UB, SB, RB) even if the models do not capture very well the variability brought about by the typology of the stations. Modelling a whole decade could only be achieved at the cost of using a relatively coarse spatial resolution, making it difficult to reproduce the differences between UB, SB and RB stations.

4.1 Nitrogen dioxide

All models exhibit a negative NO_2 bias when compared to suburban stations. This feature was expected as we used at best a 50 km spatial resolution. The small bias of modelled NO_2 levels with BOLCHEM and EURAD were however unexpected at this resolution. They are probably the result of a different representation of the vertical mixing as suggested by their strong seasonal cycle but we cannot rule out an influence of heterogeneous chemistry in the NO_x removal (which would be corroborated in the strong difference on total PM_{10} discussed below in Sect. 4.4). The other models perform better when compared to RB stations, as expected given the resolution.

Note that the average bias of global models is in-line with RCTMs such as CHIMERE and EMEP even considering their much coarser resolution. This result was not expected and constitutes an interesting finding of the study. However, the comparison might have been less favourable to GCTMs if we had focused on higher-quantile metrics (such as daily maximum values that were unfortunately unavailable in some of the global model outputs).

It is also interesting to point out the moderate importance of the seasonality in emissions. All regional models use the seasonal profile recommended by EMEP while – in these simulations – global models have no seasonality in anthropogenic emissions. The results shown on Fig. 4 show that the main driver of seasonality is probably not the prescribed cycle of emission but rather other factors such as vertical mixing (main driver of the wintertime maximum) or biogenic emissions (that could be responsible for the summer secondary maxima modelled by OSLOCTM2).

4.2 Ozone

As far as ozone is concerned, the results are in line with previous model inter-comparison initiatives (van Loon et al., 2007; Vautard et al., 2009). BOLCHEM is the only model to have a negative (albeit small) bias at suburban stations, owing to the larger NO_2 concentrations compared to other models. All the other regional CTMs show a positive bias. The best example of this behaviour is CHIMERE that has the largest bias but a very good correlation, hence similar RMSE scores than the other models.

The seasonal cycle of ozone is also very insightful (Fig. 4b). The springtime ozone build-up is quite consistent in all models but the summer time behaviour is very different. The correlation of this average monthly cycle (compared to observations) is 0.97, 0.99, 0.95, 0.85, 0.96 and 0.96 for BOLCHEM, CHIMERE, EMEP, EURAD, OSLOCTM2 and MOZART, respectively. Average O_3 concentrations level off between June and August in CHIMERE, EMEP and BOLCHEM (and in the observations), while they keep increasing according to EURAD, MOZART and OSLOCTM2. This characteristic is attributed to the reactivity of the chemical mechanism. A couple of peculiar features could not be explained such as the wintertime secondary maximum modelled by EURAD and the summertime secondary minimum of EMEP. We checked however that these features were not induced by a single event and found that they were recurrent every year over the decade.

4.3 O_x

The O_x ($=NO_2 + O_3$) climatology (global average over 10 yr) is displayed on Fig. 5. By filtering out the titration impact of NO_x on O_3 levels, this quantity gives an insight into the degree of photochemical

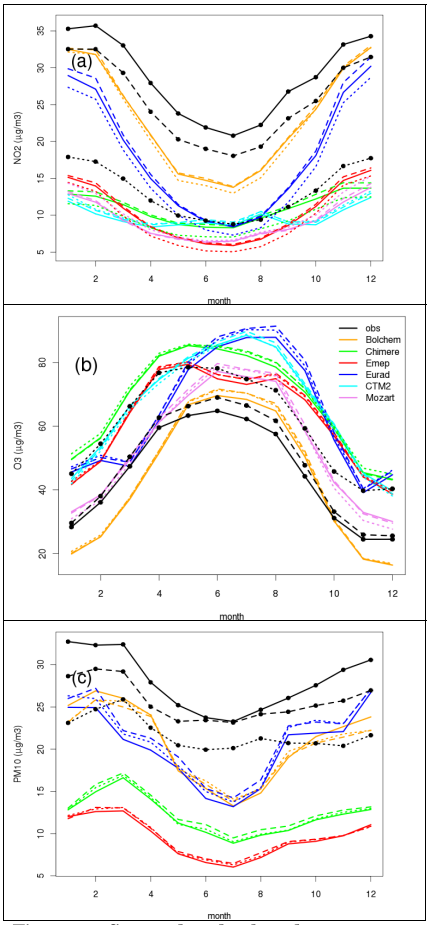

Fig. 4. Seasonal cycles based on 10 yr of daily mean values for NO_2 (top), O_3 (middle), and PM_{10} (bottom) observed (black) and modelled by BOLCHEM (orange), CHIMERE (green), EMEP (red), EURAD (blue), OSLOCTM2 (cyan) and MOZART (violet). Solid lines for urban background, dashed: suburban, and dotted: rural AIRBASE stations.

activity of the models. BOLCHEM appears as one of the least photochemically active models (spatial and temporal global average of $62.6 \pm 6.2\,\mu g\,m^{-3}$), and to a lesser extent MOZART is also in the lower part of the sample ($63.9 \pm 9.8\,\mu g\,m^{-3}$). OSLOCTM2 ($70.4 \pm 13.9\,\mu g\,m^{-3}$), EMEP ($72.8 \pm 11.1\,\mu g\,m^{-3}$) and EURAD ($74.7 \pm 14.9\,\mu g\,m^{-3}$) exhibit more similar figures while CHIMERE ($80.8 \pm 10.0\,\mu g\,m^{-3}$) is the most active. Note that the spatial variability is high as shown on the maps as well as in the standard deviation given in brackets above. Hence these global averages are not representative of the photochemical activity over populated areas, where only CHIMERE, EURAD and OSLOCTM2 can be considered as more active. All models but BOLCHEM show very high O_x concentrations above the Mediterranean. Note also the strong influence of O_3 dry deposition schemes as shown by the sharp land/sea gradient.

4.4 Particulate matter

PM_{10} scores (Table 4) are not available in global model outputs which usually calculate BC/OC rather than total particulate matter. PM_{10} correlations are much lower than for NO_2 or O_3; which is a commonplace feature in such studies. Biases are consistently negative but slightly lower in magnitude for BOLCHEM and EURAD. We will see below that this could be due to a compensation of errors, the bias for ammonium, nitrate and sulphate being quite high for these models. Again, the seasonal cycle (Fig. 4c) is much more pronounced for BOLCHEM and EURAD than for CHIMERE and EMEP, the first two models are subsequently better compared with urban and suburban stations, while the latter two are more representative of rural stations.

4.5 Nitrate, ammonium and sulphate

The overestimation of NH_{4t} and NO_{3t} mentioned above for BOLCHEM and EURAD can be seen on Fig. 6. EMEP, CHIMERE and OSLOCTM2 have a lower bias compared to the EMEP observations, and the seasonal cycle is quite synchronous with the observations for the last two. The seasonal cycle of MOZART is however slightly stronger. Gaseous sulphur dioxide is well captured by EMEP and CHIMERE but EURAD and BOLCHEM produce a strong overestimation as well as a too strong seasonal cycle. Performances in terms of particulate sulphate are very variable, the best seasonal cycle being that of the EMEP model, while EURAD and OSLOCTM2 exhibit a too strong seasonal cycle attributed by Berglen et al. (2004) to missing oxidation pathways in wintertime, especially by H_2O_2.

5 Modelled trends

The capability of chemistry transport models to capture the observed trends of major atmospheric pollutants is discussed in this section.

5.1 Nitrogen dioxide

The modelled trend of NO_2 over the whole of Europe is shown in Fig. 7 for each model. The main feature is a pronounced decrease over most of Western Europe (more specifically United Kingdom, Germany, Benelux and Italy) except France and Spain, reflecting the trend of primary emission reductions reported in the inventory (Fig. 3). By contrast NO_2

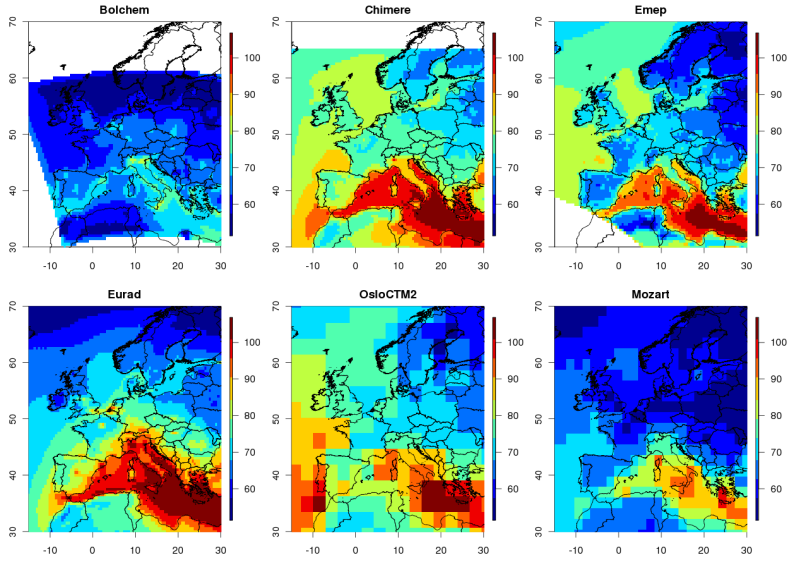

Fig. 5. Average modelled O_x ($\mu g\,m^{-3}$) [$=NO_2 + O_3$] fields over 10 yr for each model.

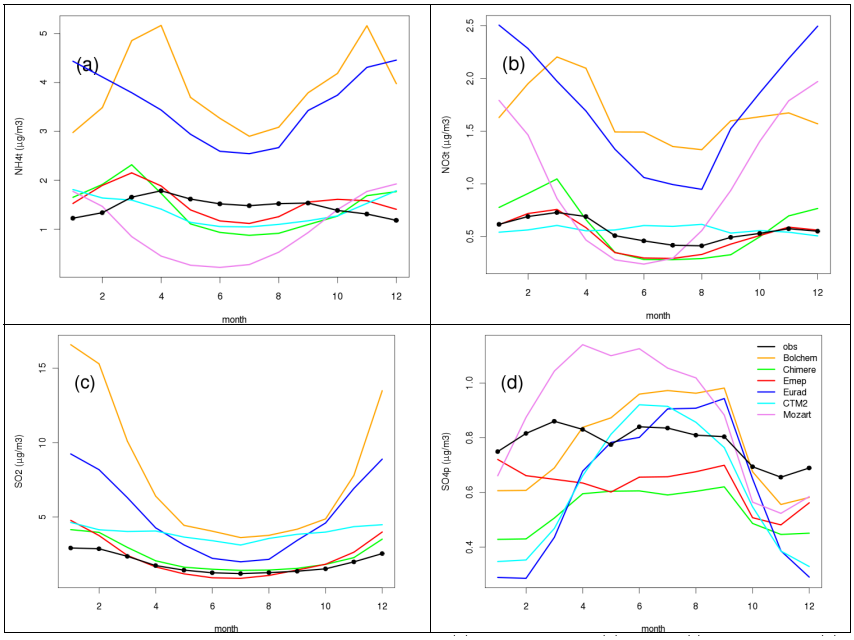

Fig. 6. Same as Fig. 4 for total NH_{4t} **(a)**, total NO_{3t} **(b)**, SO_2 **(c)** and SO_{4p} **(d)** recorded at EMEP background stations.

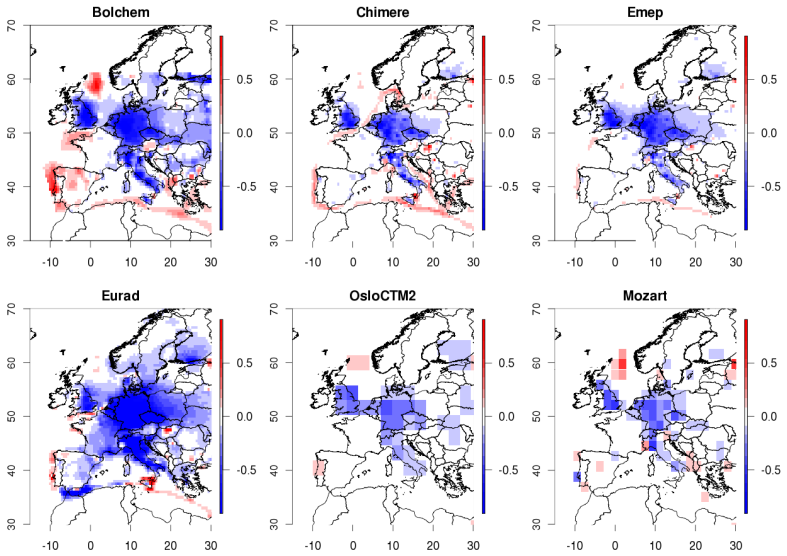

Fig. 7. Modelled NO_2 trend ($\mu g\,m^{-3}\,yr^{-1}$) for each CTM and at each grid point computed on the basis of monthly means of daily means over the 1998–2007 period with a linear least square fit of de-seasonalised values.

tends to increase over the main ship tracks. These dominating patterns are consistently captured by all models. An exception is seen in EURAD which calculates a wider extent of the NO_2 decreasing trend (especially in France), even reaching the ship track north of Morocco and Algeria. The use of identical anthropogenic emissions rules out the evolution of ship emissions to explain this feature. Meteorology is probably a dominating factor here as the PBL depth (not shown) appears to exhibit a positive trend in the EURAD simulation in that area, explaining the increased dilution of NO_2.

Before proceeding to the quantitative assessment of model performances, a visual comparison of the modelled (Fig. 7) and observed (Fig. 1) geographical patterns of these trends suggests that the models are quite successful in capturing NO_2 trends, especially in the UK, Germany, Benelux and Czech Republic. The lack of decrease or slight increase over Spain, Poland and Austria is reproduced as well as the more noisy behaviour over Italy. However, the models seem to underestimate the trends in France. The fact that these patterns match quite well with national boundaries suggests that total emissions reported to EMEP at the national level may play a significant role here, as will be confirmed below.

A more detailed comparison of modelled versus observed trends is provided in Fig. 8. The composite time series on panel (a) consists in an average of all monthly time series observed and modelled at AIRBASE background rural and background suburban stations. It reflects some of the findings discussed in Sect. 4.1 in terms of NO_2 model performances. It also shows that EURAD and BOLCHEM behave very similarly at the beginning of the decade, while the NO_2 decrease by the end of the period is much stronger in EURAD. All other models exhibit very similar behaviours.

While the composite on Fig. 8a offers a visual picture of the trend, it consists in an average of stations spread across the whole of Europe, hence aggregating different trends. Panel (b) of Fig. 8 shows the scatter between observed and modelled trends (defined as the slope of the de-seasonalised monthly mean time series) at each individual station. Such a result requires that each individual record is sufficiently reliable to assess a trend, which could only be achieved with the subset of long term time series presented in Sect. 2.2. This figure un-ambiguously shows that the correlation between modelled and observed trends is not perfect. Even if all the models used in the present study obtain decent scores in capturing NO_2, the interannual trend appears to be more challenging and most points are located quite a distance away from the 1-1 line on that scatter plot. Nevertheless the sign of the trend seems to be quite well captured at most locations; a hit-rate metric (percentage of sites where the sign of the trend is captured by the model) for model performance is thus preferred to a quantitative correlation. When considering only stations where a significant NO_2 trend is measured (according to the Mann-Kendall test, see Sect. 2.3) – i.e. 235 background suburban and rural sites – the sign of the trend is well captured at 68, 72, 81, 80, 70 and 67 % of the stations for BOLCHEM, CHIMERE, EMEP, EURAD,

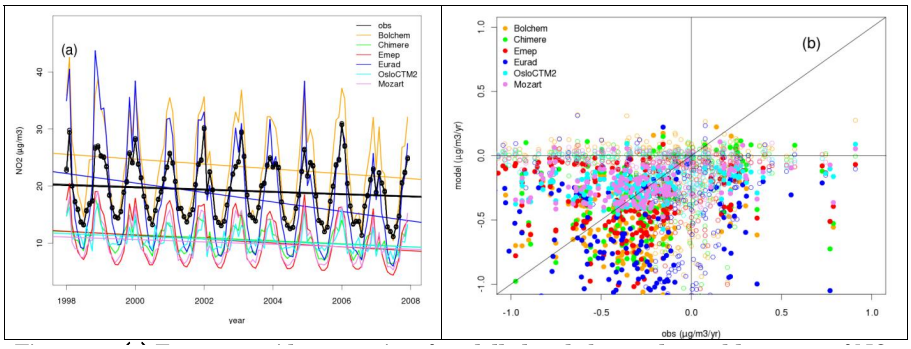

Fig. 8. (a) European-wide composite of modelled and observed monthly means of NO_2 trend ($\mu g\,m^{-3}$) at the air quality monitoring stations of background suburban and rural type. The straight line shows the best linear least square fit. **(b)** Scatter plot of modelled and observed trend (computed as linear least square of the de-seasonalised time series, in $\mu g\,m^{-3}\,yr^{-1}$) at each individual station. Sites where a significant slope is computed are marked with a filled symbol.

Table 5. Fraction of sites where the sign of the NO_2 trend is correctly captured by the models (average – avg – and standard deviation – σ – of the individual fraction correct of each model) for the countries where a significant trend is observed at 5 stations at least (number of selected stations – nst – provided on the last row).

	Europe	AT	CH	CZ	DE	FR	NL
Avg (σ)	0.73 (0.06)	0.56 (0.07)	1 (0)	0.86 (0)	0.8 (0.05)	0.39 (0.29)	0.8 (0.25)
nst	235	14	6	7	35	12	5

OSLOCTM2 and MOZART, respectively. That is a good overall performance of 73 % ($\sigma = 6$ %) on average across all models. This indicator varies widely on the country-level basis for rural sites (Table 5), the scores are much worse for all models in France and Austria. In Austria the trends are small in magnitude, making it more challenging to capture the sign correctly, this is illustrated by the spread of the distribution of model minus observed trend bias: average $-0.05\,\mu g\,m^{-3}\,yr^{-1}$, $\sigma = 0.11$. In France all models underestimate the bias (the average difference between the modelled minus observed trends is $0.67\,\mu g\,m^{-3}\,yr^{-1}$, $\sigma = 0.09$). Such country-level discrepancies – consistently produced by all 6 models – are pointing towards inaccuracies in the national inventory (in which the decreasing trend of NO_2 emission is milder than what was actually observed). However that this is contradictory with the results of (Konovalov and Beekmann, 2008) who compared satellite-derived trends and EMEP inventories and found a good agreement for France. It should be noted that they focused on a different time period (1996–2005) and also a different version of the EMEP expert emissions.

5.2 Ozone

The maps of ozone trends are provided in Fig. 9. When compared to emissions (Fig. 3) and NO_x concentrations trends (Fig. 7) these maps should be interpreted in terms of photochemical regimes. The fact that we include results of six distinct CTMs also gives a robust insight into the model uncertainty, and the comparison of model versus observed trends can be used to infer the most reliable behaviour.

The strongest pattern is an increase of daily O_3 in the Southern UK, Benelux and Germany. This behaviour relates to the switch from a VOC-sensitive towards a more NO_x-sensitive regime (Beekmann and Vautard, 2010; von Schneidemesser et al., 2010) because of the sharp decrease of NO_x emissions not accompanied by a significant reduction of VOCs (Sillman, 1999). It is worth noting that this feature is produced by all models (even the global models, although the signal in OSLOCTM2 is milder) and is also detected in the observations (Sect. 2.3), hence demonstrating the robustness of this statement.

On the contrary, Poland seems to have switched to a VOC-sensitive regime from the beginning of the period since the increased VOC emissions (with little changes of NO_x emissions, see Fig. 3) does not yield a stronger O_3 production.

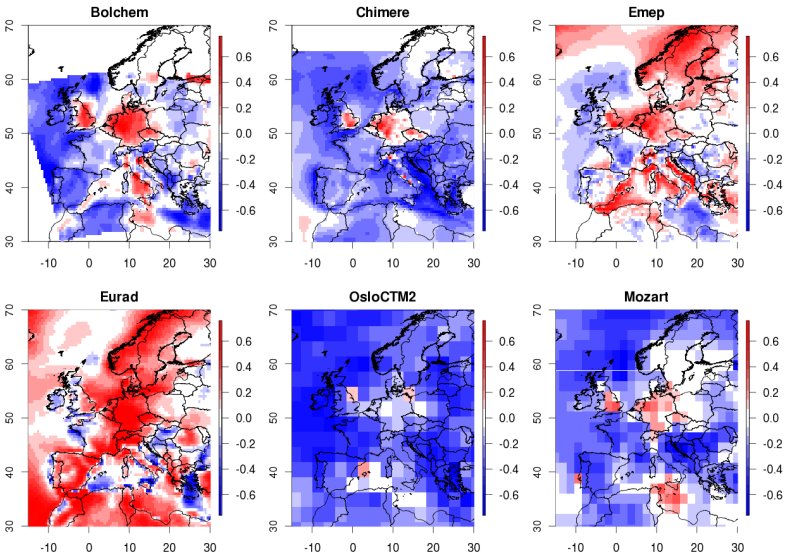

Fig. 9. Same as Fig. 7 for O_3.

Over France, the observed trend is very noisy for suburban and rural background stations. It is thus difficult to identify which model is doing best. Given the higher uncertainty on NO_2 trends discussed above (Sect. 5.1) it is thus more cautious to leave this country out of the O_3 trend analysis.

Over Northern Italy, the modelled geographical patterns are highly variable, as well as trends in observations. This apparently noisy behaviour is thus quite plausible in this area dominated by very stagnant meteorological conditions.

The very different behaviour in the Mediterranean region is interesting as it highlights the much larger model uncertainty in this area. However the lack of measurements prevents us from concluding on the most reliable trends.

Overall, although the scatter between modelled and observed trends (Fig. 10) is large, the models perform decently considering that ozone precursor emissions are very uncertain over relatively large areas. Considering only sites where a significant trend is observed the percentage of RB and SB stations where the sign of the trend is correctly captured is 58, 58, 66, 71, 39, and 51 % for BOLCHEM, CHIMERE, EMEP, EURAD, OSLOCTM2 and MOZART respectively.

5.3 Particulate matter

The modelled PM_{10} trends obtained by the regional CTMs are displayed on Fig. 11. A widespread decrease of PM_{10} is modelled over most of Europe, except for Spain, Portugal and France. More peculiar features include localised increases over Bulgaria and part of Portugal that can be related to changes in the trends of total primary particulate matter in the EMEP inventory (Fig. 3). The increase in PM over the north Atlantic simulated by EMEP results probably from a meteorological change which has an impact on sea-salt emissions (as this feature also appears in the constant emission simulations, see Sect. 7).

The decreasing trend is not reflected in the composite on Panel (a) of Fig. 12 because this composite is influenced by Czech and Spanish stations where an increase is observed. Panel (b) of Fig. 12 confirms that positive trends are virtually not captured by any model (without distinction of the countries: all stations are displayed on Fig. 12b) thus questioning the role of anthropogenic emissions (Sect. 2.3). The fact that models perform well elsewhere shows that this mismatch is not due to a model shortcoming. Such trends are thus either inappropriately reported in the EMEP inventory or the observed trends are induced – in part – by classes of emissions not adequately included in the inventory (wildfires, domestic wood burning, or re-suspension of terrigenous particulate matter). Nevertheless, apart from the Czech Republic and Spain, we can conclude that the models are quite successful at capturing the trend of PM_{10} with a fraction of significant trends with correct sign of 65, 62, 68, and 71 % respectively for BOLCHEM, CHIMERE, EMEP and EURAD.

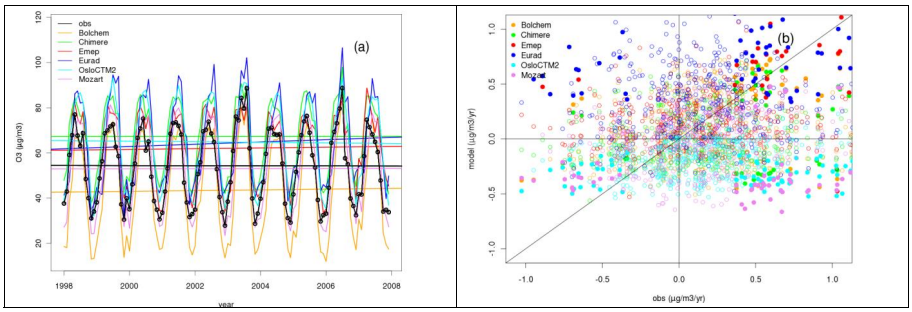

Fig. 10. Same as Fig. 8 for O_3.

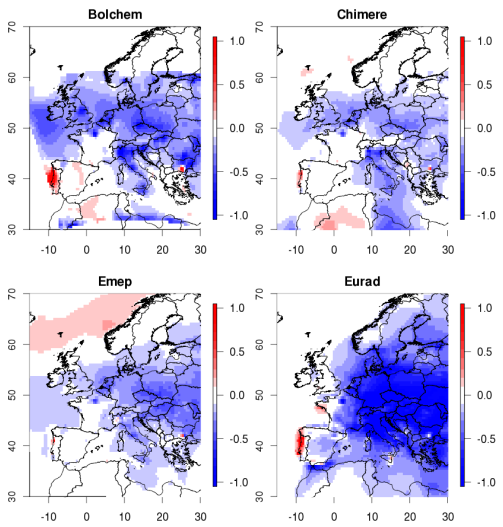

Fig. 11. Same as Fig. 7 for PM_{10}.

6 Interannual variability

One of the scopes of the present study is to prepare future air quality projections, and hence to assess the skill of the models in capturing the interannual variability. To reach this goal, we discussed above their capability to reproduce past trends. In the present Section we focus on the spread around that trend, i.e. the year to year variability.

For both AIRBASE measurements (background suburban and rural stations exclusively) and the model output interpolated at the measurement sites, we compute the residual between the time series of ozone and their linear least-square fit. The standard deviation of these residuals is thus a proxy of the temporal variability in addition to the long term changes. Note however that at this stage the seasonal variability is included in that metric of the interannual variability. Hence, in order to investigate exclusively the interannual variability we also consider the standard deviation of the residuals between the de-seasonalised time series and their linear least-square fit. At each station we obtain two standard deviations (monthly and de-seasonalised). For each model, Fig. 13 shows the quantile-quantile distribution of these two proxies, the reference (x-axis) being the distribution of the observations. The dots are equally spaced by quantiles of multiples of 10 percent. So that for example, the 5th dot represents the median of the variability in the observations (x-axis) and in the model (y-axis).

From the top panel, it appears that the month-to-month variability (once the long term trend is removed) is very well captured by all models (except at sites where the variability is very high, outside of the 10 %–90 % percentile ranges). The characteristics of the modelled seasonal cycles discussed in Sect. 4.2 are reflected here: EMEP and CHIMERE showing less variability in the higher quantiles.

The results on the bottom panel are not as good. A large part of the monthly O_3 variability is driven by the seasonal cycle. And once that cycle has been removed, the remaining variability (interannual) is more challenging to capture. Here the quantile-quantile plot shows that all models underestimate the variability compared to the observations. The median is underestimated by 28.8, 30.7, 26.3, 17.6, 53.8, and 40.3 % by BOLCHEM, CHIMERE, EMEP, EURAD, OSLOCTM2, and MOZART respectively. When split by country (Table 6), it appears that this performance is very variable according to the country, similarly to the estimate of the trend in Table 5. It is therefore likely that an underestimation of the year-to-year changes of anthropogenic emissions could be partly responsible for the inability of the models to capture the observations.

Nevertheless, if such models are used for the projections of future changes, it will be essential to investigate the relevance of implementing quantile-matching corrections (Panofsky

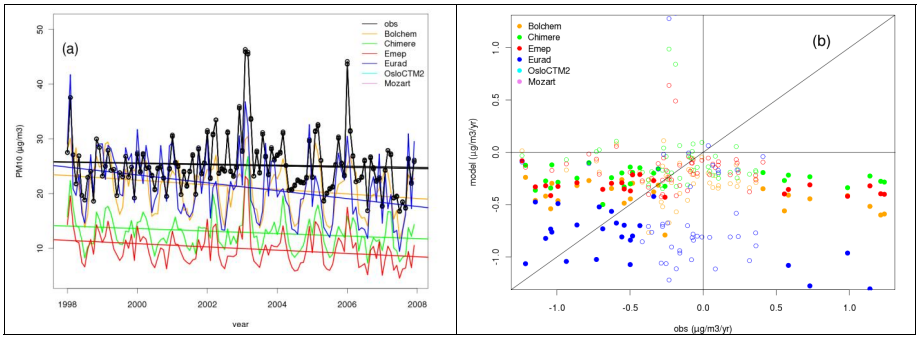

Fig. 12. Same as Fig. 8 for PM_{10}.

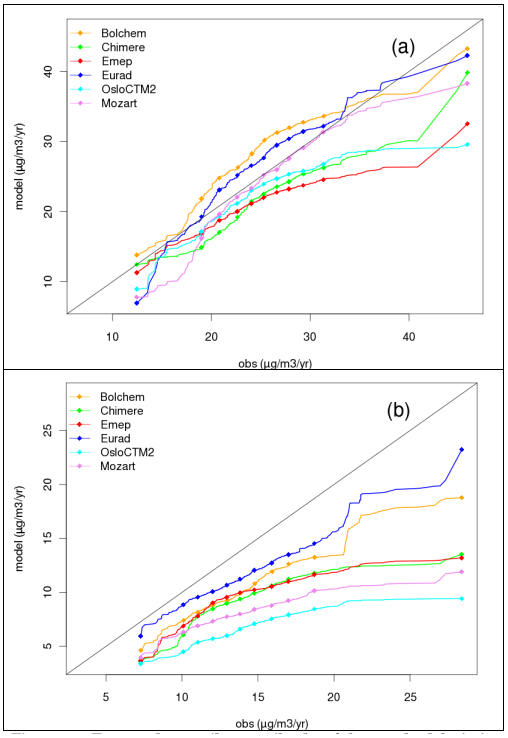

Fig. 13. Top panel: quantile-quantile plot of the standard deviation of the residuals of monthly mean O_3, once the linear trend has been removed, observations (x-axis) being used as a reference. In the bottom panel, the seasonal cycle has also been removed. The dots indicate the percentiles by multiples of 10 (0, 10th, 20th, . . . , 100th).

and Brier, 1968; Li et al., 2010) to account for this underestimation of the remaining variability.

7 Anthropogenic emission reduction versus natural meteorological variability

Each of the four regional chemistry transport models repeated the 10-yr simulation using constant emissions. The emissions of the last year of the decade (2007) were considered more reliable and therefore chosen for this experiment. The comparison of the trend modelled with constant (CST) and time-varying (CTRL) emissions can be used to infer the respective role of meteorological variability and anthropogenic emissions changes on the modelled concentrations of major pollutants.

We make use of a normalised relative trend (NRT): a quantitative metric defined in EEA (2009). This metric is the ratio between the trend brought about by the anthropogenic emission changes divided by the meteorological variability:

– At each grid point, the difference CTRL minus CST annual means is computed. The trend of this difference is directly related to emission changes. Assuming no trends of any factor besides anthropogenic emissions changes, this quantity would be positively correlated with the anthropogenic emissions changes.

– The meteorological variability is estimated as the standard deviation of the simulation with constant emissions. Although, as we discussed in Sect. 6, the interannual variability might be underestimated, these model simulations with constant emissions represent the only available proxy to estimate the specific impact of meteorology.

In both cases, these quantities are computed using annual values. The map of the ratio obtained for each models are displayed on Fig. 14, Fig. 15, and Fig. 16 for NO_2, O_3 and PM_{10} respectively. When the absolute value of this metric exceeds

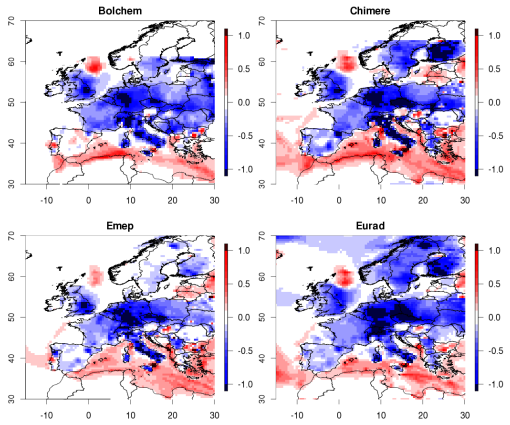

Fig. 14. Trend of NO_2 due to the anthropogenic emission evolution alone (linear least square fit of the difference between the reference run and a simulation with constant – 2007 – emissions), normalised by the interannual meteorological variability (standard deviation of the simulation with constant emissions).

1, the role of emission reduction on the modelled trend can be considered as more important than the interannual meteorological variability over the 1998–2007 decade.

The patterns of NO_2 NRT are widely consistent with NO_2 emission changes (Fig. 3) because NO_2 concentrations are directly influenced by primary emissions. The areas where all four models consistently identify a consistent decrease of NRT higher than unity are: the greater London area (UK), the Ruhr (Germany), Benelux, the Czech Republic and Italy. At this stage it is important to recall that the present discussion involves exclusively models, it is thus essential to go back to our assessment of the validity of the modelled trends against observations in Sect. 5.1. In Table 5, we provided a quantification of model performances in reproducing the trends on a country-level basis. We found that all models were quite successful in the Czech Republic, Germany, and the Netherlands and performing less well in France. Unfortunately, most other European countries did not offer an appropriate monitoring network to be included in the comparison. Nevertheless, we can be quite confident in the behaviour of the models in Germany, Benelux and the Czech Republic and thus conclude that the significant NRT identified there is a robust finding.

We saw before (Sect. 5.2) that the observed and modelled trends of O_3 in Europe during the 1998–2007 period are slightly positive over European megacities where the confidence on NO_2 trends is higher (UK, Benelux, Germany). These positive trends are however small and usually not significant in the CTRL simulation, and this is even more true for the CST simulation. Nevertheless, and interestingly enough, EMEP and EURAD seem to capture a positive O_3 trend in the CST experiment, reflecting either a direct impact of temperature changes over that period, or a reinforced role of biogenic emissions in these models (indirectly related to temperature changes). The consequence is a modulation of the widespread O_3 increase modelled by EMEP and EURAD for the CTRL simulation (Fig. 9) so that the patterns of NRT are less pronounced for these models on Fig. 15.

In the CST simulation, PM_{10} concentrations exhibit very small trends except in France where a slight positive trend is captured by all models and over the North Atlantic where EMEP shows an increase of sea-salt (already mentioned in Sect. 5.3). The NRT patterns on Fig. 16 are thus very close to the modelled trends on Fig. 11, except in France where the decrease is stronger, and over the North Atlantic where the positive trend in EMEP results vanishes. Perhaps the most surprising finding is a relatively similar trend for PM_{10} in EURAD results in the CST and CTRL simulations, yielding milder patterns on Fig. 16 compared to Fig. 11 (see e.g. the absence of a negative trend North of Morocco and Algeria on Fig. 16). Otherwise most models show that the order of magnitude of the decrease of PM_{10} due to anthropogenic emissions management reaches or exceeds the natural variability over most of Europe.

8 Conclusions

This paper contributes to the assessment of the capacity of state-of-the-art regional and global chemistry transport models (RCTM and GCTM) to capture the interannual variability of air pollution in major anthropogenic emission hotspots in Europe. A special attention is given to the cluster of large European cities in Northern France, Southern United Kingdom, Benelux and Western Germany. The purpose of the study is to investigate past modelled trends in order to demonstrate the potential and limitations of existing models for assessing the impact of future air pollution control strategies. To address these points a coordinated numerical experiment covering a period of 10 yr and involving six modelling groups was conducted. It is the first time that the air quality modelling community performs a modelling exercise covering such a time scale.

A model evaluation was performed to understand the respective strengths and weaknesses of the models. Although the scope of the study was focused on trends and interannual variability, it was also the opportunity to propose a multi-annual model evaluation. The most striking result is the consistency of model performances between regional and global chemistry-transport models induced by the scope of the study (focused on daily mean scores rather than on hourly or peak values, Valari and Menut, 2008) and the use of a common emission inventory. Another interesting conclusion in terms of scale errors regards the dissimilarity of seasonal cycles amongst RCTMs, given that they rely on identical seasonal

Table 6. Percentage of underestimation in the modelled median interannual variability (average – avg - and standard deviation – σ) at all stations of a given country and across all models. The interannual variability is estimated as the distribution of residuals of the de-seasonalised residuals of the linear fit of monthly time series. Only countries where at least 5 stations are available are shown (number of selected stations – nst – provided on the last row).

	AT	BE	CH	CZ	DE	ES	
Avg (σ)	34.1 (14.1)	15.8 (10.1)	20.7 (10.95)	23.4 (13.65)	34.3 (16.0)	30.4 (16.0)	
nst	45	15	7	13	62	17	
	FI	FR	GB	IT	NL	NO	PL
Avg (σ)	17.6 (22.6)	42.4 (12.8)	49.3 (13.6)	48.98 (14.3)	47.7 (13.8)	34.4 (11.5)	31.9 (12.8)
nst	5	43	14	8	11	5	7

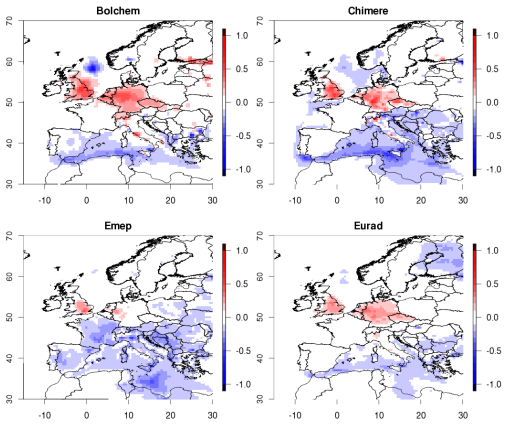

Fig. 15. Same as Fig. 14 for O_3.

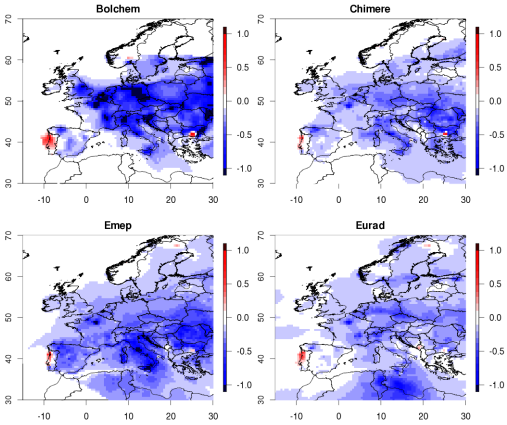

Fig. 16. Same as Fig. 14 for PM_{10}.

profiles in the emissions inventories. We also found that the models exhibited various degree of photochemical activity, hence leading to quite variable O_3 modelling skills. The performances of the RCTM to model aerosols could be divided in two broad types of behaviour: small bias in total PM_{10} due to an overestimation of ammonium nitrate, or a strong negative PM_{10} bias. We conclude that the ensemble of models implemented here covers a wide envelope of behaviours. This leads to a higher confidence in the representativeness of this set of models, and shows that they reflect well the modelling capacities of the atmospheric chemistry modelling community.

The CTMs proved to be quite successful in capturing the decreasing trend of primary pollutants, especially in the emission hotspot areas around the Benelux region. Note that we focused here exclusively on background stations and on aggregated metrics such as daily and monthly means. The results might have been substantially different at urban or traffic monitoring sites or when investigating peak values, but such proxies were considered irrelevant in a multi-model study involving global models. Downwards trends of NO_2 were successfully captured at 73 % of the stations on average for all models. Important mismatches were systematically modelled (e.g. France) pointing towards caveats in the emissions inventory. PM_{10} trends were also quite well captured, although the validation could not be as quantitative because of the relative lack of long term measurements. O_3 trends turned out to be much more challenging to reproduce, partly because the trends are small in magnitude during the period under consideration. Nevertheless, the models capture the trend in the majority of stations and we could discuss O_3 evolution in terms of photochemical regimes. As suggested elsewhere (Beekmann and Vautard, 2010), it is found that the NO_x-reduction policy yields moderate increases in O_3 over the Benelux hotspot of emissions. Given the NO_x-saturated photochemical regimes dominating there, the titration of NO_x on O_3 dominates and more ambitious NO_x reduction measures could be considered in future policies.

We also devoted a special focus on the modelled temporal variability (apart from the linear trend mentioned above). It appears that the variability of the residual between the monthly means and the linear trend is well reproduced. However, this variability is heavily influenced by the seasonal cycle. Hence the capacity of the models to capture this variability does not reflect their performance in reproducing year-to-year changes. Once the seasonal cycle is removed, the interannual variability is less well modelled. This result clearly shows that caution needs to be taken when using these models to assess future air quality variability.

In a last part, the respective role of meteorology and anthropogenic emission changes is addressed by comparing model simulations with constant emissions. We find out that the magnitude of the anthropogenic NO_2 decrease exceeds the natural variability over most of Europe. This demonstrates that emission reduction strategies enforced over the past decade led to the reduction of NO_2 background levels. Consequently, this result suggests that ambitious environmental policies have a beneficial impact on NO_2 ambient concentrations, even if this effect was not as large as expected when the emission control strategies were decided (partly because of an increased proportion of diesel engines and a subsequent change in the NO/NO_2 ratio).

To summarize, the trend assessment conducted here shows that reductions of anthropogenic emissions of nitrogen oxides and particulate matter effectively lead to reductions of atmospheric loading of primary constituents. However, the insufficient efforts on volatile organic compounds in areas exposed to a VOC-sensitive photochemical regime associated to a decrease of NO_x titration of O_3 in NO_x saturated areas lead to localised increases of ozone, especially sensitive over the most urbanised areas. The model assessment proved that the models were efficient at capturing the trend of primary species but the more limited magnitude of ozone changes was more challenging to reproduce. Nevertheless we conclude that these models capture most of the important features to justify their implementation for future projections of air quality provided that enough attention is given to their underestimation of interannual variability.

Acknowledgements. The research leading to these results has received funding from the European Union's Seventh Framework Programme (FP7/2007-2013) under grant agreement no. 212095 (CityZen). Anthropogenic emissions were provided by EMEP and complemented for global models in the framework of the MACC FP7 Project (grant agreement no. 218793). Surface observations were obtained through the AIRBASE (EEA) and EBAS (NILU) repositories. Large scale reanalyses used to drive the mesoscale meteorological models were provided by ECMWF and NCEP/NCAR.

Edited by: L. Molina

References

Ackermann, I. J., Hass, H., Memmesheimer, M., Ebel, A., Binkowski, F. S., and Shankar, U.: Modal aerosol dynamics model for Europe: development and first applications, Atmos. Environ., 32, 2981–2999, 1998.

Beekmann, M. and Vautard, R.: A modelling study of photochemical regimes over Europe: robustness and variability, Atmos. Chem. Phys., 10, 10067–10084, doi:10.5194/acp-10-10067-2010, 2010.

Berglen, T. F., Berntsen, T. K., Isaksen, I. S. A., and Sundet, J. K.: A global model of the coupled sulfur/oxidant chemistry in the troposphere: The sulfur cycle, J. Geophys. Res., 109, D19310, doi:10.1029/2003JD003948, 2004.

Berntsen, T. K. and Isaksen, I. S. A.: A global three-dimensional chemical transport model for the troposphere 1. Model description and CO and ozone results, J. Geophys. Res., 102, 21239–21280, 1997.

Bessagnet, B., Menut, L., Curci, G., Hodzic, A., Guillaume, B., Liousse, C., Moukhtar, S., Pun, B., Seigneur, C., and Schulz, M.: Regional modeling of carbonaceous aerosols over Europe – focus on secondary organic aerosols, J. Atmos. Chem., 61, 175–202, 2008.

Binkowski, F. S. and Roselle, S. J.: Models-3 Community Multiscale Air Quality (CMAQ) model aerosol component 1. Model description, J. Geophys. Res., 108, 4183, doi:10.1029/2001JD001409, 2003.

Braniš, M.: Long Term Trends in Concentration of Major Pollutants (SO_2, CO, NO, NO_2, O_3 and PM_{10}) in Prague – Czech Republic (Analysis of Data Between 1992 and 2005), Water Air Soil Pollut. Focus, 8, 49–60, 2008.

Buzzi, A., Fantini, M., Malguzzi, P., and Nerozzi, F.: Validation of a limited area model in cases of mediterranean cyclogenesis: Surface fields and precipitation scores, Meteorol. Atmos. Phys., 53, 137–153, 1994.

CAFE: Communication from the Commission to the Council and the European parliament : Thematic Strategy on air pollution SEC(2005)1132 et SEC(2005)1133 European Commission, Brussels, 2005.

Carslaw, D., Beevers, S., Westmoreland, E., Williams, M., Tate, J., Murrells, T., Stedman, J., Li, Y., Grice, S., Kent, A., and Tsagatakis, I.: Trends in NO_x and NO_2 emissions and ambient measurements in the UK, Defra, London, 2011.

Carter, W. P. L.: A detailed mechanism for the gas-phase atmospheric reactions of organic compounds, Atmos. Environ.. Part A. General Topics, 24, 481–518, 1990.

Derwent, R. G., Jenkin, M. E., Saunders, S. M., Pilling, M. J., Simmonds, P. G., Passant, N. R., Dollard, G. J., Dumitrean, P., and Kent, A.: Photochemical ozone formation in north west Europe and its control, Atmos. Environ., 37, 1983-1991, 2003.

EC: Directive 2001/42/EC of the European Parliament and of the Council of 27 June 2001 on the assessment of the effects of certain plans and programmes on the environment, 2001.

EEA: Assessment of ground-level ozone in EEA member countries, with a focus on long-term trends, European Environment Agency, Copenhagen, 56, 2009.

Emmons, L. K., Walters, S., Hess, P. G., Lamarque, J.-F., Pfister, G. G., Fillmore, D., Granier, C., Guenther, A., Kinnison, D., Laepple, T., Orlando, J., Tie, X., Tyndall, G., Wiedinmyer, C., Baughcum, S. L., and Kloster, S.: Description and evaluation of

the Model for Ozone and Related chemical Tracers, version 4 (MOZART-4), Geosci. Model Dev., 3, 43–67, doi:10.5194/gmd-3-43-2010, 2010.

Endresen, Ø., Sørgård, E., Behrens, H. L., Brett, P. O., and Isaksen, I. S. A.: A historical reconstruction of ships' fuel consumption and emissions, J. Geophys. Res., 112, D12301, doi:10.1029/2006JD007630, 2007.

Eyring, V., Isaksen, I. S. A., Berntsen, T., Collins, W. J., Corbett, J. J., Endresen, O., Grainger, R. G., Moldanova, J., Schlager, H., and Stevenson, D. S.: Transport impacts on atmosphere and climate: Shipping, Atmos. Environ., 44, 4735–4771, 2010.

Favez, O., Cachier, H., Sciare, J., and Le Moullec, Y.: Characterization and contribution to $PM_{2.5}$ of semi-volatile aerosols in Paris (France), Atmos. Environ., 41, 7969–7976, 2007.

Geiger, H., Barnes, I., Bejan, I., Benter, T., and Spittler, M.: The tropospheric degradation of isoprene: an updated module for the regional atmospheric chemistry mechanism, Atmos. Environ., 37, 1503–1519, 2003.

Giorgi, F., Jones, C., and Asrar, G. R.: Addressing climate information needs at the regional level: the CORDEX framework, WMO Bulletin, 58, 175–183, 2009.

Graf, H.-F., Feichter, J., and Langmann, B.: Volcanic sulfur emissions: Estimates of source strength and its contribution to the global sulfate distribution, J. Geophys. Res., 102, 10727–10738, 1997.

Granier, C., Lamarque, J. F., Mieville, A., Muller, J. F., Olivier, J., Orlando, J., Peters, J., Petron, G., Tyndall, G., and Wallens, S.: POET : A Database of Surface Emissions of Ozone Precursors, Paris, 2005.

Granier, C., Bessagnet, B., Bond, T., D'Angiola, A., Denier van der Gon, H., Frost, G., Heil, A., Kaiser, J., Kinne, S., Klimont, Z., Kloster, S., Lamarque, J.-F. o., Liousse, C., Masui, T., Meleux, F., Mieville, A., Ohara, T., Raut, J.-C., Riahi, K., Schultz, M., Smith, S., Thompson, A., van Aardenne, J., van der Werf, G., and van Vuuren, D.: Evolution of anthropogenic and biomass burning emissions of air pollutants at global and regional scales during the 1980–2010 period, Climatic Change, 109, 163–190, 2011.

Grell, G. A., Duddhia, J., and Staufer, D.: A description of the fifth-generation Penn State/Ncar meso-scale model (MM5), National Center of Atmospheric Research, Boulder, 1994.

Guenther, A., Karl, T., Harley, P., Wiedinmyer, C., Palmer, P. I., and Geron, C.: Estimates of global terrestrial isoprene emissions using MEGAN (Model of Emissions of Gases and Aerosols from Nature), Atmos. Chem. Phys., 6, 3181–3210, doi:10.5194/acp-6-3181-2006, 2006.

Harrison, R. M., Stedman, J., and Derwent, D.: New Directions: Why are PM_{10} concentrations in Europe not falling?, Atmos. Environ., 42, 603–606, 2008.

Hauglustaine, D. A., Hourdin, F., Jourdain, L., Filiberti, M. A., Walters, S., Lamarque, J. F., and Holland, E. A.: Interactive chemistry in the Laboratoire de Météorologie Dynamique general circulation model: Description and background tropospheric chemistry evaluation, J. Geophys. Res., 109, D04314, doi:10.1029/2003JD003957, 2004.

Hesstvedt, E., Hov, Ö., and Isaksen, I. S. A.: Quasi-steady-state approximations in air pollution modeling: Comparison of two numerical schemes for oxidant prediction, International Journal of Chemical Kinetics, 10, 971–994, 1978.

Hipel, K. W. and McLeod, A. I.: Time Series Modelling of Water Resources and Environmental Systems, Elsevier, Amsterdam, 2005.

Hollander, M. and Wolfe, D. A.: Nonparametric Statistical Methods., in, 2 ed., John Wiley & Sons, New York, 27–33, 68–75, 1999.

Holtslag, A. A. M., De Bruijn, E. I. F., and Pan, H. L.: A High Resolution Air Mass Transformation Model for Short-Range Weather Forecasting, 118, 1561–1575, doi:10.1175/1520-0493(1990)118<1561:AHRAMT>2.0.CO;2, 1990.

Honoré, C., Menut, L., Bessagnet, B., Meleux, F., Rouïl, L., Vautard, R., Poisson, N., Peuch, V. H., and Carlos Borrego and Eberhard, R.: Chapter 3.4 PREV'AIR: A platform for air quality monitoring and forecasting, in: Developments in Environmental Sciences, Elsevier, Burlington, 293–300, 2007.

Isaksen, I. S. A., Zerefos, C., Kourtidis, K., Meleti, C., Dalsøren, S. B., Sundet, J. K., Grini, A., Zanis, P., and Balis, D.: Tropospheric ozone changes at unpolluted and semipolluted regions induced by stratospheric ozone changes, J. Geophys. Res., 110, D02302, doi:10.1029/2004JD004618, 2005.

Jakobs, H., Tilmes, S., Heidegger, A., Nester, K., and Smiatek, G.: Short-Term Ozone Forecasting with a Network Model System during Summer 1999, J. Atmos. Chem., 42, 23–40, 2002.

Jonson, J. E., Simpson, D., Fagerli, H., and Solberg, S.: Can we explain the trends in European ozone levels?, Atmos. Chem. Phys., 6, 51–66, doi:10.5194/acp-6-51-2006, 2006.

Karl, M., Dorn, H. P., Holland, F., Koppmann, R., Poppe, D., Rupp, L., Schaub, A., and Wahner, A.: Product study of the reaction of OH radicals with isoprene in the atmosphere simulation chamber SAPHIR, J. Atmos. Chem., 55, 167–187, 2006.

Kendall, M. G.: Rank Auto Correlation Methods, 4 ed., Griffin, Oxford, 1976.

Konovalov, I. B. and Beekmann, M.: On the Use of Air Quality Monitoring Networks for the Evaluation of Nitrogen Oxide Emission Inventories, The Open Atmospheric Science Journal, 2, 232–248, 2008.

Konovalov, I. B., Beekmann, M., Richter, A., and Burrows, J. P.: Inverse modelling of the spatial distribution of NO_x emissions on a continental scale using satellite data, Atmos. Chem. Phys., 6, 1747–1770, doi:10.5194/acp-6-1747-2006, 2006.

Konovalov, I. B., Beekmann, M., Richter, A., Burrows, J. P., and Hilboll, A.: Multi-annual changes of NO_x emissions in megacity regions: nonlinear trend analysis of satellite measurement based estimates, Atmos. Chem. Phys., 10, 8481–8498, doi:10.5194/acp-10-8481-2010, 2010.

Lamb, B., Gay, D., Westberg, H., and Pierce, T.: A biogenic hydrocarbon emission inventory for the U.S.A. using a simple forest canopy model, Atmos. Environ. Part A., 27, 1673–1690, 1993.

Lattuati, M.: Impact des émissions européennes sur le bilan d'ozone troposphérique à l'interface de l'Europe et de l'Atlantique nord: apport de la modélisation lagrangienne et des mesures en altitude, Univ. Pierre et Marie Curie, Paris, 1997.

Li, H., Sheffield, J., and Wood, E. F.: Bias correction of monthly precipitation and temperature fields from Intergovernmental Panel on Climate Change AR4 models using equidistant quantile matching, J. Geophys. Res., 115, D10101, doi:10.1029/2009JD012882, 2010.

Logan, J. A.: An analysis of ozonesonde data for the troposphere: Recommendations for testing 3-D models and development of

a gridded climatology for tropospheric ozone, J. Geophys. Res., 104, 16115–16149, 1999.

Logan, J. A., Megretskaia, I. A., Miller, A. J., Tiao, G. C., Choi, D., Zhang, L., Stolarski, R. S., Labow, G. J., Hollandsworth, S. M., Bodeker, G. E., Claude, H., De Muer, D., Kerr, J. B., Tarasick, D. W., Oltmans, S. J., Johnson, B., Schmidlin, F., Staehelin, J., Viatte, P., and Uchino, O.: Trends in the vertical distribution of ozone: A comparison of two analyses of ozonesonde data, J. Geophys. Res., 104, 26373–26399, 1999.

Løvblad, G., Tarrasón, L., Tørseth, K., and Dutchak, S.: EMEP Assessment, Part I, European Perspective, met.no, Oslo, 47–62, 2004.

Memmesheimer, M., Friese, E., Ebel, A., Jakobs, H. J., Feldmann, H., Kessler, C., and Piekorz, G.: Long-term simulations of particulate matter in Europe on different scales using sequential nesting of a regional model, 1–2, Inderscience Enterprises, Geneva, SUISSE, 25 pp., 2004.

Memmesheimer, M., Wurzler, S., Friese, E., Jakobs, H. J., Feldmann, H., Ebel, A., Kessler, C., Geiger, J., Hartmann, U., Brandt, A., Pfeffer, U., Dorn, H. P., and Carlos Borrego and Eberhard, R.: Chapter 2.8 Long-term simulations of photo-oxidants and particulate matter over Europe with emphasis on North Rhine-Westphalia, in: Developments in Environmental Sciences, Elsevier, 158–167, 2007.

Metzger, S., Dentener, F., Pandis, S., and Lelieveld, J.: Gas/aerosol partitioning: 1. A computationally efficient model, J. Geophys. Res., 107, 4312, doi:10.1029/2001JD001102, 2002.

Mircea, M., D'Isidoro, M., Maurizi, A., Vitali, L., Monforti, F., Zanini, G., and Tampieri, F.: A comprehensive performance evaluation of the air quality model BOLCHEM to reproduce the ozone concentrations over Italy, Atmos. Environ., 42, 1169–1185, 2008.

Monks, P. S., Granier, C., Fuzzi, S., Stohl, A., Williams, M. L., Akimoto, H., Amann, M., Baklanov, A., Baltensperger, U., Bey, I., Blake, N., Blake, R. S., Carslaw, K., Cooper, O. R., Dentener, F., Fowler, D., Fragkou, E., Frost, G. J., Generoso, S., Ginoux, P., Grewe, V., Guenther, A., Hansson, H. C., Henne, S., Hjorth, J., Hofzumahaus, A., Huntrieser, H., Isaksen, I. S. A., Jenkin, M. E., Kaiser, J., Kanakidou, M., Klimont, Z., Kulmala, M., Laj, P., Lawrence, M. G., Lee, J. D., Liousse, C., Maione, M., McFiggans, G., Metzger, A., Mieville, A., Moussiopoulos, N., Orlando, J. J., O'Dowd, C. D., Palmer, P. I., Parrish, D. D., Petzold, A., Platt, U., Pöschl, U., Prévôt, A. S. H., Reeves, C. E., Reimann, S., Rudich, Y., Sellegri, K., Steinbrecher, R., Simpson, D., ten Brink, H., Theloke, J., van der Werf, G. R., Vautard, R., Vestreng, V., Vlachokostas, C., and von Glasow, R.: Atmospheric composition change – global and regional air quality, Atmos. Environ., 43, 5268–5350, 2009.

Myhre, G., Grini, A., and Metzger, S.: Modelling of nitrate and ammonium-containing aerosols in presence of sea salt, Atmos. Chem. Phys., 6, 4809–4821, doi:10.5194/acp-6-4809-2006, 2006.

Nenes, A., Pilinis, C., and Pandis, S. N.: ISORROPIA: a new thermodynamic equilibrium model for multiphase multicomponent marine aerosols., Aquat. Geochem., 4, 123–152, 1998.

Olivier, J., Peters, J., Granier, C., Petron, G., Müller, J. F., and Wallens, S.: Present and future surface emissions of atmospheric compounds, POET Rep. 2/ Eur. Union, Brussels, 2003.

Ordóñez, C., Mathis, H., Furger, M., Henne, S., Hglin, C., Staehelin, J., and Prévôt, A. S. H.: Changes of daily surface ozone maxima in Switzerland in all seasons from 1992 to 2002 and discussion of summer 2003, Atmos. Chem. Phys., 5, 1187–1203, doi:10.5194/acp-5-1187-2005, 2005.

Panofsky, H. A. and Brier, G. W.: Some Applications of Statistics to Meteorology, The Pennsylvania State University, 224 pp., 1968.

Prather, M. J.: Numerical advection by conservation of second-order moments, 6, American Geophysical Union, Washington, DC, ETATS-UNIS, 1986.

Schell, B., Ackermann, I. J., Hass, H., Binkowski, F. S., and Ebel, A.: Modeling the formation of secondary organic aerosol within a comprehensive air quality model system, J. Geophys. Res., 106, 28275–28293, 2001.

Schultz, M. G., Heil, A., Hoelzemann, J. J., Spessa, A., Thonicke, K., Goldammer, J. G., Held, A. C., Pereira, J. M. C., and van het Bolscher, M.: Global wildland fire emissions from 1960 to 2000, Global Biogeochem. Cy., 22, GB2002, doi:10.1029/2007GB003031, 2008.

Sillman, S.: The relation between ozone, NO_x and hydrocarbons in urban and polluted rural environments, Atmos. Environ., 33, 1821–1845, 1999.

Simpson, D.: Biogenic emissions in Europe 2. Implications for ozone control strategies, J. Geophys. Res., 100, 22891–22906, 1995.

Simpson, D., Andersson-Skold, Y., and Jenkin, M. E.: Updating the chemical scheme for the EMEP MSC-Woxidant model : current status, The Norwegian Meteorological Institute, EMEP, Oslo, 1993.

Simpson, D., Fagerli, H., Jonson, J., Tsyro, S., Wind, P., and Tuovinen, J.-P.: The EMEP Unified Eulerian Model. Model Description, The Norwegian Meteorological Institute, EMEP, Oslo, 2003.

Simpson, D., Benedictow, A., Berge, H., Fagerli, H., Gauss, M., Jonson, J. E., Nyiri, A., Semeena, V., Steensen, B. M., Tsyro, S., Valdebenito, A., and Wind, P.: The EMEP MSC-W Chemical Transport Model I: Model Description, in preparation, 2011.

Skamarock, W. C., Klemp, J. B., Dudhia, J., Gill, D. O., Barker, D. M., Duda, M. G., Huang, X. Y., Wang, W., and Powers, J. G.: A Description of the Advanced Research WRF Version 3, NCAR, 2008.

Søvde, O. A., Gauss, M., Smyshlyaev, S. P., and Isaksen, I. S. A.: Evaluation of the chemical transport model Oslo CTM2 with focus on arctic winter ozone depletion, J. Geophys. Res., 113, D09304, doi:10.1029/2007JD009240, 2008.

Spiro, P. A., Jacob, D. J., and Logan, J. A.: Global Inventory of Sulfur Emissions With $1^\circ \times 1^\circ$ Resolution, J. Geophys. Res., 97, 6023–6036, 1992.

Stockwell, W. R., Kirchner, F., Kuhn, M., and Seefeld, S.: A new mechanism for regional atmospheric chemistry modeling, J. Geophys. Res., 102, 25847–25879, 1997.

Symeonidis, P., Poupkou, A., Gkantou, A., Melas, D., Devrim Yay, O., Pouspourika, E., and Balis, D.: Development of a computational system for estimating biogenic NMVOCs emissions based on GIS technology, Atmos. Environ., 42, 1777–1789, 2008.

Thouret, V., Marenco, A., Logan, J. A., Nédélec, P., and Grouhel, C.: Comparisons of ozone measurements from the MOZAIC airborne program and the ozone sounding network at eight locations, J. Geophys. Res., 103, 25695–25720, 1998.

Tiedtke, M.: A comprehensive mass flux scheme for cumulus pa-

rameterization in large-scale models, 11, 1989.

Undén, P., Rontu, L., H., J., Lynch, P., and Calvo.J.: HIRLAM-5 Scientific Documentation, HIRLAM-5 project, SMHI, Norrköping, Sweden, 2003.

UNECE: The 1999 Gothenburg Protocol to Abate Acidification, Eutrophication and Ground-level Ozone UNECE, Gothenburg, Report, 1999.

Valari M. and Menut, L.: Does increase in air quality models resolution bring surface ozone concentrations closer to reality?, J. Atmos. Ocean. Tech., 25, 1955–1968, doi:10.1175/2008JTECHA1123.1, 2008.

van der Werf, G. R., Randerson, J. T., Giglio, L., Collatz, G. J., Kasibhatla, P. S., and Arellano Jr., A. F.: Interannual variability in global biomass burning emissions from 1997 to 2004, Atmos. Chem. Phys., 6, 3423–3441, doi:10.5194/acp-6-3423-2006, 2006.

van Loon, M., Vautard, R., Schaap, M., Bergström, R., Bessagnet, B., Brandt, J., Builtjes, P. J. H., Christensen, J. H., Cuvelier, C., Graff, A., Jonson, J. E., Krol, M., Langner, J., Roberts, P., Rouil, L., Stern, R., Tarrasón, L., Thunis, P., Vignati, E., White, L., and Wind, P.: Evaluation of long-term ozone simulations from seven regional air quality models and their ensemble, Atmos. Environ., 41, 2083–2097, 2007.

Vautard, R., Szopa, S., Beekmann, M., Menut, L., Hauglustaine, D. A., Rouil, L., and Roemer, M.: Are decadal anthropogenic emission reductions in Europe consistent with surface ozone observations?, Geophys. Res. Lett., 33, L13810, doi:10.1029/2006GL026080, 2006.

Vautard, R., Schaap, M., Bergström, R., Bessagnet, B., Brandt, J., Builtjes, P. J. H., Christensen, J. H., Cuvelier, C., Foltescu, V., Graff, A., Kerschbaumer, A., Krol, M., Roberts, P., Rouïl, L., Stern, R., Tarrason, L., Thunis, P., Vignati, E., and Wind, P.: Skill and uncertainty of a regional air quality model ensemble, Atmos. Environ., 43, 4822–4832, 2009.

Vestreng, V., Breivik, K., Adams, M., Wagener, A., Goodwin, J., Rozovskkaya, O., and Pacyna, J. M.: Inventory Review 2005, Emission Data reported to LRTAP Convention and NEC Directive, Initial review of HMs and POPs, MSC-W, 2005.

Vestreng, V., Ntziachristos, L., Semb, A., Reis, S., Isaksen, I. S. A., and Tarrasón, L.: Evolution of NO_x emissions in Europe with focus on road transport control measures, Atmos. Chem. Phys., 9, 1503–1520, doi:10.5194/acp-9-1503-2009, 2009.

Vignati, E., Wilson, J., and Stier, P.: M7: An efficient size-resolved aerosol microphysics module for large-scale aerosol transport models, J. Geophys. Res., 109, D22202, doi:10.1029/2003JD004485, 2004.

von Schneidemesser, E., Monks, P. S., and Plass-Duelmer, C.: Global comparison of VOC and CO observations in urban areas, Atmos. Environ., 44, 5053–5064, 2010.

Wesely, M. L.: Parameterization of surface resistances to gaseous dry deposition in regional-scale numerical models, Atmos. Environ., 23, 1293–1304, 1989.

IV

A model study of the Eastern Mediterranean ozone levels during the hot summer of 2007

Ø. Hodnebrog[1], S. Solberg[2], F. Stordal[1], T. M. Svendby[2], D. Simpson[3,4], M. Gauss[3], A. Hilboll[5], G. G. Pfister[6], S. Turquety[7], A. Richter[5], J. P. Burrows[5], H. A. C. Denier van der Gon[8]

[1]Department of Geosciences, University of Oslo, Norway

[2]Norwegian Institute for Air Research, Kjeller, Norway

[3]Norwegian Meteorological Institute, Oslo, Norway

[4]Dept. Earth & Space Sciences, Chalmers University of Technology, Göteborg, Sweden

[5]Institute of Environmental Physics, University of Bremen, Germany

[6]Atmospheric Chemistry Division, National Center for Atmospheric Research, Boulder, CO, USA

[7]Laboratoire de Météorologie Dynamique/IPSL, UPMC Univ. Paris 06, Paris, France

[8]TNO, Business unit Environment, Health and Safety, Utrecht, The Netherlands

Correspondence to: Ø. Hodnebrog (oivind.hodnebrog@geo.uio.no)

Abstract

The hot summer of 2007 in southeast Europe has been studied using two regional atmospheric chemistry models; WRF-Chem and EMEP MSC-W. The region was struck by three heat waves and a number of forest fire episodes, greatly affecting air pollution levels. We have focused on ozone and its precursors using state-of-the-art inventories for anthropogenic, biogenic and forest fire emissions. The models have been evaluated against measurement data, and processes leading to ozone formation have been quantified. Heat wave episodes are projected to occur more frequently in a future climate, and therefore this study also makes a contribution to climate change research.

The plume from the Greek forest fires in August 2007 is clearly seen in satellite observations of CO and NO_2 columns, showing extreme levels of CO in and downwind of the fires. Model simulations reflect the location and influence of the fires relatively well, but the modelled magnitude of CO in the plume core is too low. Most likely, this is caused by underestimation of CO in the emission inventories, suggesting that the CO/NO_X ratios of fire emissions should be re-assessed. Moreover, higher maximum values are seen in WRF-Chem than in EMEP MSC-W, presumably due to differences in plume rise altitudes as the first model emits a larger fraction of the fire emissions in the lowermost model layer. The model results are also in fairly good agreement with surface ozone measurements.

Biogenic VOC emissions reacting with anthropogenic NO_X emissions are calculated to contribute significantly to the levels of ozone in the region, but the magnitude and geographical distribution depend strongly on the model and biogenic emission module used. During the July and August heat waves, ozone levels increased substantially due to a combination of forest fire emissions and the effect of high temperatures. We found that the largest temperature impact on ozone was through the temperature dependence of the biogenic emissions, closely followed by the effect of decreased dry deposition. The impact of high temperatures on the ozone chemistry was much lower. The results suggest that forest fire emissions, and the temperature effect on biogenic emissions and dry deposition, will potentially lead to substantial ozone increases in a warmer climate.

1 Introduction

Three distinct heat waves and associated forest fire events led to elevated ozone (O_3) and particulate matter (PM) levels in the Eastern Mediterranean region during the summer of 2007 (Eremenko et al., 2008; Liu et al., 2009). In Greece, more than 12 % of the forested area burnt (Kaskaoutis et al., 2011), contributing substantially to the air pollution levels in Athens (Liu et al., 2009). Extreme levels of carbon monoxide (CO) were observed from satellites, indicating up to 22 ppmv close to the fires and 4 ppmv in the plume transported above the Mediterranean Basin (Turquety et al., 2009). The Greek forest fires were the most extensive and destructive in the recent history of the country, and they were a consequence of several heat waves and long periods of drought (Founda and Giannakopoulos, 2009). In fact, several stations in Greece reported record breaking temperatures (up to 47°C), making this the hottest summer on record.

Ozone is formed from photochemical reactions, following emissions of the ozone precursors CO, nitrogen oxides (NO_X) and Non-Methane Volatile Organic Compounds (NMVOC) (e.g. Crutzen, 1974; Atkinson, 2000), and is also strongly affected by meteorological conditions (e.g. Jacob and Winner, 2009). In particular, temperature has a large impact on ozone and substantial increases in surface ozone have previously been documented during heat wave episodes, e.g. during the European heat wave in the summer of 2003 (Vautard et al., 2005; Solberg et al., 2008). The impacts of temperature on atmospheric ozone occur both directly through the temperature dependence of ozone forming reactions (Sillman and Samson, 1995), and indirectly through the temperature dependence of dry deposition and biogenic emissions of ozone precursors, all of which favours ozone formation when temperatures increase. Additional meteorological factors associated with heat waves, causing higher ozone, include: increased solar radiation leading to both more intense photochemistry and enhanced biogenic emissions, high-pressure areas leading to stagnant conditions and thereby less ventilation of air pollution in the boundary layer, and lower soil moisture causing the plants' stomata to close and thereby reducing the biogenic uptake. An exception from these positive ozone responses is that dryer air leads to less formation of the OH radical and thereby slower oxidation of the NMVOCs, the "fuel" in the ozone formation.

The Eastern Mediterranean basin is constantly exposed to air pollution from the surrounding densely populated areas (Kanakidou et al., 2011). Furthermore, the region is presently experiencing a rapid urbanization. Maximum ozone mixing ratios in and downwind

of major urban areas in Greece are found to exceed the European Union (EU) health risk threshold level of 180 μg m^{-3} (Poupkou et al., 2009), and throughout the year in large parts of the Eastern Mediterranean region, ozone concentrations exceed levels known to cause vegetation damages (Kourtidis et al., 2002). The region acts as a reservoir for anthropogenic pollutants originating from the nearby emission hotspots Cairo, Istanbul and Athens, from maritime transport emissions (Poupkou et al., 2008), and from more distant sources, particularly the European continent (Gerasopoulos et al., 2005). Additionally, biogenic emissions of isoprene, monoterpenes and other VOCs are large on the Balkan Peninsula, and represent 70-80 % of the annual total NMVOC emissions in most of the countries in this region (Symeonidis et al., 2008). Considering that isoprene is about a factor of three more photochemically reactive than a weighted average of VOCs emitted by e.g. motor vehicle exhaust (Benjamin et al., 1997), the potential impact of biogenic emissions on air pollution is strong. Ozone formation is also favoured by the meteorological conditions typical of the Mediterranean climate; strong insolation, high temperatures, and a low number of precipitation days. Results from regional climate models indicate that heat waves may occur more frequently in the future (Beniston, 2004; Schär et al., 2004), and that the maximum daily temperatures observed over southeastern Europe during the exceptionally hot and dry summer of 2007 may be more frequent in the latter half of the 21st century (Founda and Giannakopoulos, 2009). Such conditions also imply an increased risk of forest fires, which would further increase future air pollution levels.

The impact of temperature changes on ozone in the Eastern Mediterranean was recently studied by Im et al. (2011a). They found an almost linear ozone increase with temperature of 0.9 ± 0.1 ppb O_3 K^{-1}, and a temperature-induced increase in biogenic isoprene emissions of 9 ± 3 % K^{-1}. Both Vieno et al. (2010) and Solberg et al. (2008) highlighted the role of surface dry deposition during the European summer 2003 heat wave, indicating that reduced uptake from vegetation due to drought contributed significantly to high ozone levels. Furthermore, biogenic isoprene emissions contributed up to 20 % of the peak ozone values, and a 10 K increase led to a 5 % increase in peak ozone (Solberg et al., 2008).

The present study was carried out as part of the EU FP7 project CityZen, which aimed at determining the air pollution distribution and change in and around emission hotspots in Europe and Asia. The Eastern Mediterranean, which is the focus here, was one of the selected hotspots within this project and the extreme summer 2007 was selected as a case study. This

study aims at quantifying the influences of various processes on the elevated ozone levels in the Eastern Mediterranean during summer 2007. Several simulations have been conducted for this purpose, using two regional atmospheric chemistry models. Descriptions of the model tools, emissions and simulation setups are given in Section 2, while the results including comparisons with observations are presented and discussed in Section 3. Finally, our conclusions are given in Section 4.

2 Models and methodology

Two regional atmospheric chemistry models were applied; WRF-Chem (Grell et al., 2005) and EMEP MSC-W (Simpson et al., 2011). Both models used a horizontal resolution of 25 km × 25 km, and have been run for three summer months of 2007; June, July and August (plus two weeks of spin-up in May). The WRF-Chem model domain is centred over the Balkan peninsula, covers most of the Mediterranean sea in the south, and extends up to mid-Germany in the north, while the EMEP model domain is much larger, covering all of Europe (Figure 1). In order to simplify the presentation of results, a common domain has been defined, which covers the region of most interest in the Eastern Mediterranean (hereafter denoted EM), and which is well within the domain borders of both models. A comparison of the model properties and setups is given in Table 1, while brief descriptions of each of the models are given below.

2.1 WRF-Chem model

The Weather Research and Forecasting model with Chemistry (WRF-Chem) (Grell et al., 2005) consists of a mesoscale meteorological model (WRF) (Skamarock and Klemp, 2008) coupled with a chemistry module. In this study, WRF-Chem version 3.2 has been used with the RADM2 gas-phase chemistry scheme (Stockwell et al., 1990). The modules and meteorological physics schemes are the same as in Hodnebrog et al. (2011), but the following modification has been applied to the FTUV (Madronich, 1987) photolysis scheme. Instead of a fixed overhead ozone column amount, the model uses a domain-averaged total O_3 column value in the calculation of photolysis rates for each day of the simulation. The overhead ozone column is calculated by the global Oslo CTM2 model (Søvde et al., 2008) using a simulation

setup described in Colette et al. (2011). Meteorological initial and boundary conditions are taken from ECMWF-IFS model analysis at a resolution of 0.25° × 0.25° and updated every 6 hours (http://www.ecmwf.int/research/ifsdocs/). Furthermore, meteorological parameters calculated by WRF are nudged towards the ECMWF-IFS data every time step. Initial and boundary conditions for the chemical species are updated every 6 hours from results obtained with the Oslo CTM2 model. As the Oslo CTM2 and RADM2 chemistry schemes differ, the NMVOC species in the Oslo CTM2 model had to be mapped to the appropriate RADM2 components. The calculation of biogenic emissions is done online using the Model of Emissions of Gases and Aerosols from Nature (MEGAN) version 2.04 (Guenther et al., 2006), and the calculation of dry deposition uses the Wesely (1989) scheme.

2.2 EMEP MSC-W model

The EMEP MSC-W model is a chemical transport model (CTM) developed at the EMEP Meteorological Synthesizing Centre – West (EMEP MSC-W) at the Norwegian Meteorological Institute. The model is a development of the 3D model of Berge and Jakobsen (1998), extended with photo-oxidant chemistry (Andersson-Sköld and Simpson, 1999; Simpson et al., 2011) and the version used here (rv. 3.7.7) makes use of the EQSAM gas/aerosol partitioning model (Metzger et al., 2002). Anthropogenic emissions from European ground-level sources are supplied as gridded annual fields of NO_X, NH_3, SO_2, fine and coarse particulate matter, CO, and non-methane VOC (NMVOC), modified with monthly and daily factors. The methodology for biogenic emissions used in the EMEP model has undergone a substantial update during 2011, now building upon maps of 115 forest species generated by Köble and Seufert (2001). Emission factors for each forest species and for other land-classes are based upon Simpson et al. (1999), updated with recent literature (see Simpson et al. (2011) and references therein), and driven by hourly temperature and light using algorithms from Guenther et al. (1993). Other emissions include NO_X from aircraft and lightning, marine emissions of dimethlysulphide, and SO_2 from volcanoes.

Dry deposition is calculated using a resistance analogy combined with stomatal and non-stomatal conductance algorithms (Emberson et al., 2001; Simpson et al., 2003a; Simpson et al., 2003b), whereas wet deposition uses scavenging coefficients applied to the 3-D rainfall. The model has traditionally been used at 50 × 50 km^2 resolution over Europe, but is flexible

with respect to input meteorological data and domain, with applications ranging from 5 × 5 km^2 over the UK to 1° × 1° globally (Jonson et al., 2010a; Jonson et al., 2010b; Vieno et al., 2010). Full details of the EMEP model are given in Simpson et al. (2011).

2.3 Emissions

Emissions of the ozone precursors CO, NO_X and NMVOC have been included in the models from anthropogenic and biogenic sources, as well as emissions originating from forest fires. In both models, the anthropogenic emissions are based on the country total emissions officially reported to EMEP, but the methods used to grid the emissions to fine scale are different. In WRF-Chem we have used the TNO-MACC emission inventory (Kuenen et al., 2011), which has a resolution of 1/8° longitude × 1/16° latitude (approximately 10 km × 7 km in the EM region). Over North Africa, including Cairo, emissions from the RETRO (2006) inventory were used. Emissions from both inventories were horizontally interpolated to the model grid. Next, a splitting of the aggregated NMVOC component in the TNO-MACC inventory was made based on the UK emissions of the 50 most significant NMVOC species (Dore et al., 2007). Factors were derived for each NMVOC species and each emission sector, and then applied to each grid cell in order to obtain individual NMVOC species, which were then lumped to the RADM2 components. The emissions used in the EMEP model are country totals redistributed using Visschedijk et al. (2007), and are provided for 10 anthropogenic source-sectors denoted by so-called SNAP codes. The emissions database is available from http://www.emep.int and further details can be obtained at that site. Before implementing the anthropogenic emissions into the models, factors to account for diurnal, weekly, and monthly cycles, as well as the vertical distribution, were applied to both inventories according to Simpson et al. (2003a; 2011).

Table 2 lists the emission totals used in this study, while Figure 2 and Figure 3 show the horizontal distribution and the time evolution, respectively, of the NO_X emissions from the various inventories for the Eastern Mediterranean region. The anthropogenic emission inventories have similar distributions, and show hotspots in Po Valley, Athens, Istanbul and Cairo, as well as fairly large emissions coming from ship traffic in the Mediterranean Sea (Figure 2). In total, however, the anthropogenic emissions of CO, NO_X and NMVOC are higher in the TNO-MACC inventory compared to the regridded EMEP inventory (Table 2).

Both emission inventories are largely based on official reported emission to EMEP but gaps are filled using expert estimates. This is relevant for a number of countries in the region of study e.g., Turkey, Serbia and Ukraine. The origin of the emission data used in the TNO-MACC emission inventory as well as the procedure to grid the emissions over the domain is described in detail by Denier van der Gon et al. (2010).

Forest fires turned out to be an important contribution to the atmospheric pollution level during the East Mediterranean heat waves in summer 2007. Thus, such emissions had to be included in the WRF-Chem and EMEP models. Forest fire emissions were taken from the Global Fire Emission Database version 2 (GFEDv2) (van der Werf et al., 2006) and from the newly developed Fire INventory from NCAR version 1 (FINNv1) (Wiedinmyer et al., 2011). The temporal and spatial resolutions differ substantially between the two inventories; the first providing 1° × 1° gridded data for 8-day averages, whereas the latter provides daily emissions on 1 km × 1 km resolution. According to Table 2, the total emissions provided by each inventory for the summer 2007 forest fires in the EM are also quite different, at least for NO_X and CO, showing higher emissions in the GFEDv2 inventory compared to FINNv1. Figure 2 shows that the GFED NO_X emissions are higher than FINN for both the Albanian and Greek forest fire episodes, but slightly lower for the fires occurring in Italy. One of the most intense forest fire episodes took place between July 20 – 31 (Figure 3), when fires broke out both at Peloponnese in Greece, and along the coast of Albania. Around August 21, new intense fires emerged, mainly in southern Greece, and continued into early September.

Figure 4 shows that the summer 2007 was exceptional when it comes to forest fire emissions in the Eastern Mediterranean, with more than 1,800 kt of CO emitted in the EM domain. Within the period of available GFEDv2 monthly data (1997-2008), the vast forest fire emissions of CO during the summer of 2007 are only exceeded by the summer of 2000.

The WRF-Chem model has been run with the FINN emissions, except for a sensitivity test with GFED. For both inventories, a diurnal profile was added according to WRAP (2005), and the WRF-Chem online plume rise routine (Freitas et al., 2007) was applied in order to vertically distribute the fire emissions. The 8-day GFEDv2 inventory (van der Werf et al., 2006) only contains gridded emissions for total NMVOCs, but not for the individual NMVOC species required for the RADM2 and EMEP MSC-W chemistries. The individual NMVOC components were calculated from the GFEDv2 dry matter burned data in combination with the GFEDv2 vegetation map and updated vegetation-type specific emission

factors based on Andreae and Merlet (2001). The EMEP model also makes use of the 8-daily fire emissions from GFED, for SO_2, CO, NO_X, NMHC, and particles. The emissions are homogeneously distributed over the eight lowest layers of the model (to about 1.8 km), based on recommendations by Sofiev et al. (2009) to use a PBL height as an approximate height for emission injection. For comparison, the vertical distribution of the GFED emissions calculated with the plume rise routine in WRF-Chem is very inhomogeneous. About 70 % is emitted in the lowermost layer (to about 60 m) and about 15 % above 1.8 km height, while the remaining 15 % are distributed between 60 and 1,800 m.

Biogenic emissions are calculated online in both models, and depend on land-use data and weather conditions. In WRF-Chem, the MEGAN module depends on ambient temperature, photosynthetic active radiation, humidity, wind speed and soil moisture when estimating emissions of isoprene, monoterpenes, other biogenic VOCs, and nitrogen emissions from soil. In the EMEP model biogenic emissions of isoprene and monoterpenes are calculated at every model timestep using near-surface air temperature and photosynthetically active radiation, the latter being calculated from the model's solar radiation, modified by the total cloud fraction.

The temporal evolution of biogenic isoprene emissions calculated by WRF-Chem and EMEP MSC-W is very similar (Figure 3), but there is a difference in the magnitude (Table 2) and in the horizontal distribution of the emissions (Figure 3). The isoprene emissions calculated by WRF-Chem/MEGAN is systematically higher than that predicted by the EMEP model. These differences could be attributed to different emission factors and land use classifications. In particular, MEGAN predicts large isoprene emissions from shrublands in the western part of Turkey and southern Greece, and from broadleaf trees northwest on the Balkan peninsula. However, the differences are well within known uncertainties, which are at least a factor of 2 for natural emissions (Simpson et al., 1995; 1999).

2.4 Simulations

For each model, one reference simulation and a number of sensitivity simulations have been performed in order to study the impact of different processes on surface ozone levels (Table 3). The impacts of fire emissions, biogenic emissions, anthropogenic emissions and dry

deposition on ozone have been investigated by turning off the respective emission sector or process in the sensitivity simulations. In addition, as this study aims at quantifying the impact of high temperatures on surface ozone, sensitivity simulations have been performed with temperatures restricted to a maximum of 28°C in the calculations of chemical reactions, biogenic emissions, and dry deposition. Regarding the latter simulation (MD), the Wesely (1989) scheme in WRF-Chem uses the surface skin temperature to calculate dry deposition, but the 28°C limit has been applied to the 2 m temperature in order for the test to be comparable with the other simulations involving the 28°C limit (MC and MB). The 28°C limit has been chosen because it represents a typical summer temperature in the EM region. For comparison, at the National Observatory of Athens the summer (JJA) normal values (based on 1961-1990 averages) are 31.6°C and 26.1°C for the daily maximum and mean air temperatures, respectively (Founda and Giannakopoulos, 2009).

3 Results and discussion

3.1 Meteorological conditions

The synoptic situation during summer 2007 is described in Founda and Giannakopoulos (2009), who attribute the heat waves to horizontal advection, downward motion causing adiabatic heating, and the preceding winter which was warm and dry in large parts of southeastern Europe (Luterbacher et al., 2007) impacting land-atmosphere interactions. The WRF-Chem output of surface temperatures and horizontal winds is given in Figure 5 as three-day averages for each of the heat waves occurring in the EM during summer 2007. The wind fields indicate that a high pressure area is located near southern Italy in all three cases, leading to transport of dry and warm air from northern Africa towards the Balkans. The heat wave in June was most severe in Greece, southeastern Italy and western Turkey, while the July heat wave was more widespread with daily maximum temperatures around 40°C throughout most of the Balkan peninsula. The August heat wave was somewhat less intense, but still the surface temperatures exceeded 35°C in many places in the EM region. It is worth noting that both the July and August heat waves coincide with the two most destructive forest fire episodes that struck the EM area during summer 2007 (Section 2.3), and this increases the potential for ozone production.

3.2 Comparison with observations

The model results have been compared to ground-based measurements of ozone and satellite observations of the ozone precursors CO and NO_2. The plume from the Greek forest fires was rapidly advected towards the sea and therefore not captured by ground-based measurements. Satellite observations therefore proved to be most relevant when evaluating the modelled forest fire plumes and the forest fire emission inventories used. The comparison with ozone measurements is included to provide an evaluation of how the models perform with the current setup and in the region of interest, although it should be noted that model validation is not the main purpose of this study.

3.2.1 CO

The Infrared Atmospheric Sounding Interferometer (IASI) onboard the MetOp-A satellite monitors the abundance of a number of atmospheric species (Clerbaux et al., 2009). CO is measured on a global scale twice a day and was shown to agree well with the retrievals of other satellite instruments (George et al., 2009). However, according to Turquety et al. (2009), who thoroughly investigated the Greek forest fire episode in August 2007, the elevated IASI CO concentrations during the 2007 fire episode were on average 35 % higher than MOPITT observations (Deeter et al., 2003).

The IASI CO columns presented here are the same as in Turquety et al. (2009), where the Fast Optimal Retrievals on Layers for IASI (FORLI) algorithm was used. When interpreting the observational data, it is important to keep in mind the sources of uncertainties, e.g. aerosol contamination, and inhomogeneities in the IASI pixels. In particular, as the IASI operational retrievals for water vapour and temperature were not available for August 2007, these profiles were taken from the ECMWF analysis data. The uncertainties are also larger in the fire plumes than in background conditions, especially close to the emissions. This means that the emphasis should be put more on a qualitative rather than a quantitative level, i.e. to identify locations for high CO rather than focusing on exact CO column values. In order to account for the different sensitivities to each vertical layer in the satellite retrievals, the model data have been weighted with IASI averaging kernels, i.e. artificial satellite retrievals were

made from the model data. The IASI retrievals are performed on a 1 km vertical grid, and here we have used averages on a 0.2° × 0.2° horizontal grid. For comparison, the model data were first interpolated temporally to the satellite overpass time, and spatially to the same horizontal and vertical grids. The averaging kernels were then applied to partial columns in each grid box using the formula

$$\boldsymbol{x}_r = \boldsymbol{A} \cdot \boldsymbol{x}_m + (\mathbf{I} - \boldsymbol{A}) \cdot \boldsymbol{x}_a \quad (1)$$

where $\boldsymbol{x}_r$ is the modelled satellite retrieval (molec cm^{-2}), $\boldsymbol{A}$ is the IASI averaging kernel vector for the total column, $\boldsymbol{x}_m$ is the model data vector (molec cm^{-2}), $\mathbf{I}$ is the identity matrix, and $\boldsymbol{x}_a$ is the IASI a priori profile (molec cm^{-2}) (Rodgers, 2000; George et al., 2009). In the comparison below, the EMEP model has been excluded because the comparison is very sensitive to processes occurring in the upper troposphere, while the EMEP model is intended for use in the lower troposphere. If a meaningful comparison were to be made, the global EMEP model (Jonson et al., 2010a; Jonson et al., 2010b) should have been used, but this would have put constraints on other factors important for this study (such as the horizontal resolution).

Figure 6 shows the observed and simulated total atmospheric column of CO for the intense Greek forest fire episode occurring in late August 2007. The daytime and nighttime CO columns are shown separately since the different thermal contrasts lead to large differences in the CO retrievals for day versus night (Clerbaux et al., 2009). The high pressure area located over southern Italy leads to strong winds from north-northeast above Greece (Figure 5), rapidly advecting the Greek fire plumes towards the Mediterranean Sea and the North African coast (Figure 6). At the end of the period, the plumes mix with emissions from intense fires in Algeria, leading to enhanced CO levels over North Africa (Turquety et al., 2009). The satellite data show that forest fires in Ukraine, Albania and Italy also lead to CO enhancements, but the signal is weaker and the transport less efficient than for the fire plume originating from the Peloponnese fires.

The locations of the Greek forest fire plumes are reflected fairly well in the simulated retrievals, but the magnitude of the CO column in the core of the plumes is strongly underestimated by the model (Figure 6). Also the fire plumes originating from Ukraine and Algeria, evident in the daytime retrievals, are too low in the model results, while the background levels of CO are overestimated. There are several possible reasons for the

discrepancies between the model and observations. First, it should be noted that the overestimation of background CO is much less pronounced when the averaging kernels were not applied (not shown). As the sensitivity of the satellite observations is stronger at higher altitudes, the averaging kernels give more weight to the upper model layers, and this will cause an amplification of possible enhanced CO at these heights. Second, the comparison is also very sensitive to how the emissions are distributed vertically, and to the vertical transport in the models. If the fire emissions are implemented too close to the surface in the models, the simulated CO retrievals (modelled CO columns with averaging kernels applied) in the plume will be too low as the sensitivity of the satellite observations decreases rapidly towards the surface. As previously mentioned, about 70 % of the forest fire emissions in WRF-Chem are emitted in the lowermost layer. The diurnal profile applied to the forest fire emissions also contribute to the uncertainties, particularly because it affects how much of the emissions is in the boundary layer, which is normally more shallow during night. Other sources of uncertainty include dilution and chemical reactivities in the model, and the uncertainties related to the observations, as previously mentioned.

Underestimation of CO fire emissions is perhaps the most important reason for the discrepancies explained above. Based on the observed and modelled fire plumes (Figure 6), the CO emissions from forest fires seem significantly underestimated in both the inventories applied (FINN and GFED). The maximum observed CO column, which occurred on August 25, exceeded 25×10^{18} molec cm^{-2} (not shown), while the corresponding model values were about one order of magnitude lower. However, one should consider that the GFED simulation may not realistically represent maximum values due to the 8-day averaging. Turquety et al. (2009) highlighted the large uncertainties associated with the calculation of fire emissions. They used the IASI CO burden and a bottom-up approach to estimate 30 and 41 % larger CO emissions, respectively, compared to the numbers reported in the GFED inventory for the Greek forest fires in August 2007. Also, Pfister et al. (2011) estimated that FINN emissions of CO during a forest fire episode in California in June 2008 may have been underestimated by nearly a factor 4, and they attributed this to possible errors in the MODIS land cover data, which is critical input to FINN as the land use category determines the emission factor.

3.2.2 NO_2

Modelled tropospheric columns of NO_2 have been compared to observations from the Ozone Monitoring Instrument (OMI), which is onboard the Earth Observing System Aura satellite (Levelt et al., 2006). OMI covers the globe daily with a spatial resolution of 24 km × 13 km at nadir. In this study level 2 data containing the individual pixels has been provided by IUP-Bremen using NASA NO_2 slant columns and the tropospheric column retrieval method described in Richter et al. (2005), and later gridded to a resolution of 1/16° × 1/16°. This data set does not provide averaging kernel information and is compared to the original vertical NO_2 column from the model. Since the tropospheric columns of NO_2 are mostly influenced by processes occurring in the lower troposphere (mainly due to strong surface emission sources and relatively short lifetime of NO_X), it was possible to include the EMEP model in this comparison.

Figure 7 shows the observed and modelled tropospheric column of NO_2 averaged over the period 21-28 August 2007. This 8-day period is chosen because it coincides both with the Greek forest fire episode and with the 8-day period in the GFED data set. As for CO, the fire plumes are clearly visible in the observations, and both models are able to capture the locations and influences of the fires. The evolution of the fire impact is much the same as for CO with northeasterly winds transporting the Peloponnese fire plume towards the Mediterranean Sea. However, the NO_2 plume is more confined to the origin of the fires due to the shorter lifetime of NO_2. The results indicate that the emissions of NO_2 from the Albanian forest fires may be overestimated in the GFED inventory as the modelled NO_2 plume with GFED data gives much higher levels than observed and also compared to the model results using FINN emissions. The WRF-Chem results show that the impact of the Ukrainian forest fire emissions is much more pronounced for NO_2 than what was the case for CO. However, the observations show a more widespread NO_2 impact, and this could indicate that a too low injection height has been used, as this would cause underestimation of transport due to the rapid increase of NO_2 lifetime with altitude.

The underestimation of the Greek fire emissions seen for CO is not evident for NO_2 (Figure 7; bottom). On the contrary, the column values in the plume modelled using GFED are now overestimated and due to the coarse spatial resolution of the emissions, the simulated plume covers a too large area. The FINN simulation yields NO_2 columns which are in the

same range as the observations. This is in agreement with Pfister et al. (2011) who also found negative bias only for CO fire emissions, while other components in the FINN inventory, including NO_X, did not show such bias. As CO and NO_X are co-emitted species calculated using fixed emission factors, our results suggest that the CO/NO_X emission ratio should be re-assessed. Maximum values for the Peloponnese fires occurred on August 26 and were about 17×10^{15}, 25×10^{15}, 18×10^{15}, and 8×10^{15} molec cm^{-2} (not shown) for OMI, WRF-Chem with FINN, WRF-Chem with GFED, and EMEP MSC-W with GFED, respectively. The higher maximum value in the simulation with FINN compared to GFED is not surprising as the spatial and temporal resolution is much coarser in the latter inventory, leading to emissions being smeared out over a larger area and averaged in time. The simulation with FINN emissions shows remarkably good agreement with OMI with respect to location and magnitude of the forest fire plumes (Figure 7; bottom). Surprisingly, when comparing the GFED simulations of WRF-Chem and EMEP MSC-W, the fire plume is much less pronounced in the latter model. On the other hand, the EMEP model gives higher NO_2 levels in the plume downwind of the fires, and this is particularly evident when looking at vertical cross-sections on August 26 (not shown), which is the day of maximum NO_2 impact from the Greek fires. This inter-model difference can mainly be explained by differences in the vertical distribution of fire emissions. Although an online plume rise routine has been applied in the WRF-Chem simulations, a much larger fraction of the forest fire emissions is placed near the surface compared to the EMEP model, which evenly distributes the emissions throughout the model's lowest eight layers (to about 1.8 km). However, other possible explanations such as differences in model dilution and reactivity of NO_X to NO_Y can not be ruled out.

The observed and modelled tropospheric columns of NO_2 (Figure 7) reveal not only the location and influences of forest fire plumes, but a number of anthropogenic emission hotspots can also be recognized. NO_2 levels in the Po Valley tend to be underestimated by the models, while Cairo is relatively well represented in the WRF-Chem simulations (Cairo is outside the EMEP model domain). It should be noted, however, that any over- or underestimation in emissions may also be caused by the relatively crude temporal scaling factors that have been applied, and not only by potential errors in the annual numbers provided in the emission inventories. Istanbul is underestimated by both models and this is probably caused by too low emissions. A new emission inventory for the greater Istanbul area had 2-7 times higher annual emissions compared with the EMEP and TNO-MACC emissions

(Im et al., 2010), mainly due to lack of officially reported emissions of Turkey to EMEP. Several other cities, including Athens, Rome and Napoli, were also captured by the observations and models, although the signal was weaker.

3.2.3 Ozone

The reference simulations of the WRF-Chem and EMEP models have been compared with ozone measurements (Hjellbrekke et al., 2011) from the 10 surface monitoring sites shown in Figure 8 (top left). The Eastern Mediterranean region has a rather sparse selection of ground-based O_3 measurement stations categorized as rural background, which is needed for a meaningful comparison considering the model resolution used. For this reason we have extended the region for comparison to also include sites in central Europe, but only those that are well within the borders of the WRF-Chem domain. The selection of stations is also based on data coverage, data quality, and geographic location (to represent as wide a region as possible). The modelled ozone values are extracted from the lowest model layer in WRF-Chem, corresponding to approximately 28 m height, while the extraction in EMEP MSC-W is based on a vertical gradient from the lowest model layer (~45-50 m) to 2 m height using boundary layer theory as described in Simpson et al. (2003a). Previously, WRF-Chem simulations have been compared to European ground-based O_3 measurements in Zabkar et al. (2011), Hodnebrog et al. (2011) and Schürmann et al. (2009), while comprehensive validations of EMEP model results are given in the annual EMEP status reports (e.g. Gauss et al., 2011). One of the reports (Aas et al., 2010) included a special section on the Mediterranean region and pointed out the many modelling limitations in this area, with special emphasis on biogenic emissions and soil-moisture effects on stomatal exchange.

The comparisons are presented in Figure 8 and Table 4 as time series and statistics, respectively, for daily maximum O_3 at each station and for the whole simulation period. Overall, the models perform reasonably well with an average correlation, bias and root-mean-square error (RMSE) of 0.62/0.56 (WRF-Chem/EMEP MSC-W), -1.0/-5.5 ppbv and 9.8/11.7 ppbv, respectively, but with large variations between the stations. Correlations range from around 0.1 to 0.8 and the bias is between -14 and 6 ppbv. The fact that both models have a low correlation and relatively high RMSE at the Slovakian station Starina could indicate that the measurements are influenced by local effects (e.g. biogenic emissions from nearby

vegetation) which the models are not able to capture at this resolution, or there could be inaccuracies in the emission data. In general, ozone levels are slightly higher in WRF-Chem than in EMEP MSC-W, and this could be due to the different height extraction. The ozone mixing ratios based on the 2 m reduction in EMEP MSC-W is likely to be lower than the ozone values extracted from the lowest model layer due to the increasing impact of dry deposition near the surface, although this effect is less important when comparing daily maximum O_3. The negative bias in EMEP MSC-W is most notable for the Finokalia station, which is located near the coast of Crete. On the other hand, evaluation of the EMEP model for this site at other periods shows mixed results, also with overpredictions during some periods (Gauss et al., 2011). Im et al. (2011a) also had relatively large bias and only moderate correlation when comparing WRF/CMAQ model results to ozone observations at the Finokalia station, indicating that the ozone levels at this station are difficult to represent in a model at this resolution.

The modelled and observed ozone concentrations shown in Figure 8 are not directly influenced by the Greek forest fire emissions due to their rapid advection towards southwest. However, the July heat wave episode seems to elevate daily maximum ozone considerably at several stations. This increase in ozone levels is well represented by the models, although with underestimation of the peak in most cases (e.g. Illmitz, Payerne, K-puszta and Iskrba). The WRF-Chem simulations reveal daily maximum temperatures reaching 35°C and relatively calm winds in central/eastern Europe in the period 14-20 August (not shown), and this leads to effective build-up of ozone in this area. During the following days the combination of a temperature decrease and stronger winds causes a drop in ozone concentrations, while in the southeast, on the Balkan peninsula, an intense heat wave is established (see Section 3.1).

3.3 Processes impacting daily maximum O_3

In the following we present results from sensitivity studies where we have estimated the impact of various processes on the atmospheric chemistry. As the perspective of this study is air quality, we have focused on daily maximum ozone near the surface. Figure 9 shows the time evolution of daily maximum surface ozone (simulation REF), and the ozone impacts of the following processes; forest fire emissions (REF – NF and GF – NF), biogenic emissions

513 (REF – NB), high temperatures (>28°C) on biogenic emissions (REF – MB), high
514 temperatures on chemistry (REF – MC), and high temperatures on dry deposition (REF –
515 MD), averaged over the EM region (dashed rectangle in Figure 1). Additional sensitivity
516 studies include ozone impacts of dry deposition (REF – ND) and anthropogenic emissions
517 (REF – NA). The models show a very similar evolution of ozone in the reference run,
518 although the results from WRF-Chem are slightly higher than from the EMEP model
519 throughout the summer period (averages of 63 and 58 ppbv, respectively).

520 Two distinctive high ozone episodes can be found in the results of both models,
521 namely the latter half of July and the end of August (Figure 9). The elevated O_3
522 concentrations in these episodes can be attributed to a combination of forest fire emissions
523 (ΔO_3 up to 8 ppbv when averaged over the EM region), and heat waves leading to
524 temperature-induced increases in biogenic emissions (avg. ΔO_3 up to 3 ppbv). Additionally, a
525 sensitivity simulation with WRF-Chem reveals that the high temperatures during heat waves
526 lead to reduced dry deposition of ozone (avg. ΔO_3 up to 1.5 ppbv), and this is caused by a
527 reduction of the plant's stomatal openings. The impact of high temperatures on chemistry,
528 however, only led to relatively small perturbations in surface ozone (avg. ΔO_3 less than 1
529 ppbv) in both models. It is important to note that the numbers mentioned above are averaged
530 over a large region, while maximum O_3 perturbations have a very inhomogeneous spatial
531 distribution and can reach significantly higher values locally. This is shown in Table 5 which
532 gives maximum and percentile values for each of the processes. For example the maximum
533 O_3 impact of high temperatures on chemistry is more than two order of magnitudes larger
534 than the mean ozone impact. Another process, which is not quantified here, is the effect of
535 stagnant air and thereby slower transport, often associated with heat waves. Based on the
536 synoptic situation (Figure 5), less advection over land may have led to increased ozone during
537 the heat wave episodes.

538 During the first heat wave, occurring in late June, ozone levels were only slightly
539 elevated. The reason is probably that forest fires only took place during the latter two heat
540 waves (except a small contribution from FINN at the end of June), and emissions from these
541 fires caused significant ozone production (Figure 9). However, the magnitude of forest fire
542 impact on ozone is uncertain, with GFED emissions leading to more ozone compared to the
543 FINN emission inventory (3-month mean ΔO_3 of 1.6 and 1.2 ppbv, respectively, when

averaged over the EM region). Furthermore, GFED emissions in EMEP MSC-W caused higher ozone than GFED emissions in WRF-Chem (1.9 and 1.6 ppbv, respectively).

Figure 10 shows the spatial distribution of seasonally averaged daily maximum near-surface O_3 for the two models. The ozone distribution of both models largely reflect the distribution of precursor emissions (Figure 2), and are also in good agreement with Poupkou et al. (2009) who studied the summer 2000 and found mean daily maximum ozone mixing ratios ranging from 65 to 95 ppbv in areas influenced by the pollution plume from Athens – mainly near the east coast of Peloponnese – and corresponding values of 65 – 75 ppbv near Thessaloniki. As previously mentioned, WRF-Chem gives higher surface ozone than the EMEP model, and this is more evident over sea than land. Shipping is likely a major contributor to ozone over the Mediterranean Sea, but differences in ship emissions can not explain the differences seen between WRF-Chem and EMEP MSC-W. NO_X is the most important ozone precursor from ship emissions and the NO_X emissions from shipping used in each of the models are about the same (Figure 2). Also, the factors applied to account for diurnal variation and vertical distribution are the same in both models.

3.3.1 Impact of forest fires

Figure 11 shows the impact of forest fire emissions on daily maximum near-surface ozone. The uncertainties in the ozone impact are evident, and it is quite clear from these simulations that the choice of emission inventory is more important than the choice of model. In line with the differences in emissions (Figure 2), the WRF-Chem simulation with FINN emissions yields much lower ozone impacts from the Albanian and Greek forest fires than WRF-Chem with GFED. On the other hand, fires that took place north of the Black Sea had a much stronger impact on ozone. Although maximum NO_2 columns were higher in FINN (Figure 7), the EM maximum of summer mean daily maximum near-surface ozone concentrations (over Albania) were about three times higher with GFED (5.3 and 17.7 ppbv, respectively). The overall maximum O_3 perturbation calculated with GFED reached extremely high values, almost 160 ppbv in one grid box on August 23, compared to 65 ppbv on July 24 when using FINN emissions (Table 5). CO concentrations in this region are much smaller in the FINN simulation (Figure 6), but this is a less probable explanation of the ozone differences as CO is relatively unreactive on these temporal and spatial scales. More likely, the higher NO_X

emissions in GFED than FINN leads to increased O_3 production, but it could also be an effect of the different emission resolutions used. For this study with 25 km × 25 km model resolution, the GFED emissions (1° × 1°) are spread over approximately 16 grid cells, while FINN emissions (1 km × 1 km) can reproduce the model scales. Due to non-linearities in the ozone chemistry, NO_X concentrations are more likely to be saturated in the latter case, leading to reduced O_3 production efficiency.

The two models yield similar impact of GFED emissions on ozone concentrations. However, in WRF-Chem the ozone impact is more confined to the origin of the fires, leading to higher maximum values than in EMEP MSC-W (17.7 and 11.4 ppbv, respectively), while the latter model shows a more widespread ozone impact near the fires and particularly in the northeastern part of the region. The same signal was seen for the ozone precursor NO_2 in Section 3.2.2, and this points to differences related to plume rise in the models.

3.3.2 Impact of biogenic emissions

Sensitivity simulations with both models show that the impact of biogenic emissions on daily maximum ozone is large, but very uncertain (Figure 12). Even in the 3-months mean summer concentration, the influence of biogenic emissions is calculated to contribute significantly to daily maximum ozone; up to 10 ppbv in certain areas. The ozone impacts calculated by WRF-Chem are larger than by the EMEP model in most of the region, and reach a maximum in southwestern Turkey where impacts of about 15 ppbv are seen in WRF-Chem, while the same area in EMEP MSC-W yields less than 5 ppbv. The large impact of biogenic emissions on ozone in southwestern Turkey was also found by Im and Kanakidou (2011). On average in the EM region, the daily maximum ozone impact of biogenic emissions is 5.8 and 5.2 ppbv in WRF-Chem and EMEP MSC-W, respectively (Table 5). These differences can be attributed mainly to the differences in magnitude and distribution of biogenic isoprene emissions (Figure 2). As mentioned in Section 2.3, the isoprene emissions in WRF-Chem are significantly higher than in the EMEP model, and in addition, biogenic NO emissions from soil are only included in WRF-Chem.

It is worth noting the large ozone impact of biogenic emissions over anthropogenic hotspot regions, such as the Po Valley and Cairo in WRF-Chem, and downwind of Athens in EMEP MSC-W (Figure 12). The relatively modest biogenic emissions in these regions

suggest that the large ozone impacts are not caused by biogenic emissions alone, but most probably these emissions act to increase the ozone production efficiency in regions dominated by anthropogenic emissions. Hotspot areas are often in a VOC-limited regime, and when nearby sources add biogenic emissions of VOCs, which are dominated by the very reactive isoprene gas, the ozone production may become much more efficient (Simpson, 1995). Im et al. (2011b) showed that biogenic VOC emissions intensified ozone production downwind of Istanbul.

A similar model sensitivity study keeping the temperature below 28°C in the calculation of biogenic emissions caused a similar pattern, although much lower in magnitude (Figure 12). Also, the distribution is more influenced by the temperature distribution (Figure 5) with the strongest ozone impacts in regions where there is a combination of strong biogenic emissions and high temperatures, particularly in and downwind of Greece and southern Italy. In WRF-Chem the temperature effect on ozone through biogenic emissions is particularly strong in Cairo and southwestern Turkey, while the Po Valley is only slightly affected. The difference between the two models is large, with summer mean daily maximum ozone averaged over the EM region of 0.68 and 0.43 ppbv calculated by WRF-Chem and EMEP MSC-W, respectively (Table 5), and this is due to two reasons. Firstly, the WRF-Chem biogenic emissions are larger in regions where the temperature is high, e.g. western Turkey and southern Greece. Secondly, a comparison of the daily mean 2 m temperature fields for the heat wave periods (not shown) reveals that the HIRLAM meteorology used in EMEP MSC-W has lower temperatures over land compared to WRF, with differences up to 5°C at many places.

3.3.3 Impact of high temperatures on chemistry

The impact of increased temperatures on photo-oxidant chemistry is normally driven by several factors. As well as changing emissions of BVOC and deposition processes as already addressed, higher temperature affects many reaction rates, usually promoting ozone production. An important mechanism is that enhanced dissociation of PAN to NO_2 leads to more production of ozone (Sillman and Samson, 1995). Solberg et al. (2008) demonstrated the large impact (order of 5 %) high temperatures had on peak ozone during the European heat wave in August 2003. From Figure 9 and Table 5 it seems that the effect of high

637 temperatures on chemistry calculations in the EM region is relatively small with summer
638 mean daily maximum ozone contributions of 0.063 and 0.069 ppbv calculated by the WRF-
639 Chem and EMEP models, respectively; much lower than the ozone impact of high
640 temperatures on biogenic emissions and dry deposition. However, there are large differences
641 in the horizontal distribution (Figure 13). The summer mean impact on daily maximum ozone
642 is up to 1 ppbv in many places, particularly over large cities located in areas strongly affected
643 by the heat waves, such as Thessaloniki and Athens. Additionally, large signals are seen near
644 regions influenced by biogenic emissions, as e.g. southwest Turkey (in WRF-Chem), south
645 Italy, and the northern part of the Balkan Peninsula. A small signal is also seen where the
646 Albanian forest fires took place.

647 In the WRF-Chem model results, regions with slightly negative (down to -0.3 ppbv)
648 ozone impacts of high temperatures can be seen, most notably over the Mediterranean Sea
649 and North Africa. The reason is that high temperatures lead to faster decomposition of PAN to
650 NO_2, and as a consequence the ozone formation will take place closer to the emission sources.
651 As the winds come from north during the heat waves (Figure 5), high temperatures lead to
652 lower production of ozone south (downwind) of the major emission regions. This is related to
653 the findings of Sillman and Samson (1995) who suggested that ozone in the free troposphere
654 did not increase with temperatures in the polluted PBL, because decreased export of PAN
655 balances the increased export of ozone.

656

657 ### 3.3.4 Impact of dry deposition

658 Dry deposition is the major sink for surface ozone, and contributes to a summer mean
659 decrease in daily maximum ozone of 17 ppbv in the EM region (Table 5). The effect on daily
660 mean concentrations would probably be even larger as dry deposition is more important
661 during night when the PBL height is low. The horizontal distribution of the dry deposition
662 effect on daily maximum ozone shows impacts between -20 and -30 ppbv over, and north of,
663 the Balkan peninsula (Figure 14). Areas further south are more sparsely vegetated,
664 particularly the desert in North Africa, and the impacts are therefore lower in these regions. It
665 should be noted, however, that any ozone reduction due to dry deposition taking place outside
666 the model domain has not been taken into account, as the lateral boundary conditions are the
667 same in all simulations. Furthermore, the total impact of heat waves on dry deposition is

probably underestimated as the Wesely (1989) dry deposition scheme used in WRF-Chem only considers changes in temperature, and not in soil moisture or near-surface humidity. The extremely low soil moisture in the summer 2007 (Founda and Giannakopoulos, 2009) is likely to have caused a significant increase in the deposition surface resistance, as highlighted by Vautard et al. (2005), Solberg et al. (2008) and Vieno et al. (2010) for the European summer 2003 heat wave.

The temperature effect on dry deposition gives increases in summer mean daily maximum ozone up to 1.5 ppbv in several places (Figure 14). Both the magnitude and geographical distribution is similar to the temperature effect on biogenic emissions, but dry deposition has a stronger impact in the northern part of the domain. A few exceptions from the sparse vegetation in North Africa can be seen over the Nile Delta north of Cairo, and over the northern parts of Algeria and Tunisia. The temperature impact on dry deposition is relatively strong here, which is partly because these areas rather frequently experience summer temperatures above 28°C, not only during heat wave episodes.

3.3.5 Impact of anthropogenic emissions

Ozone precursor emissions from anthropogenic sources are the single most important factor impacting ozone among the sensitivity tests studied here. In the EM region, the increase in daily max ozone concentration averaged over the summer, due to anthropogenic emissions, is 26 ppbv (Table 5), and in some regions the concentration change exceeds 45 ppbv (Figure 15). Note that the boundary conditions are the same in all simulations, excluding impacts of anthropogenic emissions taking place outside the model domain. The horizontal distribution largely follows the pattern of NO_X emissions (Figure 2), and also the ozone fields in the reference simulation (Figure 10). Several large cities can be recognized, but our results indicate that emissions from shipping have the strongest anthropogenic impact on ozone in the region (Figure 15). The highest contributions are found west of Crete and north of the Nile Delta, where emissions from Athens and Cairo, respectively, mix with ship emissions and effectively produce ozone. Due to the large fraction of NO_X in ship emissions, regions near the ship tracks are usually VOC-limited, and inflow of urban pollution plumes, containing a larger fraction of VOCs, therefore leads to an increase in the ozone production efficiency. The ozone levels are further intensified by the ineffectiveness of dry deposition over sea.

4 Conclusions

Model calculations for the Eastern Mediterranean hotspot area in summer 2007 are presented using the WRF-Chem and the EMEP MSC-W models. Three heat waves and numerous wildfires struck the Eastern Mediterranean area and strongly affected air pollution levels during summer 2007. Comparisons with satellite observations of CO and NO_2 columns from IASI and OMI, respectively, show that the models are able to capture the location and influence of the fires relatively well. However, the extreme levels of CO that were observed in the Peloponnese fire plume were not reflected in the model results. This is most likely caused by underestimation of CO in the forest fire emission inventories (FINN and GFED). As the magnitude of the NO_2 fire plumes were better reflected by the models, our results suggest that the CO/NO_X fire emission ratios should be re-assessed. The NO_2 comparison showed very good agreement for the simulation using FINN emissions, confirming the importance of high temporal and spatial resolution emission data. Inter-model differences were also seen, presumably caused by the different methods used for distributing the fire emissions vertically. Furthermore, the NO_2 satellite observations reveal several anthropogenic hotspots of air pollution with the Po Valley as the most dominant. The models represent the hotspot NO_2 levels relatively well, except that the tropospheric NO_2 columns over Istanbul are underestimated by at least a factor of 2 due to underestimation of emissions in this region. Model-calculated daily maximum surface O_3 concentrations are in fairly good agreement with observations from 10 European stations. Both models and observations show elevated ozone levels in mid-July due to higher temperatures and calm winds in central/eastern Europe.

Results from sensitivity simulations show that anthropogenic emissions of ozone precursors are the largest contributor to daily maximum near-surface ozone concentrations in the Eastern Mediterranean during summer 2007. In some regions the summer average concentration change due to anthropogenic emissions exceeds 45 ppbv with the largest ozone perturbations located near the ship tracks. Biogenic emissions, dominated by isoprene and terpenes, react with anthropogenic NO_X emissions and contribute up to 10 ppbv ozone (3-month mean) in certain areas. However, the model differences are large with stronger ozone impact in WRF-Chem than in EMEP MSC-W, mainly because of differences in biogenic emissions. Daily maximum ozone concentrations are reduced by 20-30 ppbv in large parts of the region due to dry deposition, the major sink for surface ozone.

Forest fire emissions from Greece and Albania contributed substantially to ozone production, particularly in the latter half of July and the end of August. Even in the seasonal (JJA) average the models calculated forest fire impacts on daily maximum ozone up to 18 ppbv in the core of the plume, but with large differences between the FINN and GFED emission inventories. The most intense forest fire episodes coincided with the two most severe heat waves, leading to more intense ozone production. Biogenic emissions increased as a response to high temperatures (> 28°C), and this led to increased daily maximum ozone by up to 3 ppbv on some days when averaged over the Eastern Mediterranean region. The high temperatures also reduced dry deposition, causing up to 1.5 ppbv increase in ozone. The direct impact of high temperatures on ozone chemistry was surprisingly low with less than 1 ppbv on average over the region, but there were large spatial differences within the region.

Thus, if summers such as in 2007 occur more frequently in the future, ozone levels in the Eastern Mediterranean region could increase substantially due to the temperature impact on biogenic emissions and dry deposition. (Future biogenic VOC emissions will likely be affected by factors other than temperature also, e.g. CO_2 levels or soil water changes, see e.g. Arneth et al. (2007), Possell and Hewitt (Possell and Hewitt, 2011), but such biogeochemical factors are beyond the scope of this study.) Moreover, heat wave episodes lead to increased risk of forest fires, which could further intensify ozone formation. As a consequence, these processes need to be taken into account when assessing mitigation options for the future.

Acknowledgements

The research leading to these results has received funding from the European Union's Seventh Framework Programme (FP7/2007-2013) under Grant Agreement no. 212095 (CityZen). Andreas Hilboll acknowledges funding by the Earth System Science Research School (ESSReS), an initiative of the Helmholtz Association of German research centres (HGF) at the Alfred Wegener Institute for Polar and Marine Research. OMI version-3 NO_2 slant column data was provided by NASA. ØH and FS want to thank Angelika Heil, Research Center Juelich, for providing GFEDv2 emission data for various species, and Christine Wiedinmyer, National Center for Atmospheric Research, for providing the FINNv1 forest fire emissions. We would also like to acknowledge the EMEP programme for access to measurement data at http://ebas.nilu.no. NOTUR, the Norwegian metacenter for

computational science, is acknowledged for giving Nilu access to the HPC (High Performance Computing) infrastructure, through the project nn9132k.

References

Aas, W., Hjellbrekke, A., Benedictow, A., Berge, H., Fagerli, H., Gauss, M., Jonson, J. E., Nyiri, A., Simpson, D., Tsyro, S., Valdebenito, A., Shamsudheen, S. V., Wind, P., Mareckova, K., Wankmüller, R., Iversen, T., Kirkevåg, A., Seland, Ø., Haugen, J. E., and Mills, G.: Transboundary Acidification, Eutrophication and Ground Level Ozone in Europe in 2008, Norwegian Meteorological Institute, Report 1/2010, 2010.

Andersson-Sköld, Y., and Simpson, D.: Comparison of the chemical schemes of the EMEP MSC-W and IVL photochemical trajectory models, Atmospheric Environment, 33 (7), 1111-1129, 10.1016/s1352-2310(98)00296-9, 1999.

Andreae, M. O., and Merlet, P.: Emission of trace gases and aerosols from biomass burning, Glob. Biogeochem. Cycle, 15 (4), 955-966, 2001.

Arneth, A., Miller, P. A., Scholze, M., Hickler, T., Schurgers, G., Smith, B., and Prentice, I. C.: CO2 inhibition of global terrestrial isoprene emissions: Potential implications for atmospheric chemistry, Geophys. Res. Lett., 34 (18), 10.1029/2007gl030615, 2007.

Atkinson, R.: Atmospheric chemistry of VOCs and NOx, Atmospheric Environment, 34 (12-14), 2063-2101, 10.1016/s1352-2310(99)00460-4, 2000.

Beniston, M.: The 2003 heat wave in Europe: A shape of things to come? An analysis based on Swiss climatological data and model simulations, Geophys. Res. Lett., 31, L02202, 10.1029/2003gl018857, 2004.

Benjamin, M. T., Sudol, M., Vorsatz, D., and Winer, A. M.: A spatially and temporally resolved biogenic hydrocarbon emissions inventory for the California South Coast Air Basin, Atmospheric Environment, 31 (18), 3087-3100, 10.1016/s1352-2310(97)00014-9, 1997.

Berge, E., and Jakobsen, H. A.: A regional scale multi-layer model for the calculation of long-term transport and deposition of air pollution in Europe, Tellus Ser. B-Chem. Phys. Meteorol., 50 (3), 205-223, 10.1034/j.1600-0889.1998.t01-2-00001.x, 1998.

Clerbaux, C., Boynard, A., Clarisse, L., George, M., Hadji-Lazaro, J., Herbin, H., Hurtmans, D., Pommier, M., Razavi, A., Turquety, S., Wespes, C., and Coheur, P. F.: Monitoring of atmospheric composition using the thermal infrared IASI/MetOp sounder, Atmospheric Chemistry and Physics, 9 (16), 6041-6054, 2009.

Colette, A., Granier, C., Hodnebrog, Ø., Jakobs, H., Maurizi, A., Nyiri, A., Bessagnet, B., D'Angiola, A., D'Isidoro, M., Gauss, M., Meleux, F., Memmesheimer, M., Mieville, A., Rouïl, L., Russo, F., Solberg, S., Stordal, F., and Tampieri, F.: Air quality trends in Europe over the past decade: a first multi-model assessment, Atmos. Chem. Phys. Discuss., 11 (7), 19029-19087, 10.5194/acpd-11-19029-2011, 2011.

Crutzen, P. J.: Photochemical Reactions Initiated by and Influencing Ozone in Unpolluted Tropospheric Air, Tellus, 26 (1-2), 47-57, 1974.

801 Deeter, M. N., Emmons, L. K., Francis, G. L., Edwards, D. P., Gille, J. C., Warner, J. X.,
802 Khattatov, B., Ziskin, D., Lamarque, J. F., Ho, S. P., Yudin, V., Attie, J. L., Packman, D.,
803 Chen, J., Mao, D., and Drummond, J. R.: Operational carbon monoxide retrieval algorithm
804 and selected results for the MOPITT instrument, J. Geophys. Res.-Atmos., 108 (D14), 4399,
805 10.1029/2002jd003186, 2003.

806 Denier van der Gon, H. A. C., Visschedijk, A., van der Brugh, H., and Dröge, R.: A high
807 resolution European emission data base for the year 2005, A contribution to UBA- Projekt
808 PAREST: Particle Reduction Strategies, TNO report TNO-034-UT-2010-01895_RPT-ML,
809 Utrecht, 2010.

810 Dore, C. J., Watterson, J. D., Murrells, T. P., Passant, N. R., Hobson, M. M., Choudrie, S. L.,
811 Thistlethwaite, G., Wagner, A., Jackson, J., Li, Y., Bush, T., King, K. R., Norris, J., Coleman,
812 P. J., Walker, C., Stewart, R. A., Goodwin, J. W. L., Tsagatakis, I., Conolly, C., Downes, M.
813 K., Brophy, N., and Hann, M. R.: UK Emissions of Air Pollutants 1970 to 2005, Technical
814 Report, 2007.

815 Emberson, L. D., Ashmore, M. R., Simpson, D., Tuovinen, J. P., and Cambridge, H. M.:
816 Modelling and mapping ozone deposition in Europe, Water Air Soil Pollut., 130 (1-4), 577-
817 582, 10.1023/a:1013851116524, 2001.

818 Eremenko, M., Dufour, G., Foret, G., Keim, C., Orphal, J., Beekmann, M., Bergametti, G.,
819 and Flaud, J. M.: Tropospheric ozone distributions over Europe during the heat wave in July
820 2007 observed from infrared nadir spectra recorded by IASI, Geophys. Res. Lett., 35 (18),
821 10.1029/2008gl034803, 2008.

822 Founda, D., and Giannakopoulos, C.: The exceptionally hot summer of 2007 in Athens,
823 Greece - A typical summer in the future climate?, Glob. Planet. Change, 67 (3-4), 227-236,
824 10.1016/j.gloplacha.2009.03.013, 2009.

825 Freitas, S. R., Longo, K. M., Chatfield, R., Latham, D., Silva Dias, M. A. F., Andreae, M. O.,
826 Prins, E., Santos, J. C., Gielow, R., and Carvalho Jr, J. A.: Including the sub-grid scale plume
827 rise of vegetation fires in low resolution atmospheric transport models, Atmos. Chem. Phys.,
828 7 (13), 3385-3398, 10.5194/acp-7-3385-2007, 2007.

829 Gauss, M., Benedictow, A. C., Fagerli, H., Steensen, B. M., and Hjellbrekke, A.: EMEP
830 Unified model performance for acidifying and eutrophying components and photo-oxidants in
831 2009, Norwegian Meteorological Institute, Report 1/2011, 2011.

832 George, M., Clerbaux, C., Hurtmans, D., Turquety, S., Coheur, P. F., Pommier, M., Hadji-
833 Lazaro, J., Edwards, D. P., Worden, H., Luo, M., Rinsland, C., and McMillan, W.: Carbon
834 monoxide distributions from the IASI/METOP mission: evaluation with other space-borne
835 remote sensors, Atmospheric Chemistry and Physics, 9 (21), 8317-8330, 2009.

836 Gerasopoulos, E., Kouvarakis, G., Vrekoussis, M., Kanakidou, M., and Mihalopoulos, N.:
837 Ozone variability in the marine boundary layer of the eastern Mediterranean based on 7-year
838 observations, J. Geophys. Res.-Atmos., 110, D15309, 10.1029/2005jd005991, 2005.

839 Grell, G. A., Peckham, S. E., Schmitz, R., McKeen, S. A., Frost, G., Skamarock, W. C., and
840 Eder, B.: Fully coupled "online" chemistry within the WRF model, Atmospheric
841 Environment, 39 (37), 6957-6975, 2005.

842 Guenther, A., Karl, T., Harley, P., Wiedinmyer, C., Palmer, P. I., and Geron, C.: Estimates of
843 global terrestrial isoprene emissions using MEGAN (Model of Emissions of Gases and
844 Aerosols from Nature), Atmospheric Chemistry and Physics, 6, 3181-3210, 2006.

Guenther, A. B., Zimmerman, P. R., Harley, P. C., Monson, R. K., and Fall, R.: Isoprene and Monoterpene Emission Rate Variability - Model Evaluations and Sensitivity Analyses, J. Geophys. Res.-Atmos., 98 (D7), 12609-12617, 10.1029/93jd00527, 1993.

Hjellbrekke, A., Solberg, S., and Fjæraa, A. M.: Ozone measurements 2009, Norwegian Institute for Air Research, EMEP/CCC-Report 2/2011, 2011.

Hodnebrog, Ø., Stordal, F., and Berntsen, T. K.: Does the resolution of megacity emissions impact large scale ozone?, Atmospheric Environment, 45 (38), 6852-6862, 10.1016/j.atmosenv.2011.01.012, 2011.

Im, U., Markakis, K., Unal, A., Kindap, T., Poupkou, A., Incecik, S., Yenigun, O., Melas, D., Theodosi, C., and Mihalopoulos, N.: Study of a winter PM episode in Istanbul using the high resolution WRF/CMAQ modeling system, Atmospheric Environment, 44 (26), 3085-3094, 10.1016/j.atmosenv.2010.05.036, 2010.

Im, U., and Kanakidou, M.: Summertime impacts of Eastern Mediterranean megacity emissions on air quality, Atmos. Chem. Phys. Discuss., 11 (9), 26657-26690, 10.5194/acpd-11-26657-2011, 2011.

Im, U., Markakis, K., Poupkou, A., Melas, D., Unal, A., Gerasopoulos, E., Daskalakis, N., Kindap, T., and Kanakidou, M.: The impact of temperature changes on summer time ozone and its precursors in the Eastern Mediterranean, Atmospheric Chemistry and Physics, 11 (8), 3847-3864, 10.5194/acp-11-3847-2011, 2011a.

Im, U., Poupkou, A., Incecik, S., Markakis, K., Kindap, T., Unal, A., Melas, D., Yenigun, O., Topcu, S., Odman, M. T., Tayanc, M., and Guler, M.: The impact of anthropogenic and biogenic emissions on surface ozone concentrations in Istanbul, Science of The Total Environment, 409 (7), 1255-1265, 10.1016/j.scitotenv.2010.12.026, 2011b.

Jacob, D. J., and Winner, D. A.: Effect of climate change on air quality, Atmospheric Environment, 43 (1), 51-63, 10.1016/j.atmosenv.2008.09.051, 2009.

Jonson, J. E., Stohl, A., Fiore, A. M., Hess, P., Szopa, S., Wild, O., Zeng, G., Dentener, F. J., Lupu, A., Schultz, M. G., Duncan, B. N., Sudo, K., Wind, P., Schulz, M., Marmer, E., Cuvelier, C., Keating, T., Zuber, A., Valdebenito, A., Dorokhov, V., De Backer, H., Davies, J., Chen, G. H., Johnson, B., Tarasick, D. W., Stübi, R., Newchurch, M. J., von der Gathen, P., Steinbrecht, W., and Claude, H.: A multi-model analysis of vertical ozone profiles, Atmos. Chem. Phys., 10 (12), 5759-5783, 10.5194/acp-10-5759-2010, 2010a.

Jonson, J. E., Valiyaveetil, S., Wind, P., Valdebenito, A., and Gauss, M.: Model validation of the global version of the EMEP Unified model, in: Development of the EMEP global modelling framework: Progress report, Joint MSC-W/MSC-E Report, EMEP/MSC-W Technical Report 1/2010, The Norwegian Meteorological Institute, Oslo, Norway, 14-31, 2010b.

Kanakidou, M., Mihalopoulos, N., Kindap, T., Im, U., Vrekoussis, M., Gerasopoulos, E., Dermitzaki, E., Unal, A., Koçak, M., Markakis, K., Melas, D., Kouvarakis, G., Youssef, A. F., Richter, A., Hatzianastassiou, N., Hilboll, A., Ebojie, F., Wittrock, F., von Savigny, C., Burrows, J. P., Ladstaetter-Weissenmayer, A., and Moubasher, H.: Megacities as hot spots of air pollution in the East Mediterranean, Atmospheric Environment, 45 (6), 1223-1235, 10.1016/j.atmosenv.2010.11.048, 2011.

Kaskaoutis, D. G., Kharol, S. K., Sifakis, N., Nastos, P. T., Sharma, A. R., Badarinath, K. V. S., and Kambezidis, H. D.: Satellite monitoring of the biomass-burning aerosols during the

889 wildfires of August 2007 in Greece: Climate implications, Atmospheric Environment, 45 (3),
890 716-726, 10.1016/j.atmosenv.2010.09.043, 2011.

891 Köble, R., and Seufert, G.: Novel Maps for Forest Tree Species in Europe, A Changing
892 Atmosphere, 8th European Symposium on the Physico-Chemical Behaviour of Atmospheric
893 Pollutants, Torino, Italy, 17-20 Sept., 2001, 2001.

894 Kourtidis, K., Zerefos, C., Rapsomanikis, S., Simeonov, V., Balis, D., Perros, P. E.,
895 Thompson, A. M., Witte, J., Calpini, B., Sharobiem, W. M., Papayannis, A., Mihalopoulos,
896 N., and Drakou, R.: Regional levels of ozone in the troposphere over eastern Mediterranean,
897 J. Geophys. Res.-Atmos., 107 (D18), 8140, 10.1029/2000jd000140, 2002.

898 Kuenen, J., Denier van der Gon, H. A. C., Visschedijk, A., and van der Brugh, H.: High
899 resolution European emission inventory for the years 2003 – 2007, TNO report TNO-060-
900 UT-2011-00588, Utrecht, 2011.

901 Levelt, P. F., Van den Oord, G. H. J., Dobber, M. R., Malkki, A., Visser, H., de Vries, J.,
902 Stammes, P., Lundell, J. O. V., and Saari, H.: The Ozone Monitoring Instrument, IEEE Trans.
903 Geosci. Remote Sensing, 44 (5), 1093-1101, 10.1109/tgrs.2006.872333, 2006.

904 Liu, Y., Kahn, R. A., Chaloulakou, A., and Koutrakis, P.: Analysis of the impact of the forest
905 fires in August 2007 on air quality of Athens using multi-sensor aerosol remote sensing data,
906 meteorology and surface observations, Atmospheric Environment, 43 (21), 3310-3318,
907 10.1016/j.atmosenv.2009.04.010, 2009.

908 Luterbacher, J., Liniger, M. A., Menzel, A., Estrella, N., Della-Marta, P. M., Pfister, C.,
909 Rutishauser, T., and Xoplaki, E.: Exceptional European warmth of autumn 2006 and winter
910 2007: Historical context, the underlying dynamics, and its phenological impacts, Geophys.
911 Res. Lett., 34, L12704, 10.1029/2007gl029951, 2007.

912 Madronich, S.: Photodissociation in the atmosphere .1. Actinic flux and the effects of ground
913 reflections and clouds, J. Geophys. Res.-Atmos., 92 (D8), 9740-9752, 1987.

914 Metzger, S., Dentener, F., Pandis, S., and Lelieveld, J.: Gas/aerosol partitioning: 1. A
915 computationally efficient model, J. Geophys. Res.-Atmos., 107 (D16),
916 10.1029/2001jd001102, 2002.

917 Pfister, G. G., Avise, J., Wiedinmyer, C., Edwards, D. P., Emmons, L. K., Diskin, G. D.,
918 Podolske, J., and Wisthaler, A.: CO source contribution analysis for California during
919 ARCTAS-CARB, Atmos. Chem. Phys., 11 (15), 7515-7532, 10.5194/acp-11-7515-2011,
920 2011.

921 Possell, M., and Hewitt, C. N.: Isoprene emissions from plants are mediated by atmospheric
922 CO2 concentrations, Global Change Biology, 17 (4), 1595-1610, 10.1111/j.1365-
923 2486.2010.02306.x, 2011.

924 Poupkou, A., Symeonidis, P., Lisaridis, I., Melas, D., Ziomas, I., Yay, O. D., and Balis, D.:
925 Effects of anthropogenic emission sources on maximum ozone concentrations over Greece,
926 Atmospheric Research, 89 (4), 374-381, 10.1016/j.atmosres.2008.03.009, 2008.

927 Poupkou, A., Melas, D., Ziomas, I., Symeonidis, P., Lisaridis, I., Gerasopoulos, E., and
928 Zerefos, C.: Simulated Summertime Regional Ground-Level Ozone Concentrations over
929 Greece, Water Air Soil Pollut., 196 (1-4), 169-181, 10.1007/s11270-008-9766-0, 2009.

930 RETRO: REanalysis of the TROpospheric chemical composition over the past 40 years.
931 http://retro.enes.org, 2006.

Richter, A., Burrows, J. P., Nuss, H., Granier, C., and Niemeier, U.: Increase in tropospheric nitrogen dioxide over China observed from space, Nature, 437 (7055), 129-132, 10.1038/nature04092, 2005.

Rodgers, C. D.: Inverse methods for atmospheric sounding: theory and practice, World Scientific, 2000.

Schär, C., Vidale, P. L., Luthi, D., Frei, C., Haberli, C., Liniger, M. A., and Appenzeller, C.: The role of increasing temperature variability in European summer heatwaves, Nature, 427 (6972), 332-336, 10.1038/nature02300, 2004.

Schürmann, G. J., Algieri, A., Hedgecock, I. M., Manna, G., Pirrone, N., and Sprovieri, F.: Modelling local and synoptic scale influences on ozone concentrations in a topographically complex region of Southern Italy, Atmospheric Environment, 43 (29), 4424-4434, 10.1016/j.atmosenv.2009.06.017, 2009.

Sillman, S., and Samson, F. J.: Impact of Temperature on Oxidant Photochemistry in Urban, Polluted Rural and Remote Environments, J. Geophys. Res.-Atmos., 100 (D6), 11497-11508, 10.1029/94jd02146, 1995.

Simpson, D.: Biogenic Emissions in Europe .2. Implications for Ozone Control Strategies, J. Geophys. Res.-Atmos., 100 (D11), 22891-22906, 10.1029/95jd01878, 1995.

Simpson, D., Guenther, A., Hewitt, C. N., and Steinbrecher, R.: Biogenic emissions in Europe .1. Estimates and uncertainties, J. Geophys. Res.-Atmos., 100 (D11), 22875-22890, 1995.

Simpson, D., Winiwarter, W., Borjesson, G., Cinderby, S., Ferreiro, A., Guenther, A., Hewitt, C. N., Janson, R., Khalil, M. A. K., Owen, S., Pierce, T. E., Puxbaum, H., Shearer, M., Skiba, U., Steinbrecher, R., Tarrason, L., and Oquist, M. G.: Inventorying emissions from nature in Europe, J. Geophys. Res.-Atmos., 104 (D7), 8113-8152, 1999.

Simpson, D., Fagerli, H., Jonson, J. E., Tsyro, S., Wind, P., and Tuovinen, J. P.: The EMEP Unified Eulerian Model. Model Description. EMEP MSC-W Report 1/2003, The Norwegian Meteorological Institute, Oslo, 2003a.

Simpson, D., Tuovinen, J. P., Emberson, L., and Ashmore, M. R.: Characteristics of an ozone deposition module II: Sensitivity analysis, Water Air Soil Pollut., 143 (1-4), 123-137, 10.1023/a:1022890603066, 2003b.

Simpson, D., Benedictow, A., Berge, H., Bergström, R., Fagerli, H., Gauss, M., Hayman, G., Jenkin, M. E., Jonson, J. E., Nyiri, A., Richter, C., Semeena, V., Tsyro, S., Valdebenito, A., and Wind, P.: The EMEP MSC-W Chemical Transport Model: Model Description in preparation, 2011.

Skamarock, W. C., and Klemp, J. B.: A time-split nonhydrostatic atmospheric model for weather research and forecasting applications, J. Comput. Phys., 227 (7), 3465-3485, 10.1016/j.jcp.2007.01.037, 2008.

Sofiev, M., Vankevich, R., Lotjonen, M., Prank, M., Petukhov, V., Ermakova, T., Koskinen, J., and Kukkonen, J.: An operational system for the assimilation of the satellite information on wild-land fires for the needs of air quality modelling and forecasting, Atmos. Chem. Phys., 9 (18), 6833-6847, 10.5194/acp-9-6833-2009, 2009.

Solberg, S., Hov, O., Sovde, A., Isaksen, I. S. A., Coddeville, P., De Backer, H., Forster, C., Orsolini, Y., and Uhse, K.: European surface ozone in the extreme summer 2003, J. Geophys. Res.-Atmos., 113 (D7), 16, D0730710.1029/2007jd009098, 2008.

975 Søvde, O. A., Gauss, M., Smyshlyaev, S. P., and Isaksen, I. S. A.: Evaluation of the chemical
976 transport model Oslo CTM2 with focus on arctic winter ozone depletion, J. Geophys. Res.-
977 Atmos., 113 (D09304), 10.1029/2007jd009240, 2008.

978 Stockwell, W. R., Middleton, P., Chang, J. S., and Tang, X. Y.: The 2nd generation regional
979 acid deposition model chemical mechanism for regional air-quality modeling, J. Geophys.
980 Res.-Atmos., 95 (D10), 16343-16367, 1990.

981 Symeonidis, P., Poupkou, A., Gkantou, A., Melas, D., Yay, O. D., Pouspourika, E., and Balis,
982 D.: Development of a computational system for estimating biogenic NMVOCs emissions
983 based on GIS technology, Atmospheric Environment, 42 (8), 1777-1789,
984 10.1016/j.atmosenv.2007.11.019, 2008.

985 Turquety, S., Hurtmans, D., Hadji-Lazaro, J., Coheur, P. F., Clerbaux, C., Josset, D., and
986 Tsamalis, C.: Tracking the emission and transport of pollution from wildfires using the IASI
987 CO retrievals: analysis of the summer 2007 Greek fires, Atmospheric Chemistry and Physics,
988 9 (14), 4897-4913, 2009.

989 van der Werf, G. R., Randerson, J. T., Giglio, L., Collatz, G. J., Kasibhatla, P. S., and
990 Arellano, A. F.: Interannual variability in global biomass burning emissions from 1997 to
991 2004, Atmos. Chem. Phys., 6, 3423-3441, 2006.

992 Vautard, R., Honore, C., Beekmann, M., and Rouil, L.: Simulation of ozone during the
993 August 2003 heat wave and emission control scenarios, Atmospheric Environment, 39 (16),
994 2957-2967, 10.1016/j.atmosenv.2005.01.039, 2005.

995 Vieno, M., Dore, A. J., Stevenson, D. S., Doherty, R., Heal, M. R., Reis, S., Hallsworth, S.,
996 Tarrason, L., Wind, P., Fowler, D., Simpson, D., and Sutton, M. A.: Modelling surface ozone
997 during the 2003 heat-wave in the UK, Atmospheric Chemistry and Physics, 10 (16), 7963-
998 7978, 10.5194/acp-10-7963-2010, 2010.

999 Visschedijk, A. J. H., Zandveld, P. Y. J., and Denier van der Gon, H. A. C.: A High
1000 Resolution Gridded European Emission Database for the EU Integrate Project GEMS, TNO
1001 report 2007-A-R0233/B, 2007.

1002 Wesely, M. L.: Parameterization of surface resistances to gaseous dry deposition in regional-
1003 scale numerical-models, Atmospheric Environment, 23 (6), 1293-1304, 1989.

1004 Wiedinmyer, C., Akagi, S. K., Yokelson, R. J., Emmons, L. K., Al-Saadi, J. A., Orlando, J. J.,
1005 and Soja, A. J.: The Fire INventory from NCAR (FINN): a high resolution global model to
1006 estimate the emissions from open burning, Geosci. Model Dev., 4 (3), 625-641, 10.5194/gmd-
1007 4-625-2011, 2011.

1008 (Western Regional Air Partnership): 2002 Fire Emission Inventory for the WRAP Region-
1009 Phase II, Project No. 178-6, available at:
1010 http://www.wrapair.org/forums/fejf/tasks/FEJFtask7PhaseII.html (last access: 27 July 2011),
1011 2005.

1012 Zabkar, R., Rakovec, J., and Koracin, D.: The roles of regional accumulation and advection of
1013 ozone during high ozone episodes in Slovenia: A WRF/Chem modelling study, Atmospheric
1014 Environment, 45 (5), 1192-1202, 10.1016/j.atmosenv.2010.08.021, 2011.

1015

1016

1017

1018

1019

1020 **Table 1. Setups of the participating models; WRF-Chem and EMEP.**

Model	WRF-Chem v. 3.2	EMEP MSC-W rv. 3.7.7
Operated by	Univ. of Oslo	NILU
Developed by	NOAA/NCAR and others	Met.no
Model type	Regional NWP + CTM	Regional CTM
Horizontal resolution	25 km × 25 km	25 km × 25 km
Horizontal grid size	104 × 99	264 × 318
Number of vertical levels	27	20
Model top	50 hPa	100 hPa
Meteorology	WRF (coupled w/chemistry)	HIRLAM (interp. from 10 km × 10 km)
Meteorological initial and boundary conditions	ECMWF-IFS[a]	ECMWF-IFS[a]
Chemistry scheme	RADM2 (Stockwell et al., 1990)	EMEP (Simpson et al., 2011)
Chemical initial and boundary conditions	Oslo CTM2 (Søvde et al., 2008; Colette et al., 2011)	Climatological, based upon measurements and ozone-sondes, see Simpson et al., (2003a; 2011)
Chemical species	63	71
Chemical reactions	158	140
Anthropogenic emissions	TNO-MACC (Kuenen et al., 2011)	Redistributed EMEP (http://www.emep.int; Visschedijk et al., 2007)
Biomass burning emissions	FINNv1 (Wiedinmyer et al., 2011) / GFEDv2 (van der	GFEDv2 (van der Werf et al., 2006)

	Werf et al., 2006)	
Biogenic emissions	MEGAN v. 2.04 (Guenther et al., 2006) online calculation	EMEP isoprene (Simpson et al., 1999) online calculation
References	Grell et al. (2005)	Simpson et al. (2003a; 2011)

[a]Documentation can be found at http://www.ecmwf.int/research/ifsdocs/

Table 2. Emissions from various sources averaged over the region marked by the dashed line in Figure 2 and for the summer period (June, July, August) of 2007, as used in the reference simulations of the two models.

	NO_X (kg(N) km^{-2} yr^{-1})	CO (kg(C) km^{-2} yr^{-1})	NMVOC (kg(NMVOC) km^{-2} yr^{-1})
WRF-Chem			
TNO-MACC anthropogenic	364.1	860.4	791.1
FINNv1 forest fires	30.9	809.1	413.7
MEGANv2 biogenic / soil	23.9	-	1,918.0[a]
EMEP MSC-W			
Regridded EMEP anthrop.	338.2	743.7	565.3
GFEDv2 (8-day) forest fires	49.0	1,233.9	387.8
EMEP biogenic / soil	-	-	949.4[a]

[a]Only isoprene emissions (kg(C_5H_8) km^{-2} yr^{-1}) given here, but note that the biogenic emission modules include also other NMVOCs such as terpenes.

Table 3. Overview of the model simulations performed by each of the two models. The WRF-Chem simulations include only gas-phase chemistry, while the EMEP MSC-W simulations include also aerosol chemistry.

Acronym	Description	WRF-Chem	EMEP MSC-W
REF	Reference (setup described in Sect. 2.1-2.3)	X	X
GF	FINN emissions replaced by GFED emissions	X[a]	
NF	No fire emissions	X	X
NB	No biogenic emissions	X	X
NA	No anthropogenic emissions	X	
ND	No dry deposition	X	
MC	Max. 28°C for chemistry calculations in the PBL[b]	X	X
MB	Max. 28°C when calculating biogenic emissions	X	X
MD	Max. 28°C when calculating dry deposition	X	

[a]FINN fire emissions are used in the WRF-Chem REF simulation, but an additional WRF-Chem simulation has been done with GFED fire emissions (GF) for comparison with EMEP MSC-W simulations.

[b]Planetary Boundary Layer (PBL) taken here as the lowest 2.5 km.

1040

1041 **Table 4. Comparison between observed and modeled daily maximum O_3 mixing ratios (ppbv) for 10**
1042 **stations (see http://ebas.nilu.no).**

	Observed	WRF-Chem				EMEP MSC-W			
Station	Mean	Mean	Bias	RMSE	*r*	Mean	Bias	RMSE	*r*
Illmitz	60.1	60.7	0.6	11.0	0.68	54.5	-5.6	11.4	0.77
Payerne	51.5	50.9	-0.6	7.7	0.71	48.9	-2.6	8.8	0.65
Svratouch	48.6	54.6	6.1	9.9	0.80	51.6	3.0	9.6	0.72
Kosetice	52.5	53.9	1.3	8.5	0.75	49.8	-2.8	10.4	0.62
Finokalia	69.9	66.3	-3.4	9.2	0.36	55.4	-14.4	16.5	0.35
K-puszta	65.8	59.3	-6.5	9.3	0.75	55.7	-10.1	13.2	0.56
Montelibretti	69.5	66.1	-3.3	11.3	0.68	60.5	-9.0	14.4	0.65
Iskrba	58.5	56.4	-2.1	10.2	0.63	53.9	-4.6	11.5	0.56
Stara Lesna	54.0	52.1	-1.9	7.3	0.70	50.3	-3.7	8.4	0.63
Starina	54.4	54.4	0.0	13.5	0.12	49.1	-5.3	12.8	0.11
Average	58.5	57.5	-1.0	9.8	0.62	53.0	-5.5	11.7	0.56

1043

1044

Table 5. Surface ozone mixing ratios (ppbv) in the reference run (1st row), and perturbations of surface O_3 due to various processes (rows 2-9). All values are based on model output of daily maximum surface O_3 in each gridbox the EM region for the summer 2007. Note that for dry deposition the percentiles and the maximum represent the highest negative values.

	WRF-Chem				EMEP MSC-W			
	Mean	99th percentile	99.99th percentile	Maximum	Mean	99th percentile	99.99th percentile	Maximum
Reference run	62.7	93.6	139.7	190.8	57.7	88.8	131.2	158.2
Forest fires (GFED)	1.6	23.4	90.2	157.5	1.9	23.9	69.4	94.0
Forest fires (FINN)	1.2	10.1	39.7	64.7				
Biog. emissions	5.8	19.4	37.5	55.0	5.2	17.4	38.6	63.8
High T in biog. emis.	0.7	5.0	11.6	17.7	0.5	4.2	10.5	19.4
High T in chemistry	0.1	2.3	12.4	18.8	0.1	1.4	7.7	14.3
High T in dry dep.	0.5	3.3	6.2	8.4				
Dry dep.	-16.9	-37.7	-49.8	-55.4				
Anthrop. emis.	25.7	57.0	99.2	154.9				

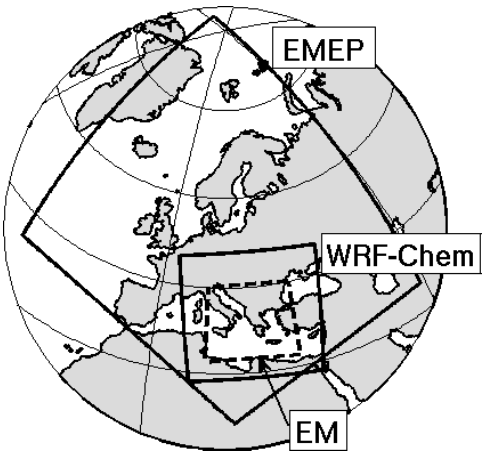

Figure 1. Locations of the domains used in the EMEP MSC-W and WRF-Chem simulations, and of the study region (11E-30E, 32N-45N) covering most of the Eastern Mediterranean (EM).

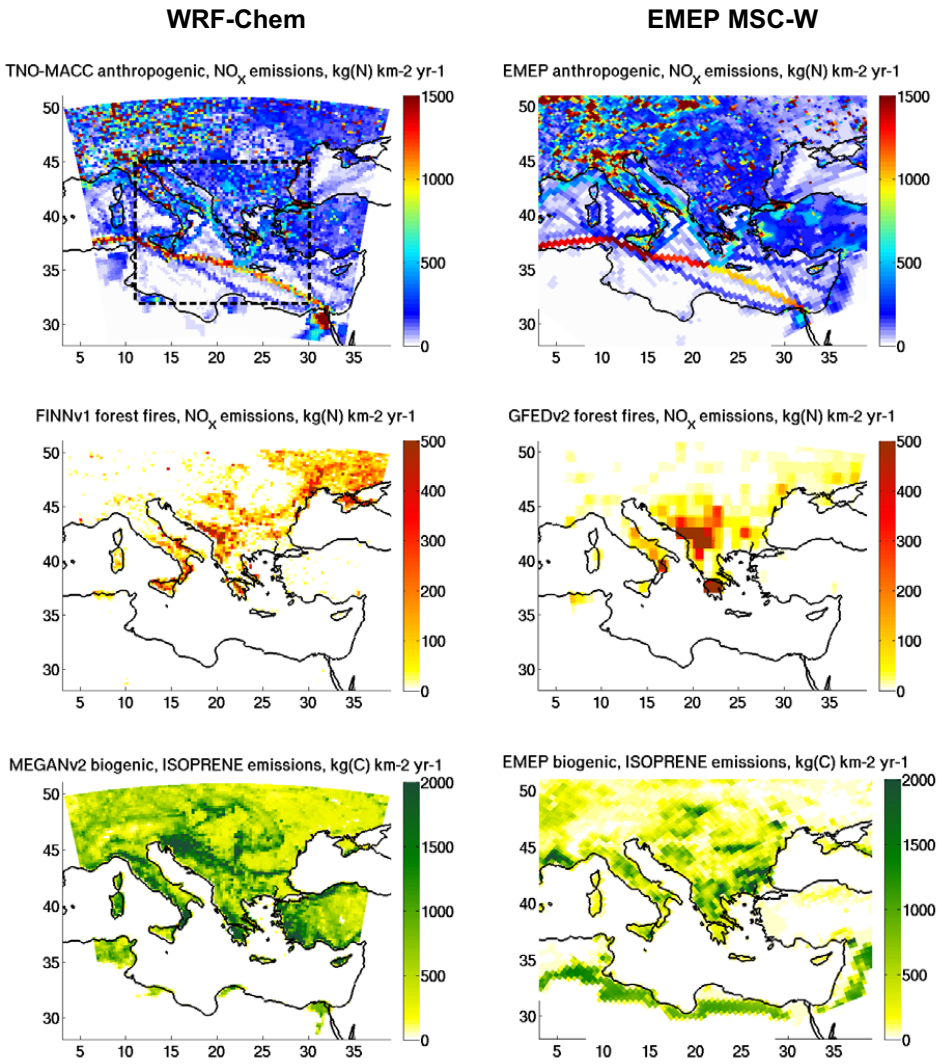

Figure 2. Seasonally (June, July, August) averaged emissions of NO_X (kg(N) km^{-2} yr^{-1}) from anthropogenic sources (top) and forest fires (middle), and emissions of isoprene (kg(C) km^{-2} yr^{-1}) from biogenic sources (bottom) as used in the reference simulations of the WRF-Chem (left) and EMEP MSC-W (right) models. The dashed rectangle in the topleft plot marks the EM region.

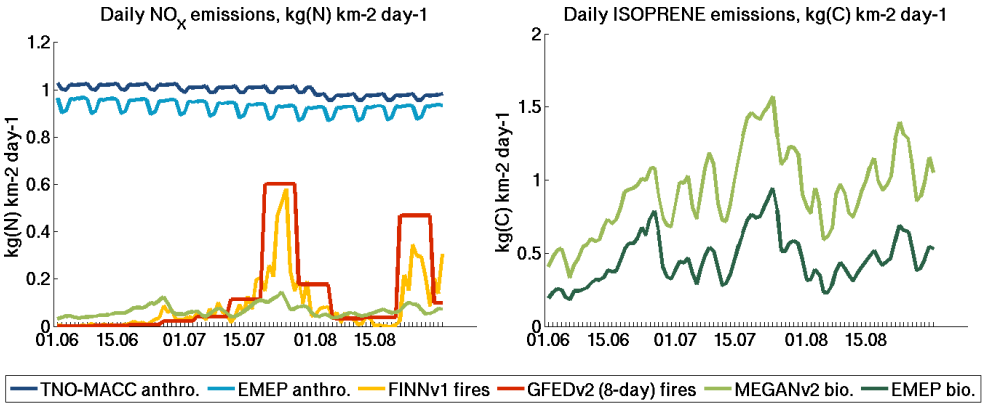

Figure 3. Temporal evolution of NO_X emissions from various sources (left; kg(N) km^{-2} day^{-1}), and of isoprene from biogenic sources (right; kg(C) km^{-2} day^{-1}) averaged over the region marked by the dashed rectangle in Figure 2. Biogenic soil emissions of NO are not included in the EMEP model.

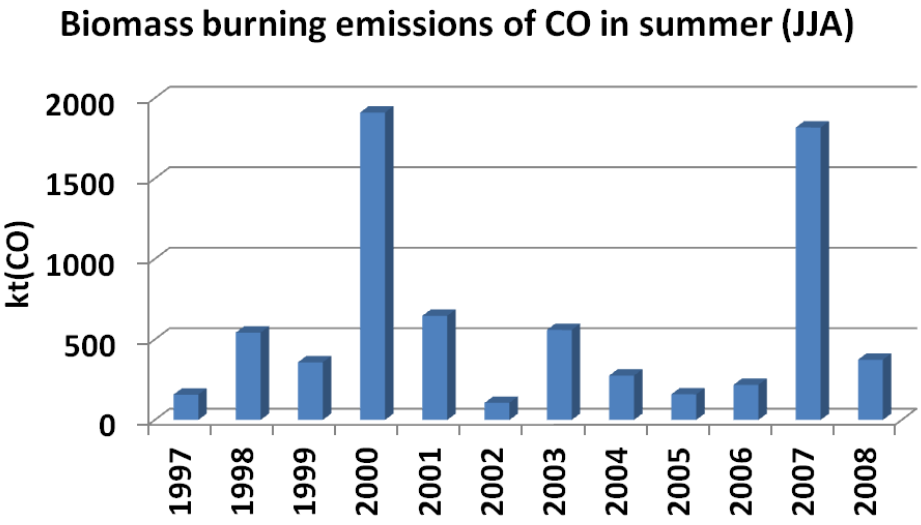

Figure 4. Biomass burning emissions of CO (kt CO) integrated over the summer period (June, July, August) and over the region marked by the dashed rectangle in Figure 2, as reported in the GFEDv2 emission inventory (van der Werf et al., 2006).

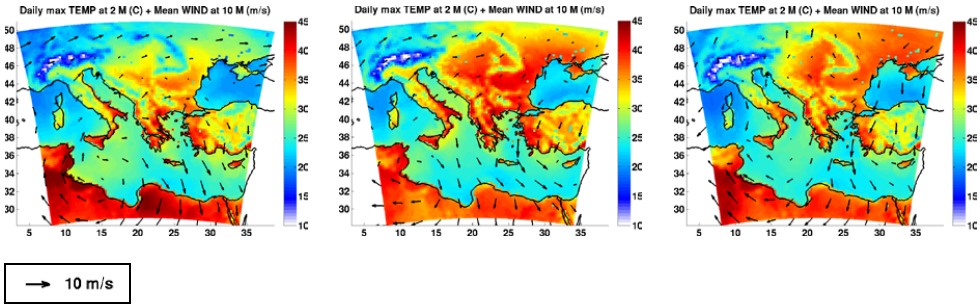

Figure 5. Daily maximum 2 m temperature (°C) and mean 10 m wind vectors (10 m s^{-1} vector shown for scale in legend) averaged over the periods June 22-24 (left), July 22-24 (middle), and August 24-26 (right) in 2007, based on hourly output from the WRF-Chem model.

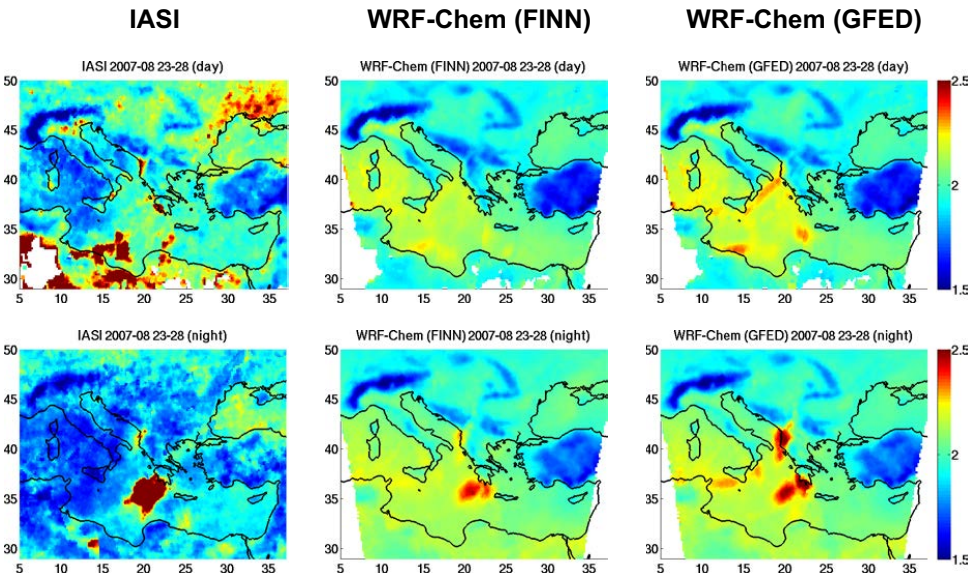

Figure 6. Kernel weighted total columns of CO (10^{18} molec cm^{-2}) as retrieved from the IASI satellite instrument (left), and as modelled with WRF-Chem using FINN (middle) and GFED (right) forest fires emissions. The data is averaged over the period 23-28 August 2007 for daytime (top) and nighttime (bottom) retrievals. The model data has been weighted with the same averaging kernels as the IASI data.

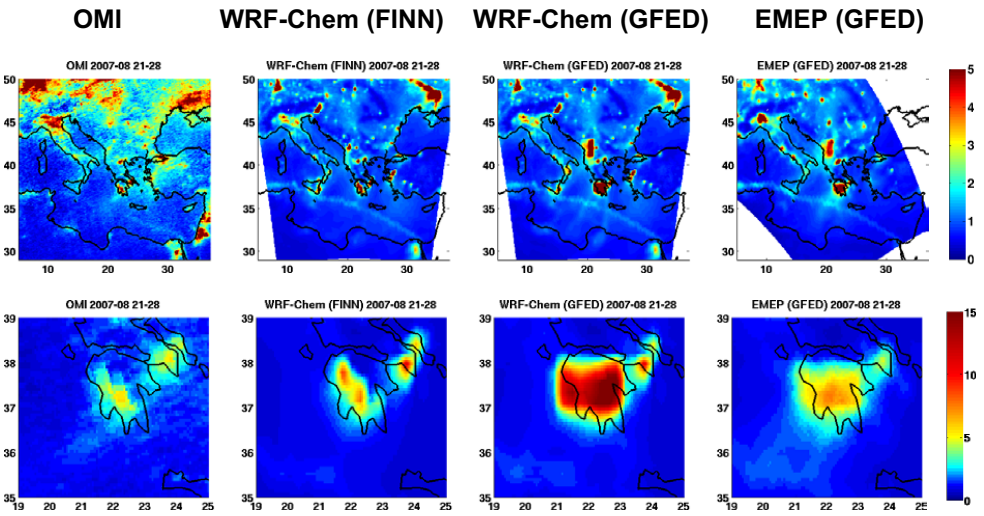

Figure 7. Tropospheric columns of NO_2 (10^{15} molec cm^{-2}) as retrieved from the OMI satellite instrument (1st column), and as modelled with the WRF-Chem (2nd and 3rd columns) and EMEP (4th column) models, averaged over the period 21-28 August 2007 (corresponding to the 8-day period in the GFED data set). In the second column, FINN forest fire emissions have been used in the simulations, while in the two rightmost columns, GFED emissions have been used. The bottom plots have different colour scale and are zoomed in on the Peloponnese fires.

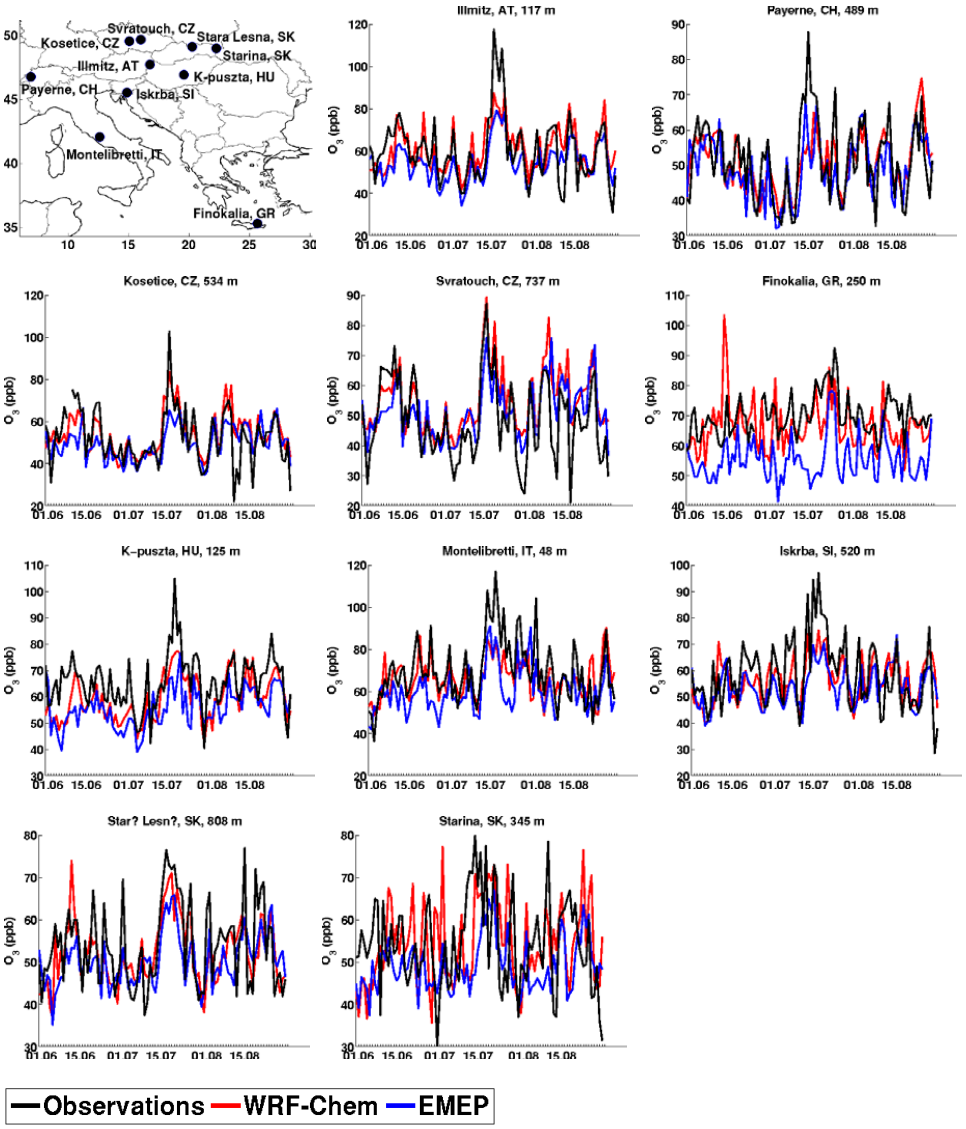

Figure 8. Time evolution of daily maximum surface O_3 (ppbv) as measured and modeled by WRF-Chem and EMEP MSC-W for 10 stations during the summer 2007. The top left plot marks the location of each station included in the comparison. Note that the scales on the vertical axes differ.

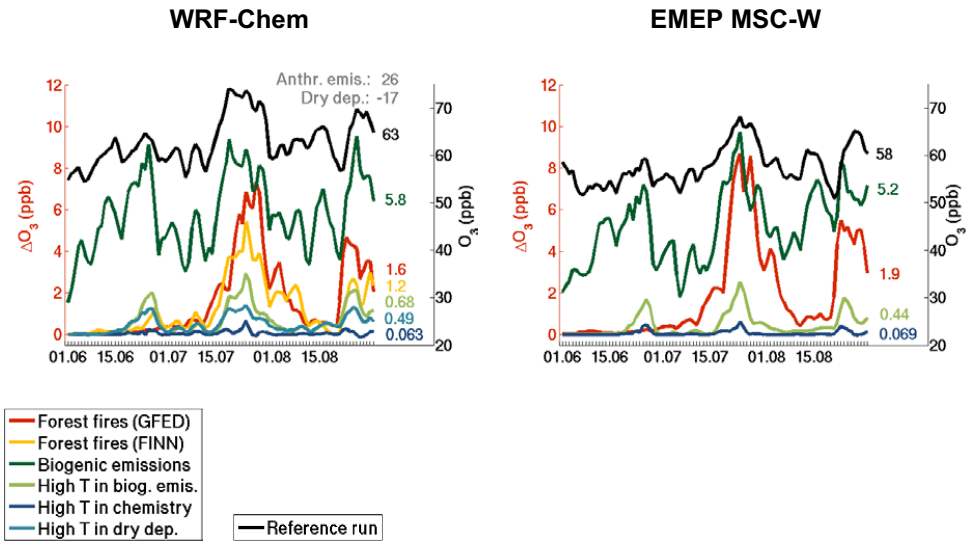

Figure 9. Daily maximum surface ozone in the reference run (ppbv; right y-axis) and the differences between the reference run and the sensitivity runs showing the impact of various processes on daily maximum surface ozone (ppbv, left y-axis), averaged over the EM region, calculated by the WRF-Chem (left) and EMEP (right) models. Seasonally averaged values are shown next to the curves.

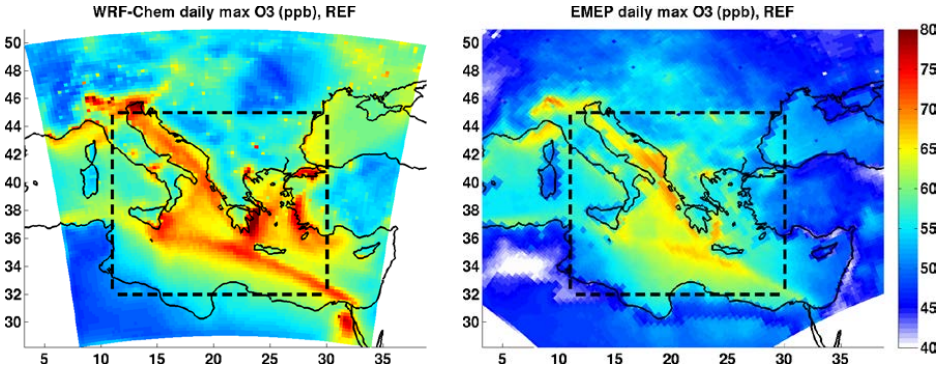

Figure 10. Daily maximum near-surface ozone (ppbv) calculated by WRF-Chem (left) and EMEP MSC-W (right) averaged over the summer (JJA) 2007. The dashed rectangle marks the common EM region.

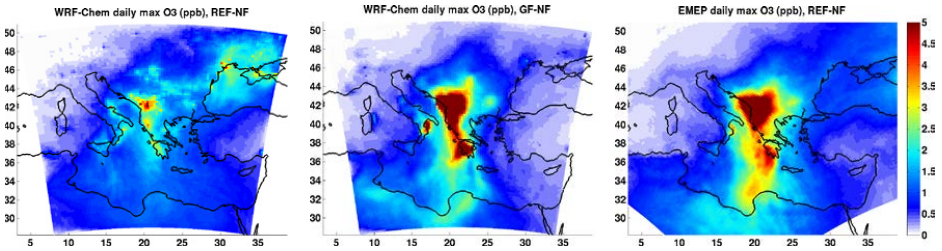

Figure 11. Change in daily maximum near-surface ozone (ppbv) due to forest fire emissions (REF-NF and GF-NF) calculated by WRF-Chem using FINN emissions (left), WRF-Chem using GFED emissions (middle), and EMEP MSC-W using GFED emissions (right) averaged over the summer (JJA) 2007.

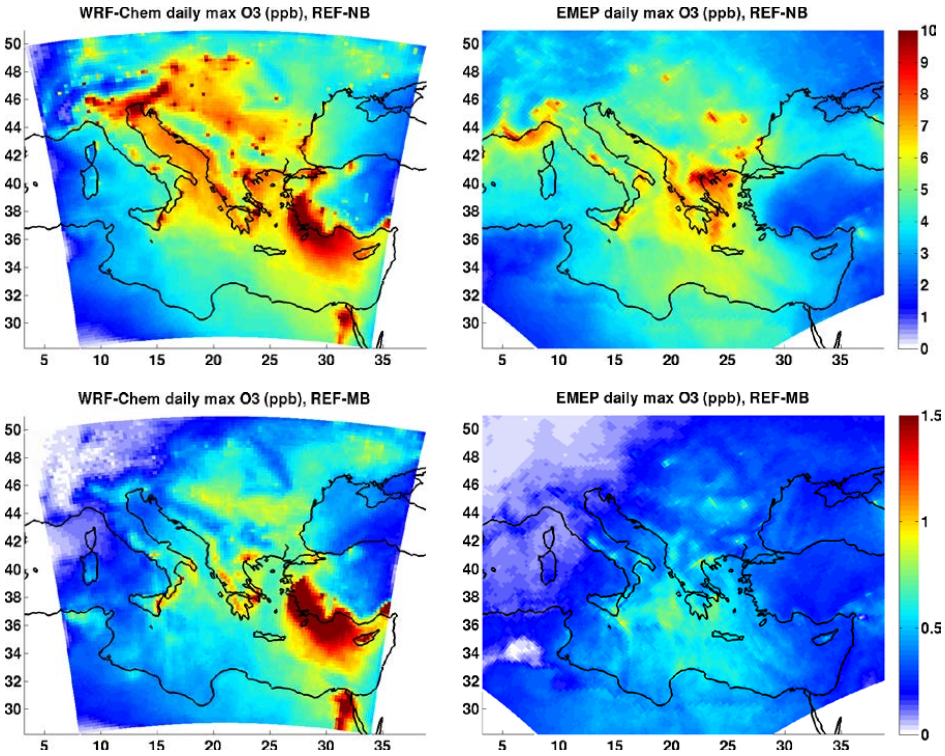

Figure 12. Change in daily maximum near-surface ozone (ppbv) due to biogenic emissions (REF-NB) (top) and due to high temperatures (above 28°C) in the computation of biogenic emissions (REF-MB) (bottom), calculated by WRF-Chem (left) and EMEP MSC-W (right) averaged over the summer (JJA) 2007.

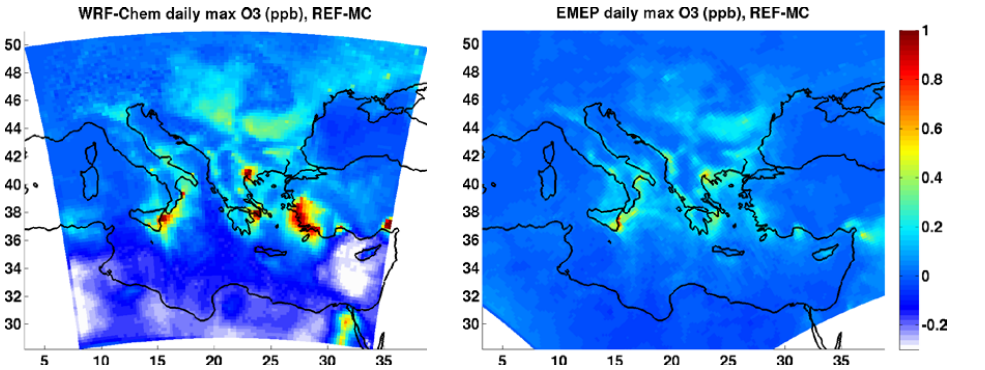

Figure 13. Change in daily maximum near-surface ozone (ppbv) due to due to high temperatures (above 28°C) in the chemistry computations (REF-MC), calculated by WRF-Chem (left) and EMEP MSC-W (right) averaged over the summer (JJA) 2007.

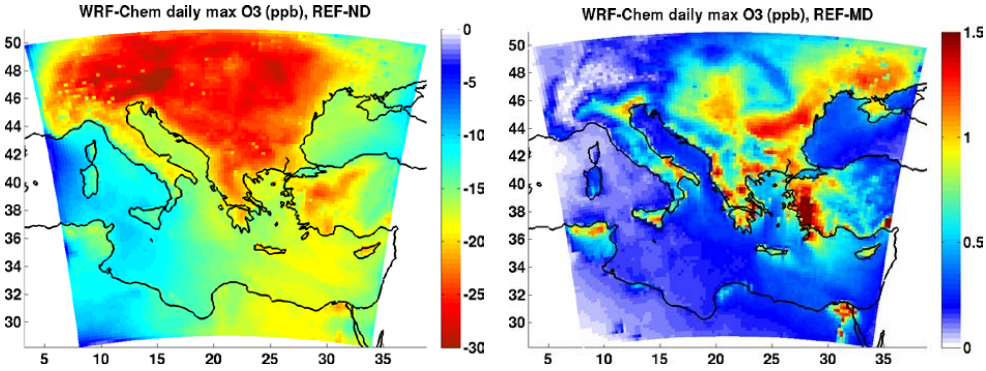

Figure 14. Change in daily maximum near-surface ozone (ppbv) due to dry deposition (REF-ND) (left) and due to high temperatures (above 28°C) in the computation of dry deposition (REF-MD) (right), calculated by WRF-Chem and averaged over the summer (JJA) 2007.

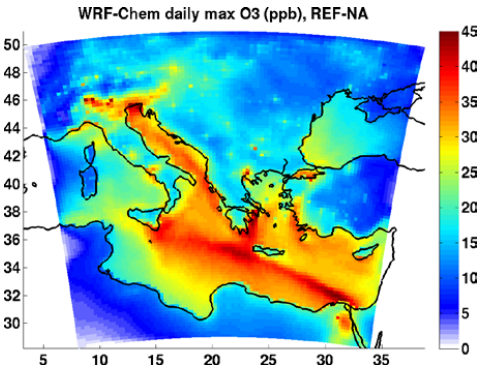

Figure 15. Change in daily maximum near-surface ozone (ppbv) due to anthropogenic emissions (REF-NA) calculated by WRF-Chem and averaged over the summer (JJA) 2007.